FINAL REPORT TO THE ACI FOUNDATION: CRC #80

REEXAMINATION OF PUNCHING SHEAR STRENGTH AND DEFORMATION CAPACITY OF CORNER SLAB-COLUMN CONNECTION

Prepared by:

MARNIE B. GIDUQUIO

MIN-YUAN CHENG

LANGA S. DLAMINI

DECEMBER, 2017

REEXAMINATION OF PUNCHING SHEAR STRENGTH AND DEFORMATION CAPACITY OF CORNER SLAB-COLUMN CONNECTION

Principal Investigator:	**Dr. Min-Yuan Cheng**
Graduate Research Assistant:	**Dr. Marnie B. Giduquio**
	Langa S. Dlamini

Sponsored by:

Ministry of Science and Technology, Taiwan.

The American Concrete Institute Foundation, Concrete Research Council

ABSTRACT

Effects of slab flexural reinforcement on the punching shear strength and deformation capacity of corner slab-column connections without shear reinforcement are evaluated in this study. Six isolated corner slab-column subassemblages were tested under combined gravity-type loading and lateral displacement reversals. Results from present and previous studies indicate that punching shear strength and deformation capacity per ACI 318-14 is not conservative for corner slab-column connections. For connections subjected to gravity-type loads only, a shear strength model considering effects of the equivalent slab top flexural reinforcement ratio and the critical section aspect ratio (b_o/d) is proposed. For connections subjected to combined gravity-type loads and lateral displacement reversals, the gravity shear ratio determined based on the proposed model improves applicability of the shear decay model per ACI 318-14.

TABLE OF CONTENTS

LIST OF FIGURES

CHAPTER 1

CHAPTER 2

CHAPTER 3

CHAPTER 4

CHAPTER 5

LIST OF TABLES

CHAPTER 2

CHAPTER 3

CHAPTER 4

CHAPTER 5

NOTATIONS

A_c = area of the critical section for punching shear per ACI Committee 318 since ACI 318-71 (1971a), can be determined as $b_o d$.

A_{cp} = area bounded by the basic control perimeter per fib Model Code (2010).

A_T = area of the critical section for punching shear per ACI Committee 318 (1963a, 1963b).

A_x, A_y = coordinate of point A with respect to the *x*-*y* coordinate system.

A_1, A_2 = coordinate of point A with respect to the 1-2 coordinate system.

B_x, B_y = coordinate of point B with respect to the *x*-*y* coordinate system.

B_1, B_2 = coordinate of point B with respect to the 1-2 coordinate system.

b_{etw} = critical section dimension parallel to the axis of unbalanced moment per ACI Committee 318 (1963a, 1963b).

b_{ew} = slab effective width.

b_s = $1.5\sqrt{r_{s,x} r_{s,y}}$, the support strip of the considered direction of moment transfer per fib Model Code (2010).

b_{sr} = maximum value for b_s per fib Model Code (2010).

b_o = perimeter of the critical section for punching shear per ACI Committee 318 since ACI 318-71 (1971a).

$b_{o,EC2}$ = basic control perimeter per Eurocode 2 (2004).

$b_{o,EC2,red}$ = reduced control perimeter per Eurocode 2 (2004).

$b_{o,MC}$ = shear resisting control perimeter per fib Model Code (2010).

b_1 = critical section dimension measured in the direction of the span for which moments are determined.

$b_{1,MC}$ = basic control perimeter per fib Model Code (2010).

$b_{1,MC,red}$ = reduced basic control perimeter per fib Model Code (2010).

b_2 = critical section dimension measured in the perpendicular direction to b_1.

b_u = diameter of a circle with the same surface area as the region inside the basic control perimeter per fib Model Code (2010).

C_{AB}, C_{BC} = distance from centroid of the critical section to the point of interest, measured perpendicular to the axis of unbalanced moment M_{uy} and M_{ux}, respectively.

c_x, c_y = column dimension along the x- and y- axis, respectively.

c_1, c_2 = distance from centroid of the critical section to the point of interest, measured perpendicular to the axis of unbalanced moment M_2 and M_1, respectively.

D = dead load.

d = effective depth of the slab or drop panel.

d_b = nominal diameter of steel bar.

d_g = maximum aggregate size, taken as not less 16mm per fib Model Code (2010).

E_s = modulus of elasticity of steel reinforcement.

e_u the eccentricity of the resultant shear with respect to the centroid of the basic control perimeter per fib Model Code (2010).

$e_{u,i}$ = e_{ux} or e_{uy} depending on the direction considered.

e_{ux}, e_{uy} = e_u along x- and y-direction, respectively.

$f_c^{'}$ = specified concrete compressive strength or concrete cylinder strength.

f_p = steel coupon peak tensile stress.

f_y = specified steel yield stress or yield stress of the steel coupons.

f_u = steel coupon peak tensile stress corresponding to 10% drop from peak or at fracture, whichever is longer.

h = slab thickness.

h_{dp} = drop panel thickness.

I_x, I_y = second moment area of the critical section about x- and y-axis, respectively, per ACI Committee 421 (2008, 2010).

I_{xy} = product of inertia of the critical section per ACI Committee 421 (2008, 2010).

I_1, I_2 = second moment area of the critical section about 1- and 2-axis, respectively, per ACI Committee 421 (2008, 2010).

J_c = property of the critical section analogous to polar moment of inertia.

J_{cx}, J_{cy} = J_c associated with unbalanced moment M_{uy} and M_{ux}, respectively.

j = ratio of lever arm resistance couple to slab effective depth d.

k = a coefficient to consider column rectangularity per Eurocode 2 (2004).

k_{dg} = a factor accounts for aggregate size and slab size per fib Model Code (2010).

k_e = a factor accounts for eccentricity per fib Model Code (2010).

k_s = a factor accounts for slab size per Eurocode 2 (2004).

k_x, k_y = k in x- and y- direction, respectively.

k_ψ = a factor to evaluate $v_{c,MC}$ per fib Model Code (2010).

L = live load

L_x, L_y = slab span taken from center-to-center of column support in x- and y-direction, respectively, per fib Model Code (2010).

l_{AB} = length of the line segment AB.

l_1, l_2 = projected dimension of critical section along 1- and 2-axis, respectively, per ACI Committee 421 (2008, 2010).

M_{ED} = transfer moment at the critical section per Eurocode 2 (2004).

$M_{ED,x}$, $M_{ED,y}$ = M_{ED} about x- and y-axis, respectively, per Eurocode 2 (2004).

M_d = $\sqrt{M_x{}^2+M_y{}^2}$.

M_T = moment transferred by torsion per ACI Committee 318 (1963a, 1963b)

M_{ub} = unbalanced moment at centroid of the critical section.

M_{ux}, M_{uy} = M_{ub} about x- and y-axis, respectively.

M_x, M_y = unbalanced moment about x- and y-axis, respectively, at centroid of the supporting column.

M_1, M_2 = unbalanced moment about 1- and 2-axis, respectively, at the centroid of critical section per ACI Committee 421 (2008, 2010).

m_n = nominal flexural strength per unit length within the support strip, b_s, per fib Model Code (2010).

m_{nx}, m_{ny} = m_n about x- and y-axis, respectively, per fib Model Code (2010).

m_u = flexural strength demand per unit length within the support strip, b_s, per fib Model Code (2010).

m_{ux}, m_{uy} = m_u about x- and y-axis, respectively, per fib Model Code (2010).

q_u = design load on the slab per fib Model Code (2010).

r_r = ratio between the area of negative (top) reinforcement that crosses entirely over the column capital or over the drop panel and the total area of negative reinforcement within the two column strips of both orthogonal directions, and in no case shall be less than 0.25, as per the Joint Committee on Standard Specifications for Concrete and Reinforced Concrete (1921).

r_s = the position where the radial bending moment is zero with respect to the support axis per fib Model Code (2010).

r_{sx}, r_{sy} = r_s about x- and y-axis, respectively, per fib Model Code (2010).

S = snow load.

V = vertical shear demand at the critical section in the ACI Building Code (1927, 1936, 1941,1947, and 1951).

V_g = connection shear due to gravity loading only.

$V_{g,flex}$ = level shear force leading to failure in bending.

V_{gs} = factored gravity shear including seismic effects.

V_o = shear force demand assumed to be transferred uniformly at the critical section when the connection is subjected to combined gravity-type loading and unbalanced moment.

V_{ug} = factored shear stress on the slab critical section calculated from the load combination $1.2D+1.0L+0.2S$.

$V_{u,318b}$ = connection shear demand per ACI 318-14 considering biaxial moment transfer.

$V_{u,318u}$ = connection shear demand per ACI 318-14 considering uniaxial moment transfer.

V_v = shear force demand at the critical section due to vertical load per ACI Committee 318 (1963a, 1963b).

v_c = punching shear stress capacity.

$v_{c,ACI}$ = v_c per ACI 318-14.

$v_{c,EC2}$ = v_c per Eurocode 2 (2004).

$v_{c,MC}$ = v_c per fib Model Code (2010).

$v_{c,prop}$ = v_c proposed in this study.

v_{ED} = factored gravity shear on the control perimeter per Eurocode 2(2004).

v_u = shear stress demand at the critical section due to combined gravity-type loading and unbalanced moment.

$v_{u,EC2}$ = v_u per Eurocode 2(2004).

$v_{u,318b}$ = v_u considering biaxial moment transfer per ACI Committee 318 (2014).

$v_{u,318u}$ = v_u considering uniaxial moment transfer per ACI Committee 318 (2014).

$v_{u,421}$ = v_u per ACI Committee 421 (2008, 2010).

v_{ug} = $V_{ug}/b_o d$.

W_1 = a factor associated with the shear stress distribution along the basic control perimeter, $b_{o,EC2}$, per Eurocode 2 (2004).

$W_{1,x}$, $W_{1,y}$ = W_1 about x- and y-axis, respectively, per Eurocode 2 (2004).

α = a coefficient to consider ρ_l in $v_{c,prop}$.

α_s = constant to calculate v_c.

β = a factor to consider shear amplified by the unbalanced moment per Eurocode 2 (2004).

β_c = ratio of long to short dimension of the supporting column.

ε_p = steel coupon tensile strain corresponding to peak stress f_p.

ε_{sh} = steel coupon tensile strain at the onset of strain hardening.

ε_t = net tensile strain in the extreme layer of the longitudinal reinforcement at nominal flexural strength.

ε_u = steel coupon tensile strain corresponding to fracture stress f_u.

ε_y = yield strain of steel coupon.

γ_c = partial safety factor for concrete material properties, specified in Eurocode 2 (2004) and fib Model Code (2010).

γ_f = a factor to determine the fraction of unbalanced moment to be transferred by flexure.

γ_v = a factor to determine the fraction of unbalanced moment transferred by shear.

γ_{vx}, γ_{vy} = the factor to determine the fraction of unbalanced moment transferred by shear for unbalanced moment M_{uy} and M_{ux}, respectively.

γ_{v1}, γ_{v2} = the factor to determine the fraction of unbalanced moment transferred by shear for unbalanced moment M_1 and M_2, respectively.

ρ_b = the balanced reinforcement ratio using the effective slab width.

ρ_l = $\sqrt{\rho_{tx}\rho_{ty}}$

$\rho_{l,EC2}$ = $\sqrt{\rho_{tx,EC2}\rho_{ty,EC2}}$

ρ_{tx}, ρ_{ty} = Slab top flexural reinforcement ratios in the *x*- and *y*- directions respectively, considering a slab effective width per ACI Committee 318 (2014).

$\rho_{tx,EC2}$, $\rho_{ty,EC2}$ = slab top flexural reinforcement ratios in the *x*- and *y*- directions respectively, considering a slab effective width equal to the column width plus 3*d* each side per Eurocode 2 (2004).

ϕ_v = strength reduction factor for shear.

ψ = rotation of the slab around the supported area per fib Model Code (2010).

θ = rotation angle of axes, positive clockwise per ACI Committee 421 (2008, 2010).

CHAPTER 1
INTRODUCTION

1.1 FLAT-PLATE FRAMING SYSTEM

Reinforced concrete (RC) flat-plate frame (Fig. 1.1) consisting of slabs that are directly supported by columns without the use of beams has been popularly used in practice as the primary system to support gravity-type loads due to its obstruction-free slab underside configuration that promotes architectural versatility, easy installation of pipelines, and most importantly cost efficiency.

Fig.1.1– Flat-Plate Structure
(http://www.houstonarchitecture.com/haif/topic/15624-2929-weslayan-40-story-residential-tower-by-pm-realty/page-10. Retrieved February 15, 2016)

Its beamless feature, however, inevitably results in a more flexible response when subjected to lateral forces. As a result, the flat-plate framing system is typically designed for gravity type loads while a stiffer element such as shear walls or moment-resisting frames are incorporated to resist the lateral forces. Another major concern for the use of flat-plate framing system is the punching shear failure at the connection, as shown in Fig. 1.2. Punching shear failure, typically observed around the vicinity of the column, is believed to be caused by the combined effect of gravity-type load and unbalanced moment that are transferred at the connection. Punching shear failure is brittle in nature and may cause catastrophic damage to properties and even loss

of lives (Wood, 2004; King and Delatte, 2004; Park, 2012; and among others). Despite the extensive research works conducted in the past to minimize the likelihood of punching shear failure, controversial issues (Dilger et al., 2005; Widianto et al., 2009, Cheng and Giduquio, 2014a, 2014b; Ghali et al., 2015, and among others) still exist. The strength and deformation capacity of corner slab-column connection is of interest in this research.

Fig.1.2 – Punching Shear Failure
(https://reidmiddleton.files.wordpress.com/2011/03/ddd2.jpg. Retrieved June 1, 2016)

A corner and interior slab-column connection is surrounded by slabs from two and four sides, respectively. As a result, the confining effects for the two types of connections are different. However, test results of corner slab-column connections are relatively limited, especially for specimens subjected to combined gravity-type loads and lateral displacement reversals. Most of the design provisions in the ACI 318-14 have been developed based on test results of interior slab-column specimens. Whether the code-specified design provisions are applicable to corner slab-column connections is of particular concern. This research, through analyses of test results from previous and the present studies, aims to provide more information of punching shear strength and deformation capacity for the design of corner slab-column connections.

1.2 CURRENT DESIGN PRACTICE OF SLAB-COLUMN CONNECTIONS

The current ACI Building Code (ACI Committee 318, 2014), referred as ACI 318-14 hereafter in this report, prohibits the use of flat-plate framing system as the primary seismic-force-resisting system in regions with high seismicity, more specifically in regions assigned to seismic design category (SDC) D, E, or F (ASCE/SEI 7, 2016). Within such regions, flat-plate framing systems are designed to support gravity-type loads. According to ACI 318-14, the flat-plate framing system in SDC D, E, or F is required to satisfy two-step design processes, i.e. satisfy "strength check" provisions followed by "deformation check" provisions.

"Strength check" provisions require connection shear capacity to be greater than the shear demand under gravity-type loads at the critical section, i.e., $v_u \leq \phi_v v_{c,ACI}$. In which, the strength reduction factor ϕ_v is 0.75 and the critical section is located at $d/2$ distance away from the column faces. An eccentric shear stress model per Section 8.4.4.2 of the ACI 318-14 (ACI Committee 318, 2014), as shown in Eq. 1.1, is provided to evaluate connection shear demand, $v_{u.}$. On the other hand, shear capacity $v_{c,ACI}$ per the code is determined by Eq. 1.2. Notations used in both Eqs. 1.1 and 1.2 will be explained later in Chapter 2.

"Deformation check" provisions intend to ensure enough connection deformation capacity. Previous research works have shown that connection deformation capacity is greatly influenced by the connection gravity shear. A bilinear interaction diagram shown in Fig. 1.3 is provided by the ACI 318-14 (ACI Committee 318, 2014) to evaluate connection deformation capacity. In Fig. 1.3, the $v_{ug}/\phi_v v_{c,ACI}$ for the horizontal axis is defined as the factored gravity shear at the critical section connection using a specified code-defined load combination divided by the punching shear capacity determined per Eq. 1.2. The connection design drift must be less than the larger of $0.035 - (1/20)\left(v_{ug}/\phi_v v_{c,ACI}\right)$ and 0.005. Shear reinforcement is needed if the demand is greater than the capacity in either of the two design step.

$$v_u = \frac{V_o}{b_o d} \pm \left(\frac{\gamma_v M_{ub} c}{J_c}\right) \qquad \text{Eq. 1.1}$$

$$v_{c,ACI} = \text{Least of} \left\{ \begin{array}{l} \text{(a)} \left(2 + \frac{4}{\beta}\right) \sqrt{f_c'(\text{psi})} \\ \text{(b)} \left(\frac{\alpha_s d}{b_o} + 2\right) \sqrt{f_c'(\text{psi})} \\ \text{(c)} \quad 4\sqrt{f_c'(\text{psi})} \end{array} \right\} \qquad \text{Eq. 1.2}$$

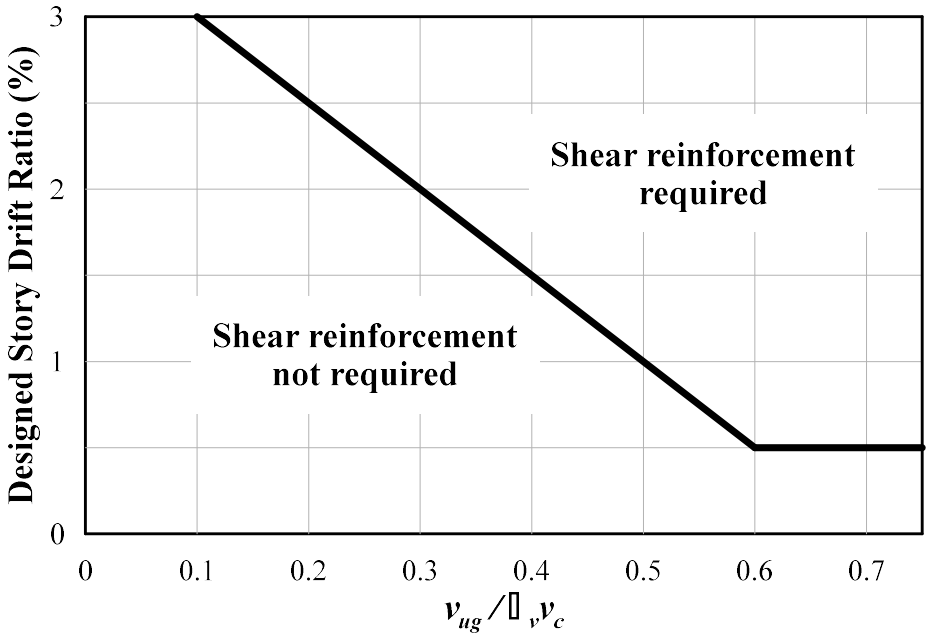

Fig.1.3 – Drift Ratio vs. Gravity Shear Ratio Interaction Diagram per ACI 318-14 (ACI Committee 318, 2014)

Several types of shear reinforcement are permitted by the ACI 318-14 (ACI Committee 318, 2014) such as stirrups and headed shear stud as presented in Fig. 1.4. In practice, headed shear stud is favored due to its installation advantage (Robertson et al., 2002). However, headed shear studs are relatively expensive. In addition, test results (Cheng et al., 2010; and Matzke et al., 2015) show that shear capacity per ACI 318-14 for headed shear studs is not conservative because of its deficiency to provide adequate confinement to concrete and bridge crack widths under large inelastic deformation.

The potential of using fiber reinforced concrete as an alternative shear reinforcement in the slab-column connection has been studied previously. Test results (Swamy and Ali, 1982; Shaaban and Gesund, 1994; McHarg et al., 2000; and Cheng and Parra-Montesinos, 2010a, 2010b) show that the application of steel fiber-reinforced concrete in the slab-column connection enhances the punching shear strength and drift capacity of the connection.

(a) Stirrups
(http://www4.eng.hawaii.edu/~ian/peer/lee-uh/lee-uh-2cs.htm. Retrieved June 3, 2016)

(b) Headed Shear Studs
(https://nees.org/warehouse/experiment/3046/project/983. Retrieved June 3, 2016)

Fig.1.4 – Slab Shear Reinforcement

1.3 RESEARCH MOTIVATION

The complexity of shear transfer mechanism in the slab-column connections results in some controversial issues. First, different research reports interpret eccentric shear stress model (Eq. 1.1) differently (Cheng and Giduquio, 2014a, 2014b). Shear stress demand (v_u) at corner slab-column connection is affected significantly due to this issue. Second, the empirically derived shear capacity per Eq. 1.2 has been criticized for its need to consider slab flexural reinforcement, as suggested by other design recommendations or research reports (European Committee for Standardization, 2004; Widianto et al., 2009; International Federation for Structural Concrete, 2013, Dam et al., 2017). This issue affects both interior and exterior slab-column connections. Third, the bilinear interaction curve, presented in Fig. 1.3, for the evaluation of

connection deformation capacity is primarily developed based on test results of interior slab-column specimens (Hueste et al, 2009; Cheng, 2009). As a result, it appears there is still some room for research in the area of punching shear strength and deformation capacity of corner slab-column connections.

1.4 RESEARCH OBJECTIVES

The objective of this study is to examine strength and deformation capacity of the corner slab-column connections. To accomplish this, six approximately full-scaled isolated corner slab-column specimens subjected to combined gravity load and lateral displacement reversals were tested. The six specimens were geometrically identical and evenly divided into two groups depending on the flexural reinforcement ratio within the effective slab width, b_{ew}, defined per ACI 318-14. In each group, the connection gravity shear ratio ($v_g/v_{c,ACI}$) of the three specimens was targeted at 0.3, 0.4 and 0.5, respectively, during the test. In which, v_g represents the shear stress demand assumed to be uniformly transferred at the critical section due to gravity-type load without induced lateral displacement and its value was recorded from a load cell at the bottom column support. Please note, v_g is V_o (Eq. 1.1) at zero lateral drift divided by the critical section area, $b_o d$. In addition, in order to better understand the influence of flexural reinforcement ratio on punching shear strength, a database consisting of 19 test results of corner slab-column connections subjected to gravity-type load from previous researches is established.

To be consistent with the design philosophy of the ACI 318-14, in this report, connection shear strength is evaluated based on test results of specimens subjected to gravity-type load. Connection deformation capacity is evaluated with respect to the gravity shear ratio, $v_g/v_{c,ACI}$.

1.5 REPORT OUTLINE

This report consists of six chapters. A brief introduction of flat-plate framing system is presented in Chapter 1. A review of related literature, comprising the historical background of the development of the punching shear provisions stipulated in the ACI Building Code (ACI Committee 318, 2014), punching shear provisions per European Code (European Committee for Standardization, 2004), design recommendations per fib Model Code or MC-10 (International Federation for Structural Concrete, 2013), and a brief description of tests conducted previously on corner slab-column connections subjected to gravity-type loads, is

outlined in Chapter 2. Details of the experimental program of this study are described in Chapter 3. Chapter 4 focuses on discussion of the test results. In Chapter 5, previous test results of corner slab-column connections subjected to gravity-type loads are collected and a database is developed. Based on test results from the present study and the database analysis, code provisions and design recommendations for punching shear strength and connection deformation capacity are evaluated. Finally, conclusions drawn from this study are summarized in Chapter 6.

CHAPTER 2
LITERATURE REVIEW

2.1 INTRODUCTION

Development of the code provisions per ACI 318-14 (ACI Committee 318, 2014) on shear strength and deformation capacity of slab-column connections is presented in this chapter. Design provisions of the European building code (European Committee for Standardization, 2004), fib model code (International Federation for Structural Concrete, 2013), ACI 352 report (Joint ACI-ASCE Committee 421, 2008 and 2010), and ACI 421 report (Joint ACI-ASCE Committee 352, 2011) on punching shear strength (capacity) are also reviewed. In the final part of this chapter, relevant research works (Zaghlool et al., 1970; Walker and Regan, 1987; Desayi and Seshadri, 1997), specifically on punching shear strength of corner slab-column connection subjected to monotonically gravity-type loading, are summarized.

2.2 DEVELOPMENT OF PUNCHING SHEAR DESIGN PROVISIONS PER ACI 318

Prior to the establishment of standards or building code in the United States, acceptance of the design of flat slab construction was based on the results of load tests (Sozen and Siess, 1963; Gasparini, 2002). The first design provision for shear appears to be first provided in the National Association of Cement Users (NACU) Report (Henley, 1908). It specified that for a concrete compressive strength of 2000 psi, the corresponding shearing strength should be assumed equal to 200 psi. It was not clear whether this stress limit was applicable to members subjected to one-way (column/beam members) or two-way (slab-column connections) shear actions. No further explanations were provided within the report on how to determine the shear demand.

For members with web reinforcement, NACU Standard No. 4 (1910) recommended that concrete shall be considered to carry 40 psi of the total shear stress demand; the remainder shear stress demand shall be resisted by the web reinforcement. This recommendation was specifically intended for beams (one-way shear). No provision was provided for shear stresses in the slab-column connection.

The term “punching shear” was first adopted in the report of the Joint Committee on Concrete and Reinforced Concrete (1913). The first design provision for punching shear stress (vertical shear) was also introduced, where the allowable punching shear stress demand shall be limited

to $0.06f_c'$. The concrete compressive strength, f_c', was based on the average strength of a set of 8 × 16 in. (200 × 400 mm) concrete cylinder samples or the recommended maximum concrete compressive strength provided by the committee (Joint Committee on Concrete and Reinforced Concrete, 1913) based on concrete mix proportion. However, it was not clear how the shear demand should be evaluated.

Later, the stress limit for punching shear was increased to $0.075f_c'$ in the report of the Committee on Reinforced Concrete Building Laws (1916).

Based on Moe's (1961) review, the report of the Joint Committee on Concrete and Reinforced Concrete (1917) indicated that the diagonal tension shall be considered for punching shear design. However, it was still not clear how the stress demand due to diagonal tension should be determined.

The American Concrete Institute (ACI), through its Standard Specifications No. 23 (1920), presented a clear definition of the two possible shear failure mechanisms in the flat slab construction including the vertical shear failure and diagonal tension failure. To prevent the vertical shear failure, punching shear stress was required to be evaluated on the vertical section, with a depth equivalent to slab effective depth *d*, along the periphery of the column or column capital. The working stress considering "punching shear" (vertical shear) was limited to $0.10f_c'$, where f_c' was the concrete compressive strength based on 6 × 12 in. (150 × 300 mm) or 8 × 16 in. (200 × 400 mm) concrete cylinder samples. To prevent the "diagonal tension" failure, two scenarios were presented. When column or column capital was used, shear stress was suggested to be evaluated within the slab effective depth *d*, on the surface of the frustum of cone or pyramid, passing though the periphery of the column or capital with a base angle of 45 degrees. In this case, the working stress on this critical section was limited to $0.035f_c'$. When drop panel was used, the shear stress limit for diagonal tension, evaluated on the vertical section along the periphery of the drop with a depth of *jd*, must not exceed $0.03f_c'$. The parameter *j* is the ratio of the lever arm resistance couple to the slab effective depth, *d*. The critical sections for both "punching shear" and "diagonal tension" failures are presented in Fig. 2.1.

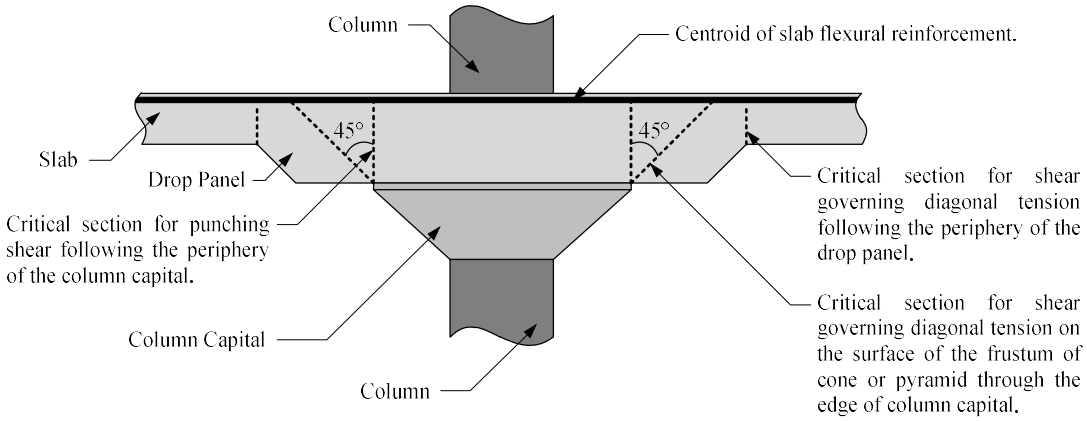

Fig.2.1– Critical Section Definition per ACI Standard Specifications No. 23 (1920)

The Joint Committee on Standard Specifications for Concrete and Reinforced Concrete (1921) submitted a report to the constituent organizations entitled "Tentative Specifications for Concrete and Reinforced Concrete." According to the report, the working shear stress capacity, v_c, can be computed based on Eq. 2.1. No further explanations were given for its associated failure mechanism (vertical shear or diagonal tension).

$$v_c \leq \min\begin{Bmatrix} 0.02f_c^{'}(1+r_r) \\ 0.03f_c^{'} \end{Bmatrix} \qquad \text{Eq. 2.1}$$

In Eq. 2.1, r_r is the ratio between the area of negative (top) reinforcement that crosses entirely over the column capital or over the drop panel and the total area of negative reinforcement within the two column strips in the two orthogonal directions, and in no case shall be less than 0.25. Throughout this report, column strip was defined as the design strip with a width of each side of a column centerline equal to 0.25 times the lesser of the bay distances in both orthogonal directions.

The critical section of connection without drop panel was defined as the vertical section having a depth of $[h-1.5](\text{in.})$ along the perimeter lying at a distance of $[h-1.5](\text{in.})$ from the edge of the column or column capital. For a connection with drop panel, two critical sections shall be considered: first was the critical section within the drop, defined as the vertical section having a depth of $0.875\left[h_{dp}-1.5\right](\text{in.})$ along the perimeter lying at a distance of $\left[h_{dp}-1.5\right](\text{in})$ from the column or column capital; and second was the critical section beyond the drop, defined as the vertical section having a depth of $0.875\left[h_{dp}-1.5\right](\text{in.})$ along the

perimeter lying at a distance of $[h - 1.5](\text{in.})$ from the edge of the drop. The definitions of h and h_{dp} are illustrated in Fig. 2.2.

The "tentative specifications" for shear in slab-column connections were later adopted and published in the final report of the same committee (Joint Committee on Standard Specifications for Concrete and Reinforced Concrete, 1924).

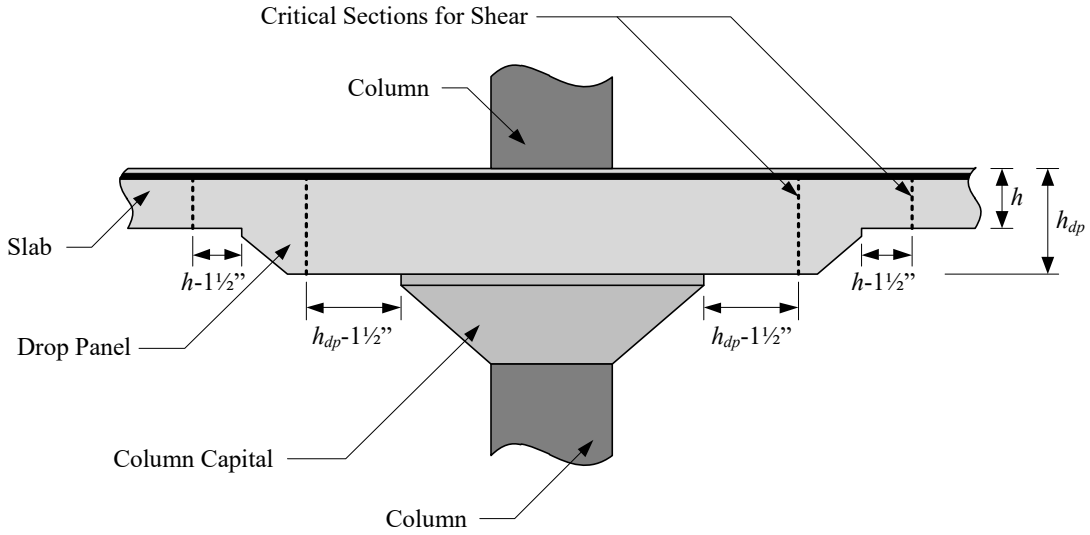

Fig.2.20 – Critical Section Definition (Joint Committee on Standard Specifications for Concrete and Reinforced Concrete, 1921)

In 1927, ACI Committee E-1 (1927) adopted Eq. 2.1 for punching shear capacity. Further requirement was made to provide at least 25% and 50% of the negative (top) reinforcement area in the column strips within the width of the strip directly above the column or capital and drop panel, respectively. Also, the punching shear stress demand was suggested to be evaluated using Eq. 2.2.

$$\text{shear stress demand} = \frac{8V}{7b_o d} \qquad \text{Eq. 2.2}$$

In Eq. 2.2, V is the vertical shear at the critical section; b_o is the perimeter of the critical section defined in Fig. 2.2; and the effective depth, d, is taken as either $[h - 1.5](\text{in.})$ or $\left[h_{dp} - 1.5\right](\text{in})$.

Few years later, slight changes were made for the punching shear provisions by ACI Committee 501 (1936). The working stress limit (shear capacity) at the critical section should be taken as follows:

(a) $0.03f_c^{'}$, when 50% of the total negative (top) reinforcement passes directly over the column capital.

(b) $0.025f_c^{'}$, when 25% of the total negative (top) reinforcement passes directly over the column capital.

(c) For intermediate percentages, intermediate values of shearing unit stress shall be used.

Shear stress demand along the critical section, on the other hand, was suggested to be evaluated using Eq. 2.3. The parameter j is the ratio of the lever arm resistance couple to the slab effective depth d, which is taken as $[h - 1.5](\text{in.})$, and b_o is the perimeter of the critical section defined lying at a distance $[h - 1.5](\text{in.})$ from the column or capital.

$$\text{shear stress demand} = \frac{V}{b_o jd} \qquad \text{Eq. 2.3}$$

No change was made for the punching shear provisions in the next few ACI Building Code versions (1941, 1947 and 1951).

In the 1956 ACI Building Code (ACI Committee 318, 1956), shear stress limits at the critical section were revised as follows. In which, shear demand was evaluated using Eq. 2.3. Critical section for the evaluation of shear strength was defined as a vertical section located at a distance d away from the column face.

(a) $0.03f_c^{'} \leq 100$ psi, when 50% of the total negative reinforcement passes directly over the column capital.

(b) $0.025f_c^{'} \leq 85$ psi, when 25% of the total negative reinforcement passes directly over the column capital.

(c) For intermediate percentages, proportionate values of shearing unit stress shall be used.

Ultimate strength design (USD) philosophy was introduced in the 1963 ACI Building Code (ACI Committee 318, 1963a). As a transition from the then widely used working stress design (WSD) approach to the USD approach, the 1963 ACI Building Code allowed the designer to

adopt any of the two design approaches in proportioning structural components. Both approaches, per ACI 318-63, intended to provide shear resistance for diagonal tension failure mechanism.

For WSD approach, the concrete shear stress capacity was limited to $2\sqrt{f_c'(\text{psi})}$. The use of shear reinforcement was permitted for sections with total slab thickness of at least 10 inches but the nominal shear capacity including shear resistance from both shear reinforcement and concrete shall be limited to $3\sqrt{f_c'(\text{psi})}$. For USD approach, shear capacity without shear reinforcement was limited to $4\sqrt{f_c'(\text{psi})}$and shear capacity with shear reinforcement as shall limited to $6\sqrt{f_c'(\text{psi})}$. The critical section perimeter for both WSD and USD was defined at a distance $d/2$ from the periphery of the column. The slab effective depth, d, was defined as the distance from extreme compression fiber to the centroid of tensile reinforcement. The nominal punching shear capacity specified in the USD method of the 1963 ACI Building Code was primarily developed based on the recommendations of the Joint ACI-ASCE Committee 326 (1962).

Shear demand for connection subjected to vertical load only was suggested to be evaluated per Eq. 2.4(a). In which, V_v is shear demand at the critical section due to vertical load, b_o is the critical section perimeter located at a distance $d/2$ away from the column face as shown in Fig. 2.3(a), and d is the slab effective depth. For connections subjected to combined vertical load and unbalanced moment perpendicular to b_{etw} shown in Fig. 2.4(b), shear demand was suggested to be evaluated per Eq. 2.4(b). In which, V_o is the shear demand assumed to be transferred uniformly at the section with a perimeter defined by points *A*, *B*, *B'*, *A'* shown in Fig. 2.3(b), A_T is the section area, M_T is the unbalanced moment transferred by torsion, and J_c refers to the polar moment of inertia of the section. This analytical model, typically referred as eccentric shear stress model, was primarily developed based on the work of Di Stasio and van Buren (1960).

$$\text{shear stress demand due to vertical load} = \frac{V_v}{b_o d} \qquad \text{Eq. 2.4 (a)}$$

$$\text{shear stress demand due to combined effect} = \frac{V_o}{A_T} \pm \frac{M_T\,(c_x + d)/2}{J_c} \qquad \text{Eq. 2.4 (b)}$$

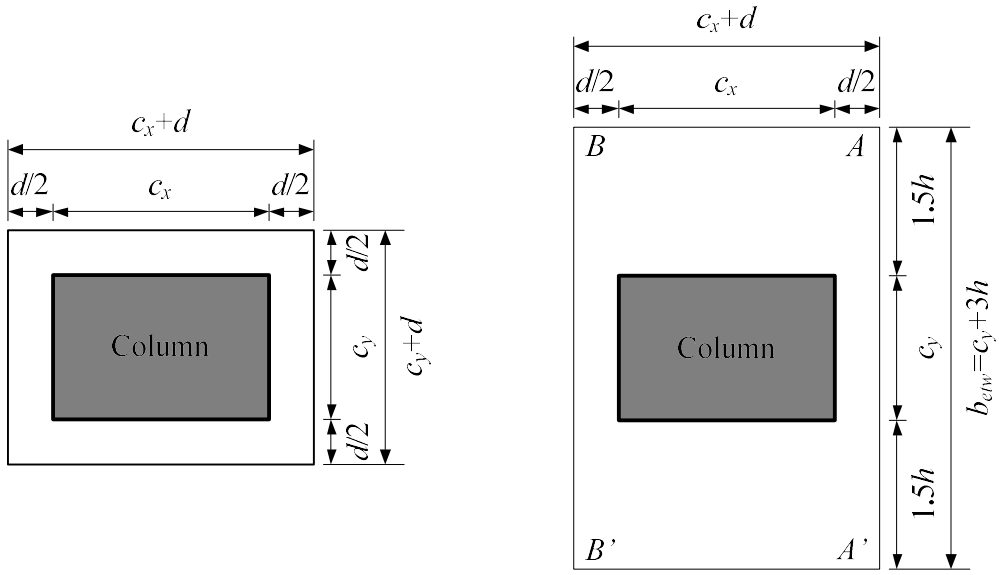

(a) Critical Section for Shear

(b) Critical Section for Combined Moment, Torsion and Vertical Load

Fig.2.30 – Critical Section Defined in the Commentary of the 1963 ACI Building Code (ACI Committee 318, 1963b)

The WSD approach was completely eliminated in the 1971 ACI Building Code (ACI Committee 318, 1971a) and its commentary (ACI Committee 318, 1971b). Punching shear provisions were slightly modified in the ACI 318-71. Shear demand at the critical section due to combined vertical and unbalanced moment was suggested to be evaluated using Eq. 2.5. The critical section was defined as a section located at a distance of $d/2$ away from the column face. Please note, Eq. 2.5 is essentially the same as Eq. 1.1 because A_c is $b_o d$. As can be seen, this model (eccentric shear stress model) has remained unchanged since then.

$$v_u = \frac{V_o}{A_c} \pm \frac{\gamma_v M_{ub} c}{J_c} \qquad \text{Eq. 2.5}$$

In Eq. 2.5, referring to a typical interior connection shown in Fig. 2.4, v_u is the combined shear stress on the critical section; V_o is shear assumed to be uniformly transferred at the critical section; $A_c = b_o d = 2d(c_x + c_y + 2d)$ is the area of the critical section; M_{ub} is the unbalanced moment acting at the centroid axis of the critical section; J_c is a property of the assumed critical section analogous to polar moment of inertia (for example, $J_c = 2\left[\left(b_1 d^3/12\right) + \left(d b_1^3/12\right)\right] + 2(b_2 d)(b_1/2)^2$ for an interior slab-column connection with parameters and direction of M_{ub}

defined in Fig. 2.4); c is the distance measured perpendicular to the axis of M_{ub} between centroid of the critical section to the point of interest (an interior connection example is presented in Fig. 2.4); and γ_v is the factor to determine the percentage of unbalanced moment transferred by shear. The factor γ_v is evaluated using Eq. 2.6.

$$\gamma_v = 1 - \gamma_f = 1 - \frac{1}{1 + \frac{2}{3}\sqrt{\frac{b_1}{b_2}}} \qquad \text{Eq. 2.6}$$

The parameters used in Eq. 2.6 are defined as follows: γ_f is the fraction of unbalanced moment transferred by flexure within the effective slab width between lines that are half the slab thickness on each side of the column; b_1 is the dimension of the critical section measured in the direction of the span for which moments are determined; and b_2 is the dimension of the critical section measured in the direction perpendicular to b_1.

In the 1974 code supplement (ACI Committee 318, 1974), the effective slab width was redefined between lines that are 1.5 times the slab thickness on each side of the column. This definition has remained unchanged since then.

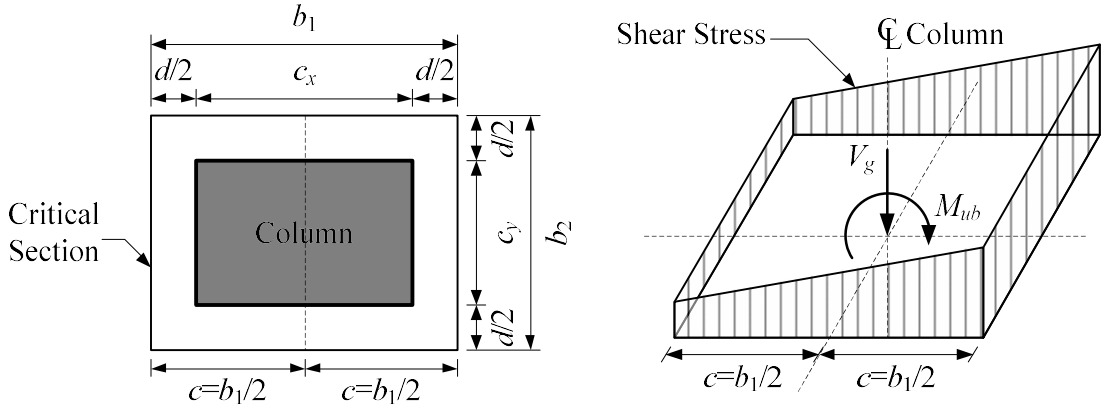

(a) Critical Section (b) Combined Shear Stress

Fig.2.40 – Combined Shear Stress Evaluation per Eccentric Shear Stress Model

The Joint ACI-ASCE Committee 426 (1974) has reported that the permissible shear stress of $4\sqrt{f_c'(\text{psi})}$ was not conservative when β_c, the ratio of long-to-short dimension of the supporting column, is larger than 2. The shear stress on the critical section is assumed to vary from a

maximum of $4\sqrt{f'_c(\text{ psi})}$ down to $2\sqrt{f'_c(\text{ psi})}$ as the β_c increases. To account for the effect of the rectangularity of the column, the 1977 ACI Building Code (ACI Committee 318, 1977) introduced an additional shear stress limit for slab-column connections without shear reinforcement, as expressed in Eq. 2.7.

$$v_c = \left(2 + \frac{4}{\beta_c}\right)\sqrt{f'_c} \le 4\sqrt{f'_c},\ \text{psi} \qquad \text{Eq. 2.7}$$

Another shear stress limitation was introduced in the 1989 ACI Building Code (ACI Committee 318, 1989) for connections without shear reinforcement, as expressed in Eq. 2.8. In Eq. 2.8, α_s is 40 for interior connections, 30 for edge connections, and 20 for corner connections. As a result, the connection shear capacity, v_c, shall be taken as the least value obtained from Eq. 2.7 to Eq. 2.8, but need not exceed $4\sqrt{f'_c(\text{ psi})}$, same as $v_{c,ACI}$ shown in Eq. 1.2 per current ACI 318-14.

$$v_c = \left(\frac{\alpha_s d}{b_o} + 2\right)\sqrt{f'_c},\ \text{psi} \qquad \text{Eq. 2.8}$$

Table 2.1 – Modified values of γ_f per ACI 318-95 (ACI Committee 318, 1995)

Column Location	Axis of Unbalanced Moment	Limitations		Modified γ_f
		Gravity Shear(1)	Slab Reinforcement Ratio(2)	
Corner	Either direction	$\le 0.50\phi_v v_c$	$\le 0.375\rho_b$(3)	1.0
Edge	Parallel to the edge	$\le 0.75\phi_v v_c$	$\le 0.375\rho_b$(3)	1.0
	Transverse to the edge	$\le 0.40\phi_v v_c$	$\le 0.375\rho_b$(3)	$\frac{1.25}{1+\frac{2}{3}\sqrt{\frac{b_1}{b_2}}} \le 1.0$
Interior	Either direction	$\le 0.40\phi_v v_c$	$\le 0.375\rho_b$(3)	$\frac{1.25}{1+\frac{2}{3}\sqrt{\frac{b_1}{b_2}}} \le 1.0$

(1) ϕ_v is the strength reduction factor for shear , v_c is the least value from Eq. 2.7, Eq. 2.8 and $4\sqrt{f'_c(\text{ psi})}$
(2) slab flexural reinforcement ratio within the effective slab width.
(3) ρ_b is the balanced reinforcement ratio using the effective slab width.

An evaluation of available test results (Moehle, 1988; and Joint ACI-ASCE Committee 352, 1988) showed that some flexibility in the distribution of unbalanced moments transferred by both shear and flexure was possible (Grossman, 1989). This led to the additional provisions for the fraction of unbalanced moment to be transferred by flexure γ_f in the 1995 ACI Building Code (ACI Committee 318, 1995). Adjustments for γ_f, as summarized in Table 2.1, were introduced in the 1995 ACI Building Code (ACI Committee 318, 1995).

No changes were made for the punching shear design provisions in the 1999 ACI Building Code (ACI Committee 318, 1999). Seismic design requirements for slab-column connections were incorporated for the first time in the 2002 ACI Building Code (ACI Committee 318, 2002). The results of the tests conducted by Pan and Moehle (1989) indicated that a lateral interstory drift of 1.5% could be achieved if the level of gravity shear acting on the slab critical section was limited to 40% of the connection shear capacity. Considering those findings, the 2002 ACI Building Code (ACI Committee 318, 2002) limited the factored gravity shear of slab-column connection without shear reinforcement to $0.40\phi_v v_c$ when the flat-plate framing system was designed as part of the lateral force-resisting system in seismic design category C (intermediate).

The 2005 ACI Building Code (ACI Committee 318, 2005) required that slab-column connections shall support the designed gravity loading when subjected to the designed lateral displacement. It provided two options in assessing the adequacy of the slab-column connection under earthquake-induced effects; (a) the shear strength check, $v_u \leq \phi_v v_{c,ACI}$, where v_u shall be determined with earthquake effects, and (b) the displacement check, that was included the first time in the building code, as presented in Fig. 1.3. In Fig. 1.3, v_{ug} is the factored shear force on the slab critical section calculated from the load combination $1.2D + 1.0L + 0.2S$, where D, L and S refer to dead, live and snow load, respectively. This interaction curve indicates that shear reinforcement is not needed in the connection when the design story drift ratio is less than the larger of 0.005 and $\left[0.035 - 0.05\left(v_{ug}/\phi_v v_{c,ACI}\right)\right]$. Unless either of the two checks is satisfied, shear reinforcement shall be provided to reduce the likelihood of punching shear failure. In the 2008 ACI Building Code (ACI Committee 318, 2008), a minor change is made pertaining to the provisions for the fraction of unbalanced moment to be transferred by flexure γ_f. The requirement for the amount of longitudinal reinforcement in the effective slab width to be less

than 37.5% of the balanced steel ratio is replaced with a steel minimum net tensile strain ε_t of 0.010. However, this change seems to be applicable only for interior connection and edge connection with unbalanced moment about an axis perpendicular to the edge. Further changes are made for the modification of the fraction of moment to be transferred by flexure γ_f in the current ACI Building Code (ACI Committee 318, 2014). The changes are summarized in Table 2.2.

Table 2.2 – Modified values of γ_f per ACI 318-14 (ACI Committee 318, 2014)

Column Location	Span Direction	Limitations		Maximum Modified γ_f
		v_{ug}	ε_t (within effective width)	
Corner	Either direction	$\leq 0.50\phi_v v_c$	≥ 0.004	1.0
Edge	Perpendicular to the edge	$\leq 0.75\phi_v v_c$	≥ 0.004	1.0
	Parallel to the edge	$\leq 0.40\phi_v v_c$	≥ 0.010	$\frac{1.25}{1+\frac{2}{3}\sqrt{\frac{b_1}{b_2}}} \leq 1.0$
Interior	Either direction	$\leq 0.40\phi_v v_c$	≥ 0.010	$\frac{1.25}{1+\frac{2}{3}\sqrt{\frac{b_1}{b_2}}} \leq 1.0$

2.3 ISSUES RELATED TO THE ECCENTRIC SHEAR STRESS MODEL

It is very controversial whether connection shear demand using Eq. 2.5 is to be evaluated with moments from both designed directions simultaneously, as shown in Eq. 2.9. In which, c_x and c_y refers to distance from centroid of critical section to the point of interest, respectively, γ_{vx} and γ_{vy} refers shear fraction factor in the *x*- and *y*- direction, respectively, and J_{cx} and J_{cy} is the inertia properties in the *x*- and *y*- direction, respectively. The combination of unbalanced moments from both directions basically results in maximum shear stress at a corner of the critical section, as shown in Fig. 2.5. A remark made by Wight and Falconer (2005) has indicated that it is unnecessary to evaluate biaxial moments simultaneously, but moment transfer should be checked individually in each designed direction and take the larger value in the design, as shown in Eq. 2.10.

$$v_{u,318b} = \frac{V_o}{b_o d} \pm \left(\frac{\gamma_{vx} M_{ux} c_{BC}}{J_{cx}} \pm \frac{\gamma_{vy} M_{uy} c_{AB}}{J_{cy}} \right) \quad \text{Eq. 2.9}$$

$$v_{u,318u} = \text{Larger of} \begin{cases} \dfrac{V_o}{b_o d} \pm \left(\dfrac{\gamma_{vx} M_{ux} c_{BC}}{J_{cx}} \right) \\ \dfrac{V_o}{b_o d} \pm \left(\dfrac{\gamma_{vy} M_{uy} c_{AB}}{J_{cy}} \right) \end{cases} \qquad \text{Eq. 2.10}$$

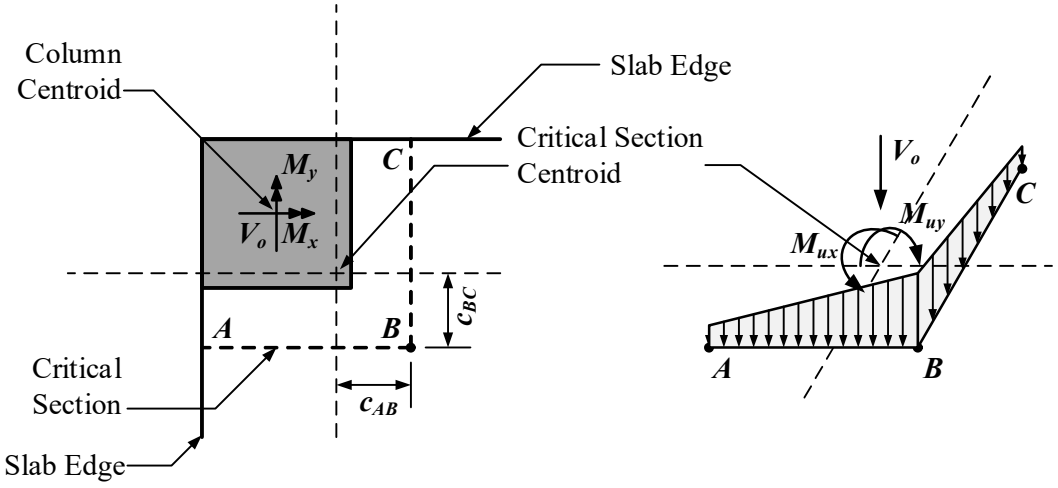

Fig. 2.50 – Punching Shear Stress Distribution due to Combined Gravity Load and Biaxial Unbalanced Moment

However, reports published by the Joint ACI-ASCE Committee 421 (2008, 2010) explicitly suggest that moment transferred in both principal directions should be considered simultaneously. As a result, shear demand should be evaluated using Eq. 2.11. Considering that peak stress at a single point on the critical section is not likely to govern the strength due to stress redistribution, the Joint ACI-ASCE Committee 421 (2008) recommends that the maximum stress to be considered in the design may be evaluated at a distance $0.4d$ from the peak point, but the reduction need not exceed 15%.

$$v_{u,421} = \frac{V_o}{b_o d} \pm \left(\frac{\gamma_{v1} M_1 c_2}{I_1} \pm \frac{\gamma_{v2} M_2 c_1}{I_2} \right) \qquad \text{Eq. 2.11}$$

Despite the similarity between Eq. 2.9 and Eq. 2.11, parameters used in the two equations are conceptually different. In Eq. 2.9, parameter J_{cx} or J_{cy} is difficult to handle for critical section with irregular geometries or with openings (Wight, 2016). On top of that, Ghali (1989) indicates that the use of Eq. 2.9 does not satisfy equilibrium. The aforementioned issues can be

resolved by replacing J_{cx} and J_{cy} with I_1 and I_2 as shown in Eq. 2.11. The subscripts 1 and 2 refer to the principal axes having a rotation angle, θ, from the axes coinciding with the column cross-section about the centroid of the critical section, as shown in Fig. 2.6. Both shear capacity and shear demand per Joint ACI-ASCE Committee 421 (2008, 2010) are evaluated with respect to the principal axes.

The inclined angle, θ, can be evaluated using Eq. 2.12, wherein two values satisfy from -180 to 180 degrees. Selection should be made for the angle which results in a larger I_1 of the critical section, i.e., $I_1 \geq I_2$. In Eq. 2.12, I_x, I_y, and I_{xy} can be determined for a critical section consisting of multiple straight sections by summing up the corresponding properties of each straight section. For example, as shown in Fig. 2.6, section AB represents one segment of the critical section. Coordinates of point A and Point B with respect to the x-y axes is (A_x, A_y), and (B_x, B_y), respectively. Using the coordinates, $(I_x)_{AB}$, $\left(I_y\right)_{AB}$, and $\left(I_{xy}\right)_{AB}$ representing I_x, I_y, and I_{xy} of this section AB can be determined using Eq. 2.13, where d is the slab effective depth, and l_{AB} is the length between A and B.

After θ is determined, I_1 and I_2 in Eq. 2.11 can be also determined by summing up the properties of each straight section as shown in Eq. 2.14. In which, the coordinates of point A, and B with respect to the principal axes, i.e. (A_1, $A2$), and (B_1, $B2$) shown in Fig. 2.6(b), respectively, can be obtained using Eq. 2.15.

$$tan\, 2\theta = \frac{-2I_{xy}}{I_x - I_y} \qquad \text{Eq. 2.12}$$

$$\begin{aligned} (I_x)_{AB} &= \frac{dl_{AB}}{3}\left(A_y^2 + B_y^2 + A_yB_y\right) \\ \left(I_y\right)_{AB} &= \frac{dl_{AB}}{3}\left(A_x^2 + B_x^2 + A_xB_x\right) \\ \left(I_{xy}\right)_{AB} &= \frac{dl_{AB}}{6}\left(2A_xA_y + 2B_xB_y + A_xB_y + A_yB_x\right) \end{aligned} \qquad \text{Eq. 2.13}$$

$$\begin{aligned} (I_1)_{AB} &= \frac{dl_{AB}}{3}\left(A_2^2 + B_2^2 + A_2B_2\right) \\ (I_2)_{AB} &= \frac{dl_{AB}}{3}\left(A_1^2 + B_1^2 + A_1B_1\right) \end{aligned} \qquad \text{Eq. 2.14}$$

$$A_1 = A_x \cos\theta + A_y \sin\theta$$
$$A_2 = -A_x \sin\theta + A_y \cos\theta \qquad \text{Eq. 2.15}$$

Elgabry and Ghali (1996) have also found that Eq. 2.6 leads to an infinite increase of punching shear demand at a certain point when critical section moves away from the column face, which is contrary to the real situation. Modifications of Eq. 2.6 have been proposed based on finite element analysis (Elgabry, 1991) and are presented in Eq. 2.16 and Eq. 2.17, in which l_1 and l_2 are illustrated in Fig. 2.7.

$$\gamma_{v1} = 0.40 \qquad \text{Eq. 2.16}$$

$$\gamma_{v2} = \begin{cases} 1 - \dfrac{1}{1 + \frac{2}{3}\sqrt{\frac{l_1}{l_2}} - 0.2}, & \text{if } \dfrac{l_1}{l_2} \geq 0.2 \\ 0, & \text{if } \dfrac{l_1}{l_2} \leq 0.2 \end{cases} \qquad \text{Eq. 2.17}$$

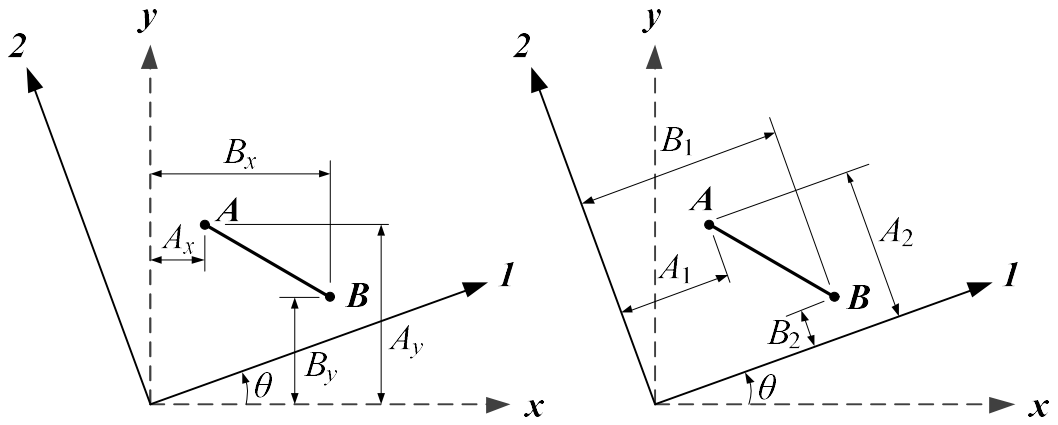

(a) With Respect to *x*-*y* Axes (b) With Respect to 1-2 Axes

Fig. 2.60 – Coordinates of Endpoints of Line AB

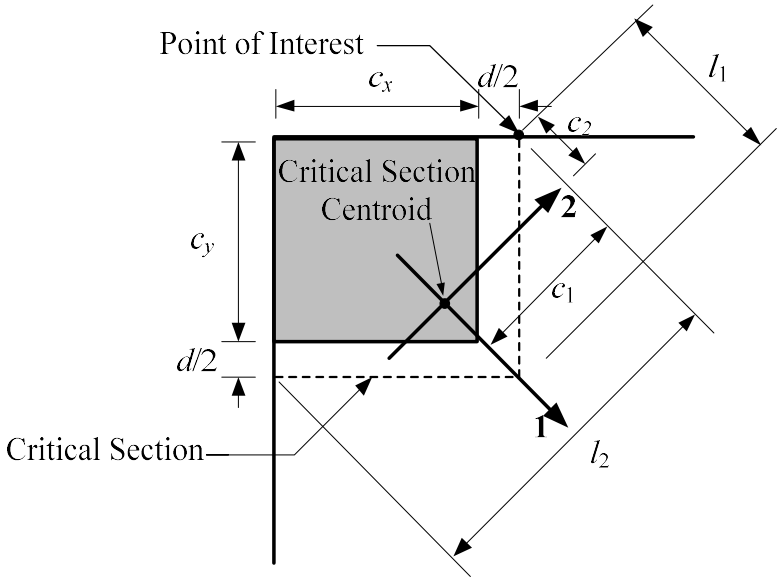

Fig. 2.7 – Illustration of Principal Axes per ACI Committee 421 (2008, 2010)

2.4 CONNECTION DISPLACEMENT CAPACITY

Slab-column connection is required to sustain its design gravity load while undergoing the expected lateral displacement. Based on test results of interior slab-column connections, Pan and Moehle (1989) have indicated that lateral drift capacity of a slab-column connection is highly dependent on the gravity shear ratio, defined as the gravity shear transferred at the connection divided by the connection shear capacity. Pan and Moehle (1989) have recommended that the gravity shear ratio should be limited to 0.4 in order to ensure a minimum drift capacity of 1.5%.

Later, a shear-drift interaction model for interior slab-column connections is proposed by Luo and Durrani (1995), as presented in Fig. 2.8. It is observed that the lateral drift capacity decreases as the gravity shear ratio increases.

Few years later, Hueste and Wight (1999) have proposed a trilinear interaction diagram between drift capacity and gravity shear ratio, as shown in Fig. 2.9. In the model, the contribution of unbalanced moments to the total punching shear stress is considered insignificant for drift ratios ranging from 0% to 0.5%, as represented by the first line segment. It is followed by a linear decrease of gravity shear ratio from 1.0 down to 0.4 as the drift increases from 0.5% to 1.5%. The limiting gravity shear ratio recommended by Pan and Moehle

(1989) appears to be incorporated in the model. The third line segment defines a slower decrease in allowable gravity shear ratio as the drift ratio increases from 1.5% to 4.0%.

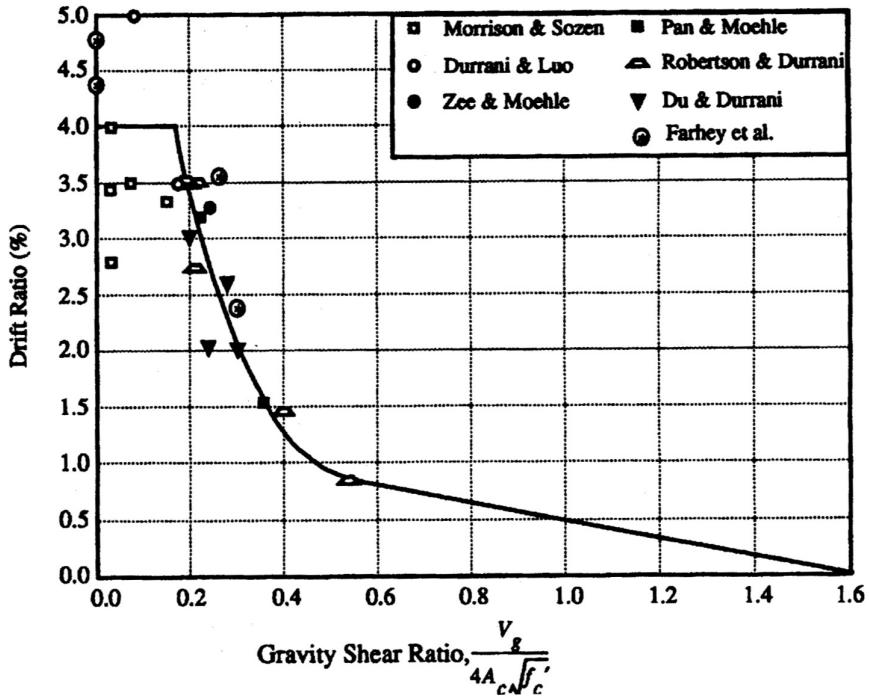

Fig. 2.8 – Shear -Drift Model by Luo and Durrani (1995)

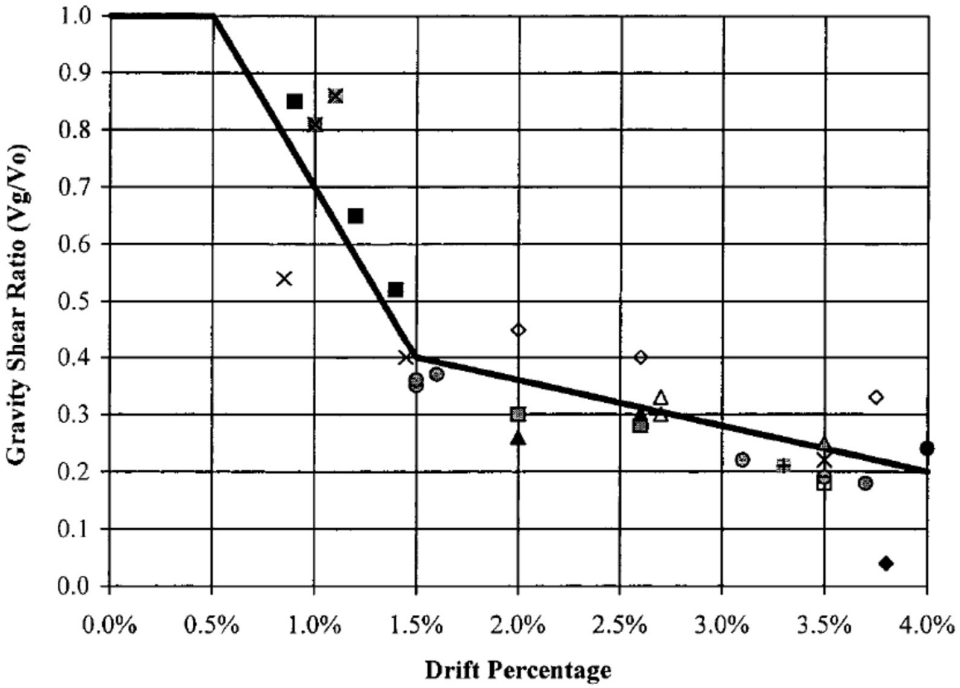

Fig. 2.9 – Shear-Drift Model by Hueste and Wight (1999)

The ACI 2005 Building Code (ACI Committee 318, 2005) has adopted a simpler bilinear interaction diagram between the gravity shear and drift ratios for slab-column connections, as shown in Fig. 1.3. Shear reinforcement is not needed for connections with design values below the bilinear curve; otherwise, minimum shear reinforcement with shear strength of at least $3.5\sqrt{f_c'(\text{psi})}\, b_o d$ shall be provided. This model has remained unchanged until the current ACI Building Code (ACI Committee 318, 2014).

The Joint ACI-ASCE Committee 421 (2010), though has adopted the bilinear interaction diagram embodied in the ACI Building Code, has added a more stringent requirement for shear reinforcement, as presented in Fig. 2.10. Shear reinforcement is not needed for slab-column connections within Zone 1 only. Minimum shear reinforcement should be provided for slab-column connections that fall within Zone 2. However, sufficient shear reinforcement should be provided for slab-column connections that are within Zone 3. For slab-column connections within Zone 4, with relatively high drift ratio, sufficient slab reinforcement should also be provided. It should be noted that the gravity shear V_{gs} presented in Fig. 2.10 considers all cases of load combinations including seismic effects as opposed to the V_{ug} ($v_{ug} b_o d$) in the ACI Building Code (ACI Committee 318, 2014).

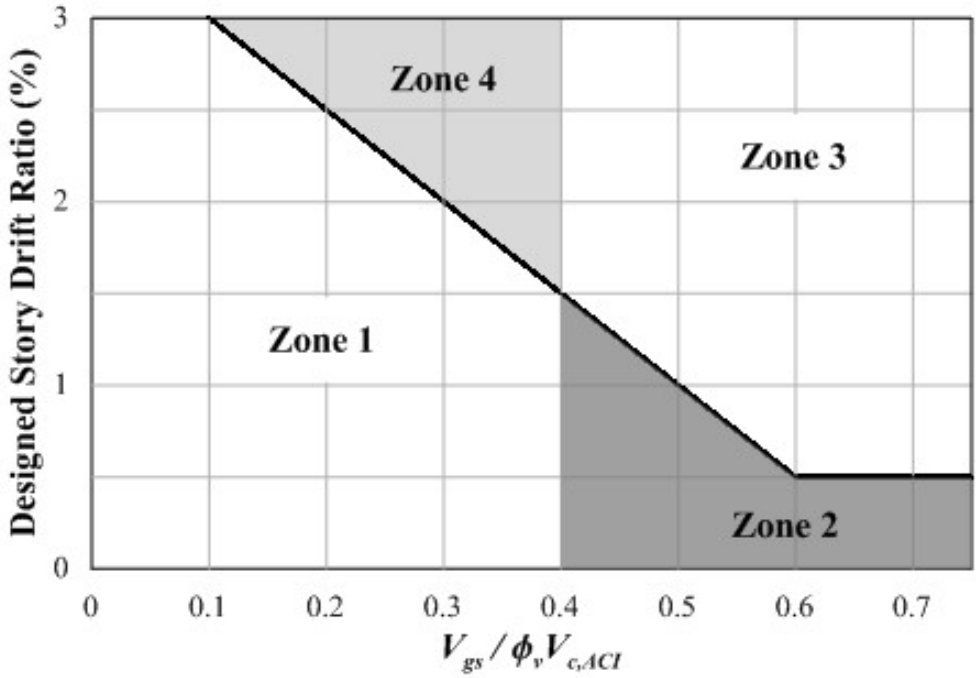

Fig. 2.10 – Shear-Drift Interaction Diagram per Joint ACI-ASCE Committee 421 (2010)

2.5 OTHER PUNCHING SHEAR STRENGTH MODELS

Two shear strength models for punching shear strength of corner slab-column connections are briefly reviewed in this section, namely the Eurocode 2 (European Committee for Standardization, 2004), here in after referred to as EC2, and the fib Model Code 2010 (International Federation for Structural Concrete, 2013).

2.5.1 Eurocode 2 (2004)

2.5.1.1 Control Perimeter

The definitions of critical sections where shear strength is evaluated according to the model adopted by EC2 are presented in Fig. 2.11. The basic control perimeter $b_{o,EC2}$ is the minimum perimeter located at a distance $2d$ from the face of the column, as shown in Figs. 2.11 and 2.12, where d is the average of the slab effective depths in the two orthogonal directions.

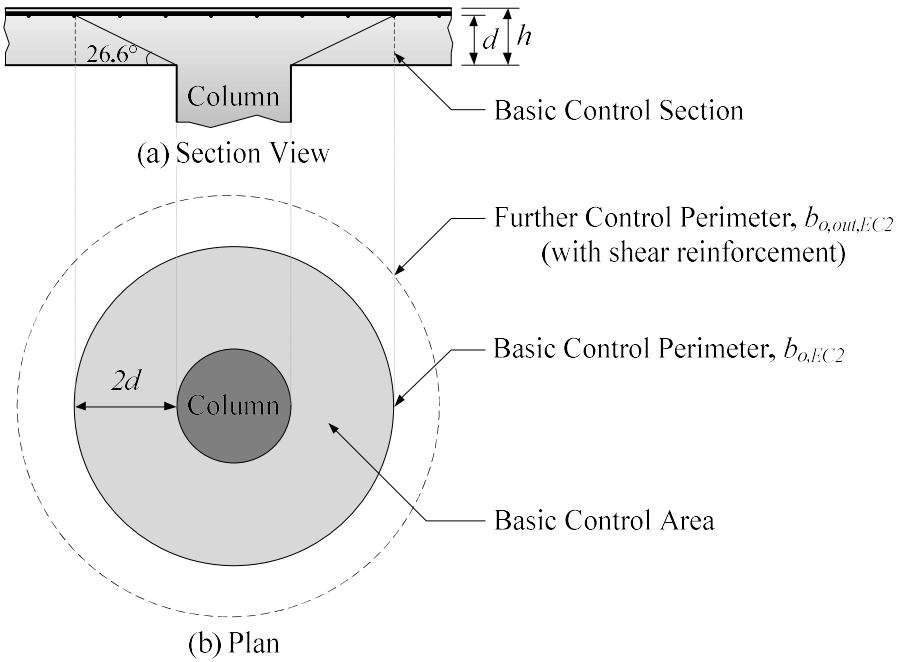

Fig. 2.11 – Critical Sections for Punching Shear per EC2 (2004)

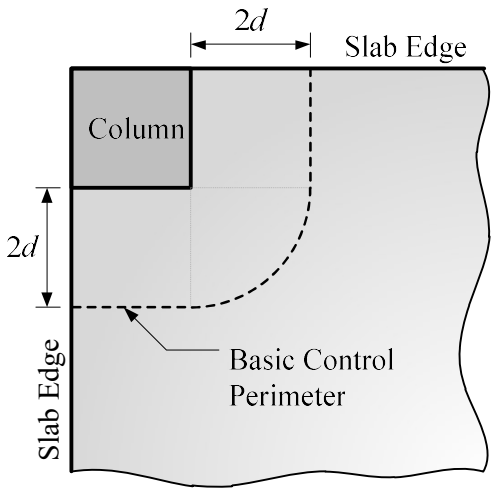

Fig. 2.12 – Corner Connection Basic Control Perimeter per EC2 (2004)

2.5.1.2 Design Shear Force (Demand)

Connection shear should be evaluated at the column perimeter and at the basic control perimeter $b_{o,EC2}$, as shown in Figs. 2.11 and 2.12. Focus is given to the shear at the basic control perimeter in this study. In this case, the connection shear demand $v_{u,EC2}$ is evaluated using Eq. 2.18, where v_{ED} is determined by dividing the factored gravity shear on the control perimeter by the critical section area, $b_{o,EC2}d$, where d is the average slab effective depth. Coefficient β that accounts for shear amplified by the unbalanced moment is determined as described in the following sections.

$$v_{u,EC2} = \beta v_{ED} \qquad \text{Eq. 2.18}$$

For corner slab-column connections, β is determined using Eq. 2.19 if the load eccentricity is toward the exterior. In Eq. 2.19, M_{ED} is the transfer moment at the critical section, coefficient k related to the support rectangularity is shown in Table 2.3. And, c_x is the dimension of the rectangular column parallel to the design direction; and c_y is the dimension of the rectangular column perpendicular to c_1. The parameter W_1 corresponds to the shear distribution along the basic control perimeter and can be determined as the first moment of critical section area with respect to the centroid of the critical section. An example to illustrate the determination of W_1 for a corner slab-column connection is provided in Appendix A. Please note, Eq. 2.19 applies to bending from one direction only. If biaxial bending is considered, based on the suggestion from German Annex (EN 1992-1-1/NA, 2013), β can be evaluated using Eq. 2.20 that is

typically adopted by most commercial software DECON EXPERT Studrails(DECON EXPERT Studrails 4.2.0.23, 2017) and Peikko Designer (Peikko Designer Ex. 1.0.2.75, 2017) in practice.

$$\beta = 1 + k\frac{M_{ED}}{v_{ED}d}\frac{1}{W_1} \qquad \text{Eq. 2.19}$$

$$\beta = 1 + \sqrt{\left(k_x\frac{M_{ED,x}}{v_{ED}d}\frac{1}{W_{1,x}}\right)^2 + \left(k_y\frac{M_{ED,y}}{v_{ED}d}\frac{1}{W_{1,y}}\right)^2} \qquad \text{Eq. 2.20}$$

Table 2.3 – Values of *k* for rectangular columns per EC2

c_x/c_y	≤ 0.5	1.0	2.0	≥ 3.0
k	0.45	0.60	0.70	0.80

For a corner slab-column connection with load eccentricity toward the interior, punching shear stress is assumed to be uniformly distributed along the reduced control perimeter $b_{o,EC2,red}$. The definition of $b_{o,EC2,red}$ is shown in Fig. 2.13. The coefficient β can be obtained using Eq. 2.21.

$$\beta = \frac{b_{o,EC2}}{b_{o,EC2,red}} \qquad \text{Eq. 2.21}$$

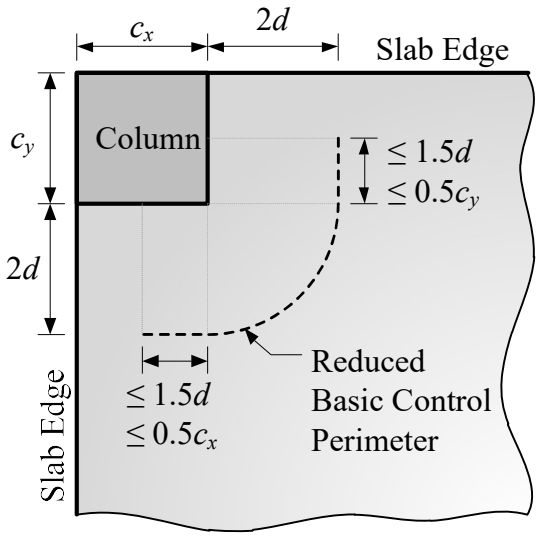

Fig. 2.13 – Reduced Basic Control Perimeter per EC2 (2004)

2.5.2.3 Punching Shear Strength (Capacity)

The punching shear resistance of the slab-column connection is evaluated at the basic control section (Figs. 2.11 and 2.12). The connection punching shear resistance without shear reinforcement, $v_{c,EC2}$, is determined using Eq. 2.22. Instead of using characteristic concrete strength originally specified in the code, this study uses f_c' in Eq. 2.22 for comparison purpose.

$$v_{c,EC2} = \frac{5}{\gamma_c} k_s \left(100 \rho_{l,EC2} f_c'\right)^{1/3} \geq 0.422 k_s^{3/2} \sqrt{f_c'}, \text{ psi} \qquad \text{Eq. 2.22}$$

where:

γ_c = partial safety factor for concrete material properties, taken as 1.5 for transient and persistent situations and 1.2 for incidental situations. In this study, γ_c is taken as 1.0 for the evaluated specimens.

$$k_s = 1 + \sqrt{\frac{7.9}{d(\text{in.})}} \leq 2.0$$

d = average slab effective depth in inch.

$$\rho_{l,EC2} = \sqrt{\rho_{tx,EC2} \cdot \rho_{ty,EC2}} \leq 0.02$$

$\rho_{tx,EC2}, \rho_{ty,EC2}$= slab reinforcement ratios in the x- and y-directions, respectively, considering a slab effective width equal to the column width plus $3d$ each side.

f_c' = concrete strength (psi)

2.5.2 FIB Model Code 2010

2.5.2.1 Control Perimeter

The FIB Model Code 2010 uses 2 different control perimeters in the design of punching shear of slab-column connections. First is the basic control perimeter, $b_{1,MC}$, for the evaluation of shear demand. The definition of $b_{1,MC}$ is presented in Fig. 2.14. To evaluate punching shear capacity, the shear-resisting control perimeter $b_{o,MC}$ is introduced and it will be explained further in the following.

Due to two-way action, shear stress is concentrated at the corner of the support. To consider this effect, a reduced basic control perimeter $b_{o,MC10} = b_{1,MC,red}$ is used, as shown in Fig. 2.15, in which the length of its straight segments does not exceed $3d$ on each side. In addition, to account for the moment transfer between the slab and the column, the shear-resisting control perimeter $b_{o,MC}$ is taken as $k_e b_{1,MC,red}$, where k_e is the coefficient of eccentricity. The

parameter k_e is $1/(1+e_u/b_u)$, where $e_u = \sqrt{e_{ux}^2 + e_{uy}^2}$ can be determined per Fig. 2.16 assuming that the simplified basic control perimeter is composed of straight line segments at $d/2$ distance away from the column face; and b_u is the diameter of a circle with the same surface area as the region inside the basic control perimeter.

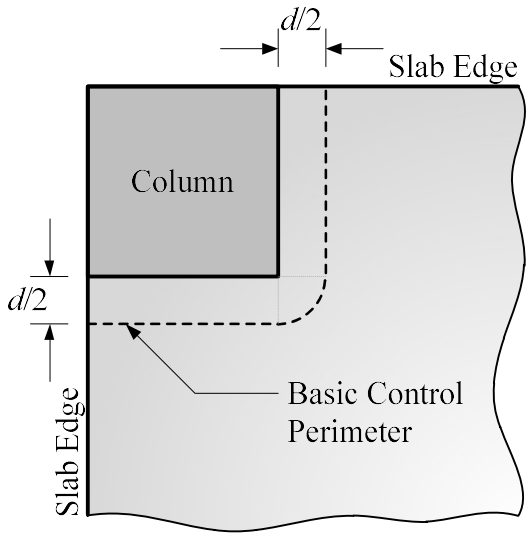

Fig. 2.14 – Basic Control Perimeter for Punching Shear per fib Model Code (2010)

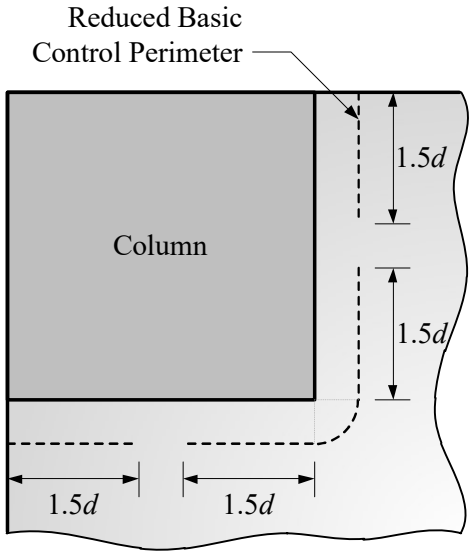

Fig. 2.15 – Reduced Basic Control Perimeter for Large Supported Areas

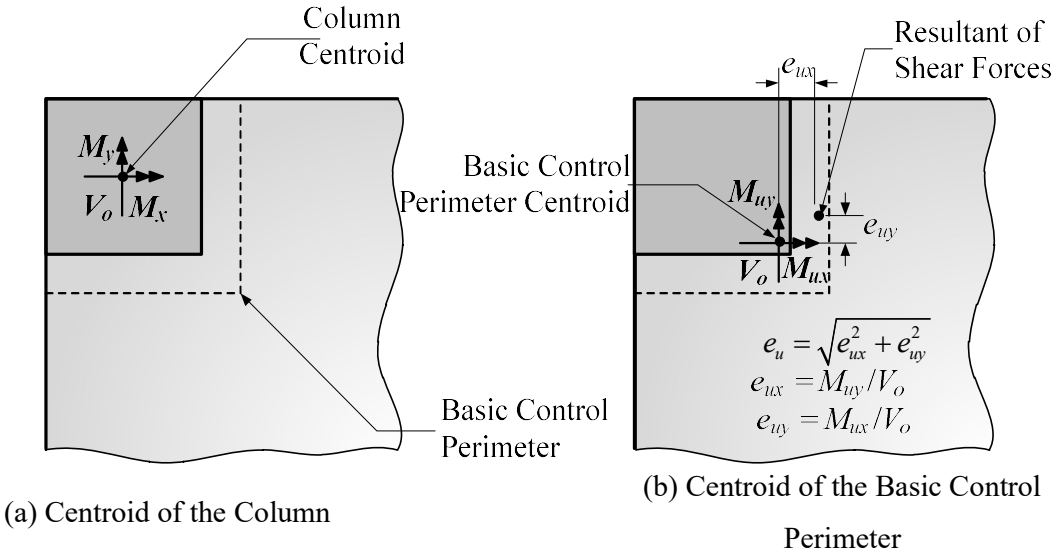

Fig. 2.16 – Resultant of Shear Forces Location per fib Model Code (2010)

2.5.2.2 Design Shear (Demand)

The shear stress demand, $v_{u,MC}$, is evaluated per Eq. 2.23. In which, V_o is the support reaction force; q_u is the design load on the slab; A_{cp} is the area within the basic control perimeter; and d is the average slab effective depth from the two directions.

$$v_{u,MC} = \frac{V_o - q_u A_{cp}}{b_{o,MC} d} \qquad \text{Eq. 2.23}$$

2.5.2.3 Punching Shear Strength (Capacity)

The concrete punching shear capacity $v_{c,MC}$ of the connection is evaluated using Eq. 2.24. In which, $f_c^{'}$ is the concrete strength; $b_{o,MC}$ is the shear-resisting control perimeter as presented above; and d is the slab effective depth. The parameter γ_c is the partial safety factor for concrete material properties, taken as 1.5 for transient and persistent situations and 1.2 for incidental situations. Similarly, γ_c is taken as 1.0 for the evaluated specimens in this study.

$$v_{c,MC} = k_\psi \frac{\sqrt{f_c^{'}}}{\gamma_c}, \text{MPa} \qquad \text{Eq. 2.24}$$

The coefficient k_ψ in Eq. 2.24 is calculated using Eq. 2.25. The parameter k_{dg} is evaluated as $32/\left(16 + d_g(\text{mm})\right)$ but may be taken as 1.0 if the maximum aggregate size (d_g) is not less than 16 mm. The parameter ψ is the rotation of the slab around the supported area. For a typical design (Level II approximation), ψ can be determined using Eq. 2.26.

$$k_\psi = \frac{1}{1.5 + 0.9k_{dg}\psi d(\text{mm})} \leq 0.60 \qquad \text{Eq. 2.25}$$

$$\psi = 1.5\frac{r_s}{d}\frac{f_y}{E_s}\left(\frac{m_u}{m_n}\right)^{1.5} \qquad \text{Eq. 2.26}$$

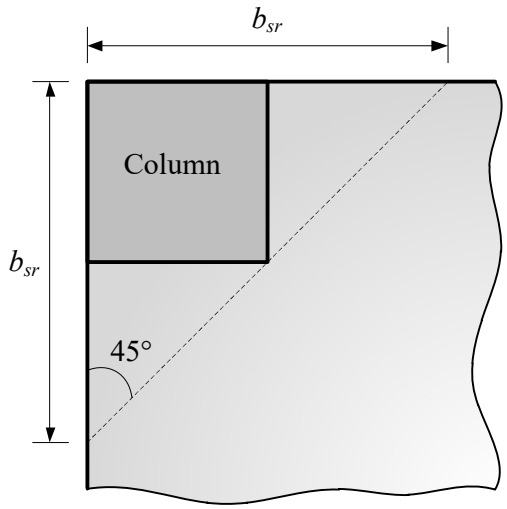

Fig. 2.17 – Support Strip Dimensions

For regular flat slabs, where the ratio of the spans (L_x/L_y) is between 0.5 and 2.0, the r_s in Eq. 2.24 denotes the position where the radial bending moment is zero with respect to the support axis and is assumed to be $0.22L_x$ or $0.22L_y$ for x- and y-directions, respectively. The parameters f_y and E_s are the yield stress and modulus of elasticity, respectively, of slab flexural reinforcement. The design moment and nominal flexural strength per unit length represented as m_u and m_n, respectively, of the slab is evaluated within the support strip b_s of the considered direction of moment transfer, where $b_s = 1.5\sqrt{r_{s,x}r_{s,y}} \leq b_{sr}$ and the definition of b_{sr} is presented in Fig. 2.17. The design moment m_u of corner connection in each direction is evaluated using Eq. 2.27, where V_o is the vertical load measured from the support center, $e_{u,i}$

is either e_{ux} or e_{uy} depending on the direction being investigated. In the end, ψ per Eq. 2.26 shall be evaluated in each direction and taken the larger value to evaluate k_{ψ} in Eq. 2.25.

$$m_u = V_o\left(\frac{1}{8} + \frac{|e_{u,i}|}{b_s}\right) \geq \frac{V_o}{2} \qquad \text{Eq. 2.27}$$

2.6 CORNER SLAB-COLUMN CONNECTION TESTS

Research works on slab-column connections subjected to combined gravity and earthquake-type loadings have been extensively started in the early 1970s. However, only a few were conducted for corner slab-column specimens.

Behaviors of corner slab-column connections under combined gravity load and unbalanced moment were experimentally evaluated using different setups. Most of these tests (Zaghlool, 1971; Zaghlool and de Paiva, 1973; van den Beukel, 1976; Hammill and Ghali, 1994; and Widjaja, 2008) were conducted using isolated corner slab-column sub-assemblage, others (Zaghlool et el., 1970; Walker and Regan, 1987; and Desayi and Seshadri, 1997) were using single-panel flat plate specimens, and a few (Gardner and Shao, 1996; Hwang and Moehle, 1990, 2000; Sudarsana, 2001; and Rha et al., 2014) were utilizing multiple-panel specimens.

To be aligned with the current ACI 318-14, connection shear capacity is evaluated based on test results of specimens primarily subjected to monotonically increasing gravity-type loading while connection deformation capacity is evaluated based on test results of specimens subjected to combined gravity-type loading and lateral displacement reversals. Unfortunately, test results of specimens subjected to combined gravity-type loading and lateral displacement reversals are not completely reported in the literature; i.e., lateral displacement data are not available. As a result, only research works on corner slab-column connections primarily subjected to monotonically increasing gravity-type loading are reviewed in this section.

2.6.1 Zaghlool, de Paiva and Glockner (1970)

Four single-panel reinforced concrete flat plate specimens, each supported by four square columns at the corners, as shown in Fig. 2.18, were tested by Zaghlool et al. (1970). The design parameters used in this study were the column width-to-slab thickness ratio and the concrete strength. The gravity load was applied at 16 points through 15-in. square steel plates resting on

rubber pads on the slab top surface, as shown in Fig. 2.18. Tripod devices were used to monitor the reaction forces at the column supports throughout the test. According to the report, flat plates I, II and IV failed in shear with relatively limited inelastic behavior observed. Flat plate II failed due to the initial failure of one of its reaction supports.

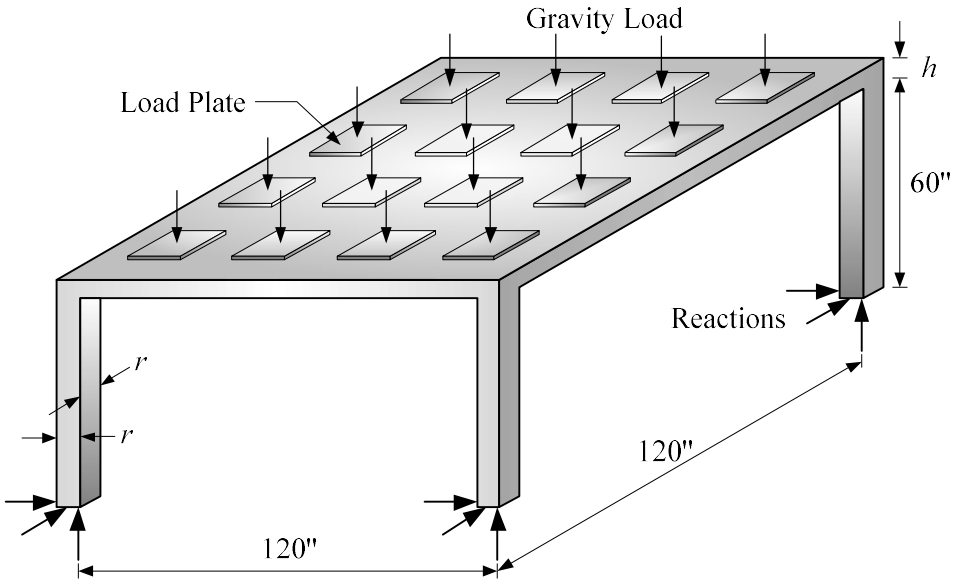

Fig. 2.18 – Single Panel Flat Plate Specimen Tested by Zaghlool et al. (1970)

The proposed model by Moe (1961) for interior connections was evaluated using the test results. The results showed that Moe's model was very conservative when applied to the corner connections. A value of 0.04 for the fraction of moment to be transferred by shear was found to provide a more reasonable prediction of strength instead of using 1/3, as recommended by Moe (1961). The proposed value of 0.04 for the fraction of moment to be transferred by shear was further evaluated in terms of linear interaction diagram between shear and moment (Hanson and Hanson, 1968) and showed good agreement with the test results. A simplified model in evaluating the punching shear strength of corner connections was proposed as expressed in Eq. 2.28. The parameters d and c_x or c_y refer to the slab effective depth and side dimension of a square column, respectively.

$$v_c = \left[5.6+2.0\left(\frac{d}{c_x}\right)\right]\sqrt{f'_c}, \text{ psi} \qquad \text{Eq. 2.28}$$

2.6.2 Walker and Regan (1987)

Eleven single panel flat plate specimens were tested by Walker and Regan (1987). The first 7 specimens were tested using the experimental setup shown in Fig. 2.19. The rest of the specimens were relatively smaller in size and had no upper columns to simulate roof slab. The test arrangement at the bottom was essentially similar with that shown in Fig. 2.19. The top reinforcement of one of the specimens was placed diagonally for some specimens, 45 degrees with the slab edges.

The bottom end of the columns was supported by spherical bearings, allowing freedom of rotation. Three of the columns were allowed to freely translate while the bearing support of the other one was fixed to the laboratory floor. Bottom columns were interconnected with pin-ended steel ties with strain gauges attached to the rod to monitor the tie forces. For specimens with upper columns, struts with rotating bearings and load cells were employed to brace apart the top ends and acting as ties. Gravity loads were applied through several points on the slab surface using strands and a jacking system.

According to the report, the ultimate failure mode of all specimens was punching, though some had attained their flexural capacities given by yield line theory especially those with lesser amount of flexural reinforcement within the effective width. Based on the test results, column dimensions were shown to have a great impact on the stiffness of the slab-column connections, and consequently, the moment transfer mechanism. The stiffness of the connections was also affected by the amount and detailing of the reinforcement. Specimen using diagonal top reinforcement produced a much greater connection stiffness compared to its equivalent specimen with a conventional, orthogonally-oriented, top reinforcement layout. The predicted design shear stresses per ACI 318-83 (ACI Committee 318, 1983), considering that unbalanced moments from the two directions are transferred simultaneous were conservative, except for the specimen with a relatively large column side length-to-slab effective depth ratio.

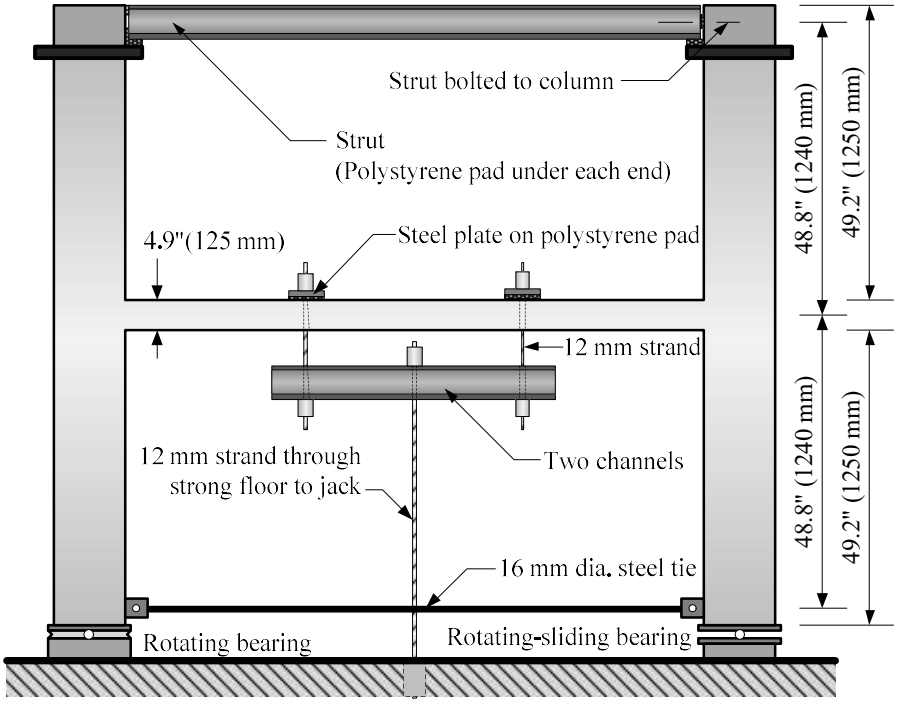

(a) Elevation

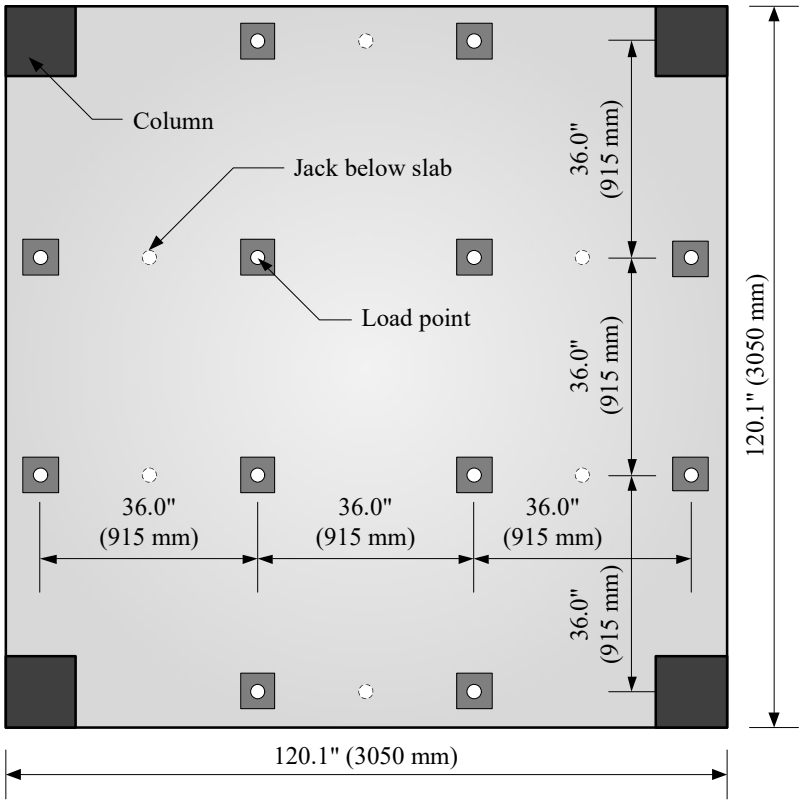

(b) Plan

Fig. 2.19 – Test Setup Adopted by Walker and Regan (1987)

2.6.3 Desayi and Seshadri (1997)

Six single panel flat plate specimens were investigated by Desayi and Seshadri (1997) under gravity-type loading until failure. The gravity load was applied at 16 discrete points on the slab and distributed as shown in Fig. 2.20. The specimens were constructed with three different slab flexural reinforcement ratios and two different moment-to-shear ratios. The base of the columns was supported by ball bearings, three of which were free to both rotate and translate while the other one was only permitted to rotate and translation was restrained.

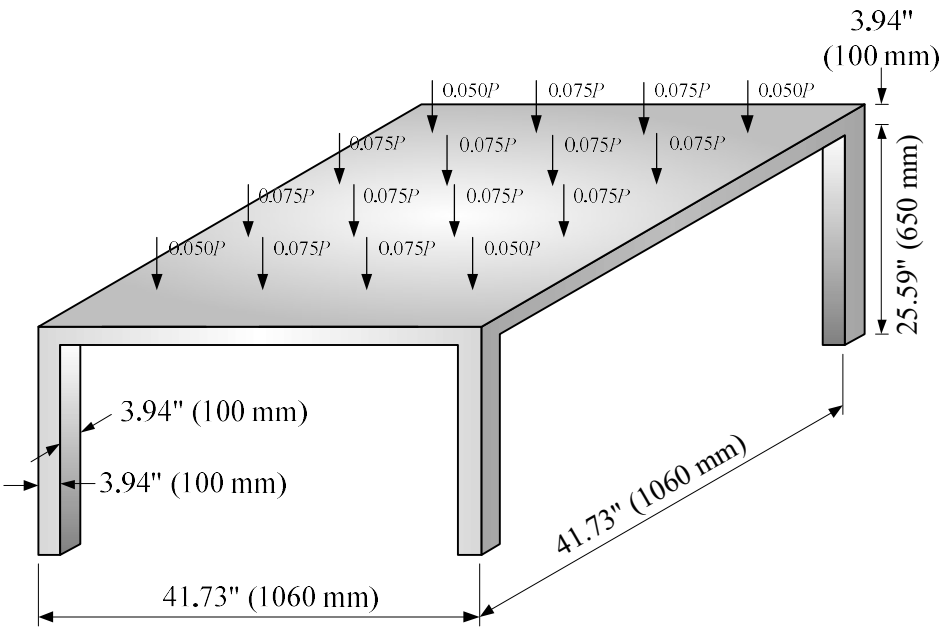

Fig. 2.20 – Single Panel Flat Plate Specimen Tested by Desayi and Seshadri (1997)

All of the specimens were reported to fail in punching with failure surfaces inclining at an angle of about 30 degrees with the horizontal. Deflections in the slabs were observed to decrease as the flexural reinforcement ratio was increased. Specimens with smaller moment-to-shear ratio had relatively lower ultimate slab deflections. A model to predict punching shear capacity of the corner slab-column connection was proposed by the authors. Details can be found elsewhere (Desayi and Seshadri, 1997).

CHAPTER 3
EXPERIMENTAL PROGRAM

3.1 INTRODUCTION

Experimental studies on the behavior of flat-plate framing system have been extensively conducted before. However, there is no clear evidence indicating that a particular experimental setup provides apparent advantages over the other. As a result, different experimental setups have been adopted by different research groups. Some researchers (Desayi and Seshadri, 1997; Rha et al., 2014; and Einpaul et al., 2015) believe that a continuous flat plate specimen is suitable to monitor the actual load redistribution throughout the duration of the test. However, isolated slab-column sub-assemblage is deemed satisfactory enough to capture the behavior of the slab-column connection under certain loading condition (Broms, 2007), provided that proper boundary conditions are carefully considered. Experimental program is usually designed based on two major factors, namely, project cost and capability of the available test facilities. In this study, the isolated slab-column sub-assemblage type of specimen is adopted. This chapter provides a detailed discussion about the experimental program implemented in this study.

3.2 PROTOTYPE FLOOR SYSTEM

The prototype floor system used in this study had a square floor plan, which was composed of 5 equivalent bays in each direction with center-to-center distance of 17.25 ft, as shown in Fig. 3.1(a). This bay distance was chosen such that the support of the test specimen would coincide with the hole pattern on the strong floor of the structural laboratory. A uniform slab thickness of 8 in. was used and it was supported by 16 in. square columns. No drop panels or column capitals were used. The slab edges were flushed to the exterior faces of the perimeter columns. Spandrel beams were not provided.

The designed forces were evaluated using ADAPT-Builder (ADAPT-Builder Ex. 3.20.1, 2008), a commercially available analysis and design software package, specifically for flat plate structures. A one-story structural model was isolated from the prototype structure for analysis. In the model, the ends of the columns above and below the slab represented the mid-height of the prototype structure as shown in Fig. 3.1(b). Boundary conditions at the column ends were set to be pinned connections, simulating the point of contra flexure at the column mid-heights during seismic event even if no lateral load was applied to the model.

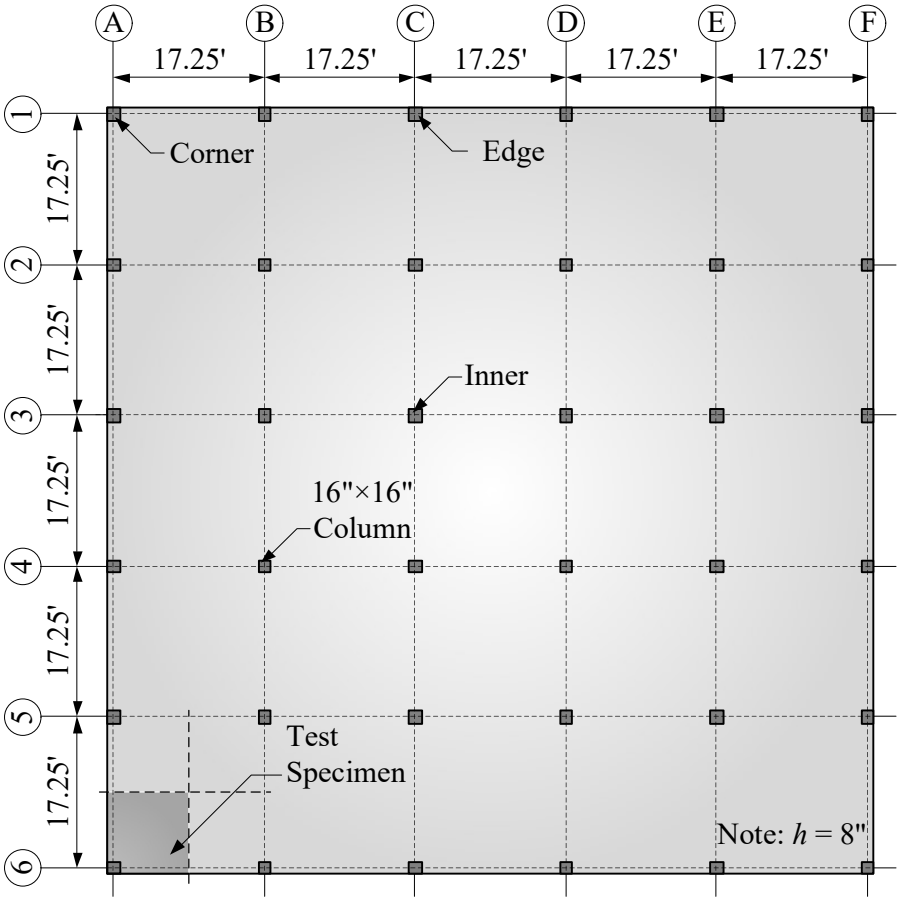

(a) Plan

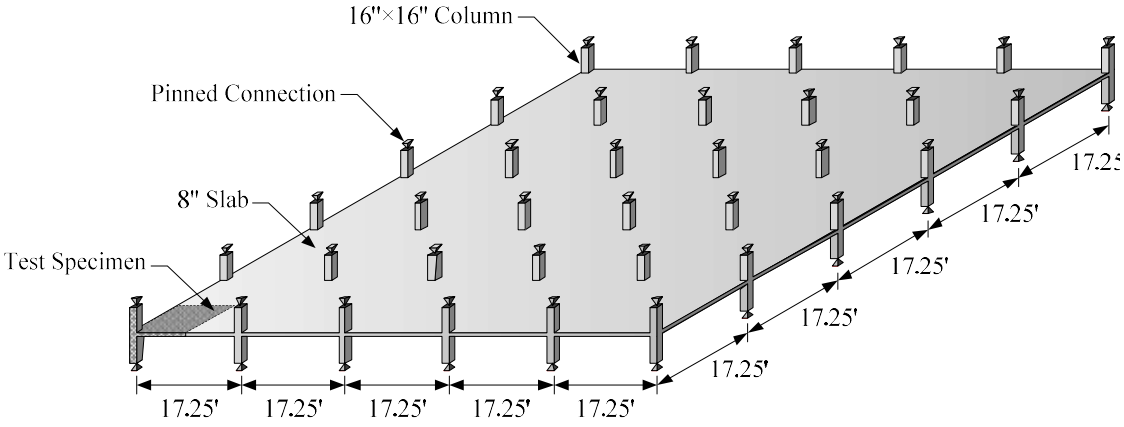

(b) Elevation

Fig. 3.1 – Prototype Floor System

A uniform gravity load was applied on the entire floor area and its magnitude was adjusted to impose a punching shear demand at the corner slab-column connection (Fig. 3.1) equivalent to a 0.45 gravity shear ratio, defined as the shear demand divided by the shear capacity per ACI

318-14 (ACI Committee 318, 2014) using a specified concrete strength of 5000 psi. Under this uniformly distributed gravity load, a gravity shear of 32.57 kips and unbalanced moment of 47.88 kip-ft in both directions were then obtained at the corner slab-column connections.

3.2 SPECIMEN DESIGN

This experimental program focused on the behavior of corner slab-column connection under combined gravity-type loading and lateral displacement reversals. An approximately full-scaled corner slab-column sub-assemblage was designed as experimental specimen of this study.

The test specimen was composed of a column stub and slab as shown in Fig. 3.2. The column stub, with a 16 in. square cross section, was 134 in. high. The 8 in. thick slab had a total edge dimension of 119.5 in. in two orthogonal directions, allowing 8 in. extension from the centerline of the slab panel described in the prototype slab system. This was to accommodate attachments to simulate boundary conditions of the pseudo-continuous edges of the slab panel. The slab edges were flushed to the outside faces of the column. The east and south sides of the slab were provided with holes for boundary condition attachments and for SW, SE and NE corner steel arm supports. Additional 3 holes with 1 in. diameter were laid near the slab-column connection at gridline intersections C-3, C-4, and B-3 for gravity load applications. The column was extended 60 in. from the top slab face. Four threaded rods were anchored at the top end of the column to fasten a steel support on which the hydraulic actuator was attached. Underneath the slab, the column was extended 66 in. downward. The six specimens in this study were geometrically similar with detailed dimensions shown in Fig. 3.2. Based on the slab reinforcement ratio, however, the six specimens were divided into two main groups, namely, the G-Series and the R-Series.

Test parameters for each specimen are summarized in Table 3.1. Connection gravity shear levels in each series are expressed in terms of $\sqrt{f_c'}b_o d$.

Table 3.1– Specimen Target Gravity Shear Level

Series	Specimen	Target Connection Gravity Shear
G-Series	G1	$1.20\sqrt{f_c'(\text{psi})}b_o d \left[0.10\sqrt{f_c'(\text{MPa})}b_o d\right]$
	G2	$2.00\sqrt{f_c'(\text{psi})}b_o d \left[0.17\sqrt{f_c'(\text{MPa})}b_o d\right]$
	G3	$1.60\sqrt{f_c'(\text{psi})}b_o d \left[0.13\sqrt{f_c'(\text{MPa})}b_o d\right]$
R-Series	R1	$1.20\sqrt{f_c'(\text{psi})}b_o d \left[0.10\sqrt{f_c'(\text{MPa})}b_o d\right]$
	R2	$2.00\sqrt{f_c'(\text{psi})}b_o d \left[0.17\sqrt{f_c'(\text{MPa})}b_o d\right]$
	R3	$1.60\sqrt{f_c'(\text{psi})}b_o d \left[0.13\sqrt{f_c'(\text{MPa})}b_o d\right]$

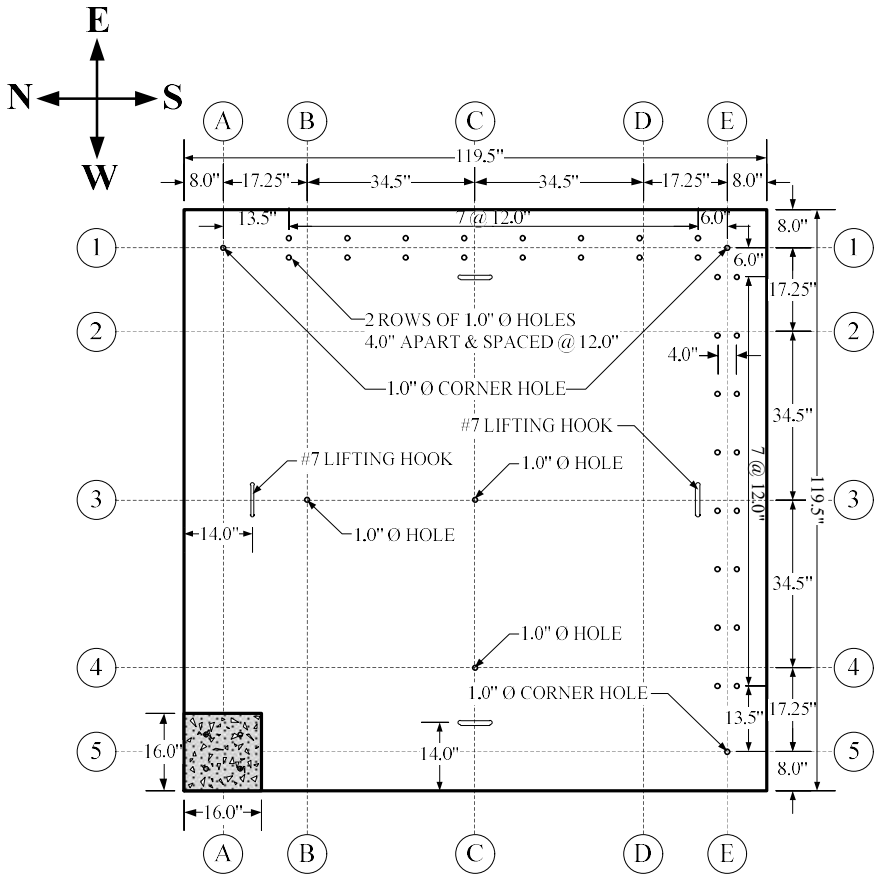

(a) Plan View

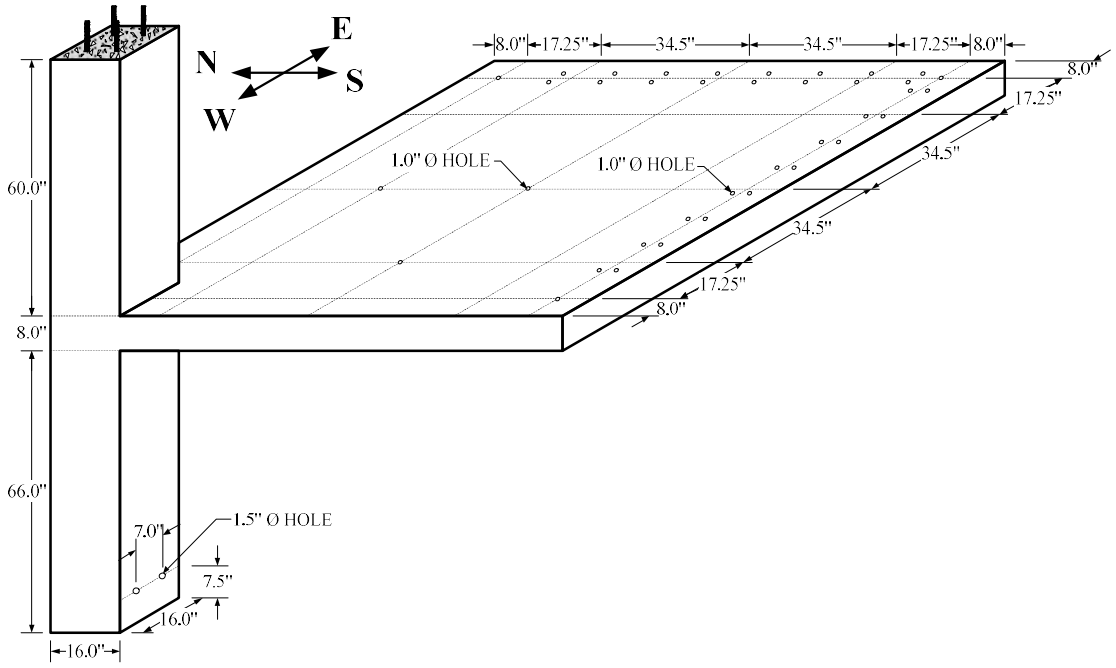

(b) Perspective View

Fig. 3.2 – Corner Slab-Column Connection Specimen

3.2.1 Slab

3.2.1.1 G-Series

The G-Series specimens were designed based on the analytical results from the prototype structural model. Direct design method specified in the ACI 318-14 (ACI Committee 318, 2014) was used in the design of the slab reinforcement. A specified concrete strength of 5000 psi and Grade 60 steel were used in the design. Four No. 5 top bars, spaced at 8 in. were provided within the effective slab width of 28 in. measured from the slab edge as depicted in the reinforcement layout shown in Fig. 3.3. Two bottom bars were provided within the column cage to satisfy integrity provision of the code. These resulted to top and bottom slab reinforcement ratios of 0.66% and 0.33%, respectively. Flexural reinforcement for the rest of the slab, outside the effective width, was governed by temperature and shrinkage requirement using No. 5 bars at 18 in. spacing on centers. The same reinforcement layout was applied to the two orthogonal directions. However, the top and bottom slab reinforcement parallel to the loading direction was placed on the outermost layer.

3.2.1.2 R-Series

The top and bottom reinforcement ratios of the R-Series specimens within the effective slab width were 1.5 times larger than those of the G-Series specimens. As a result, the R-Series specimens were reinforced with 6 No. 5 top bars that were spaced at 4.5 in., and 3 No. 5 bottom bars with 8 in. spacing as shown in Fig. 3.4. The equivalent top and bottom reinforcement ratios within the effective slab width were 0.99% and 0.50%, respectively. Three bottom bars were provided within the column cage. The rest of the slab was reinforced with No. 5 bars that were spaced at 18 in. on centers. Reinforcement layout was the same in the two orthogonal directions. Consistently, the top and bottom slab reinforcement parallel to the loading direction was placed on the outermost layer.

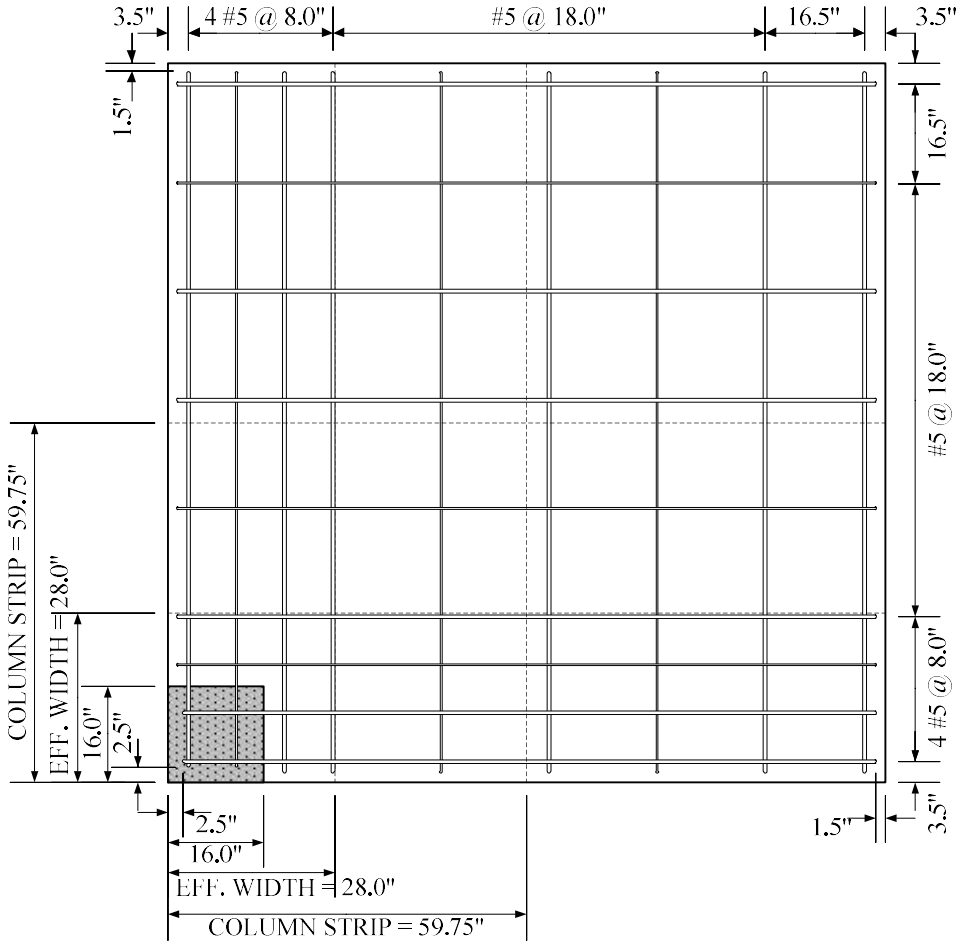

(a) Top Reinforcement

Fig. 3.3 – Slab Reinforcement Layout for G-Series Specimens

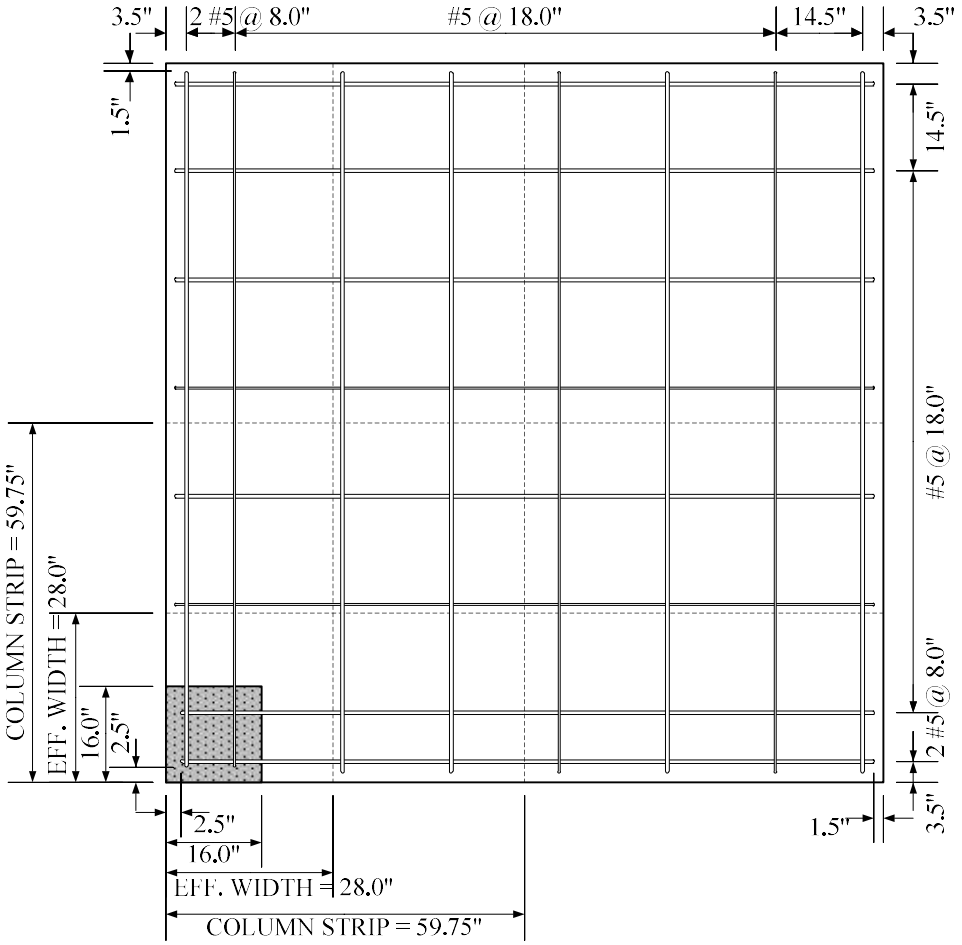

(b) Bottom Reinforcement

Fig. 3.3 – Slab Reinforcement Layout for G-Series Specimens (cont.)

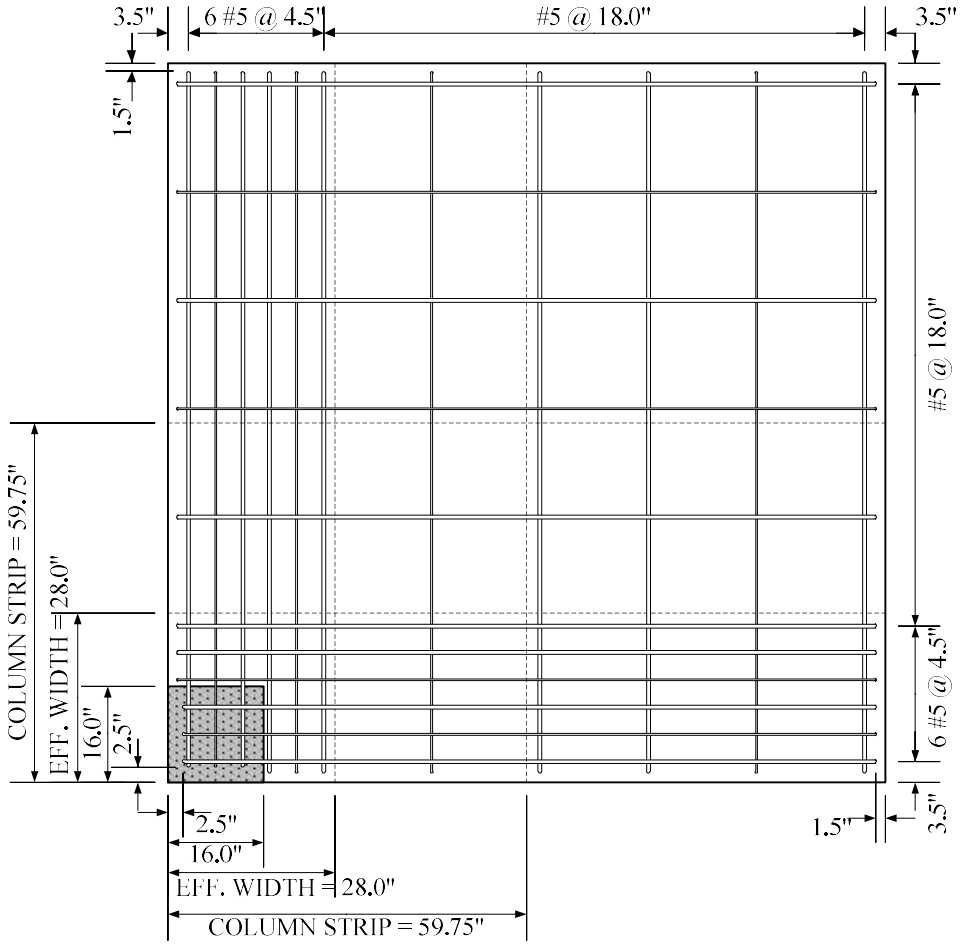

(a) Top Reinforcement

Fig. 3.4 – Reinforcement Layout for R-Series Specimens

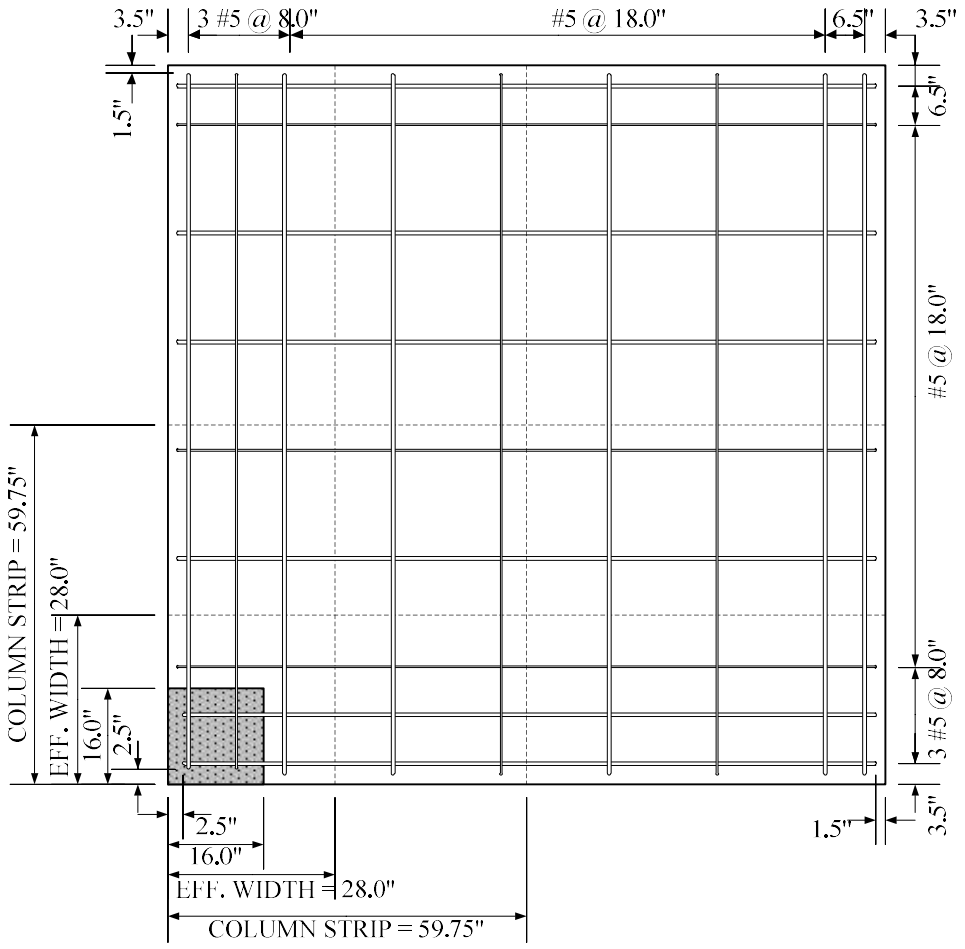

(b) Bottom Reinforcement

Fig. 3.4 – Reinforcement Layout for R-Series Specimens (cont.)

3.2.2 Column

The column was designed to remain elastic throughout the duration of the test. A higher reinforcement percentage was provided to minimize column deformation during the imposition of lateral displacement. Using specified concrete strength of 5000 psi and Grade 60 steel, the 16 in. square column was reinforced with 8 - #7 longitudinal reinforcement, 3 on each side, as shown in Fig. 3.5. The column transverse reinforcement was provided in compliance with the requirements of ACI 318-14 (ACI Committee 318, 2014) for special-moment-resisting-frame. No. 4 transverse reinforcement spaced at 4 in. was provided within the mid-height region of the column. The rest of the column section was provided with No. 4 closed hoops spaced at 5 in. on centers.

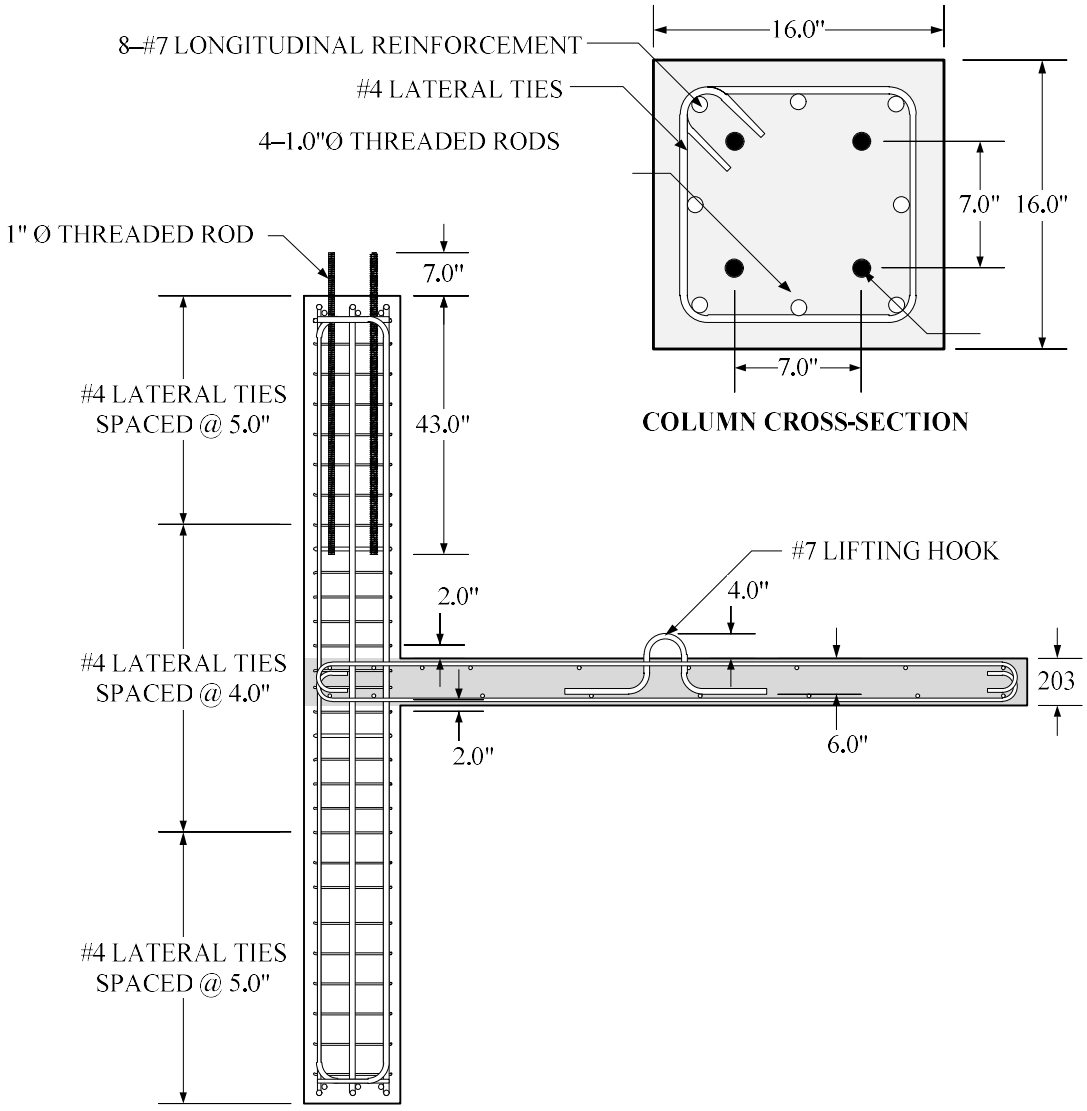

Fig. 3.5 – Typical Column Reinforcement Detail (Loading Direction)

3.3 SPECIMEN CONSTRUCTION

Specimens were constructed and cast inside the structural laboratory of the National Taiwan University of Science and Technology, Taipei City, Taiwan. Specimens G1 and G2 were constructed first, followed by specimens R1 and R2, and the last to be cast were specimens G3 and R3. Each pair of specimens was constructed with the same reinforcement. Each pair of specimens was cast with the same concrete material except for specimens G3 and R3.

After the slab formworks were finished, slab longitudinal reinforcement was laid out as shown in Fig. 3.6. The column cage was also set upright as presented in Fig 3.7(a). Before the formworks for columns were completely placed, 4 – 1 in. Ø threaded rods, used for anchoring

the steel support at the top of the column, were properly positioned, as shown in Fig. 3.7(b). Chairs were provided to ensure proper placement of the slab flexural reinforcement. A number of 1 in. PVC pipes were used to provide holes through the slab for gravity load application along the centerline of the slab panel and for the attachment of steel tubes to simulate pinned boundary conditions along the south and east sides of the slab as shown in Fig 3.8.

Concrete pouring then commenced after all reinforcement had been laid out. For each specimen, the column and slab were cast at the same time. All of the concrete mixes used were ordered from a local concrete batching plant and were delivered using concrete truck mixer. The specified concrete compressive strength was 5000 psi. The concrete was poured using a bucket and was supported and maneuvered using the structural laboratory crane, as shown in Fig. 3.9. Mechanical vibrator was used to provide adequate compaction of fresh concrete throughout the specimen. The slump of each concrete mix was obtained and a set of 4 × 8 in. concrete cylinder samples per specimen was also prepared during the concrete pouring, as shown in Fig 3.10. The specimens were left within the natural environment of the structural laboratory without special curing process.

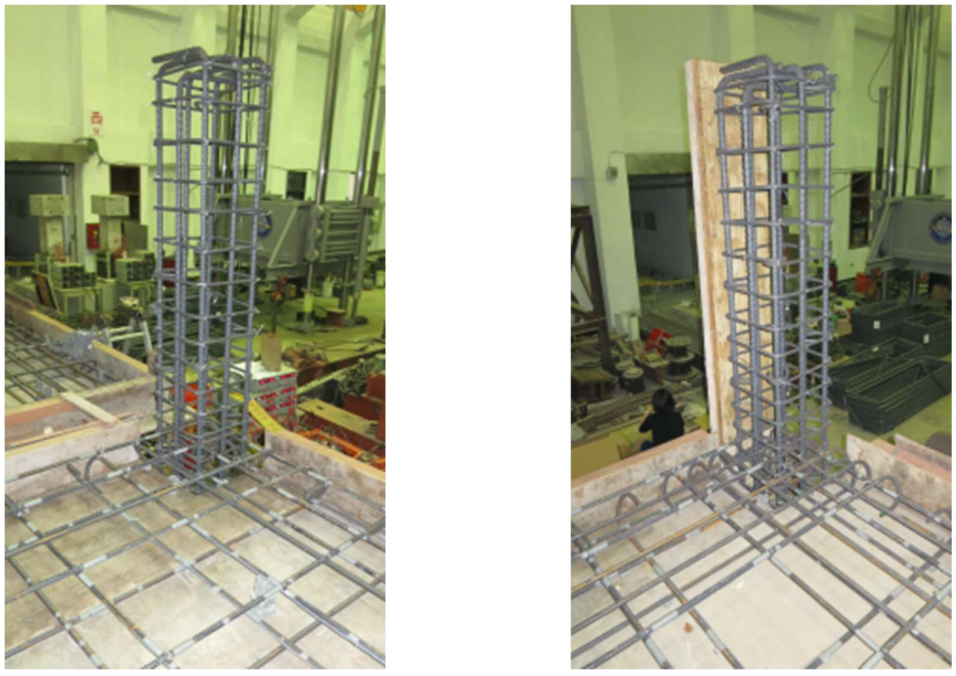

(a) G-Series (b) R-Series

Fig. 3.6 – Typical Reinforcement Detail Near the Slab-Column Connection

(a) Column Section

(b) Placement of Threaded Rods

Fig. 3.7 – Typical Column Reinforcement Detail

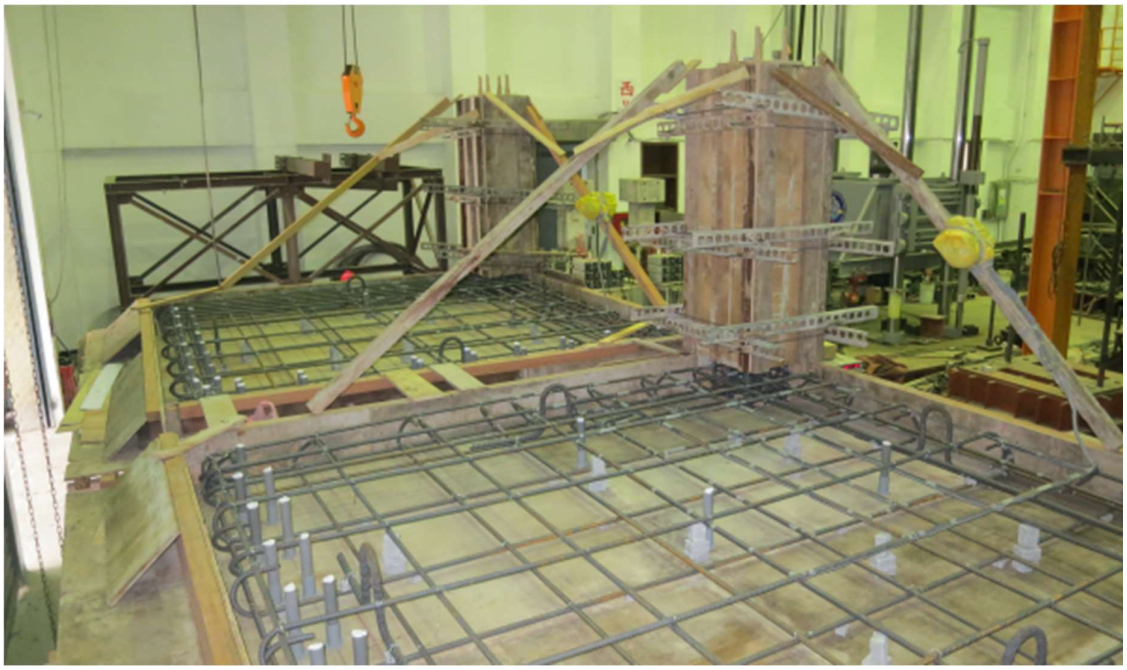

Fig. 3.8 – Specimen Prior to Concrete Pouring

Fig. 3.9 – Concrete Pouring

Fig. 3.10 – Concrete Cylinder Specimen Sample Preparation

3.4 EXPERIMENTAL SETUP AND INSTRUMENTATION

3.4.1 Experimental Setup

The experimental setup for all test specimens was essentially similar, as shown in Fig. 3.11. The base of the column was mounted at the top of the universal hinge support and fastened

with 2 - 1 in. threaded rods. The universal hinge, presented in Fig. 3.12, was composed of a 10 in. solid steel sphere, supported by a 1 in. thick and 7 in. high movable square steel section that was restrained on all four sides against lateral displacement. Each of the three other corners of the slab was supported with a roller support, attached to a steel arm that was hinged at the bottom. To avoid accidental slippage of the roller support underneath the slab during the imposition of lateral loading, an anchorage system, using 1/2 in. 7-wire prestressing strands, were provided as shown in Fig. 3.13.

(a) Overall Experimental Setup

Fig. 3.11 – Experimental Setup

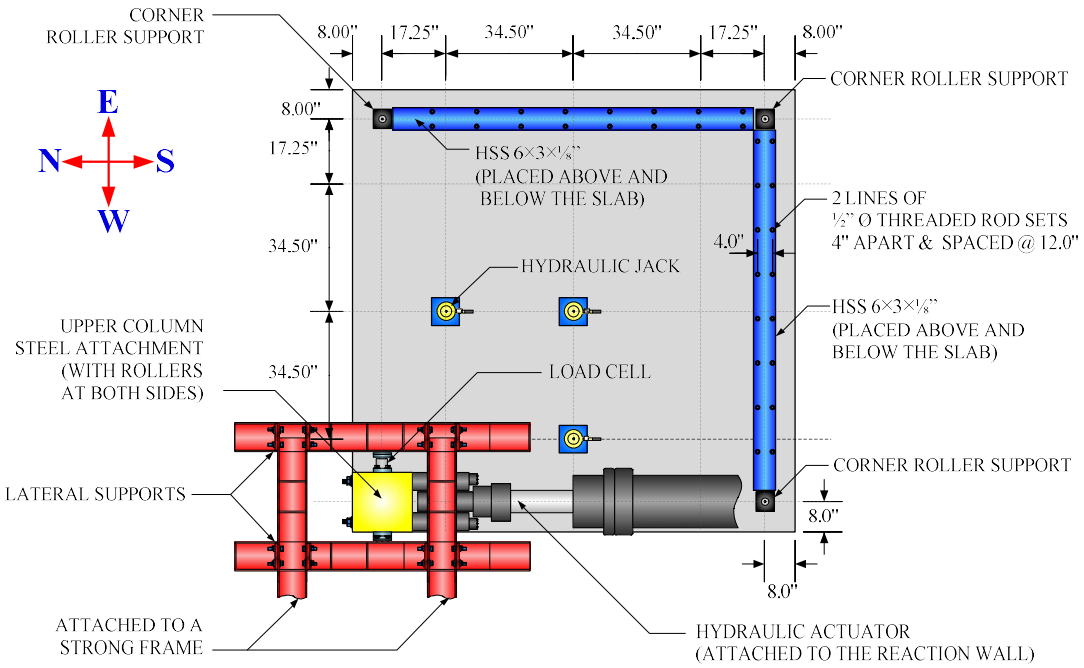

(b) Plan View

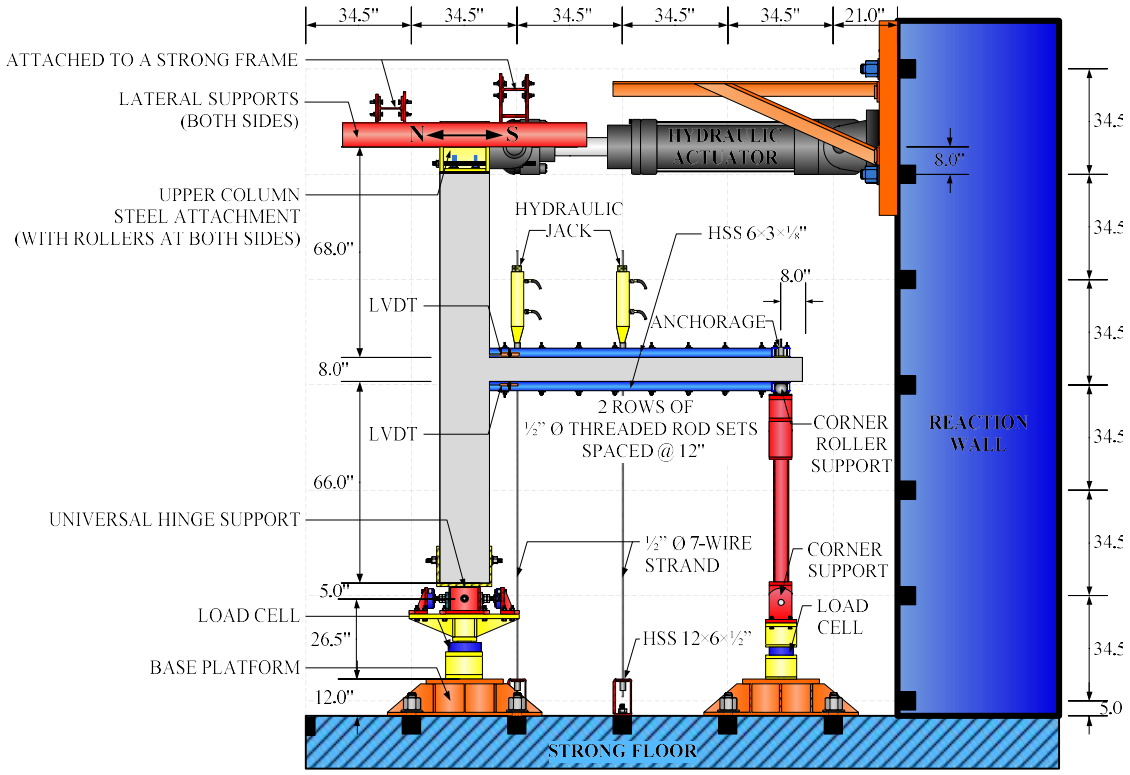

(c) Elevation View

Fig. 3.11 – Experimental Setup (cont.)

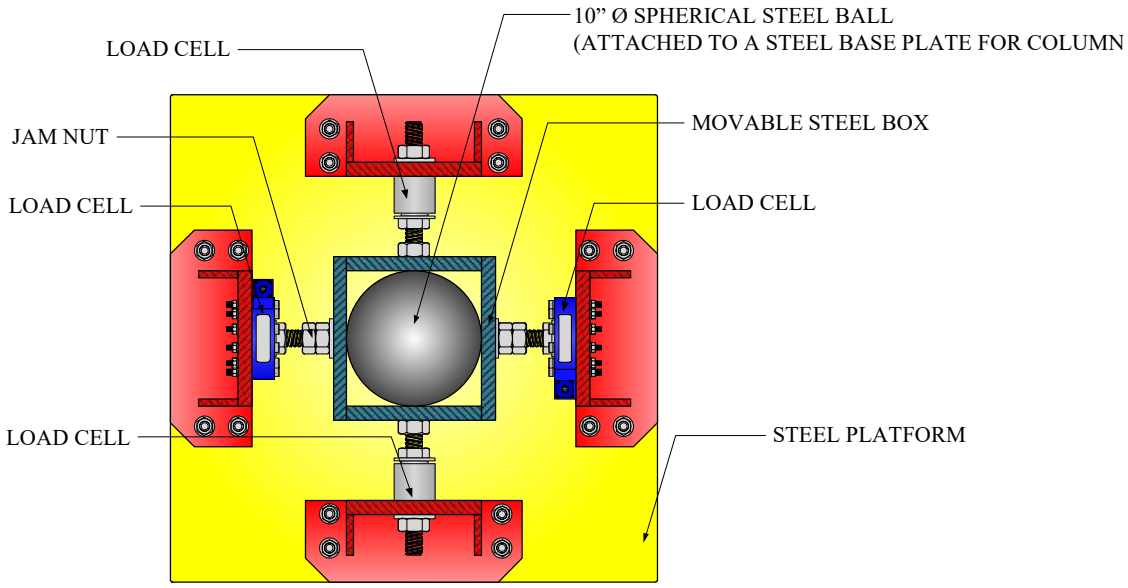

Fig. 3.12– Universal Hinge Setup

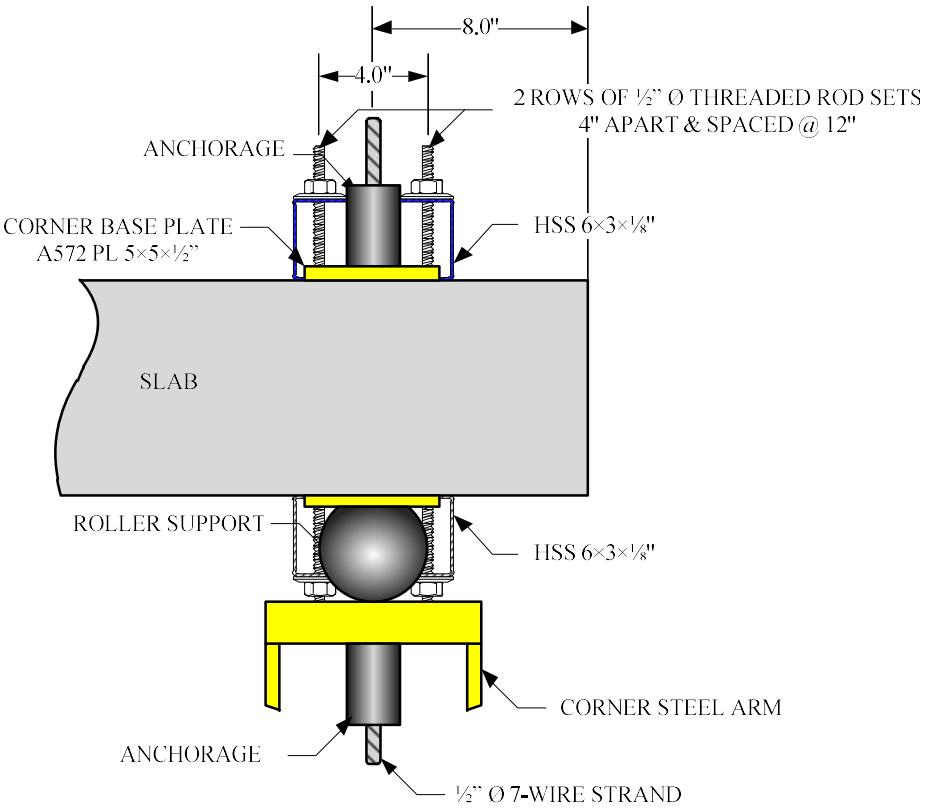

Fig. 3.13 – Roller Support at Slab Corners

The column top end was attached with a steel assembly on which the hydraulic actuator was connected. This steel assembly had rollers on its east and west sides. Two lateral supports,

sandwiching the steel support at the top of the column, were provided and acting as guided roller support to prohibit displacement in the transverse direction. For additional safety precautions against in-plane specimen rotation, roller lateral supports were also provided at selected locations along the east and west slab edges.

The pseudo-continuous boundary conditions along the east and west side edges of the slab were simulated using 4 - 3×6×1/8 in. tubes, two on each side and placed on the top and bottom faces, sandwiching the slab. They were fastened by two rows of 1/2 in. threaded rods, 4 in. apart, and spaced at 12 in. on centers.

Steel bearing plates were provided at the three gravity loading points on the slab. Three hydraulic jacks were placed vertically, above these plates, as shown in Fig. 3.14. Each hydraulic jack applied vertical load on the slab through a 1/2 in. 7-wire prestressing strand, which was anchored on the strong floor. The pressure was kept the same for all the hydraulic jacks and monitored with pressure gauges.

Fig. 3.14 – Hydraulic Jacks for Gravity Loading Application

A space steel frame was also placed beneath the test specimen, as shown in Fig. 3.11(a). This frame was not attached to the specimen and had enough clearance from the slab bottom surface. The frame was basically used to facilitate the assembly of experimental setup. It also served as a precautionary measure against unexpected sudden failure during the test. At the end of the test, the frame was also used to temporarily hold the specimen after all supports were detached.

3.4.2 Data Recording and Instrumentation

3.4.2.1 Lateral Displacement

Lateral displacement was applied to the specimen using a 220-kip hydraulic actuator. The hydraulic actuator was set to a displacement-controlled protocol with a loading rate of 0.04 in. per second. Lateral displacement was imposed using the displacement history presented in Fig. 3.15. Drift was defined as the lateral displacement of the actuator divided by the distance between the centerline of the actuator and the bottom universal hinge support, which was measured to be 147 in.. Positive and negative loading directions referred to actuator movement to the north and south, respectively. Each drift level had two cycles, which had a 0.25% drift increment until 2.00% drift level and 0.50% drift increment thereafter. A lower amplitude cycle of 1.00% was provided after 2.00% drift level and every 1.00% drift increment thereafter. Lateral displacement was measured using the built-in LVDT of the hydraulic actuator.

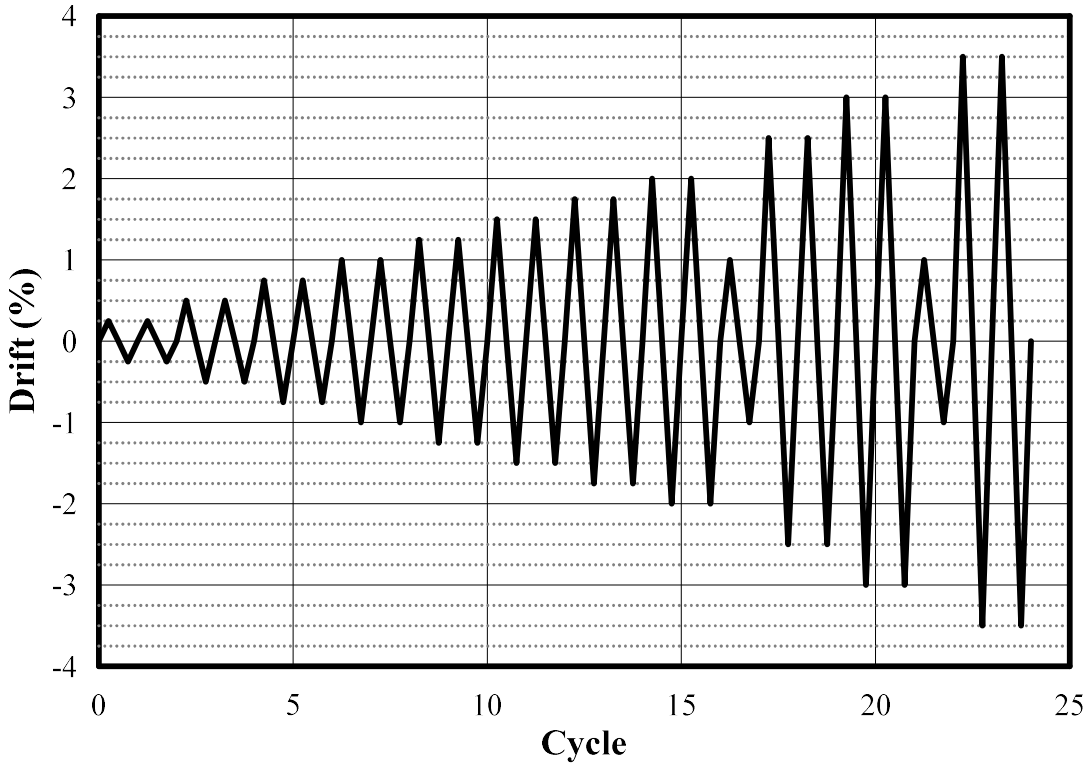

Fig. 3.15 – Displacement History

3.4.2.2 Lateral Loads

Lateral load in this study was basically the passive resistance measured at the column ends due to the imposition of lateral displacement and application of gravity load. Specimens G1 and G2 adopted the lateral load recorded from the built-in load cell of the hydraulic actuator and assumed the same lateral force at the base support but acting on the opposite direction. No load cells were provided to measure lateral loads in the transverse direction at end of the lower column.

The rest of the specimens (i.e., G3, R1, R2 and R3) were provided with 5 additional load cells to monitor reactions at both the top and bottom of the column. Four of these were placed at the bottom column support, one on each side of the steel box, supporting the universal hinge support, and were securely aligned along the reaction points, as presented in Fig. 3.12. The other load cell was attached in between the east side roller and the steel assembly at the top of the column, as depicted in Fig. 3.11(b), to monitor transverse lateral load reaction.

3.4.2.3 Gravity Load

Four load cells were used to measure the gravity load at the supports. One was mounted at the base of the universal hinge support to monitor the connection gravity load history, as shown in Fig. 3.11(c). Another 3 load cells were placed at the bases of the steel arm supports to monitor the gravity load distribution among the supports.

The G-Series and R-Series specimens were subjected with different specified gravity shear levels. The target gravity shear levels used in this study were $1.20\sqrt{f_c'(\text{psi})}b_o d$, $1.60\sqrt{f_c'(\text{psi})}\,b_o d$ and $2.00\sqrt{f_c'(\text{psi})}b_o d$ as summarized in Table 3.1. The specified gravity load was kept to be approximately the same during the test; adjustments were provided after the completion of the drift cycles when necessary.

3.4.2.4 Slab Connection Rotation

Slab connection rotations of the specimens were measured using two different instruments. This was due to the availability of instruments during the time of test. Specimens G1 and G2

used linear variable differential transducer (LVDT) while the rest of the specimens (i.e., G3, R1, R2, and R3) were using optical tracking system. The details of the instrumentation are described in the following sections.

3.4.2.4(a) LVDT System

LVDT system used in specimens G1 and G2 were set on the slab surface near the east and south column faces, as presented in Fig. 3.16. In each direction, two LVDTs were installed on the top and bottom faces of the slab and oriented perpendicularly to the face of the column, as depicted in Fig. 3.17. Each LVDT was leveled properly and fixed at a distance equivalent to the slab effective depth, d = 6.625 in., from the column face using a threaded rod embedded in the slab. The centerline of the stroke was provided with 1 in. vertical clearance from the slab surface, resulting to a 10 in. center-to-center distance between top and bottom LVDTs.

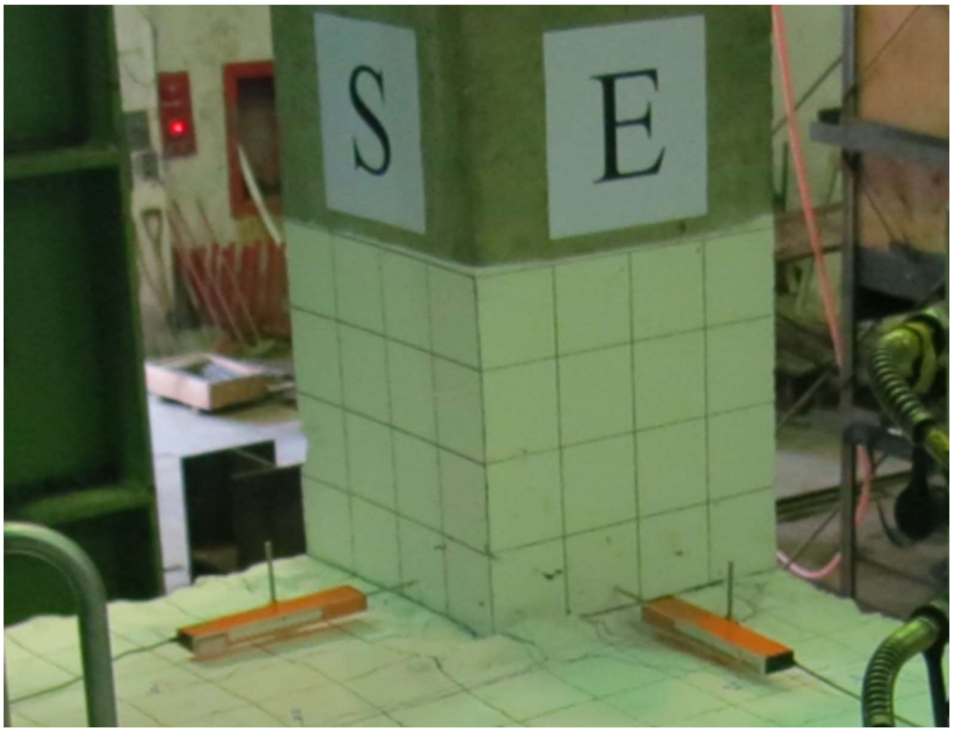

Fig. 3.16 – Actual LVDT Setup

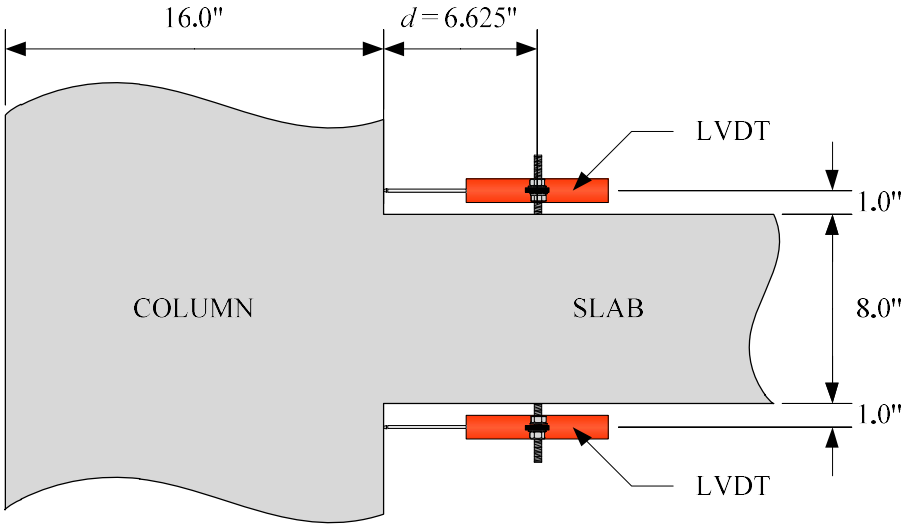

Fig. 3.17 – Typical LVDT Layout for Specimens G1 and G2

The chord rotation of the slab near the connection relative to the column face is defined as the net linear displacement of the top and bottom LVDTs divided by the center-to-center distance between top and bottom LVDTs.

3.4.2.4(b) Optical Tracking System

An optical tracking system, OptotrakCertus® by Northern Digital, Inc., was employed for Specimens G3, R1, R2 and R3 to monitor the rotation of the connection region. This tracking system had an accuracy of 0.1 mm with a resolution of 0.01 mm. It was also capable of capturing data at higher speeds with a maximum marker frequency of 4600 Hz. This system was composed of a motion capture device mounted on a stand and placed at certain distance from the specimen, tracking the positions of the optical markers in the x, y and z directions. Several optical markers were attached on the north and west slab faces of the slab specimen in a regular 3 × 4 in. grid pattern, as shown in Fig. 3.18.

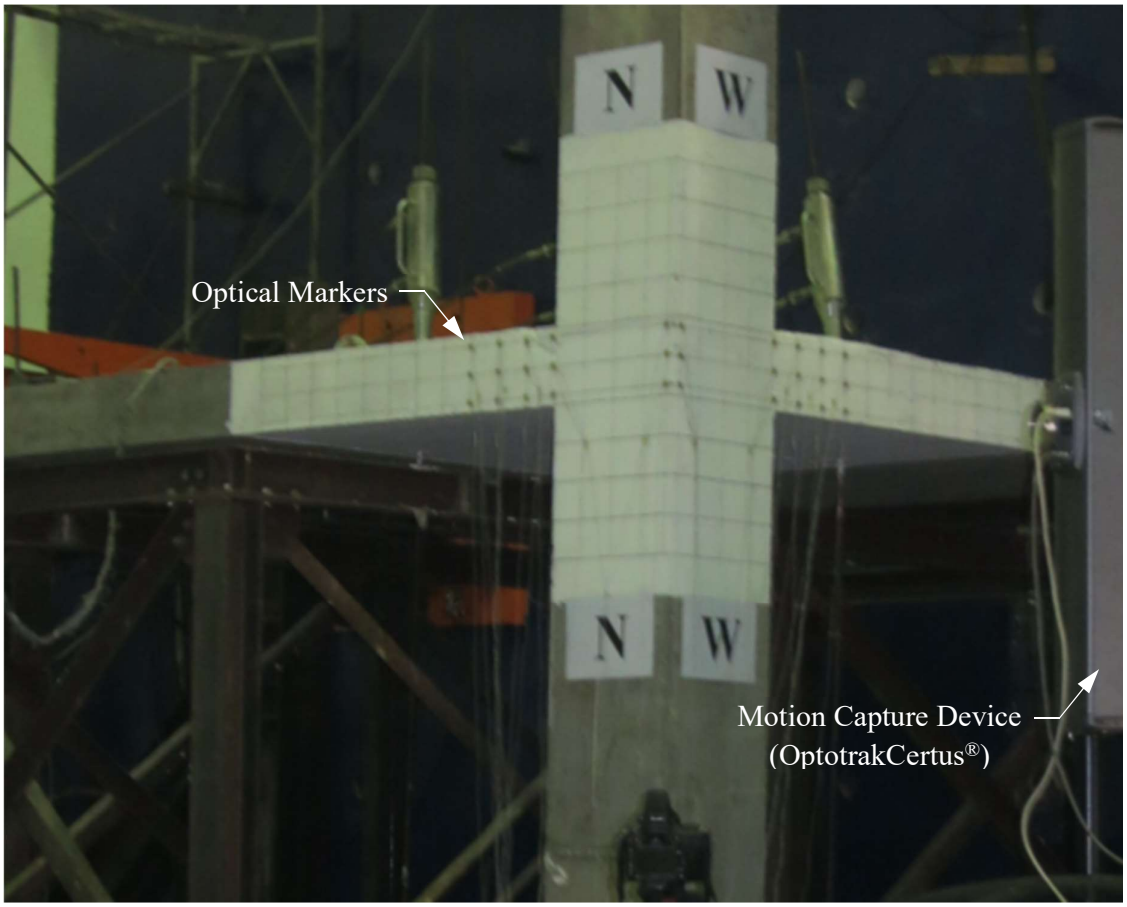

Fig. 3.18 – Typical Optical Tracking System Setup for Specimens G3, R1, R2 and R3

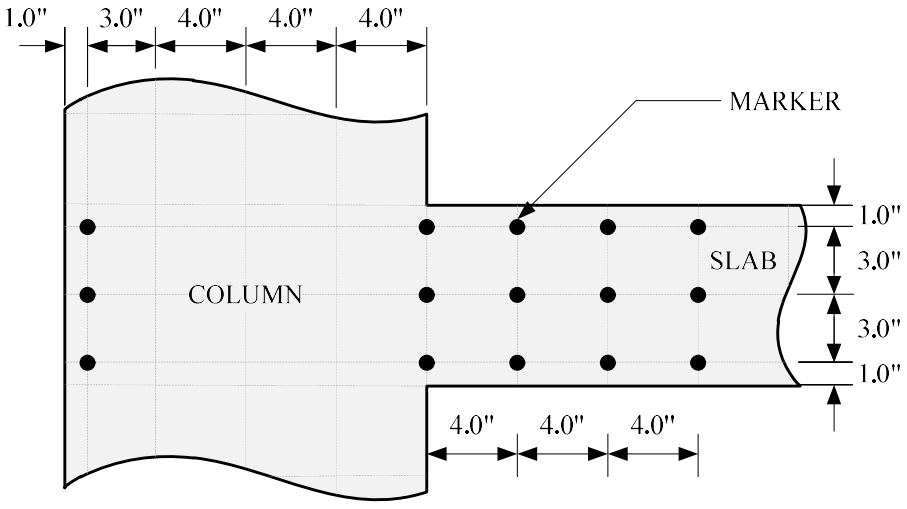

Fig. 3.19 – Typical Optical Marker Grid Pattern (West Side)

3.4.2.5 Reinforcement Strain

Several strain gauges were attached on the slab longitudinal reinforcement at designated locations to monitor the reinforcement strain within the vicinity of the connection. The first line of strain gauges were attached along the inner column face perpendicular to the longitudinal reinforcement, as shown in Fig. 3.20 to Fig. 3.22. The succeeding lines of strain gauges on the slab reinforcement were spaced at 2*d* distance.

Another four strain gauges were installed on the corner longitudinal bars of the column near the south face for specimens G1, G2, R1 and R2. Two strain gauges for each corner longitudinal bar, one was attached along the top slab face and the other one was attached along the bottom slab face. No strain gauges were attached on the column longitudinal reinforcement of specimens G3 and R3.

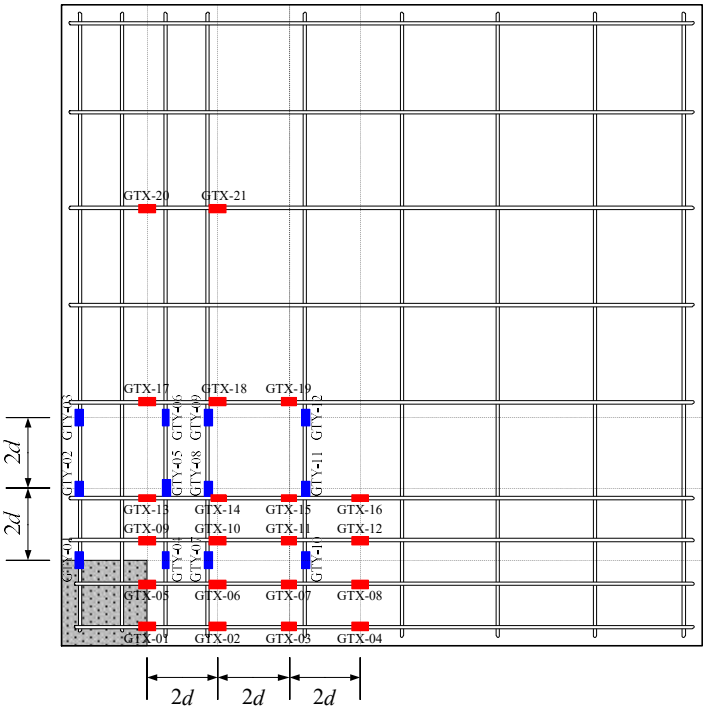

(a) Top Reinforcement

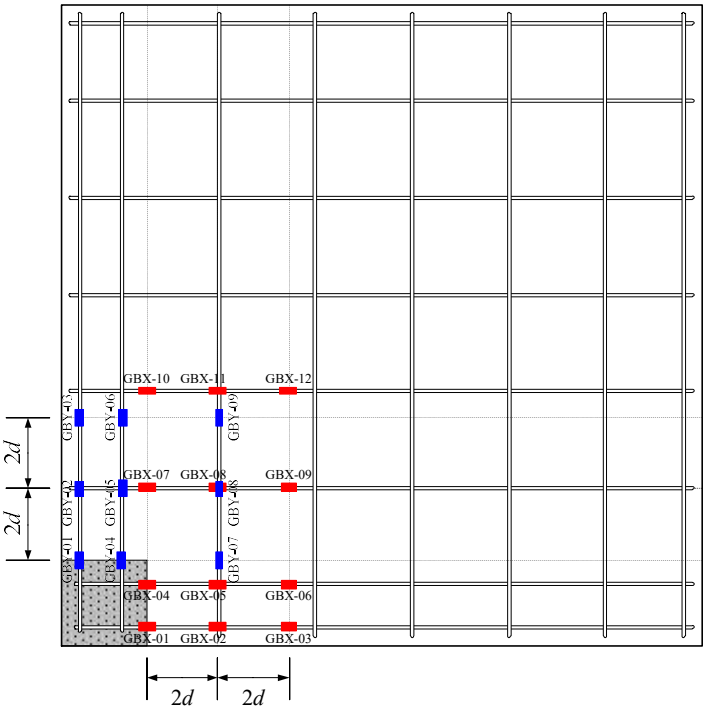

(b) Bottom Reinforcement

Fig. 3.20 – Strain Gauge Layout for Specimens G1 and G2

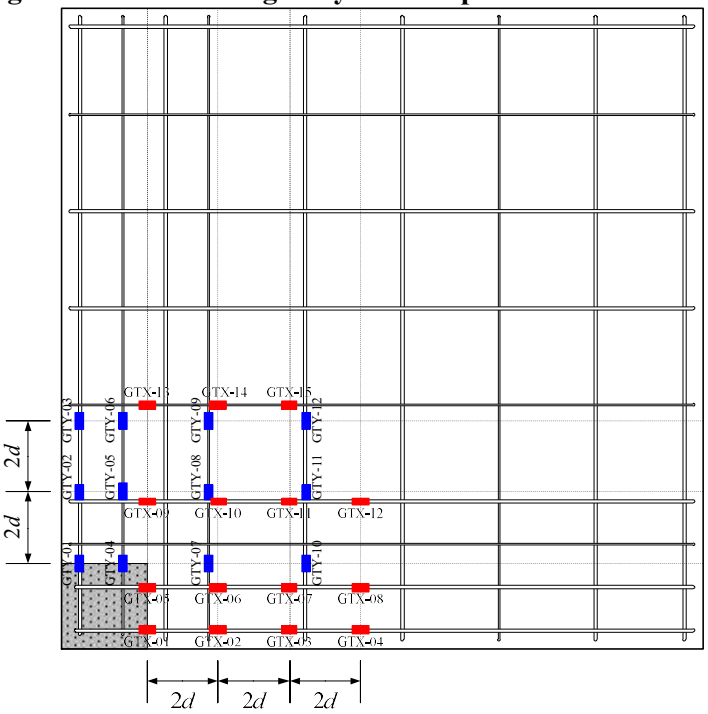

(a) Top Reinforcement

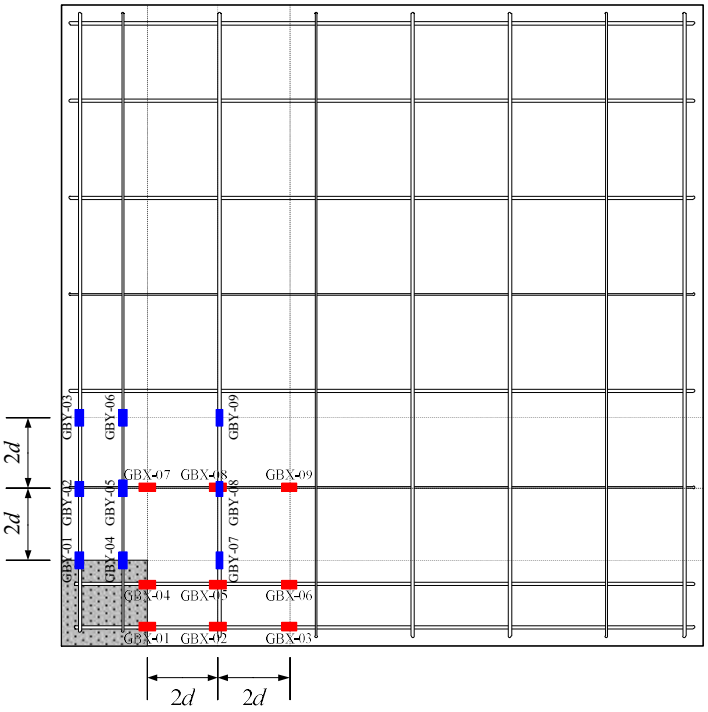

(b) Bottom Reinforcement

Fig. 3.21 – Strain Gauge Layout for Specimens G3

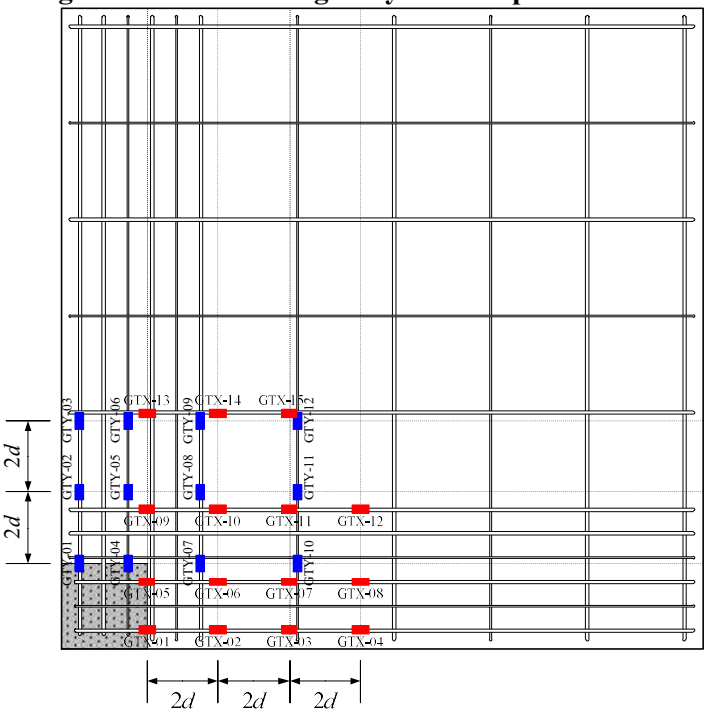

(a) Top Reinforcement

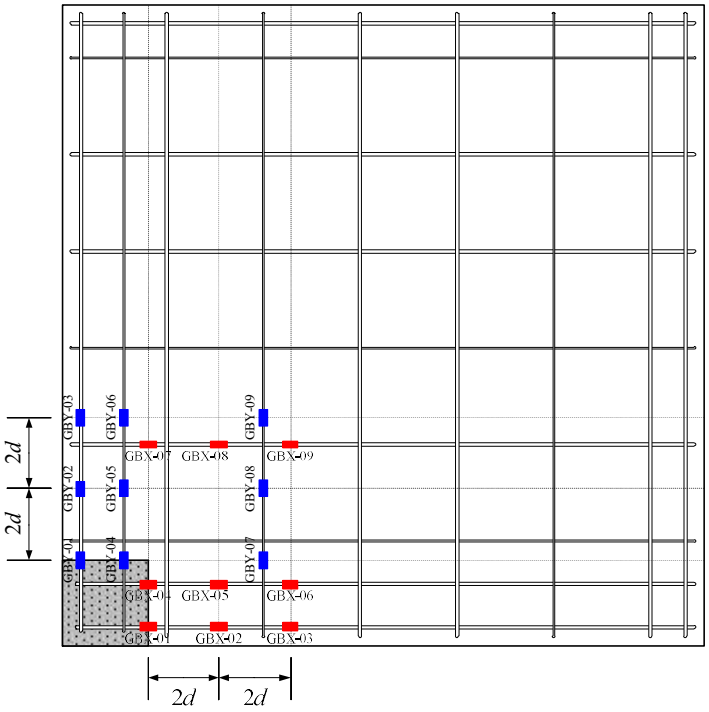

(b) Bottom Reinforcement

Fig. 3.22 – Strain Gauge Layout for R-Series Specimens

3.4.2.6 Crack Pattern

During the test, marker pens were used to trace the crack propagation at the peak of the second cycle of each drift level. Different marker colors were used to distinguish the cracks developed in the positive and negative loading directions. A regular 4 in. by 4 in. grid pattern, as shown in Fig. 3.23, was drawn on the slab and column faces, near the slab-column connection, as reference in evaluating cracks. Crack pattern was only drawn for specimens G1, G2, R1, and R2. Crack patterns of specimens G3 and R3 were not drawn to avoid unnecessary movement of the optical markers attached on the specimen. However, for the two specimens, crack propagation was still monitored through photographs and visual observations during the test.

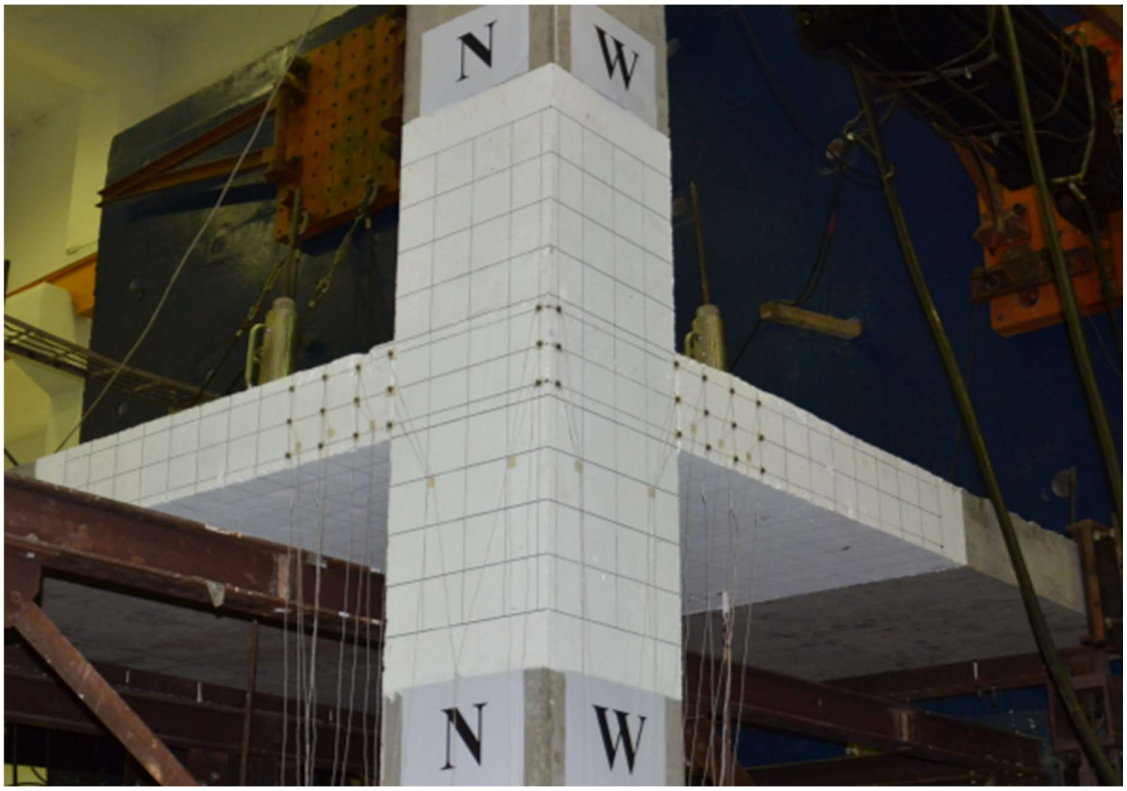

Fig. 3.23 – Gridline Pattern of the Optical System

CHAPTER 4
EXPERIMENTAL RESULTS AND OBSERVATIONS

4.1 INTRODUCTION

Six approximately full-scaled isolated corner slab-column connection specimens, with varying gravity shear ratios and flexural reinforcement ratios, were tested under combined gravity loading and lateral displacement reversals. This chapter presents test results of each specimen and the corresponding material properties.

4.2 MATERIAL PROPERTIES

4.2.1 Concrete

Concrete mixes used in all specimens were obtained from a local batching plant and were delivered using concrete mixers. The 28-day specified concrete strength was 5000 psi. All concrete mixes had a specified slump of 6 in. and a maximum aggregate size of 3/4 in..

4.2.1.1 Slump

Slump test was conducted for every batch of concrete mixture per ASTM C143/C143M (2015), as shown in Fig. 4.1. As presented in Table 4.1, specimens G1 and G3 had a slump of 6.8 in. specimens R1 and R2 had relatively lower slump of about 4.5 in.. Specimens G3 and R3 had relatively higher slump measurements of about 8.5 in. and 9.4 in., respectively.

Fig. 4.1 – Slump Test

Table 4.1– Concrete Slump Measurement

Specimen	G-Series			R-Series		
	G1	G2	G3	R1	R2	R3
Slump in. (mm)	6.8* (173)		8.5 (216)	4.5* (114)		9.4 (239)

* Same concrete batch.

4.2.1.2 Concrete Cylinder Compressive Strength

A set of six 4 in. × 8 in. concrete cylinder samples was prepared for each specimen during concrete pouring. Concrete cylinder specimens were exposed to the same environment with the slab-column specimens. Prior to compression testing, as shown in Fig. 4.2, both top and bottom ends of the concrete cylinder specimens were either smoothened or capped with gypsum paste to provide plane surfaces in accordance to ASTM C617/C617M (2015). Because the gravity load was applied directly on the slab in order to obtain the target connection shear (Table 3.1), which was related to concrete cylinder strength, the corresponding concrete cylinder samples were tested on the same day with the specimen, right before the specimen was tested. Concrete compressive strength was determined based on the average compressive strengths of six concrete cylinder samples. A summary of the results of the compression tests is presented in Table 4.2.

Fig. 4.2 – Concrete Compressive Strength Testing

Table 4.2 – Concrete Compressive Strength Summary

Specimen	G-Series			R-Series		
	G1 psi (MPa)	**G2** psi (MPa)	**G3** psi (MPa)	**R1** psi (MPa)	**R2** psi (MPa)	**R3** psi (MPa)
1	6404 (44.2)	6695 (46.2)	6250 (43.1)	6098 (42.0)	5349 (36.9)	5495 (37.9)
2	6298 (43.4)	6479 (44.7)	5784 (39.9)	5798 (40.0)	5178 (35.7)	5068 (34.9)
3	6464 (44.6)	7119 (49.1)	5859 (40.4)	6223 (42.9)	5777 (39.8)	4935 (34.0)
4	7085 (48.8)	7843 (54.1)	5601 (38.6)	6069 (41.8)	5639 (38.9)	4729 (32.6)
5	6584 (45.4)	7565 (52.2)	5297 (36.5)	5282 (36.4)	6056 (41.8)	4679 (32.3)
6	6240 (43.0)	6840 (47.2)	6272 (43.2)	5648 (38.9)	6179 (42.6)	4745 (32.7)
Average	**6513 (44.9)**	**7090 (48.9)**	**5844 (40.3)**	**5853 (40.4)**	**5696 (39.3)**	**4942 (34.1)**

4.2.2 Steel Reinforcement

All steel reinforcement used in this study had specified yield stress of 60 ksi. All reinforcing bars (rebars) were ordered from a local rebar company. A set of 3 steel coupons, with at least 24 in. long, was randomly collected for each bar size. Mechanical properties of steel reinforcement were determined by direct tensile testing in accordance with ASTM A370 (2012). A gauge length of 8 in. was used for all test coupons. Rebar strain was evaluated using an optical tracking system (Optotrak Certus® by Northern Digital, Inc.), with two optical markers attached on the steel coupon sample, as shown in Fig. 4.3. A clearance of 2 bar diameters was provided between the gauge length and the grip of the universal testing machine.

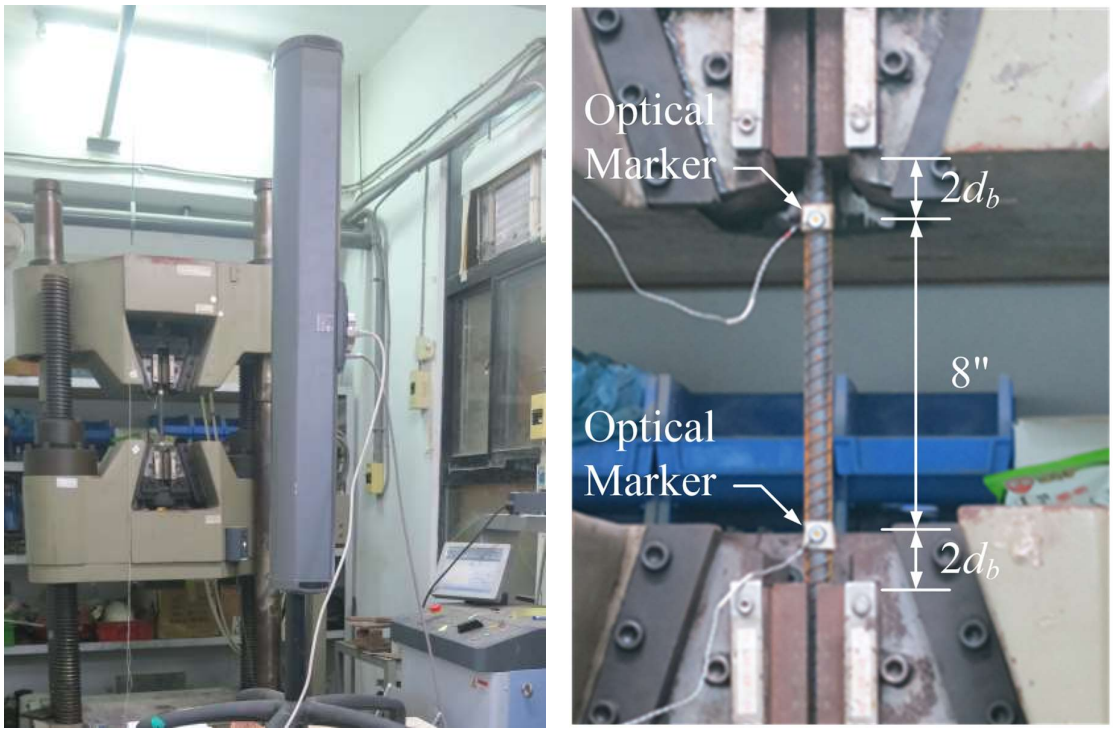

(a) Setup (b) Gauge Length and Marker Orientation

Fig. 4.3 – Direct Tensile Testing

The stress-strain relationships of all steel coupons are presented in Fig. 4.4 to Fig. 4.12. Some key mechanical properties of steel reinforcement are summarized in Table 4.3. All reported values are based on the average of the three coupon samples. For rebar specimens exhibiting a well-defined yield plateau, the yielding properties are graphically determined at the point where the slope of the stress-strain relationship curve exhibited a sharp change. For rebar specimens not exhibiting a distinct yield plateau, No. 4 bars in specimens R1 and R2, yielding point

properties are evaluated using 0.2% offset method (ASTM A370, 2012), as presented in Fig. 4.13. The peak point corresponds to the maximum stress on the stress-strain relationship curve. The ultimate point is defined as the actual fracture point or point corresponding to 10% stress drop from the maximum stress of the tested stress-strain relationship, whichever comes first (ASTM A370, 2012).

ASTM A706 (2012) provides a set of acceptance criteria for Grade 60 steel reinforcement. These criteria are presented in Table 4.4. Based on the summarized mechanical properties of rebars in Table 4.3, all rebar specimens have passed the ASTM A706 (2012) acceptance criteria except for the No. 4 rebars used in specimens R1 and R2, which do not meet the minimum yielding stress of 60 ksi (414 MPa).

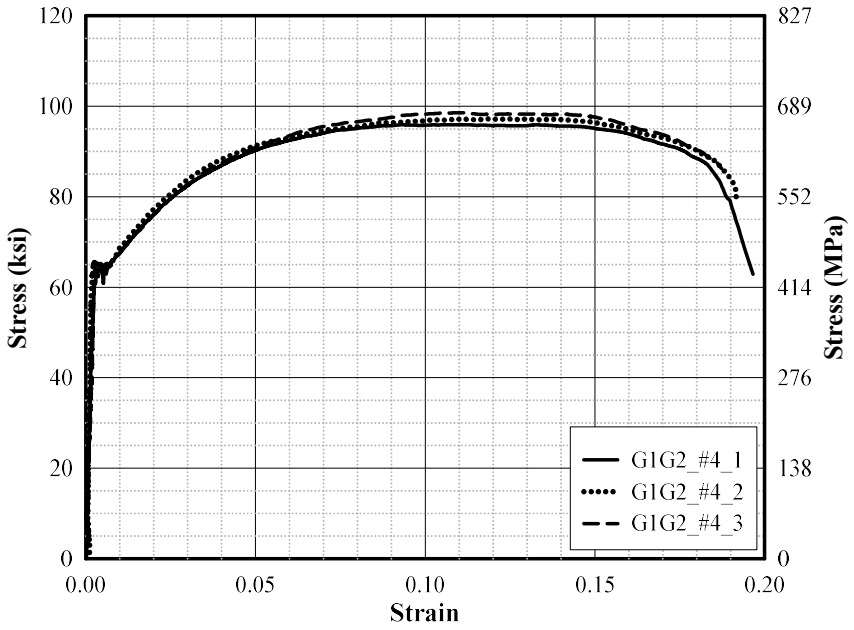

Fig. 4.4 – Specimens G1 and G2 No. 4 Steel Reinforcement Stress-Strain Relationship

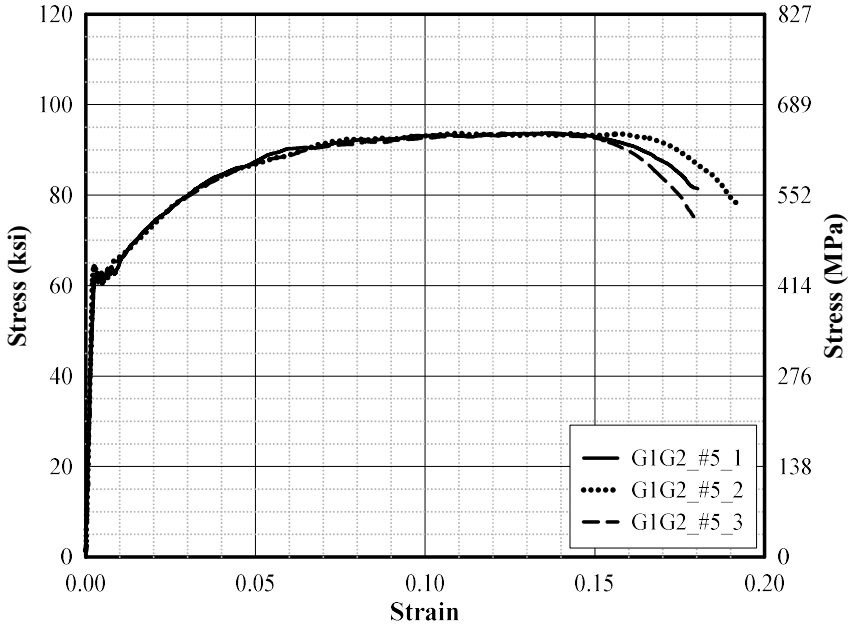

Fig. 4.5 – Specimens G1 and G2 No. 5 Steel Reinforcement Stress-Strain Relationship

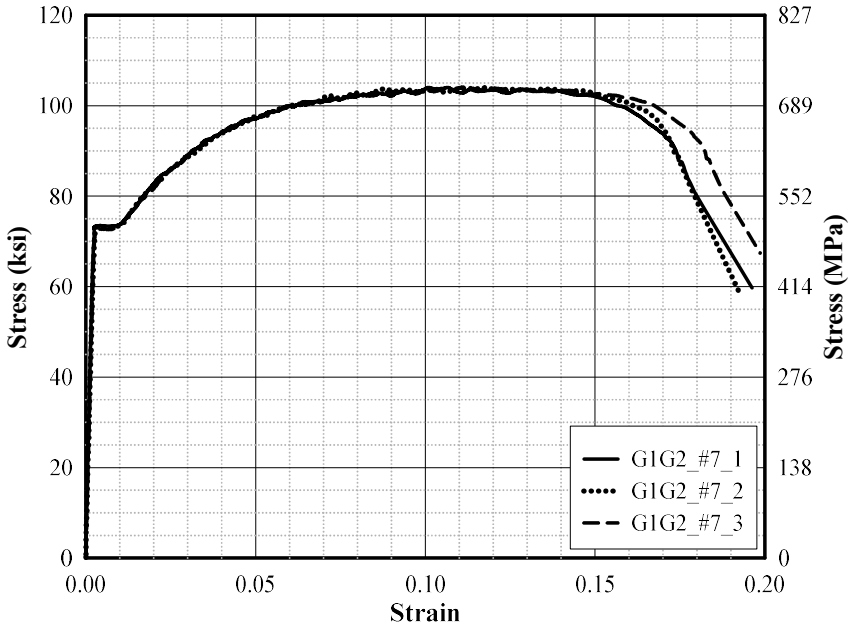

Fig. 4.6 – Specimens G1 and G2 No. 7 Steel Reinforcement Stress-Strain Relationship

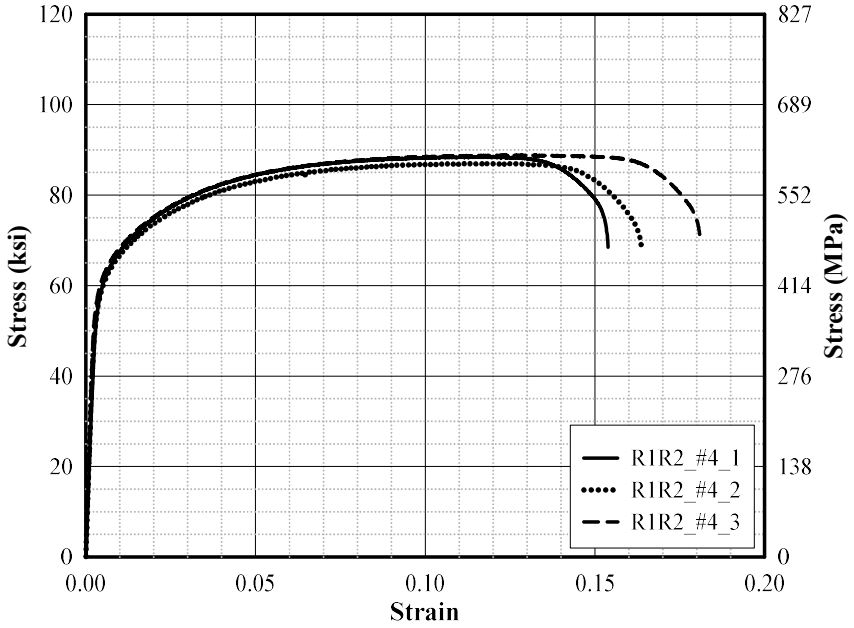

Fig. 4.7 – Specimens R1 and R2 No. 4 Steel Reinforcement Stress-Strain Relationship

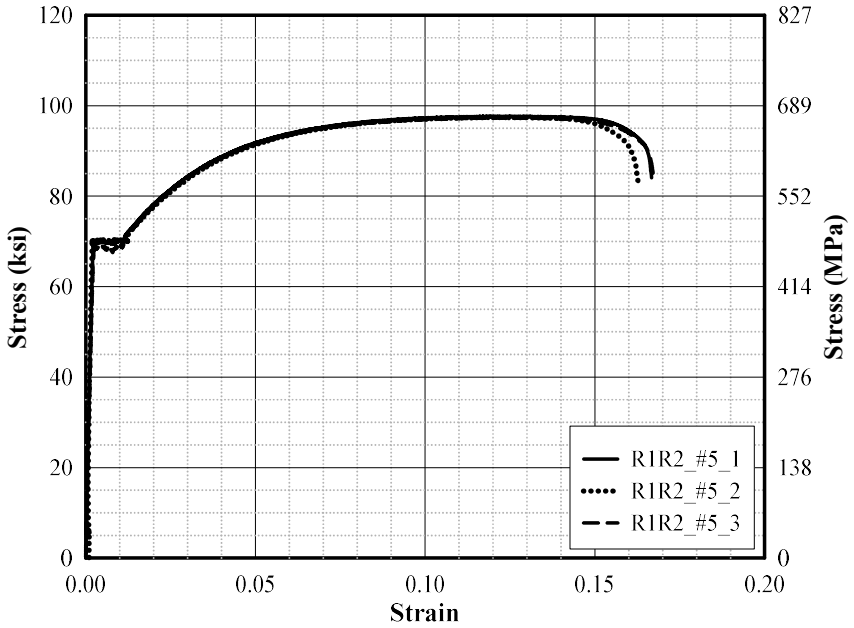

Fig. 4.8– Specimens R1 and R2 No. 5 Steel Reinforcement Stress-Strain Relationship

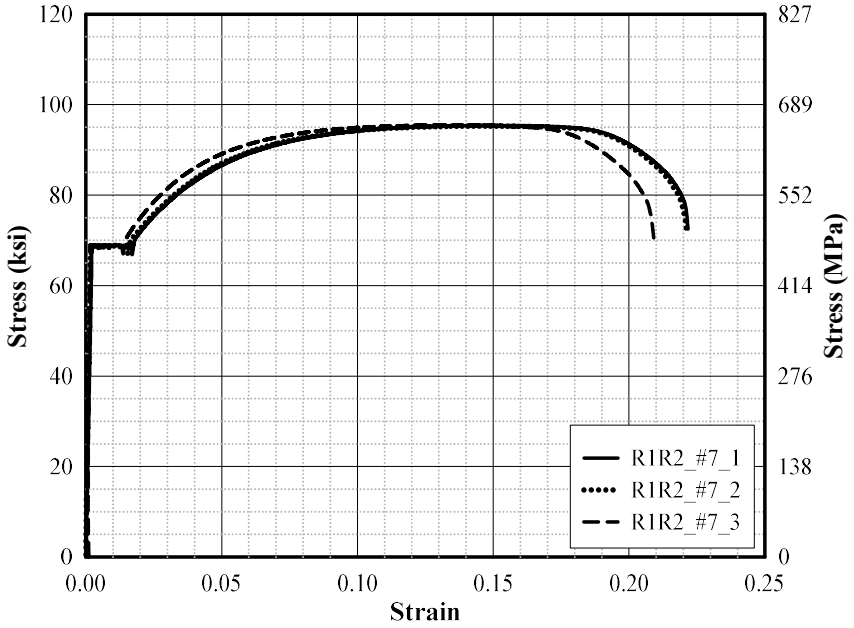

Fig. 4.9 – Specimens R1 and R2 No. 7 Steel Reinforcement Stress-Strain Relationship

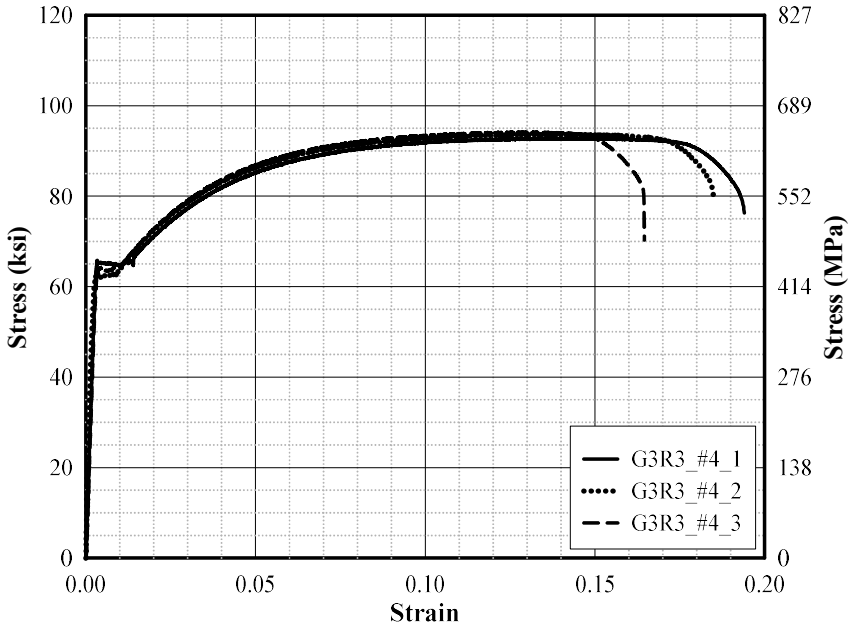

Fig. 4.10 – Specimens G3 and R3 No. 4 Steel Reinforcement Stress-Strain Relationship

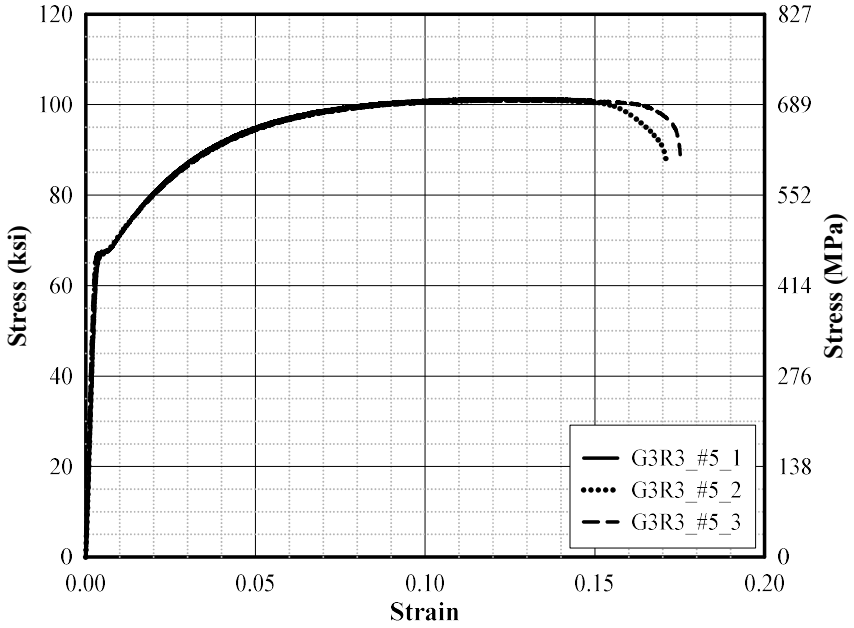

Fig. 4.11 – Specimens G3 and R3 No. 5 Steel Reinforcement Stress-Strain Relationship

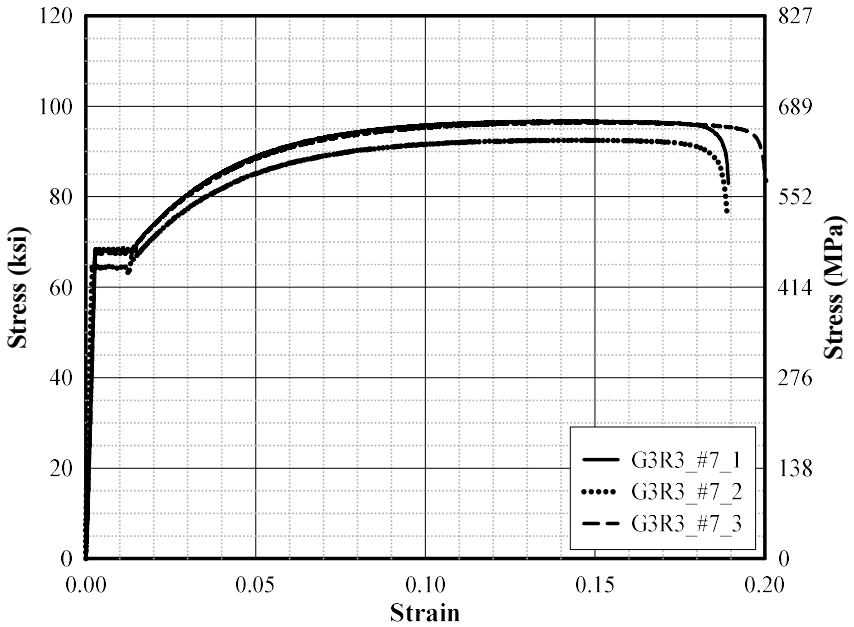

Fig. 4.12 – Specimens G3 and R3 No. 7 Steel Reinforcement Stress-Strain Relationship

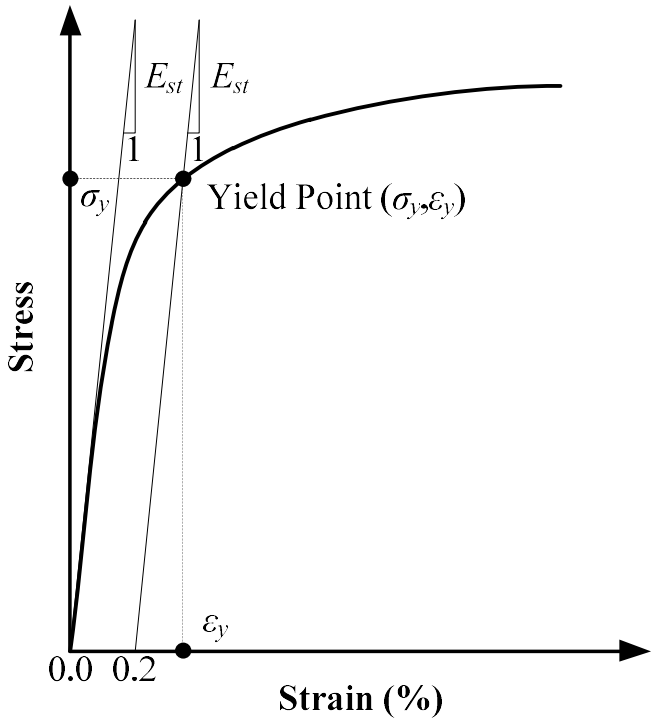

Fig. 4.13 – Yield Point Evaluation using 0.2% Offset Method

Table 4.3 – Summary of Steel Reinforcement Properties

Specimen	Bar Size	Yield			Peak		Ultimate‡		$\frac{f_p}{f_y}$
		f_y ksi (MPa)	ε_y (%)	ε_{sh} (%)	f_p ksi (MPa)	ε_p (%)	f_u ksi (MPa)	ε_u (%)	
G1 & G2	No. 4	63.8 (439.9)	0.20	0.64	97.2 (670.2)	11.32	87.5 (603.3)	18.42	1.52
	No. 5	61.6 (424.7)	0.21	0.78	93.7 (646.0)	12.48	84.3 (581.2)	17.66	1.52
	No. 7	73.0 (503.3)	0.24	0.90	104.0 (717.1)	11.00	93.6 (645.3)	17.35	1.42
R1 & R2	No. 4	57.8 (398.5)	0.41	NA*	88.1 (607.4)	12.11	79.3 (546.8)	16.10	1.52
	No. 5	69.4 (478.5)	0.21	1.14	97.5 (672.2)	12.35	87.7 (604.7)	16.48	1.40
	No. 7	68.6 (473.0)	0.18	1.54	95.4 (657.8)	14.51	85.8 (591.6)	20.69	1.39
G3 & R3	No. 4	63.6 (438.5)	0.28	1.14	93.5 (644.7)	13.89	84.2 (580.5)	17.86	1.47
	No. 5	66.0 (455.1)	0.28	0.61	101.1 (697.1)	12.79	91.0 (627.4)	17.04	1.53
	No. 7	66.7 (459.9)	0.25	1.35	95.2 (656.4)	14.78	85.7 (590.9)	19.22	1.43

‡ Actual fracture point or point corresponding to 10% drop from the peak stress.
* Determined using 0.2% offset method.

Table 4.4 - Acceptance Criteria for Grade 60 Deformed Bars per ASTM A706 (2012)

Bar Size	Minimum ε_{sh} %	Minimum ε_u %	Minimum f_y ksi (MPa)	Minimum f_p ksi (MPa)
No. 3 to No. 6	NA	14	60 (414)	80 (550)*
No. 7 to No. 11		12		

* The value of f_p shall not be less than $1.25 f_y$.

4.3 GENERAL SPECIMEN RESPONSE AND CRACK DEVELOPMENT

The response of each specimen under combined gravity-type loading and lateral displacement reversals are monitored through instrumentations and visual inspections. This section presents the visual observations on each specimen through crack patterns developed throughout the duration of the test. The extent of damage in each specimen at failure at is also presented.

4.3.1 Specimen G1

Specimen G1 had a target connection gravity shear of $1.20\sqrt{f_c'(\text{psi})}b_o d$. During the initial application of gravity load, several fine cracks appeared on the bottom surface of the slab and on the north side face of the slab. These cracks appeared to be caused by flexure, as shown in Fig. 4.14. No crack was observed on the top surface of the slab.

Fig. 4.14 –Slab Bottom Surface Crack Pattern of Specimen G1 at Initial Target Connection Shear.

At 0.25% drift, a few hairline cracks were observed on the top surface of the slab near the column. These cracks started near the north and west slab edges, about a slab effective depth d distance from the adjacent column faces, and extended toward the inner corner of the column. Vertical cracks were observed on the north and west slab faces after the completion of 0.25% drift cycles.

Within 0.50% drift cycles, inclined cracks (about 20 to 25 degree counter-clockwise from the slab bottom surface) were developed on the north side (face) of the slab. Those inclined cracks originated from the slab bottom surface at a distance of about $2h$ from the column face and extended upward toward the column, when the specimen was displaced toward the positive (N) direction. Similarly, an opposite inclined crack (about 90+27 degree counter-clockwise from the slab bottom surface) was also observed when the specimen was displaced toward the negative (S) direction. This inclined crack originated near the top face of the slab (about 2.5 slab thickness distance from the column) and extended downward toward the direction of the column. The formation of this crack appeared to be the initiation of the main inclined crack on the north face of the slab. On the west face of the slab, a new vertical crack at around $1.5h$ distance from the south column face was observed.

Several new inclined cracks were observed on the north face of the slab near the column during 0.75% drift cycles. Another new inclined crack, which originated from the bottom of the slab that was a slab thickness distance away from the column face and extended upward toward the column direction, was observed on the west face of the slab when the specimen was displaced toward the positive direction. Existing cracks extended during 0.75% drift cycles and inclined crack widths became wider.

At 1.00% drift level, the main inclined crack on the north face extended further toward the top surface, as shown in Fig 4.15. Further extension of cracks on the top surface of the slab was observed. In addition, several new cracks appeared. Cracks parallel to the slab edges in both orthogonal directions became apparent, which appeared to be the projection of the slab flexural reinforcement.

Fig. 4.15 – Initiation of the Major Diagonal Crack on the North Face of the Slab

During 1.50% drift cycles, the major inclined crack width continued to increase, as shown in Fig. 4.16(a). Further extension (parallel to the slab top surface) and widening of this crack was observed during 1.75% drift cycles. At this drift level, cracks on the west slab face were still very narrow and did not show any sign of major distress. During 2.00% drift cycles, the major inclined crack width opened up significantly as shown in Fig. 4.16(b). The main inclined crack on the north slab face widened by about an inch during 2.50% drift cycles. Cover concrete on the bottom surface of the slab around the connection region started to spall off during the 2.50% drift cycles as shown in Fig. 4.17.

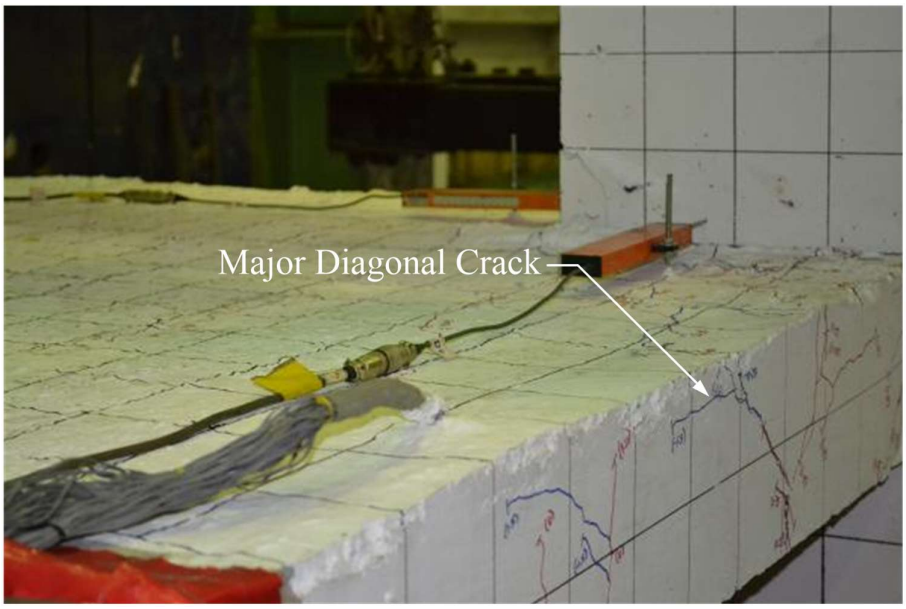

(a) 1.50% Drift

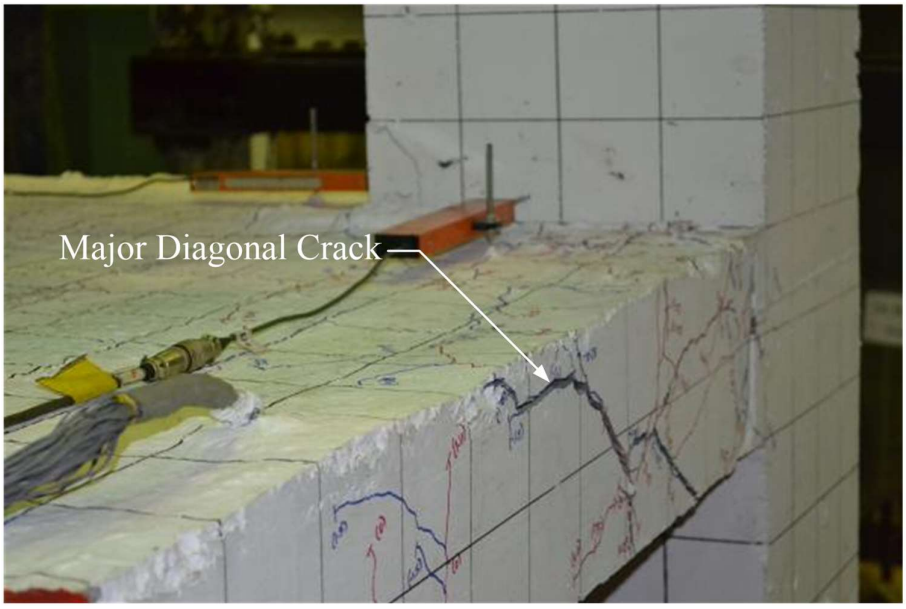

(b) 2.00% Drift

Fig. 4.16 – Main Failure Plane Projection on the North Face of the Slab

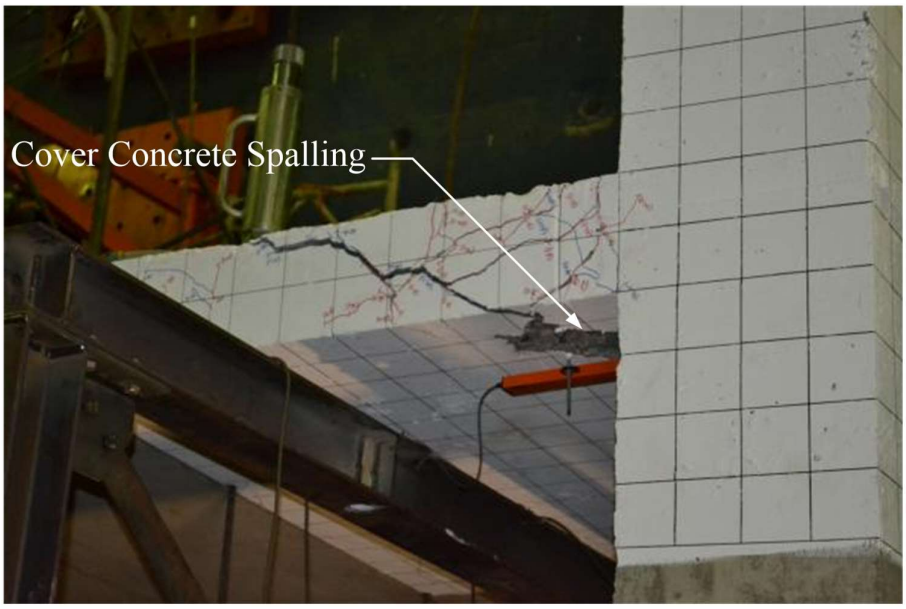

Fig. 4.17 – Cover Concrete Spalling on the Bottom Surface of the Slab

During 3.00% drift cycles, the connection lost its gravity shear significantly. An attempt to adjust the connection shear back to the target level of $1.2\sqrt{f_c^{'}(\text{psi})}b_o d$ after the completion of the 3.00% drift cycles failed and that led to the end of the test.

The specimen final states are presented from Figs. 4.18 to 4.21. As can be seen from Figs. 4.18 and 4.19, with the major inclined crack developed at around 27 degree counter-clockwise, damage was concentrated within 4*h* distance from the column faces. After removal of loose concrete, Fig. 4.19, slab flexural reinforcement was fully exposed and an apparent punching cone was observed. No extensive damage was observed on the bottom surface of the slab except for the diagonal crack that extended from the east column face to the north slab edge as shown in Fig. 4.21.

(a) At the End of the Test

(b) After Loose Concrete Removal

Fig. 4.18 – North Side of Specimen G1 at Failure

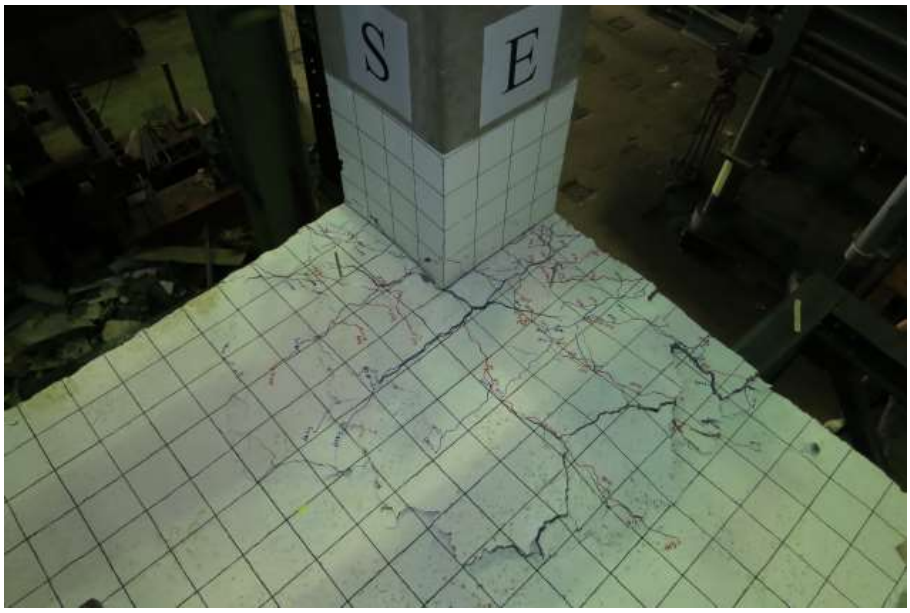

(a) At the End of the Test

(b) After Loose Concrete Removal

Fig. 4.19 – Slab Top Surface of Specimen G1 at Failure

(a) At the End of the Test

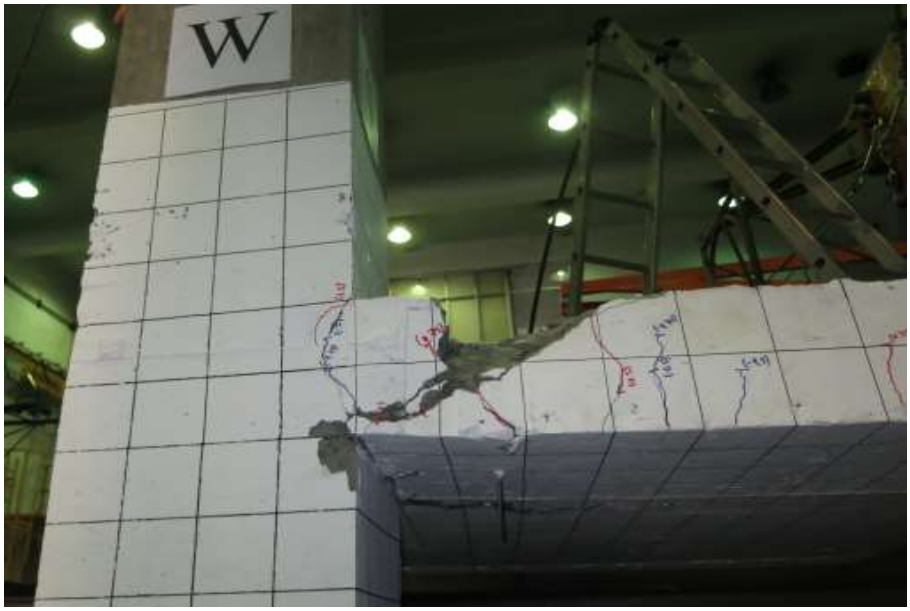

(b) After Loose Concrete Removal

Fig. 4.20 – West Side of Specimen G1 at Failure

Fig. 4.21 – Slab Bottom Surface of Specimen G1 Near the Connection at Failure

4.3.2 Specimen G2

Specimen G2 had a target connection gravity shear of $1.20\sqrt{f_c'(\text{psi})}b_o d$. However, this specimen failed during the application of gravity load, right before its target connection shear was reached. No lateral displacement was imposed to specimen G2. The cracks on the north and west slab sides cut through the full slab thickness as shown in Figs. 4.22 and 4.23. The slope of the major crack at the north and west slab sides was around 27 to 30 degrees near the column and became gentler as it extended upward when crossing the slab flexural reinforcement. The plan view from top of the slab indicated that damage was concentrated within a 4*h* distance from the inner column faces, as shown in Fig. 4.24. The extent of damage on the bottom surface of the slab was only observed along the perimeter of the column, as presented in Fig. 4.25. A punching cone became apparent after loose concrete was moved.

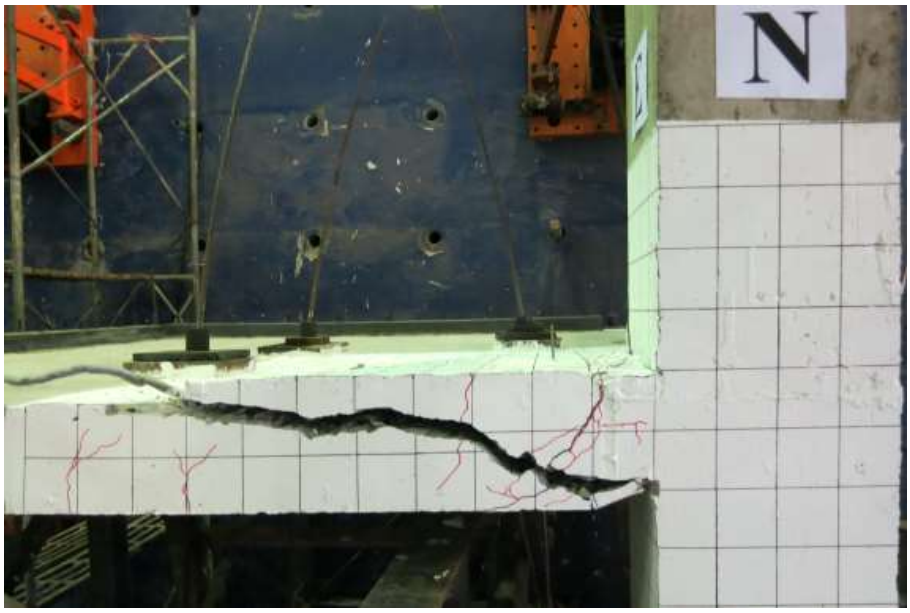

(a) At the End of the Test

(b) After Loose Concrete Removal

Fig. 4.22 – North Side of Specimen G2 at Failure

(a) At the End of the Test

(b) After Loose Concrete Removal

Fig. 4.23 – West Side of Specimen G2 at Failure

(a) At the End of the Test

(b) After Loose Concrete Removal

Fig. 4.24 – Slab Top Surface of Specimen G2 at Failure

Fig. 4.25 – Slab Bottom Surface of Specimen G2 Near the Connection at Failure

4.3.3 Specimen G3

When specimen G3 was set to its proper orientation, prior to the start of the test, a fine inclined crack on the north face of the slab was observed, as shown in Fig. 4.26. It may be caused during the set up process. It is believed that this crack would not affect the overall behavior of the specimen. Specimen G3 had a target connection gravity shear of $1.60\sqrt{f_c'(\text{psi})}b_o d$. Prior to the application of lateral displacement, the gravity shear measured at the bottom of the column gradually decreased right after the hydraulic jack pressure was locked. Despite of this loss, test continued without adjusting the gravity shear at the moment. Cracks on the slab bottom surface were apparent after the designed gravity load was applied. Crack pattern of specimen G3 was not drawn to enable full recording of marker readings and to avoid unnecessary disturbance of the optical markers attached to the specimen.

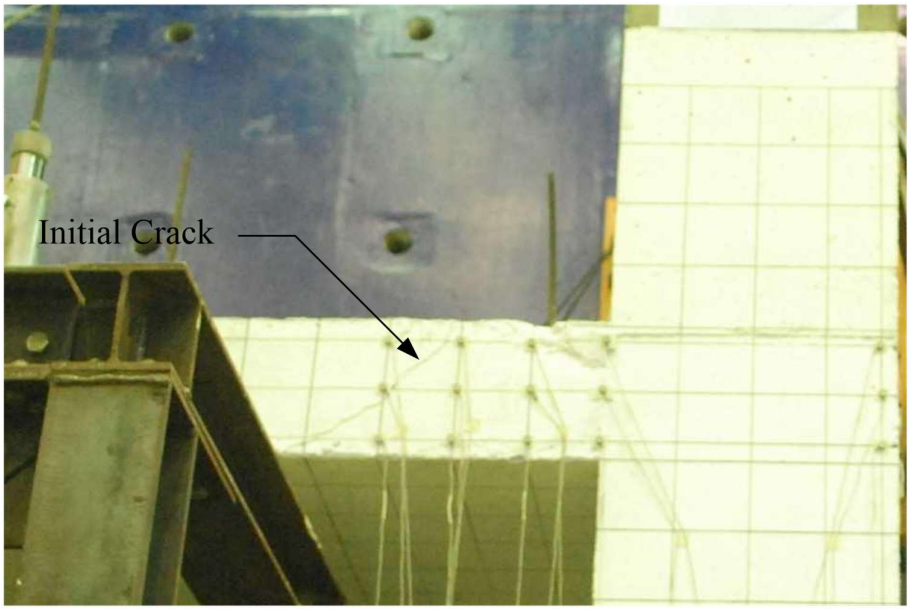

Fig. 4.26 – Initial Crack on the North Face of the Slab of Specimen G3

Inclined cracks on the north side of the slab near the column were observed during the first cycle of 0.25% drift level as shown in Fig. 4.27. At the same drift cycle, an inclined crack near the column and a vertical crack at a distance of a slab thickness away from the column face were also observed at west side of the slab as shown in Fig. 4.28. After completion of 0.25% drift cycles, gravity load was adjusted to reach a connection gravity shear of $1.47\sqrt{f_c'(\text{psi})}b_o d$ which is lower than its target level. Further increasing the stroke of hydraulic jacks was not able to raise the connection gravity shear back to its target level. Without observing obvious signs of failure, test continued.

After completion of the 1st cycle of 0.5% drift level, the inclined crack widths on both north and west sides of the slab grew significantly. A chunk of cover concrete on the north column face spalled off right before the specimen reached the 2nd cycle of -0.50% drift. Both gravity shear and lateral load dropped significantly. Test was terminated after completion of the 0.50% drift cycles.

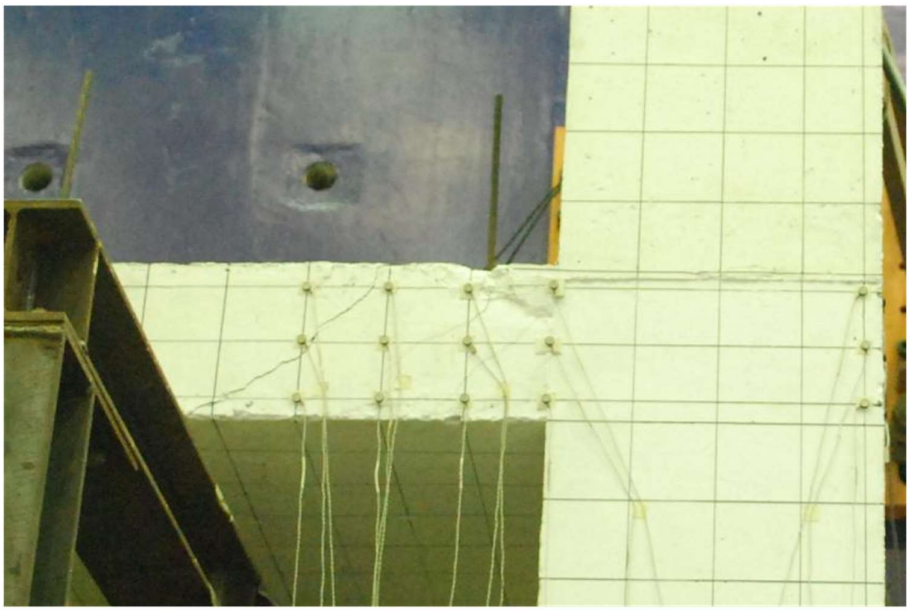

Fig. 4.27 – Crack Pattern on the North Face of the Slab of Specimen G3 at 0.25% Drift

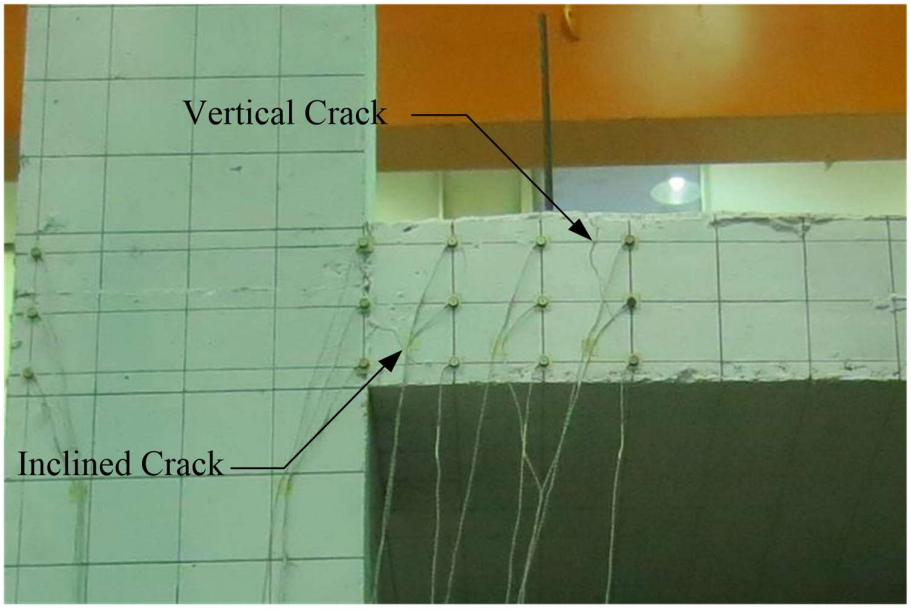

Fig. 4.28 – Crack Pattern on the West Face of the Slab of Specimen G3 at 0.25% Drift

The main inclined crack on the north face of the slab was relatively shallow, as shown in Fig. 4.29. On the west side, the main inclined crack started from the bottom of the slab, nearly a slab thickness distance away from the column face, and extended across the slab thickness toward the top of the slab as shown in Fig. 4.30. This crack started with an inclination of about 27 degrees with the horizontal, near the bottom of the slab, and gradually decreased as it

approached to the top flexural reinforcement of the slab. The damage area of the slab section was concentrated within a 4*h* distance from the inner column faces, as depicted on the top surface of the slab shown in Fig. 4.31. The bottom surface of the slab only showed fine cracks and slight spall-off of concrete cover near the inside perimeter of the column as shown in Fig. 4.32. After removal of loose concrete, a cone shape failure surface was observed.

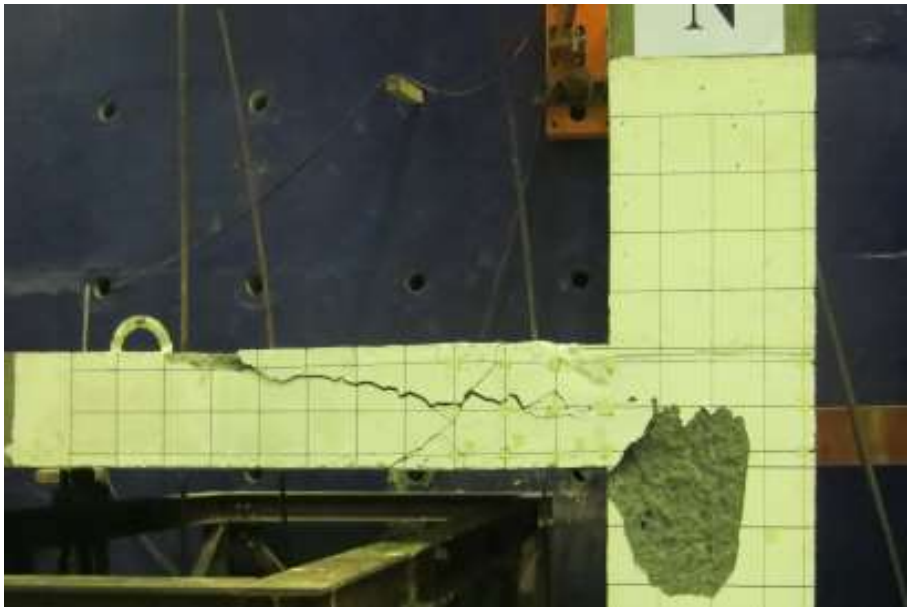

(a) At the End of the Test

(b) After Loose Concrete Removal

Fig. 4.29 – North Side of Specimen G3 at Failure

(a) At the End of the Test

(b) After Loose Concrete Removal

Fig. 4.30 – West Side of Specimen G3 at Failure

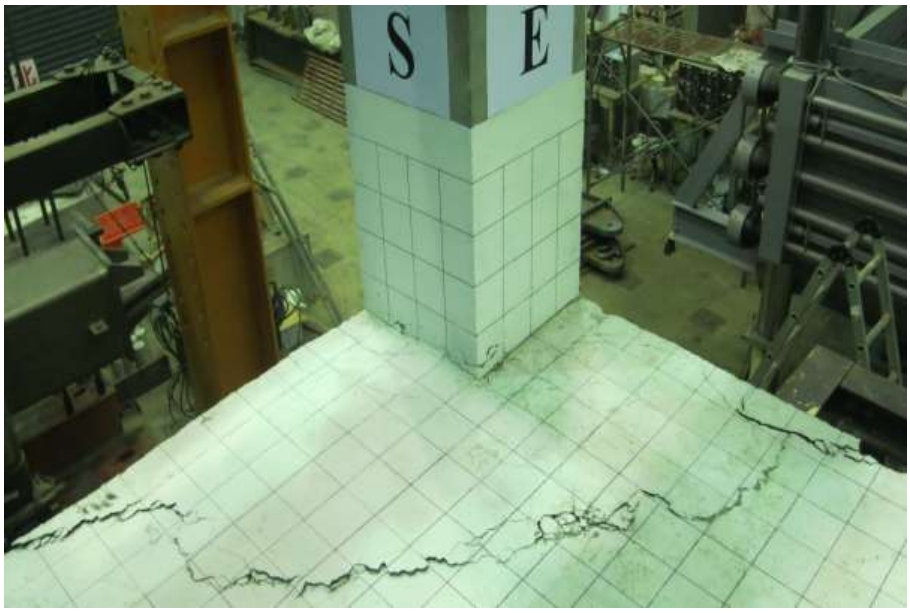

(a) At the End of the Test

(b) After Loose Concrete Removal

Fig. 4.31 – Slab Top Surface of Specimen G3 at Failure

Fig. 4.32 – Slab Bottom Surface of Specimen G3 Near the Connection at Failure

4.3.4 Specimen R1

Fine flexural cracks were observed on the bottom surface of the slab of specimen R1 after the application of the gravity load. Inclined cracks were observed on the north and west slab faces during the 0.25% drift cycles as shown in Fig. 4.33. These cracks started from the top of the slab and extended toward the bottom of the slab. Few vertical cracks were observed on the west face of the slab. An inclined crack, shown in Fig. 4.34, on the north face of the slab was developed during the 2nd cycle of the 1.00% drift. This crack eventually became the main inclined crack on the north face of the slab.

The main inclined crack on the west face of the slab was initiated as the specimen was loaded in the 2nd cycle of -1.25% drift. The inclined crack widths on both west and north slab faces continued to grow during the 1.50% and 1.75% drift cycles, as shown in Figs. 4.35. and 4.36.

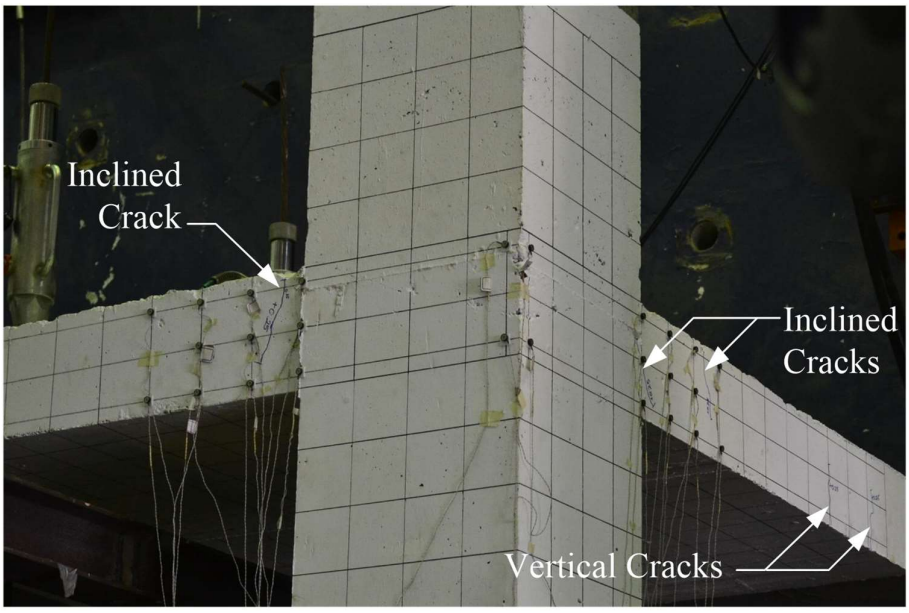

Fig. 4.33 – Crack Pattern on the North and West Slab Faces of Specimen R1 at 0.25% Drift

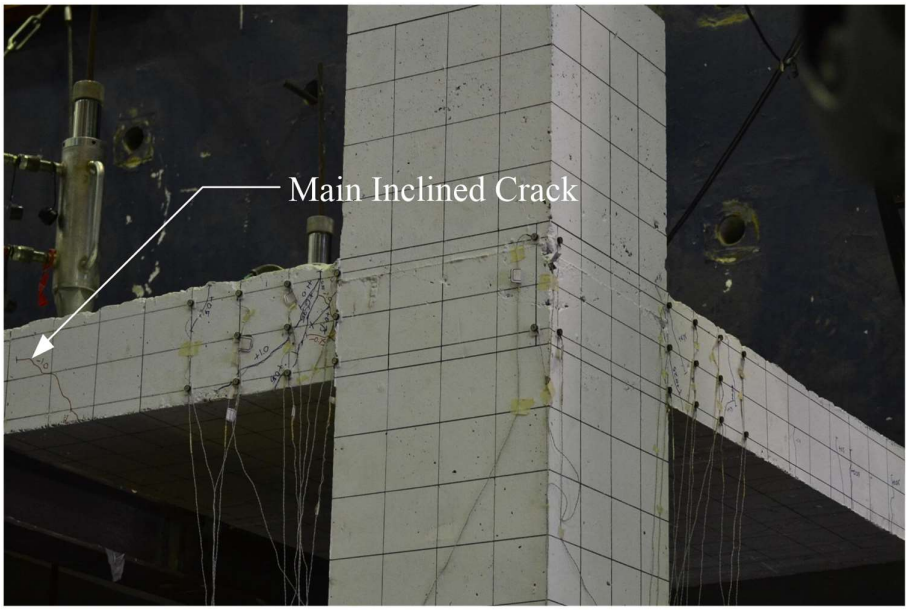

Fig. 4.34 – Initiation of the Main Inclined Crack on the North Face of the Slab of Specimen R1

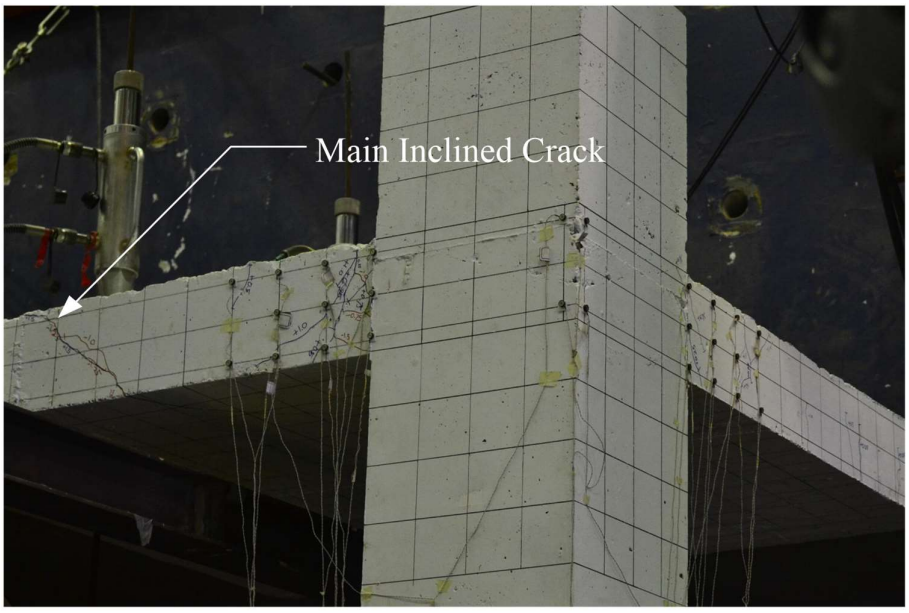

Fig. 4.35 – Crack Pattern on the North and West Slab Faces of Specimen R1 at 1.50% Drift

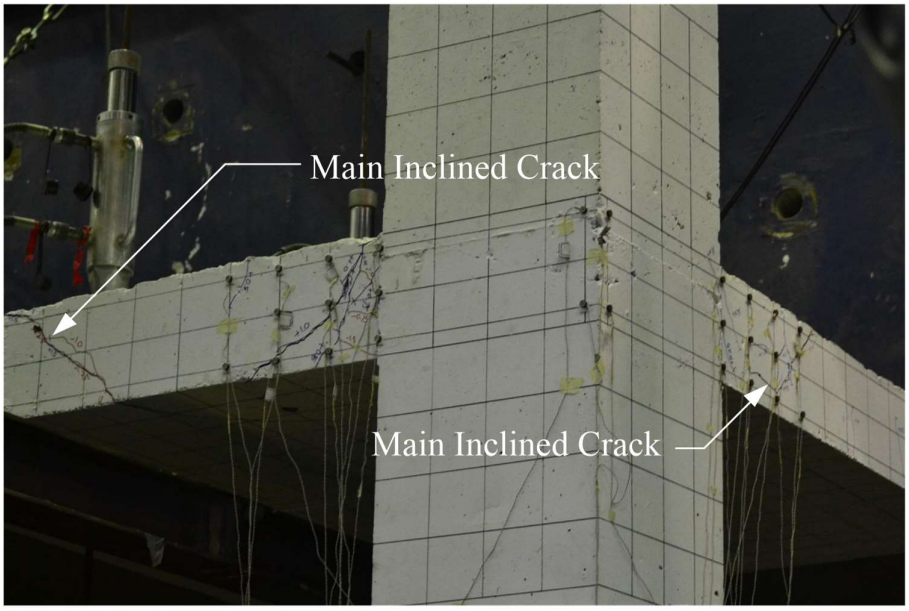

Fig. 4.36 – Crack Pattern on the North and West Slab Faces of Specimen R1 at 1.75% Drift

A large cover concrete piece became loose on the north column face, near the slab-column interface, during the 1st cycle of +2.00% drift, as shown in Fig. 4.37. A significant decrease of gravity load was observed after the 2.00% drift cycles. That loose concrete cover spalled off

during the adjustment of the connection gravity shear at end of the 2.00% drift cycles. The gravity load adjustment failed and, as a result, the test was concluded.

Fig. 4.37 – Crack Pattern on the North and West Slab Faces of Specimen R1 at 2.00% Drift

The slab section was observed to be fully disintegrated from the column after loose concrete debris were removed. The slab flexural reinforcement anchored to the column effectively held the slab section from total collapse. The main inclined crack had an angle of around 34 degree, as shown in Fig. 4.38. On the west face of the slab, the main inclined crack had an angle of about 27 degree, as presented in Fig. 4.39. In general, the damage was concentrated within a 4*h* distance from the inner column faces, as depicted in the top surface of the slab shown in Fig. 4.40. The extent of concrete spalling and damage of the slab bottom surface was within a 3*h* distance away from the column face, as presented in Fig. 4.41.

(a) At the End of the Test

(b) After Loose Concrete Removal

Fig. 4.38 – North Side of Specimen R1 at Failure

(a) At the End of the Test

(b) After Loose Concrete Removal

Fig. 4.39 – West Side of Specimen R1 at Failure

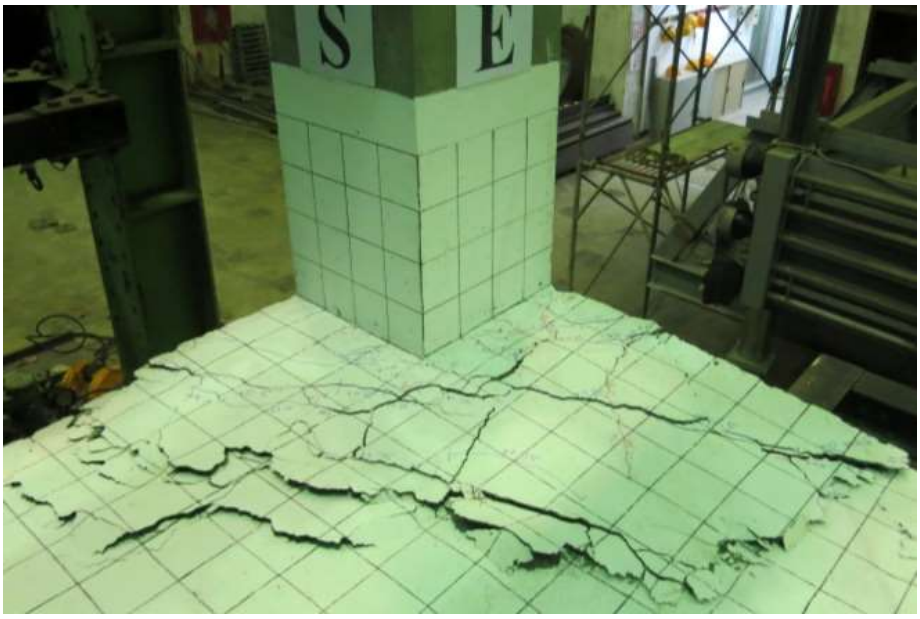

(a) At the End of the Test

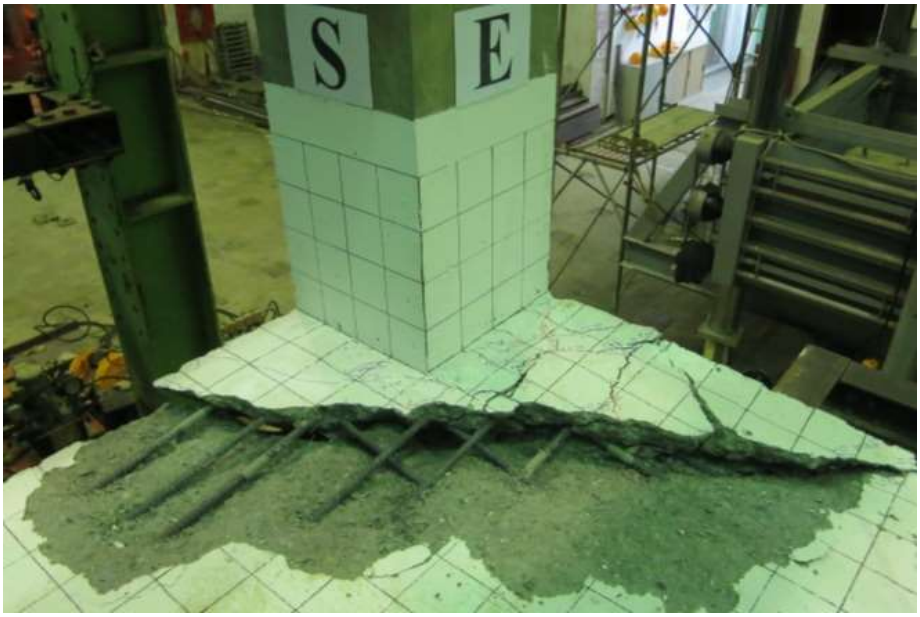

(b) After Loose Concrete Removal

Fig. 4.40 – Slab Top Surface of Specimen R1 at Failure

Fig. 4.41 – Slab Bottom Surface of Specimen R1 Near the Connection at Failure

4.3.5 Specimen R2

After application of the gravity shear, several fine cracks were observed on the bottom slab surface and on the north and west sides of the slab as shown in Fig. 4.42. During the 0.25% drift cycles, existing cracks extended accompanied by developments of some new cracks.

During the 1.25% drift cycles, as the specimen was loaded to the negative direction, a wide inclined crack appeared suddenly on the north and west slab faces, as shown in Fig. 4.43. At the end of this cycle, an attempt to adjust gravity load failed the connection suddenly. Gravity load dropped significantly after that and test was terminated.

The main inclined crack on the north slab face had an angle of about 20 degree as shown in Fig. 4.44. On the west face, the main inclined crack had an angle of about 18 degree as shown in Fig. 4.45. The damage was concentrated within a $4h$ to $5h$ distance from the inner column faces, as depicted on the top surface of the slab, as shown in Fig. 4.46. The damage on the bottom surface of the slab was concentrated within the diagonal, about 45 degrees with the slab edges, passing through the inner corner of the column, as shown in Fig. 4.47.

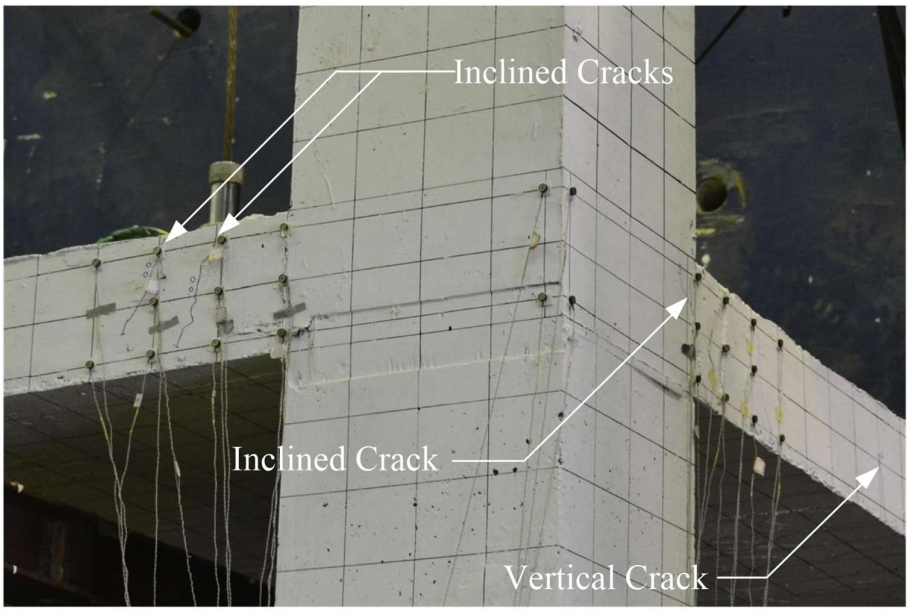

Fig. 4.42 – Crack Pattern of Specimen R2 at 0.00% Drift

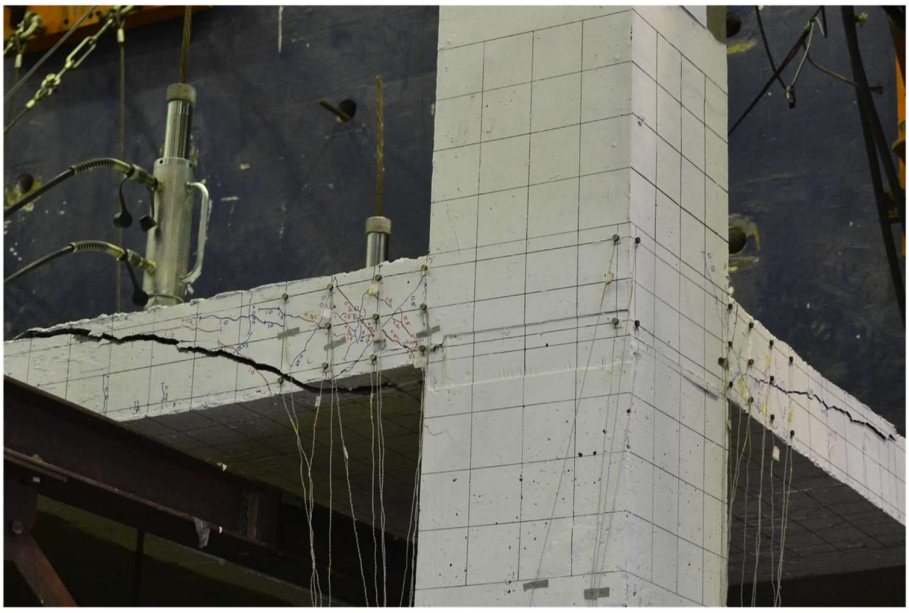

Fig. 4.43 – Crack Pattern on the North and West Slab Faces of Specimen R2 at 1.25% Drift

(a) At the End of the Test

(b) After Loose Concrete Removal

Fig. 4.44 – North Side of Specimen R2 at Failure

(a) At the End of the Test

(b) After Loose Concrete Removal

Fig. 4.45 – West Side of Specimen R2 at Failure

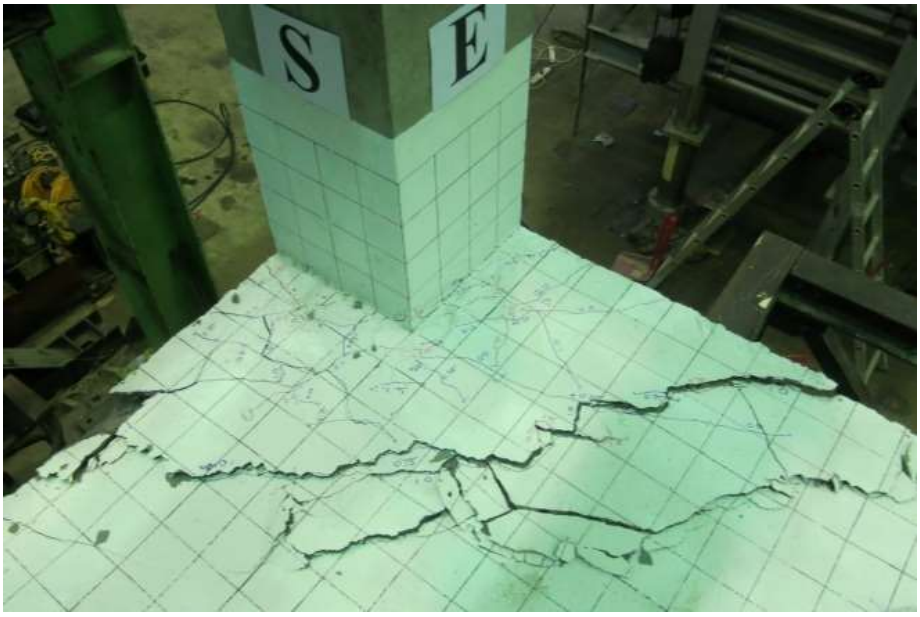

(a) At the End of the Test

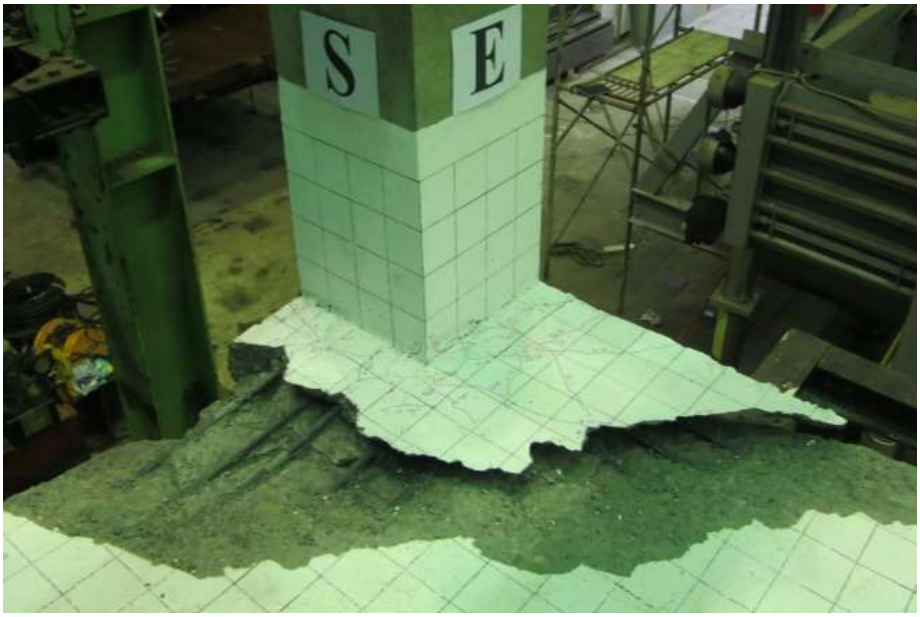

(b) After Loose Concrete Removal

Fig. 4.46 – Slab Top Surface of Specimen R2 at Failure

Fig. 4.47 – Slab Bottom Surface of Specimen R2 Near the Connection at Failure

4.3.6 Specimen R3

Before the test started, a minor crack was already observed on the north face of the slab as shown in Fig. 4.48. A fine vertical crack was also observed on the west face of the slab as shown in Fig. 4.49. These cracks were caused during the set up process. The presence of these initial cracks however, was believed to not significantly affect the overall behavior of the specimen.

Fine flexural cracks on the bottom surface of the slab were observed after the application of the target connection gravity shear. No new cracks were observed until the 0.50% drift level, wherein an inclined crack on the west slab face, near the column, was observed and became more apparent at 1.25% drift. The main inclined cracks on both the north and west slab faces were initiated during the 1.50% drift cycles and became apparent on the 1st cycle of 1.75% drift level as presented in Figs. 4.50 and 4.51. Gravity shear dropped significantly after completion of 1.75% drift cycles. However, an attempt to adjust the connection shear back to its target level resulted in significant vertical slab deformation but only moderate increase of connection shear. Due to safety concern, the gravity load was adjusted to a maximum connection gravity shear of about $1.50\sqrt{f_c'(\text{psi})}b_o d$ and specimens was then loaded to 2.00% drift cycles. Both

lateral force and gravity shear lost significantly before reaching the peak of the 1st positive 2.00% drift and the test was terminated then.

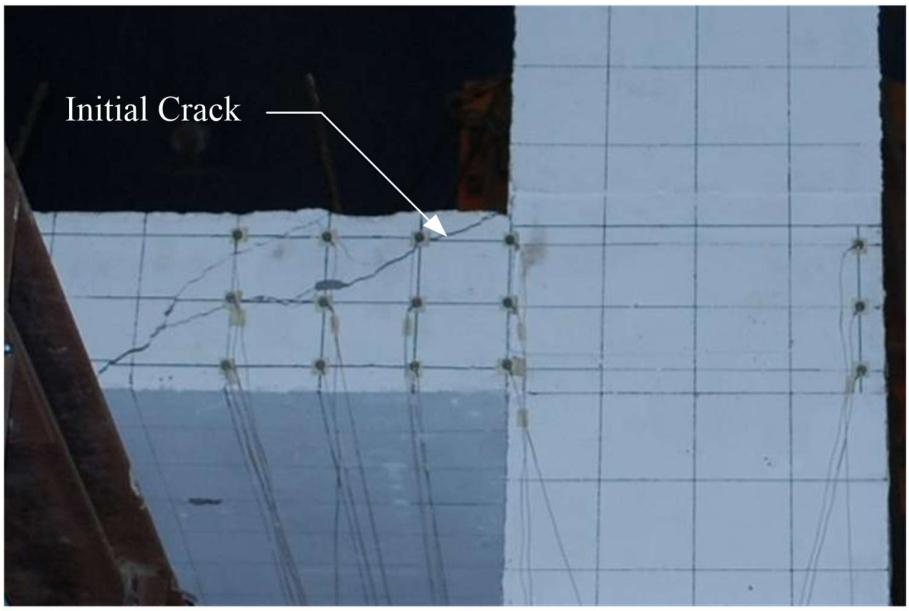

Fig. 4.48 – Initial crack on the North Face of the Slab of Specimen R3

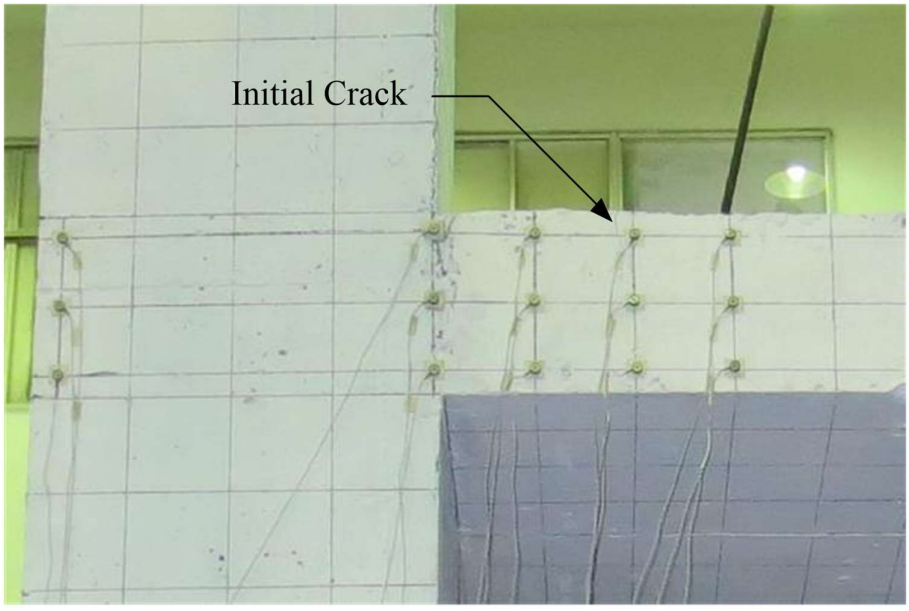

Fig. 4.49 – Initial Crack on the West Face of the Slab of Specimen R3

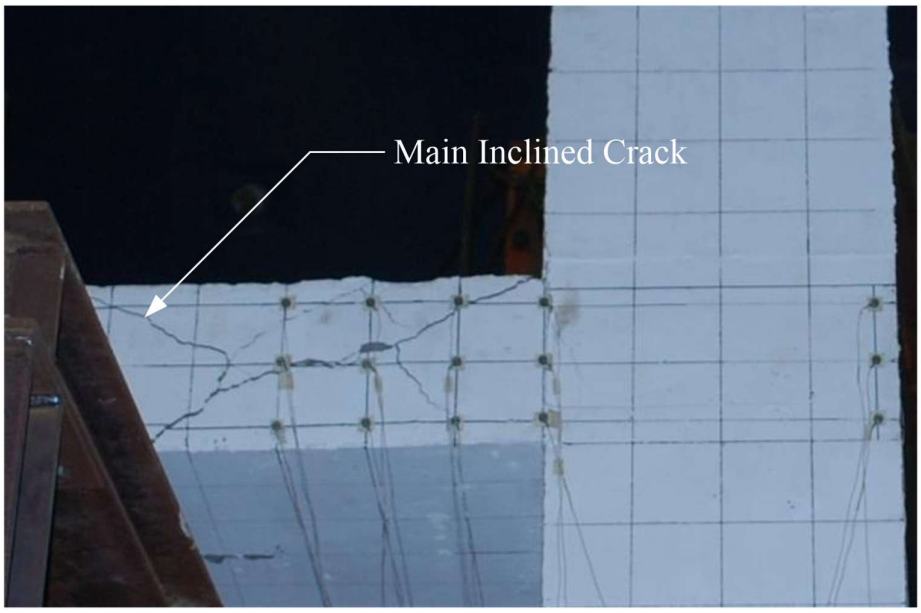

Fig. 4.50 – Crack Pattern on the West Slab Face of Specimen R3 at 1.75% Drift

Fig. 4.51– Crack Pattern on the West Slab Face of Specimen R3 at 1.75% Drift

The main inclined crack on the north face of the slab had an inclined angle of about 27 degree as shown in Fig. 4.52. On the west face of the slab, the main inclined crack had an inclined angle of about 27 degree as shown in Fig. 4.53. The damage was concentrated within a 4*h* distance from the inner column faces as depicted on the crack pattern on the top surface of the slab shown in Fig. 4.54. Aside from the chunk of concrete that fell off from the north face of

the slab, spalling on the bottom surface of the slab was only observed along the column perimeter, as shown in Fig. 4.55.

(a) At the End of the Test

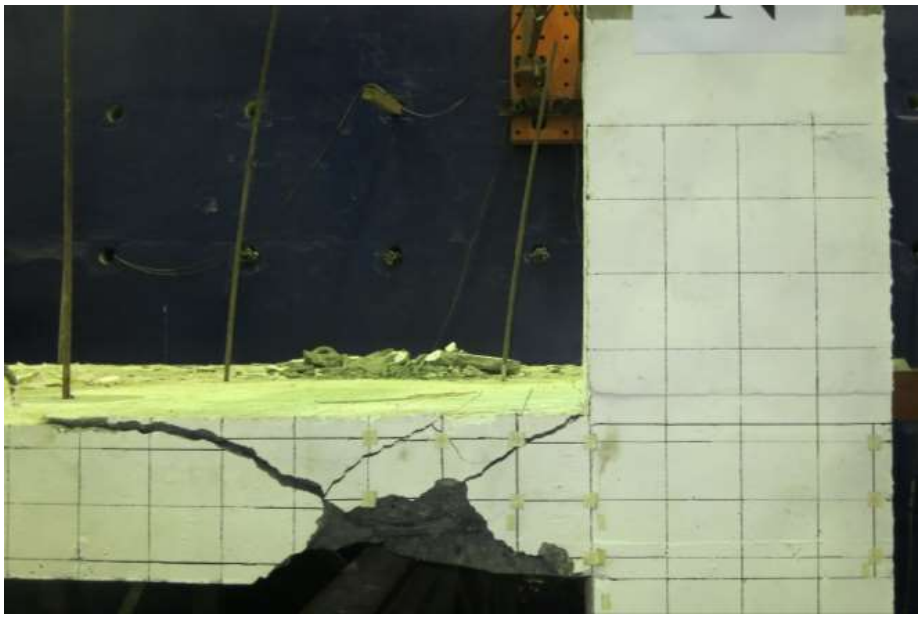

(b) After Loose Concrete Removal

Fig. 4.52 – North Side of Specimen R3 at Failure

(a) At the End of the Test

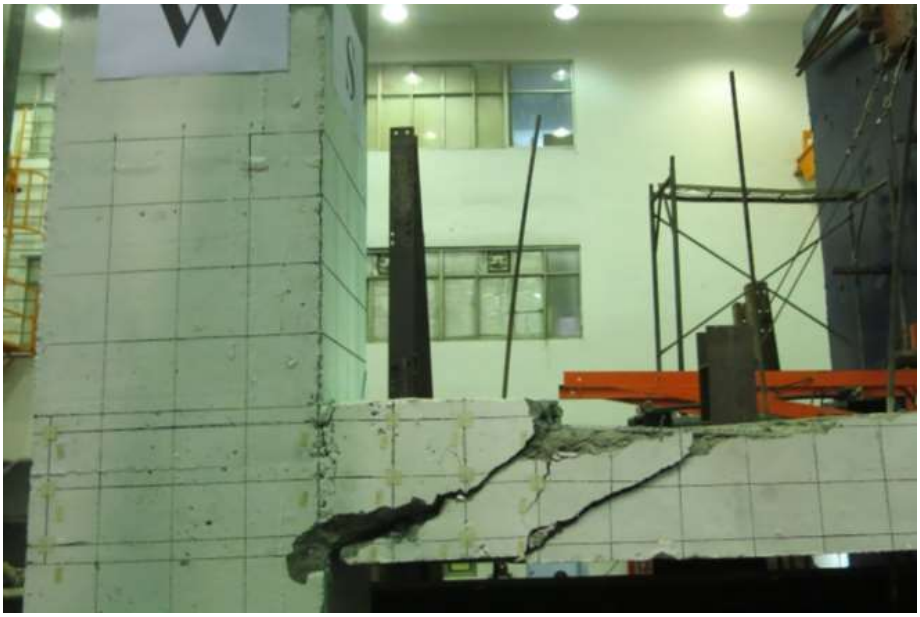

(b) After Loose Concrete Removal

Fig. 4.53 – West Side of Specimen R3 at Failure

(a) At the End of the Test

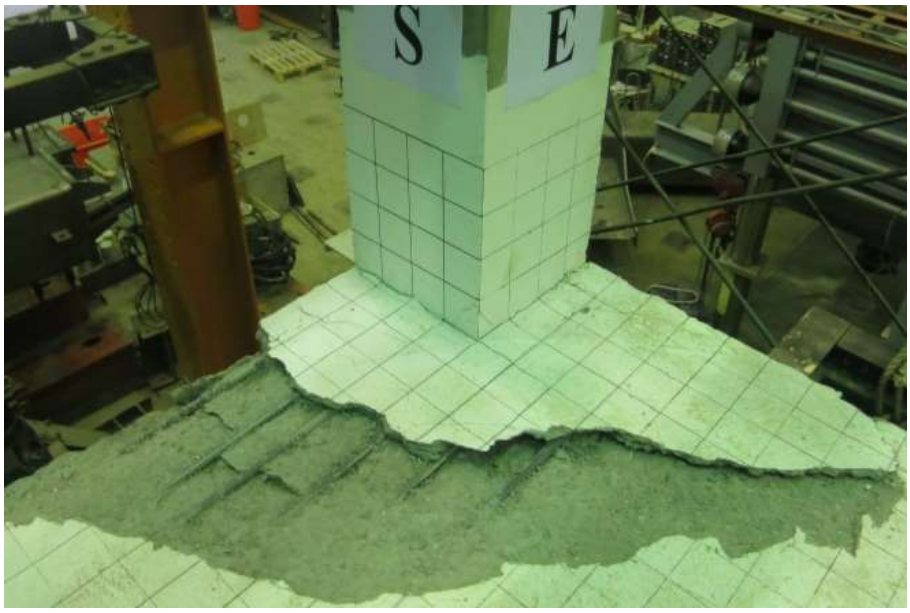

(b) After Loose Concrete Removal

Fig. 4.54 – Slab Top Surface of Specimen R3 at Failure

Fig. 4.55 – Slab Bottom Surface of Specimen R3 Near the Connection at Failure

4.4 GRAVITY SHEAR HISTORY AND LATERAL LOAD-DRIFT RESPONSE

The connection shear that is measured at the bottom of the column comprises of the shear caused by the gravity load and the induced shear due to the lateral displacement. In this report, the connection shear is denoted as V_o. And, gravity shear, denoted as V_g, is the connection shear at zero displacement. Histories of the connection shear and the vertical reactions among the four supports are presented in this section. The vertical reaction measured at bottom of each support is presented in percentage of the overall value including the slab self-weight and applied gravity load from the hydraulic jacks. Slab self-weight is assumed to be distributed equally among the four corner supports. The vertical corner supports (steel arms) are labeled based on their locations (S-W, S-E, and N-E corners), see Fig. 3.2.

Lateral loads of specimen G1 and G2 were only measured at the top of the column. Additional load cells were provided at the bottom supports for specimens G3, R1, R2 and R2 to monitor the horizontal reactions in both loading and transverse directions. Test results showed that reactions (load cell readings) in the loading direction at top of the column was practically equivalent to the value recorded at bottom. For consistency, the lateral load presented hereafter for each specimen was based on the measurements at top of the column. Drift was defined as the lateral displacement of the actuator divided by the distance between the centerline of the actuator and the bottom universal hinge support, which was measured to be 147 in.. Specimen ultimate drift, DR_u, is defined as either (1) the maximum drift achieved, when adjustment of connection gravity shear failed, or (2) the drift corresponding to 20% drop of lateral force from the peak on the positive lateral load-drift hysteretic response envelope, whichever is lesser.

4.4.1Specimen G1

The connection shear history of specimen G1 is presented in Fig. 4.56. In which, positive value for the vertical axis refers to compression. Horizontal red line represents the target connection shear of $1.20\sqrt{f_c'(\text{psi})}b_o d$. The initial value at zero time step accounts for the slab-self weight with an assumed slab density of 150 lb/ft^3. As can be seen, the measured connection gravity shear was $1.19\sqrt{f_c'(\text{psi})}b_o d$ just prior to the imposition of lateral displacement. The thick solid black lines in Fig. 4.56 indicate the adjustment of gravity load. History of support vertical reactions and the overall vertical reaction is presented in Fig. 4.57, and Fig. 4.58, respectively.

Results indicate that column support took about 50% of applied gravity load from the hydraulic jacks while the S-W and N-E steel arm each took about 20%.

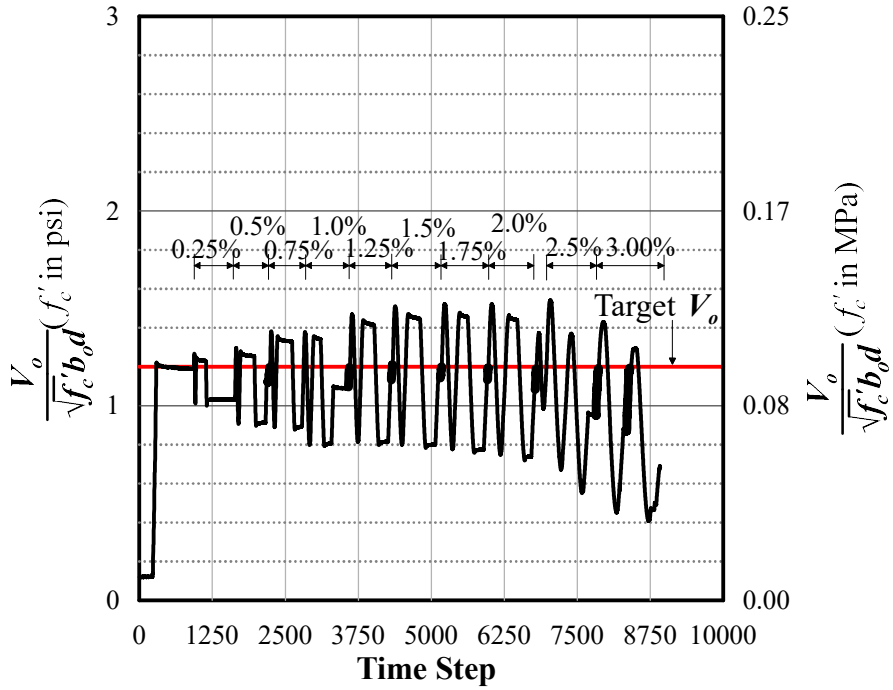

Fig. 4.56 – Connection Shear History of Specimen G1

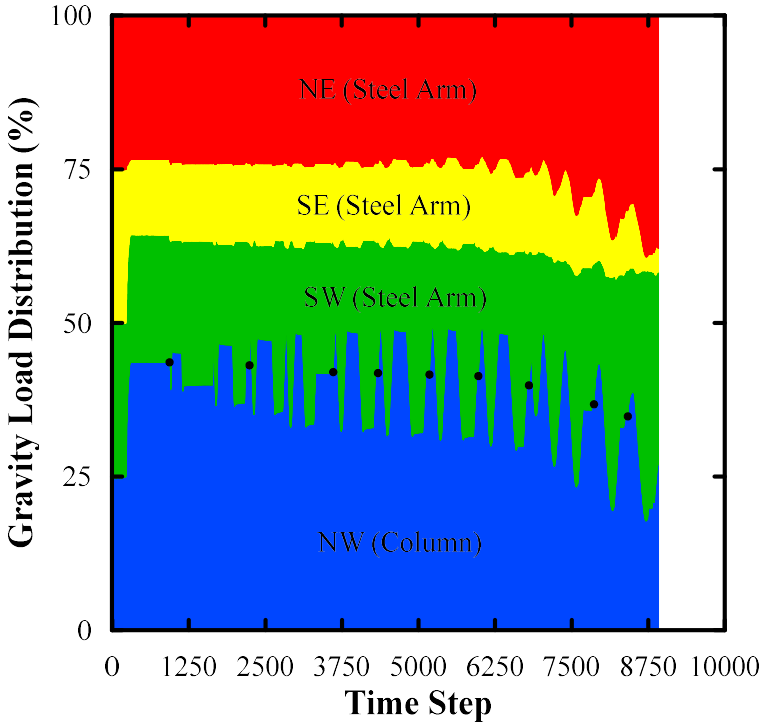

Fig. 4.57– Gravity Load Distribution History of Specimen G1

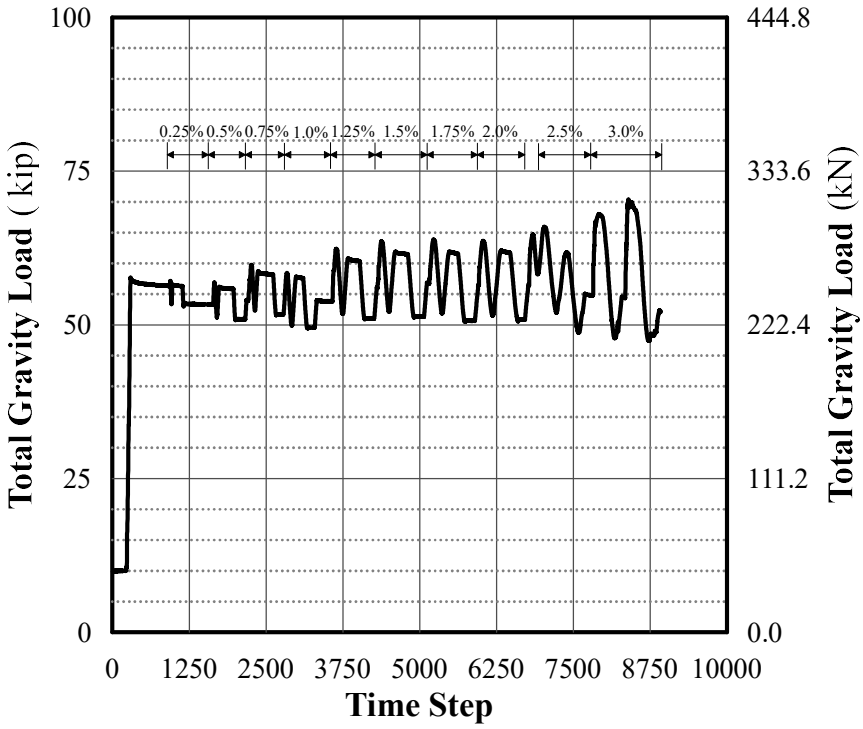

Fig. 4.58 – Total Gravity Load History of Specimen G1

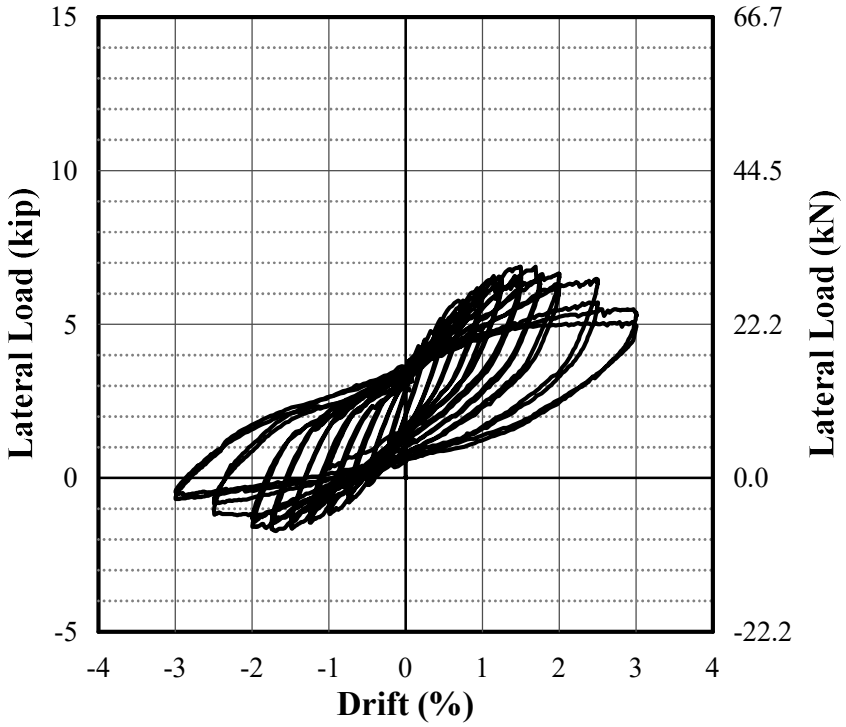

Fig. 4.59 – Lateral Load – Drift Response of Specimen G1

The lateral load-drift response of specimen G1 is presented in Fig. 4.59. Specimen G1 attained a maximum lateral load of 6.9 kips at +1.69% drift of the first cycle of 1.75% drift level. After achieving its peak, the lateral load degraded gradually as the specimens was loaded to larger displacement. At 1st cycle of +3.00% drift, the lateral load resistance was only 81% of the maximum lateral resistance. The connection gravity shear dropped significantly after the completion of 3.00% drift cycles. An attempt to adjust the gravity shear back to its target level failed and that led to termination of the test. The envelope of the lateral load-drift response of Specimen G1 is presented in Fig. 4.60. The ultimate drift, DR_u ,based on the definition earlier, is 3.00%, and the corresponding connection gravity shear, V_g, based on the last adjustment of the gravity load right before the 3.00% drift cycles is $1.19\sqrt{f_c'(\text{psi})}b_o d$.

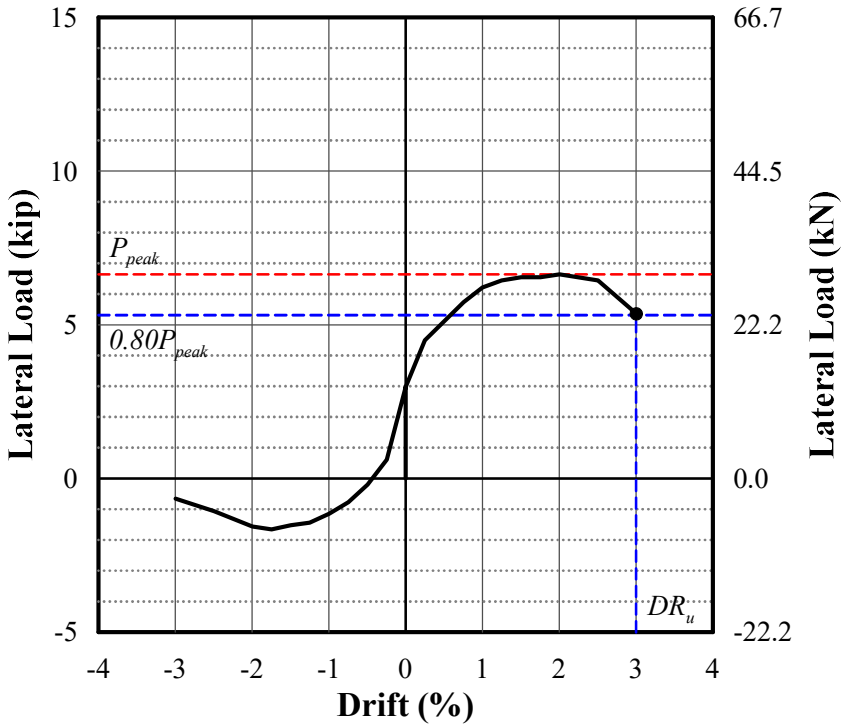

Fig. 4.60 – First Cycle Envelope Response of Specimen G1

4.4.2 Specimen G2

Specimen G2 had a target connection shear of $2.00\sqrt{f_c'(\text{psi})}b_o d$. However, it failed suddenly before reaching its target level (solid red line) as shown in Fig. 4.61. As a result, the lateral load-drift response is not available. Instead, the lateral load history is presented in Fig. 4.62. The specimen attained its maximum lateral load of 3.28 kips. The largest connection shear was

$1.89\sqrt{f_c'(\text{psi})}\,b_o d$ which is taken as V_g later in the analysis. The gravity load distribution of specimen G2 among the vertical supports is shown in Fig. 4.63. As can be seen, the column support took about 45% of the total gravity load (Fig. 4.64) prior to failure.

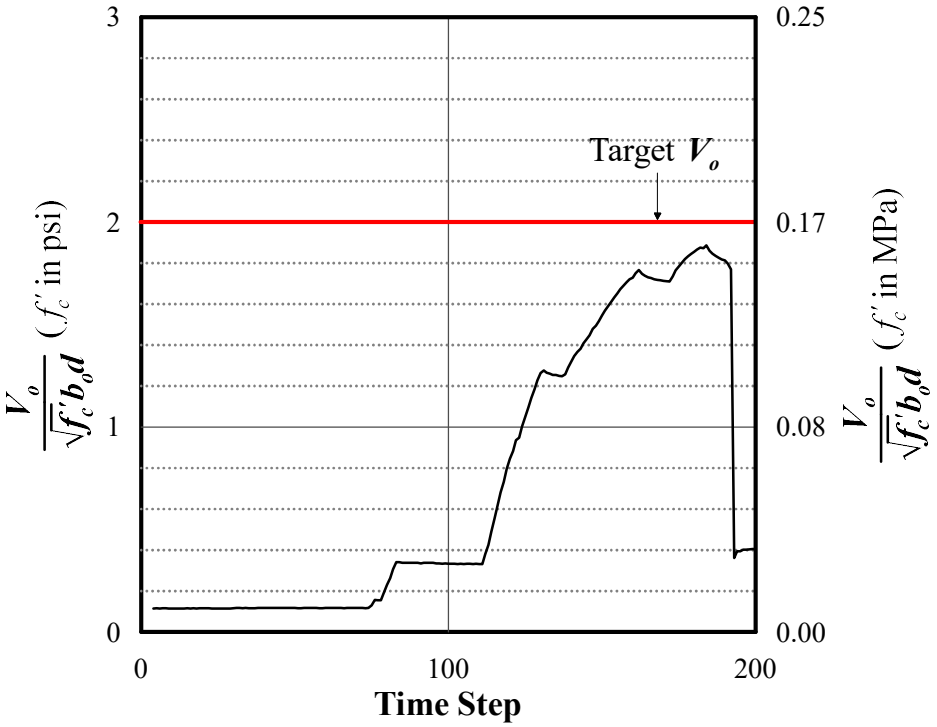

Fig. 4.61 – Connection Shear History of Specimen G2

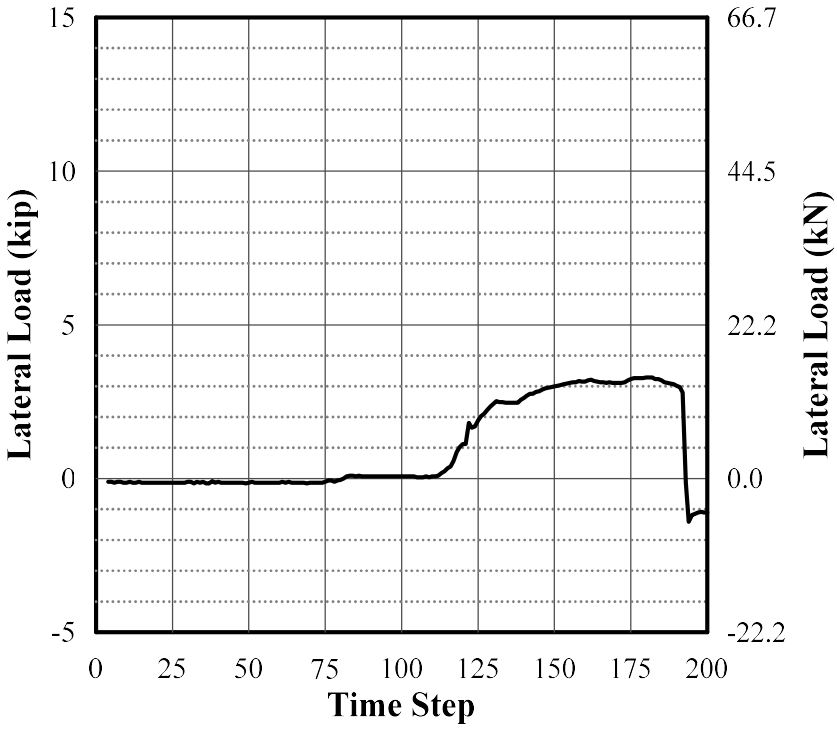

Fig. 4.62 – Lateral Load History of Specimen G2

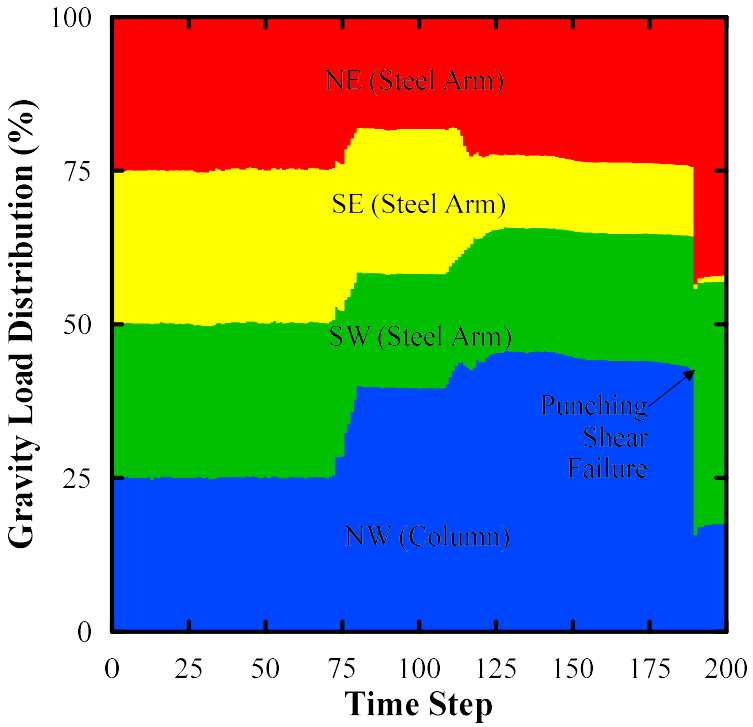

Fig. 4.63 – Gravity Load Distribution History of Specimen G2

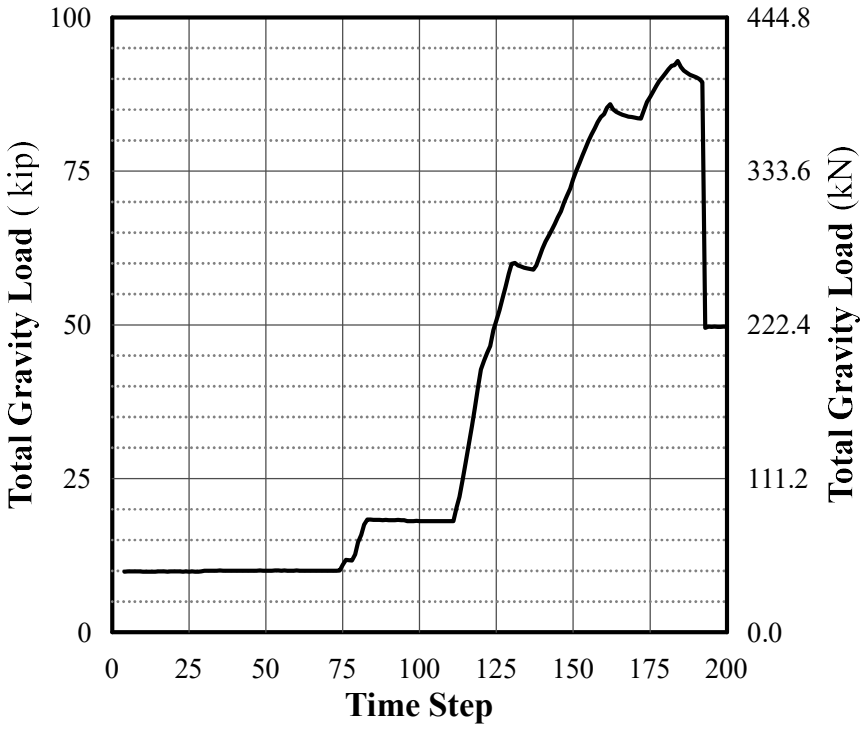

Fig. 4.64 – Total Gravity Load History of Specimen G2

4.4.3 Specimen G3

Specimen G3 had a target connection shear of $1.60\sqrt{f_c'(\text{psi})}b_o d$. The history of connection shear is shown in Fig. 4.65. The gravity shear was not sustained well in the 0.25% drift cycles. The gravity load distribution among the supports is presented in Fig. 4.66, while the overall gravity load is presented in Fig. 4.67. Similar to the previous two specimens, the column support took around 45% of the overall applied gravity load. The lateral load-drift response of specimen G3 is presented in Fig. 4.68.

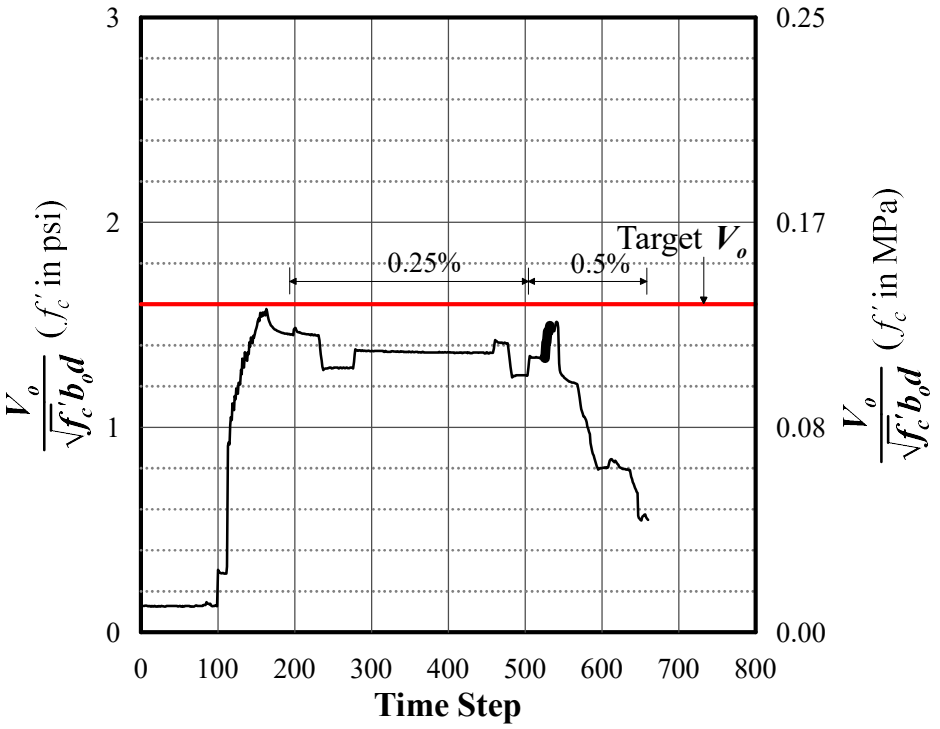

Fig. 4.65 – Connection Shear History of Specimen G3

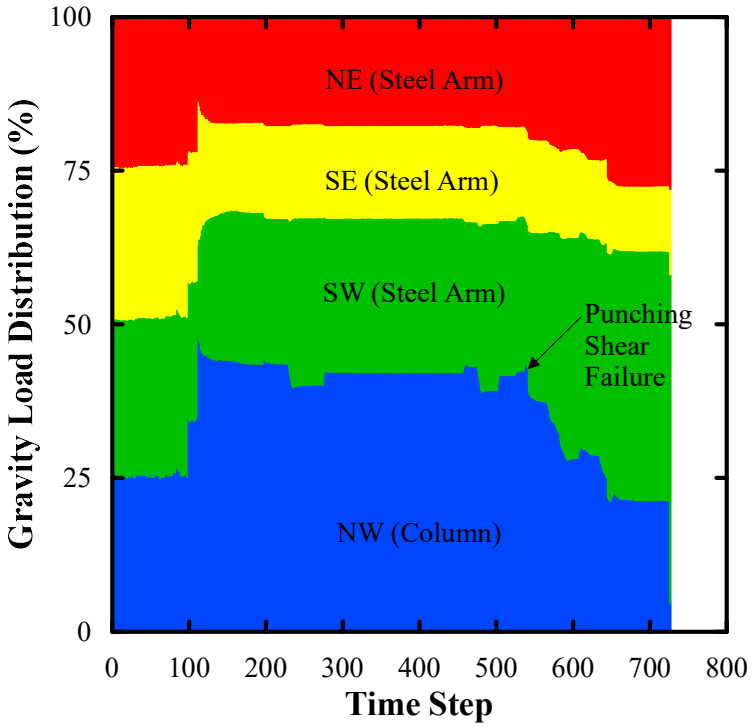

Fig. 4.66 – Gravity Load Distribution History of Specimen G3

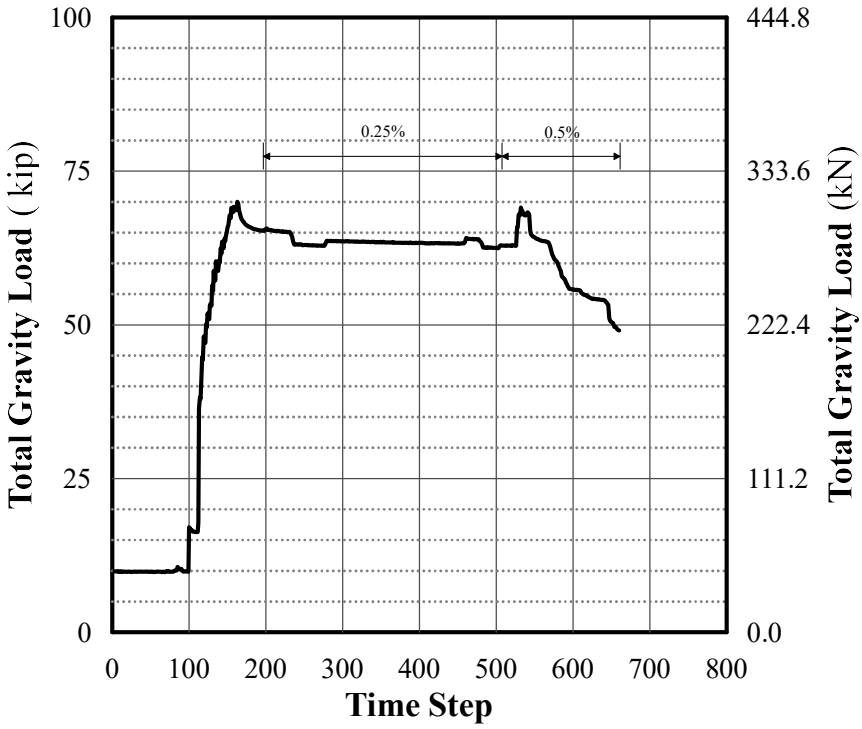

Fig. 4.67 – Total Gravity Load History of Specimen G3

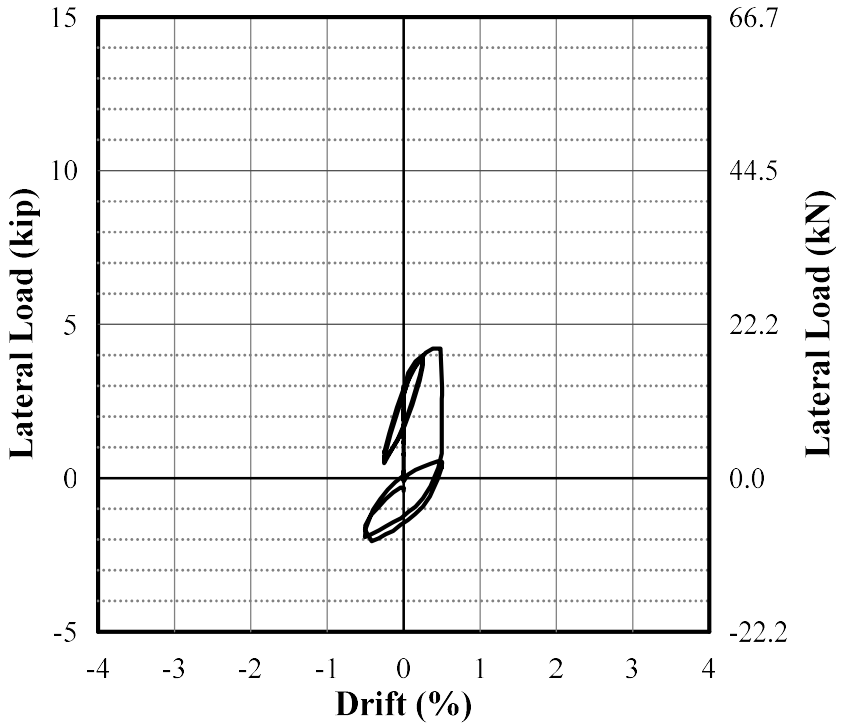

Fig. 4.68 – Lateral Load – Displacement Response of Specimen G3

As can be seen from Fig. 4.65, gravity load was adjusted after completion of 0.25% drift cycles but the adjustment only reached a connection gravity shear level of $1.47\sqrt{f_c'(\text{psi})}b_o d$. Nonetheless, succeeding displacement cycles were continued. The specimen attained a maximum lateral force of 4.21 kips at +0.38% of the 1st cycle of 0.50% drift level. The maximum lateral load was relatively sustained until +0.48% of the 1st cycle of 0.50% drifts cycles; then, the lateral load suddenly dropped. The specimen was failed by punching shear at this point. The succeeding cycles were continued but lateral load resistance was not recovered, as shown in Fig. 4.68. The ultimate drift, DR_u, of specimen G3 as shown in Fig. 4.69, is only about 0.50% and the corresponding connection gravity shear, V_g, is $1.50\sqrt{f_c'(\text{psi})}b_o d$.

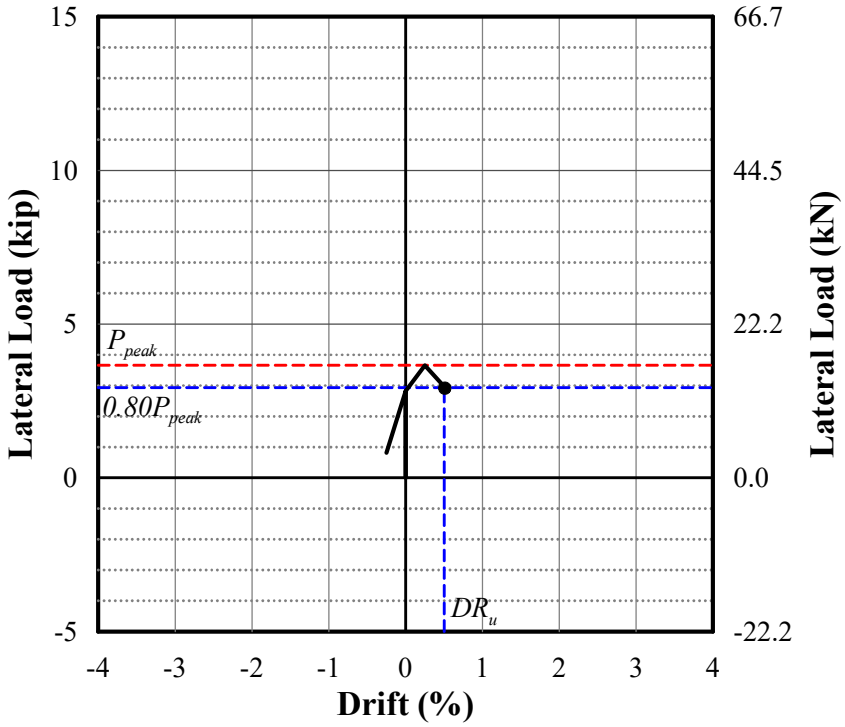

Fig. 4.69 – First Cycle Envelope Response of Specimen G3

4.4.4 Specimen R1

Specimen R1 had a target connection shear of $1.2\sqrt{f_c'(\text{psi})}b_o d$. The connection shear history is presented in Fig. 4.70 that shows that the measured gravity shear just before the imposition of lateral displacement was $1.28\sqrt{f_c'(\text{psi})}b_o d$. Consistently, based on the gravity load distribution

history presented in Fig. 4.71, the total gravity load (Fig. 4.72) was shared among the corner supports as follows: NW column supported around 45% of the total gravity load; 20% was carried by the SW steel arm; SE steel arm took the about 15%; and the remaining 20% went to NE steel arm. The specimen lateral load-drift response is presented in Fig. 4.73. The recorded lateral load prior to the imposition of lateral displacement was around 3.5 kips.

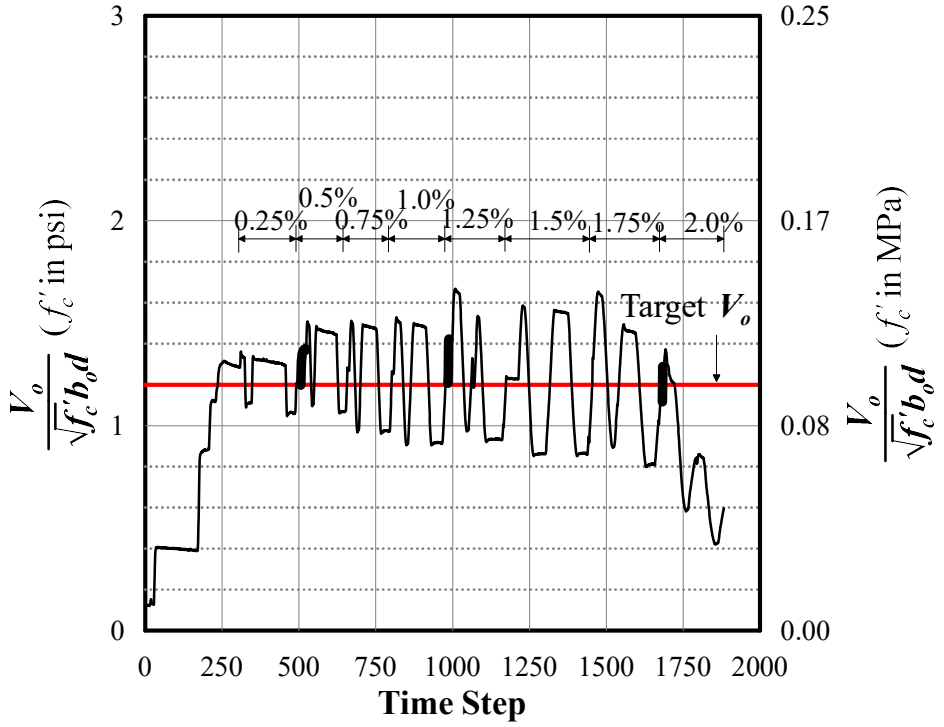

Fig. 4.70 – Connection Shear History of Specimen R1

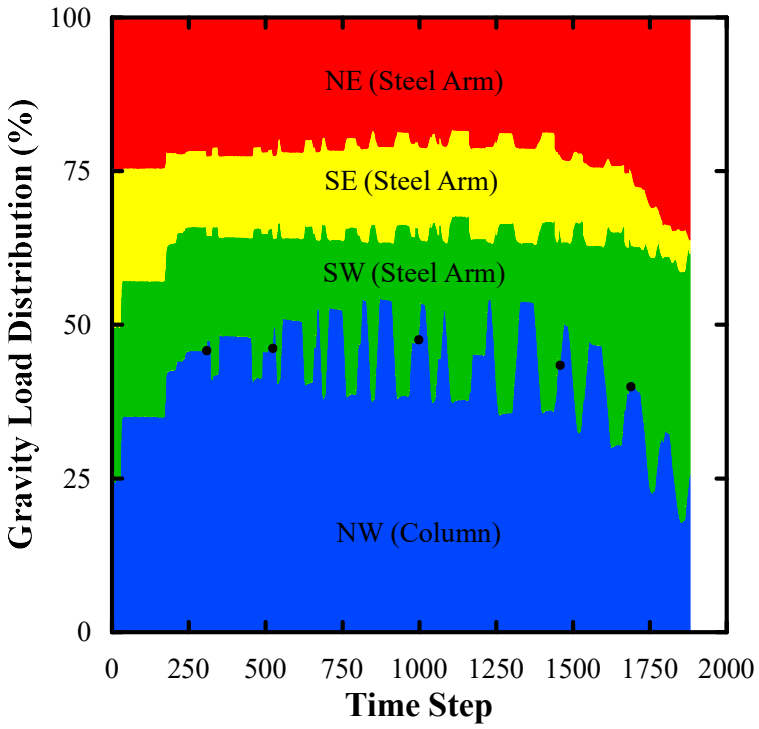

Fig. 4.71 – Gravity Load Distribution History of Specimen R1

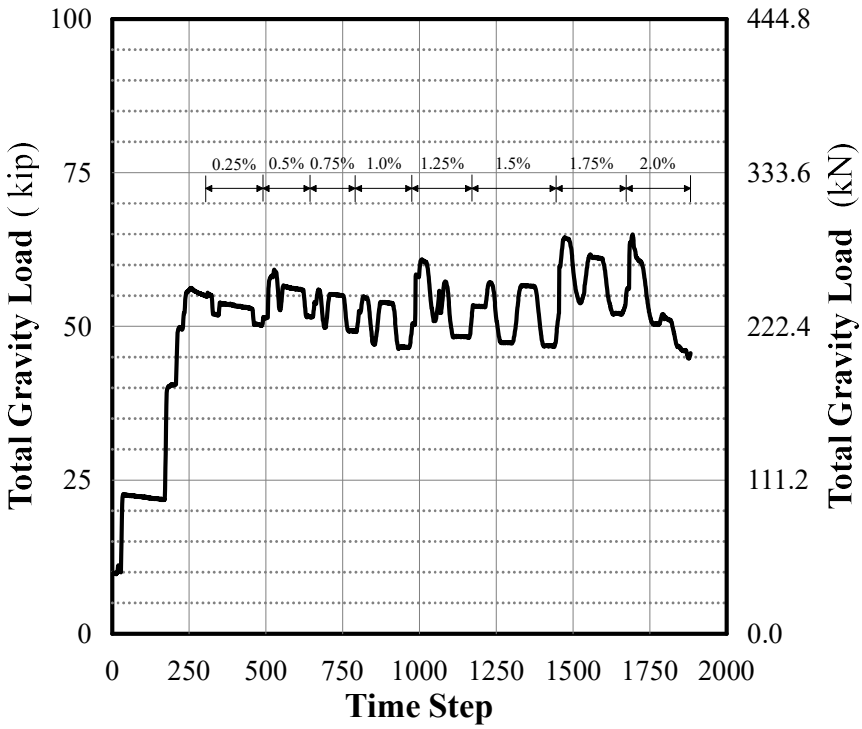

Fig. 4.72 – Total Gravity Load History of Specimen R1

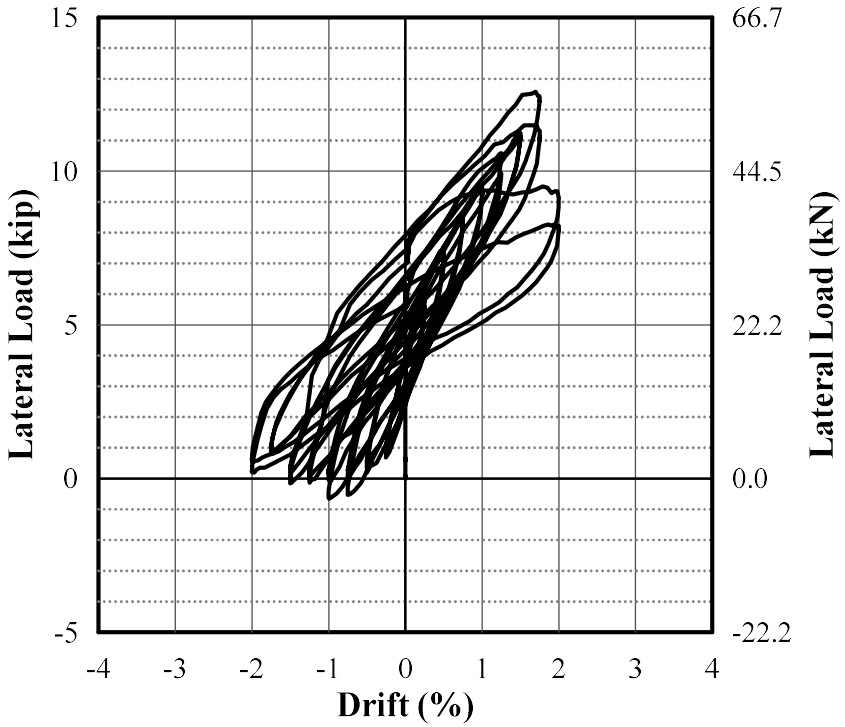

Fig. 4.73 – Lateral Load – Displacement Response of Specimen R1

Specimen R1 sustained a maximum connection shear of $1.67\sqrt{f_c'(\text{psi})}b_o d$ at 1.23% drift during the 1st 1.25% drift cycles. At this point, the corresponding lateral load was 10.56 kips. The specimen achieved a maximum lateral load of 12.59 kips at +1.70% of the 1st cycle of 1.75% drift level. The connection shear at this point was $1.65\sqrt{f_c'(\text{psi})}b_o d$. However, lateral load decreased in the repeated cycle of 1.75% drift. Gravity load appears to be redistributed among the supports during the 1.75% drift cycles, as shown in Fig. 4.71. After completion of 1.75% drift cycles, gravity load was adjusted and the connection was able to sustain the target gravity load back to its target level. Test continued as a result. During the 1st cycle of 2.00% drift, both stiffness and peak strength decreased. At the 2.00% drift, the lateral force was 9.13 kips, which was about 73% of the peak lateral force. The envelope of lateral load-drift response for specimen R1 is presented in Fig. 4.74. Based on the definition earlier, the ultimate drift, DR_u, of specimen R1 is about 1.9% and the corresponding connection gravity shear, V_g, based on the last adjustment of the gravity load is $1.30\sqrt{f_c'(\text{psi})}b_o d$.

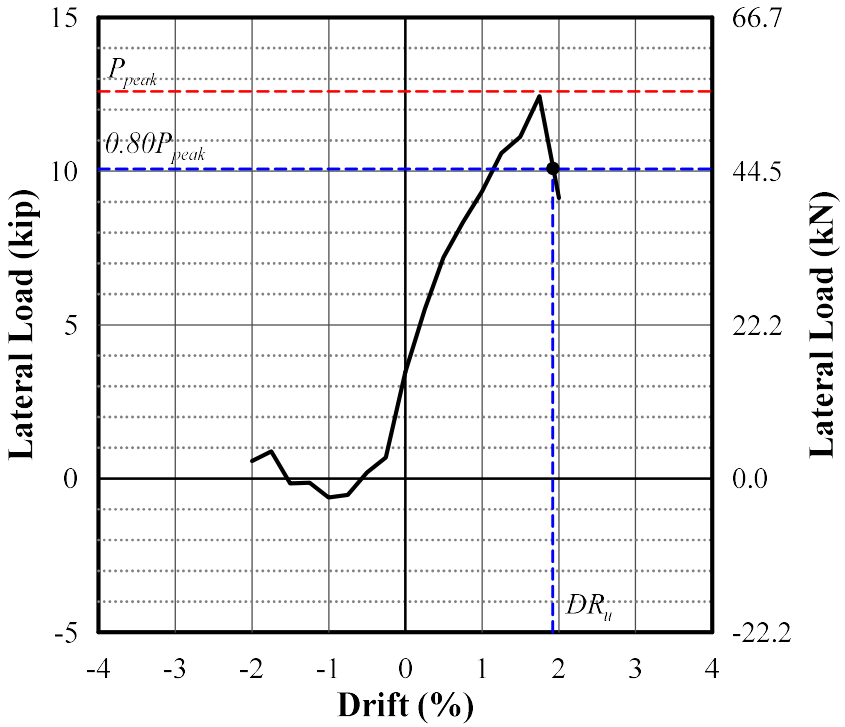

Fig. 4.74 – First Cycle Envelope Response of Specimen R1

4.4.5 Specimen R2

Specimen R2 had a target connection gravity shear of $2.00\sqrt{f_c'(\text{psi})}b_o d$ and its connection shear history is presented in Fig. 4.75. Based on the gravity load distribution history of specimen R2 shown in Fig. 4.76, this connection shear was about 50% of the total gravity load applied on the slab (Fig. 4.77). The other 50% was shared by the three corner supports. The lateral load-drift response of specimen R2 is presented in Fig. 4.78. The lateral force right before the application of lateral displacement was 5.14 kips.

Specimen R2 had reached a maximum lateral load of 8.64 kips at +0.58% of the 1st cycle of 0.75% drift. This lateral load resistance was roughly maintained up to 1.25% drift. The corresponding connection shear at peak lateral load was $2.15\sqrt{f_c'(\text{psi})}b_o d$. With the adjustments of gravity load during the test, specimen R2 managed to sustain its target connection shear until the 1st cycle of 1.25% drift.

When the specimen was displaced toward the negative direction in the 1st cycle of 1.25% drift, a major inclined crack formed and opened significantly and that accompanied by a sudden

change (kink) of the lateral load at around -0.50% drift as shown in Fig. 4.78. No succeeding drift cycles were imposed to the specimen because specimen R2 was not able to sustain the connection shear adjustment after the completion of this cycle. The lateral load-drift response envelope is presented in Fig. 4.79. The ultimate drift, DR_u, of specimen R2 is 1.25% and the corresponding connection gravity shear, V_g, is $2.02\sqrt{f_c'(\text{psi})}b_o d$.

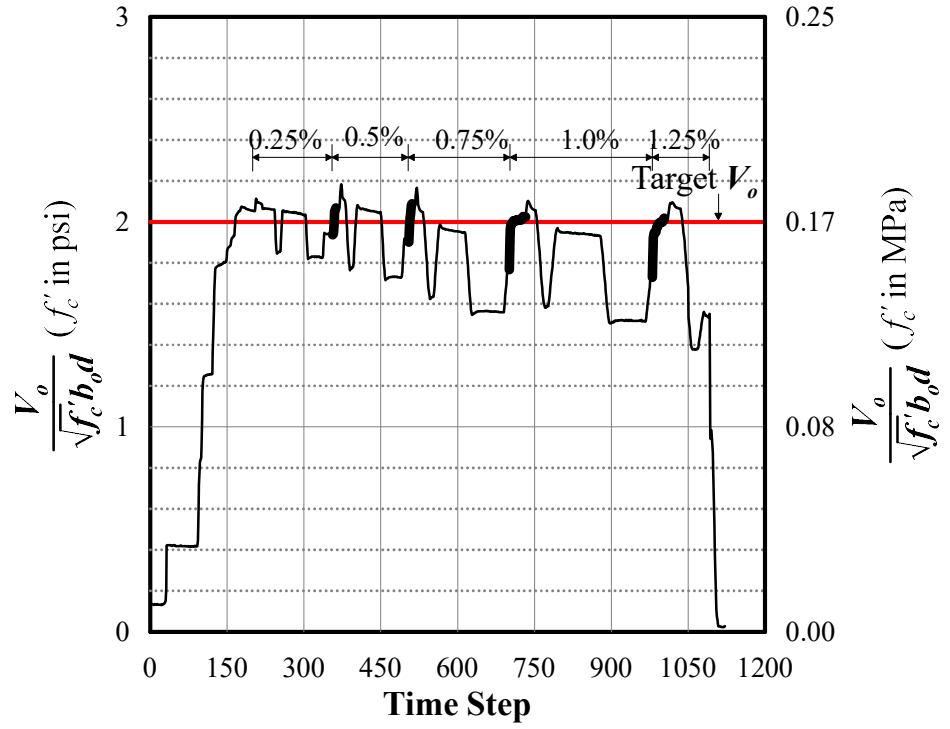

Fig. 4.75 – Connection Shear History of Specimen R2

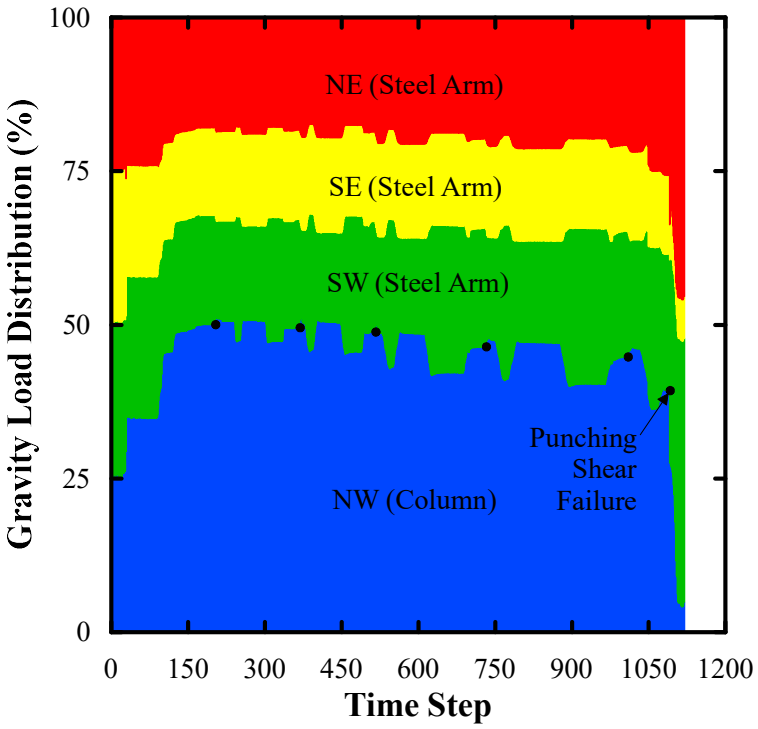

Fig. 4.76 – Gravity Load Distribution History of Specimen R2

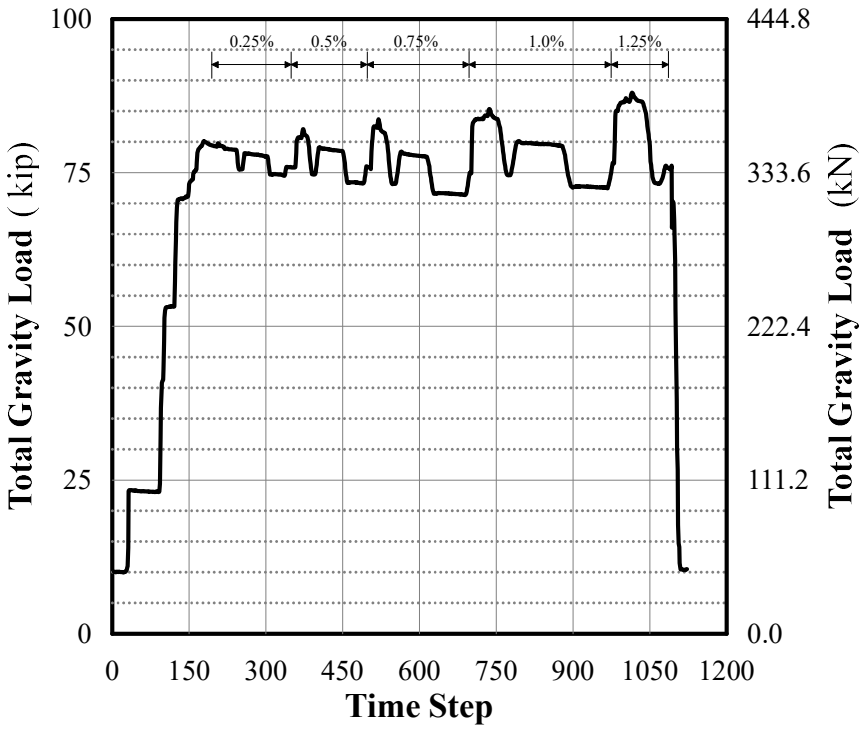

Fig. 4.77 – Total Gravity Load History of Specimen R2

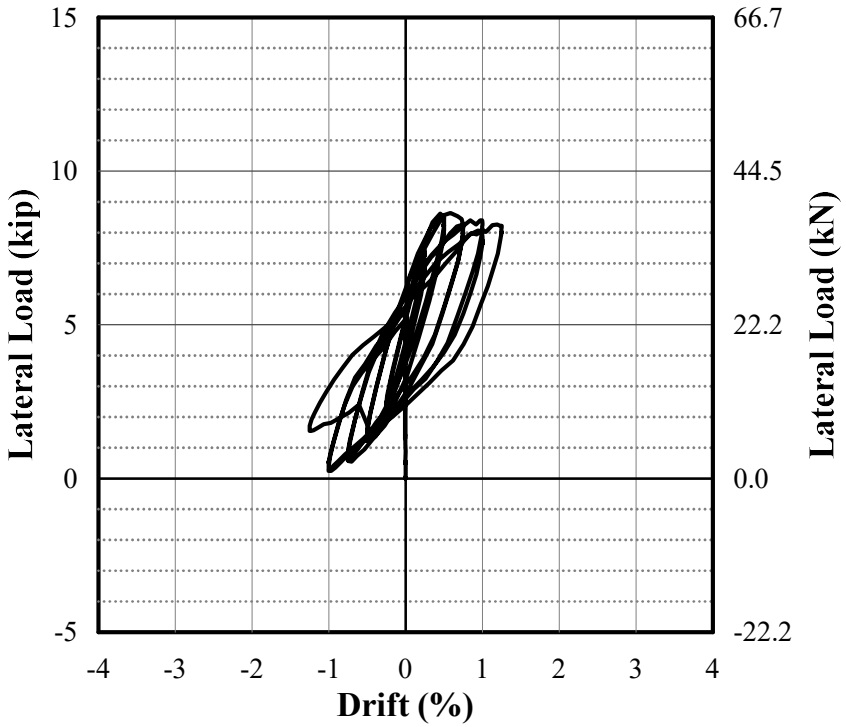

Fig. 4.78 – Lateral Load – Displacement Response of Specimen R2

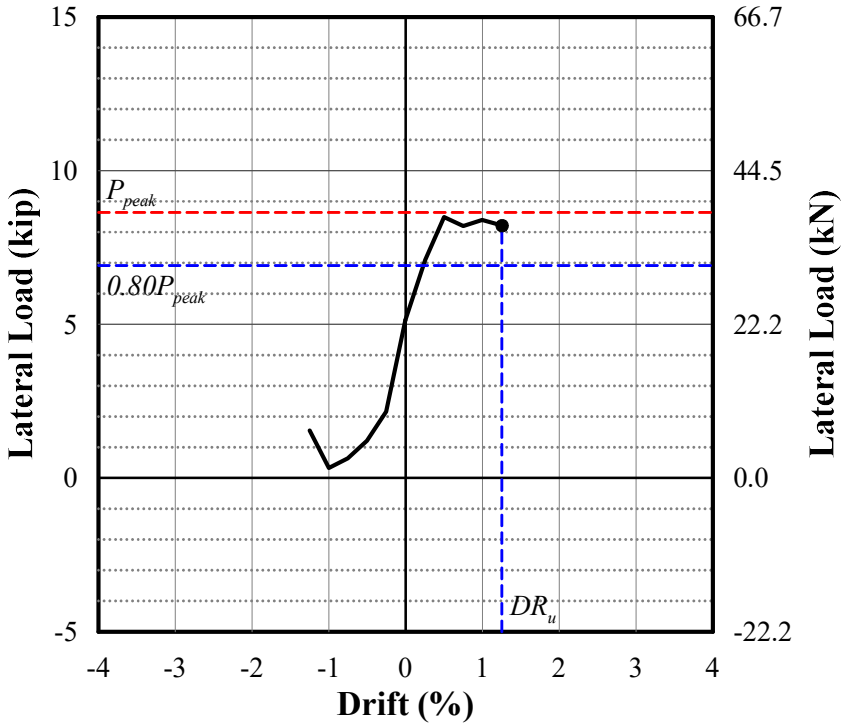

Fig. 4.79 – First Cycle Envelope Response of Specimen R2

4.4.6 Specimen R3

Specimen R3 had a target connection shear of $1.60\sqrt{f_c'(\text{psi})}b_o d$. The connection shear history is presented in Fig. 4.80. Prior to the imposition of lateral displacement, the connection shear was about $1.48\sqrt{f_c'(\text{psi})}b_o d$. Based on the gravity load distribution (Fig. 4.81), this connection shear was about 45% of the total gravity load applied on the slab (Fig. 4.82). The lateral load prior to the imposition of lateral displacement was 2.03 kips.

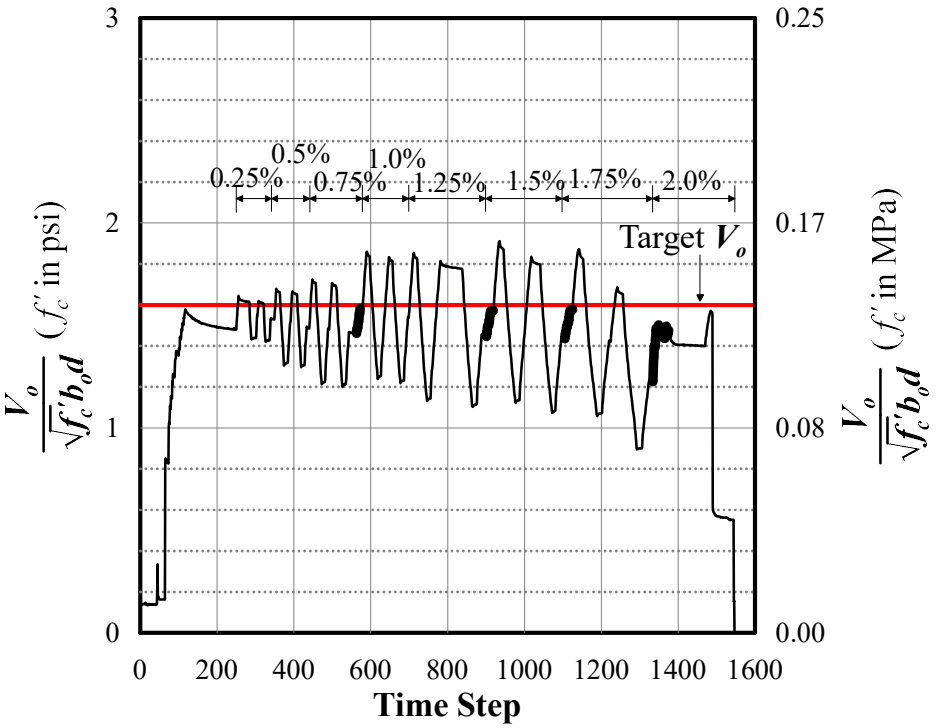

Fig. 4.80 – Connection Shear History of Specimen R3

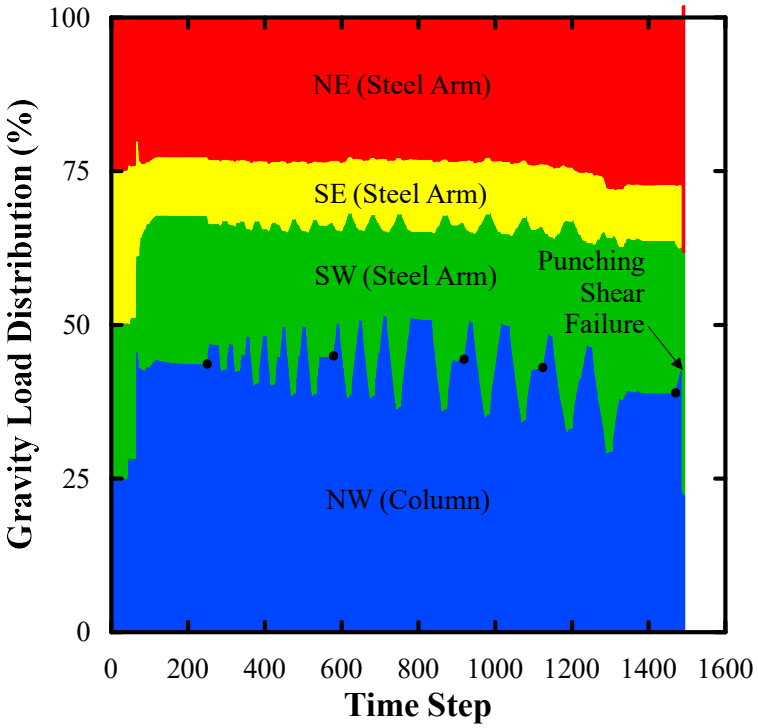

Fig. 4.81 – Gravity Load Distribution History of Specimen R3

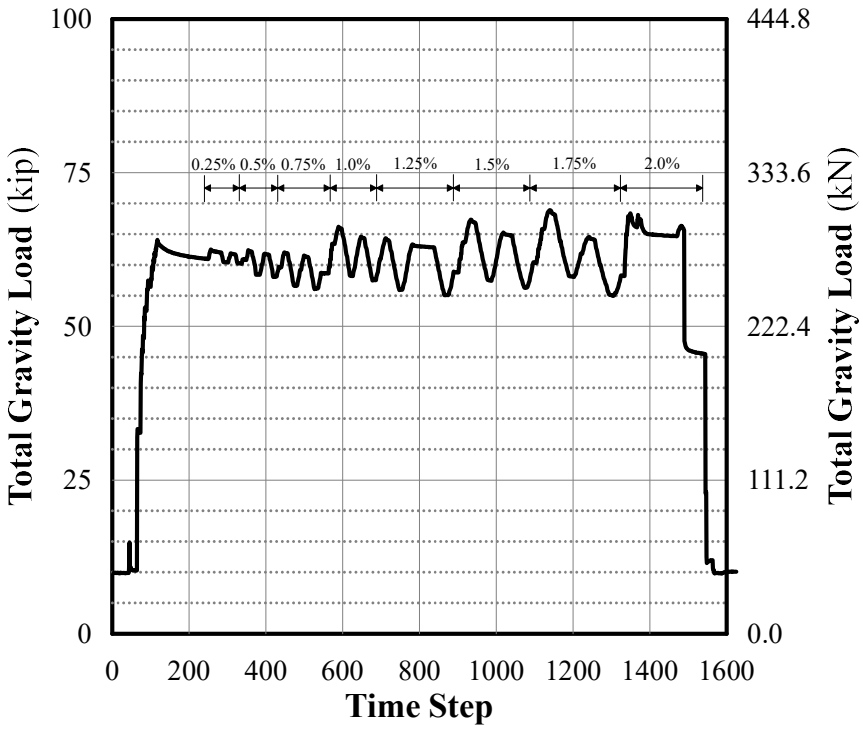

Fig. 4.82 – Total Gravity Load History of Specimen R3

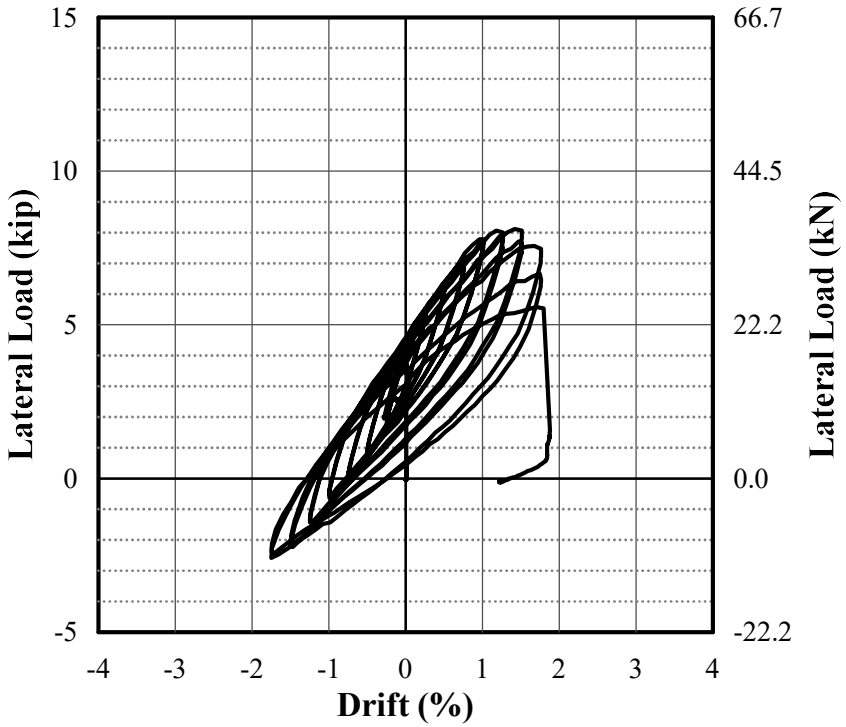

Fig. 4.83 – Lateral Load – Displacement Response of Specimen R3

The lateral load-drift response of specimen R3 is presented in Fig. 4.83. The performance of the specimen was quite stable and had reached a maximum lateral force of 8.11 kips at +1.42% of the 1st cycle of 1.50% drift. The connection shear at maximum lateral force was about $1.91\sqrt{f_c'(\text{psi})}b_o d$. The lateral force had deceased thereafter.

The degradation of lateral stiffness of specimen R3 was relatively quick after the maximum lateral resistance was attained. When the specimen was displaced toward +2.00% drift (1st cycle), the lateral force suddenly dropped at +1.80% drift, as shown in Fig. 4.83. Connection shear dropped simultaneously at this moment, see Fig. 4.80. The ultimate drift, DR_u, of specimen R3 is 1.75% and the corresponding connection gravity shear, V_g, based on the last adjustment is $1.48\sqrt{f_c'(\text{psi})}b_o d$.

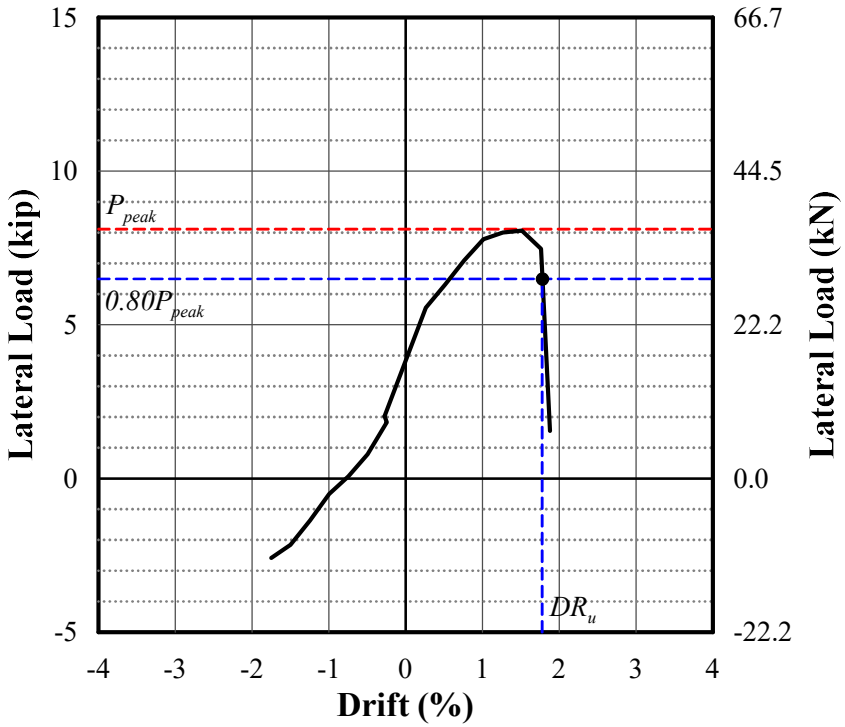

Fig. 4.84 – First Cycle Envelope Response of Specimen R3

4.5 CONNECTION ROTATION

Slab rotation was monitored using two types of instrumentations. The first one was LVDTs which were used for specimens G1 and G2 to measure the slab rotation at a d distance away from east and south faces of the column. For specimens G3, R1, R2, and R3, an optical tracking system was employed on the north and west sides of the slab to record slab rotations at $0.5h$, h and $1.5h$ distances away from the column face. As a result, the slab rotation in the north-south (lateral loading) and east-west (transverse to the lateral loading) direction is determined based on markers on the west and north sides of the slab, respectively, see Fig. 3.17.

Histories of the slab rotations are presented in Fig. 4.85 to Fig. 4.90. In those figures, rotation values are plotted with respect to the left vertical axis. Positive rotation refers to the length increased at top of the slab more than the length increased at bottom of the slab. Connection gravity shear history, which is plotted with respect to the right vertical axis, is also provided in the figure for comparison. Except specimen G2, slab rotations typically increases as the specimen drift increases. Slab rotation in the north-south (lateral loading) direction is typically larger than that in the east-west direction within the same distance away from the column face.

For specimen G1, in the loading direction as shown in Fig. 4.85, approximately 67% of the system drift is attributed to the slab rotation within a *d* distance from the column face at peaks of the positive 1.5% drift. The ratio between the slab rotation and the system drift increases to more than 90% at peaks of the positive 2.5% drift. Slab rotation in the loading direction continues to increase up to approximately 3.0% radians before the specimen failed in punching during the 3.0% drift cycles.

For specimen G2, in the loading direction shown in Fig. 4.86, slab rotation within a *d* distance away from the column face increases to approximately 2.5% radians before the slab failed in punching.

For specimen G3, results from Fig. 4.87 indicate that the slab rotation in the loading direction appears to be approximately equal within a 0.5*h*, between 0.5*h* and 1.0*h*, and between 1.0*h* and 1.5*h* distance away from the column face. At the 1st peak of positive 0.5% drift, before the connection failed in punching, the recorded maximum slab rotation in the loading direction is around 0.5%, 1.0% and 1.5% radians within a 0.5*h*, 1.0*h*, and 1.5*h* distance away from the column face, respectively.

As can be seen from Fig. 4.88, results from specimen R1 indicate that slab rotation in the loading direction is concentrated within a 0.5*h* distance away from the column face during the 2.0% drift cycles. As the specimen was loaded to the peak of the 2nd cycle at positive 2.0% drift, the recorded maximum rotation within a 0.5*h* distance is around 2.0% radian. Connection gravity shear is not able to be recovered after that.

For specimen R2, shown in Fig. 4.89, slab rotation in the loading direction also appears to be concentrated within a 0.5*h* distance away from the column face in the 1.25% drift cycles, the last drift cycle before the specimen failed in punching. At peak of the 1st positive 1.25% drift, the maximum slab within a 0.5*h* distance away from the column face is approximately 1.25% radians.

Specimen R3 has slab rotation concentrated within a 1.0*h* distance from the column face in the loading direction, Fig. 4.90. The maximum rotation within a 1.0*h* distance from the column face in the loading direction is about 2.0% radians, as the specimen failed in punching during the 2.0% drift cycles.

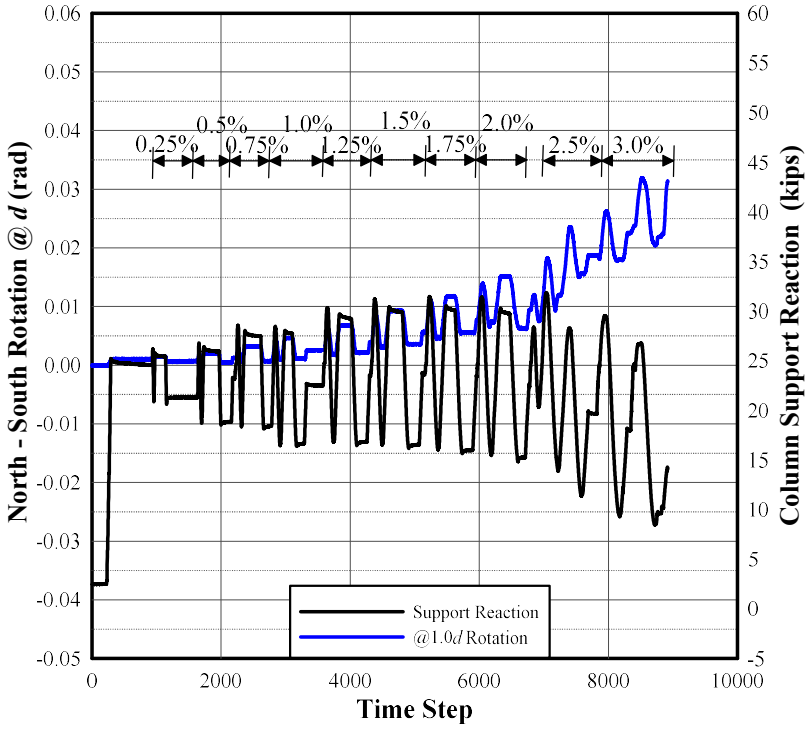

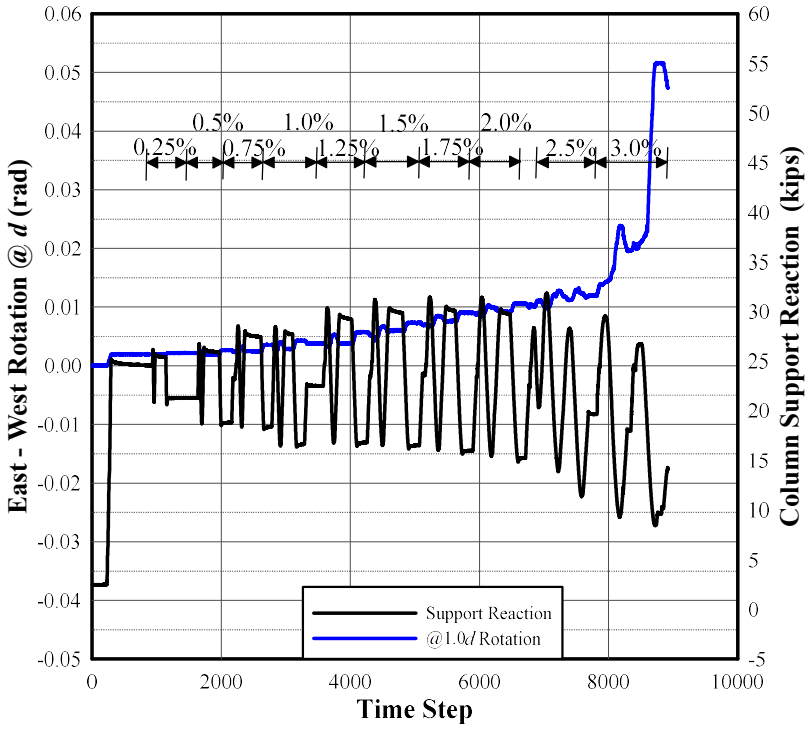

Fig. 4.85 – Slab Rotation and Support Reaction for Specimen G1

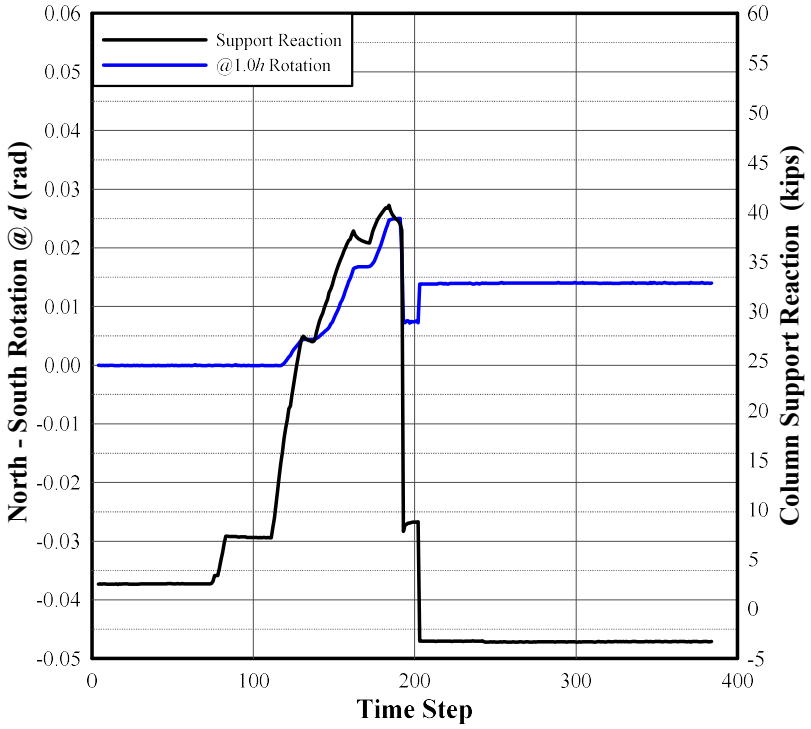

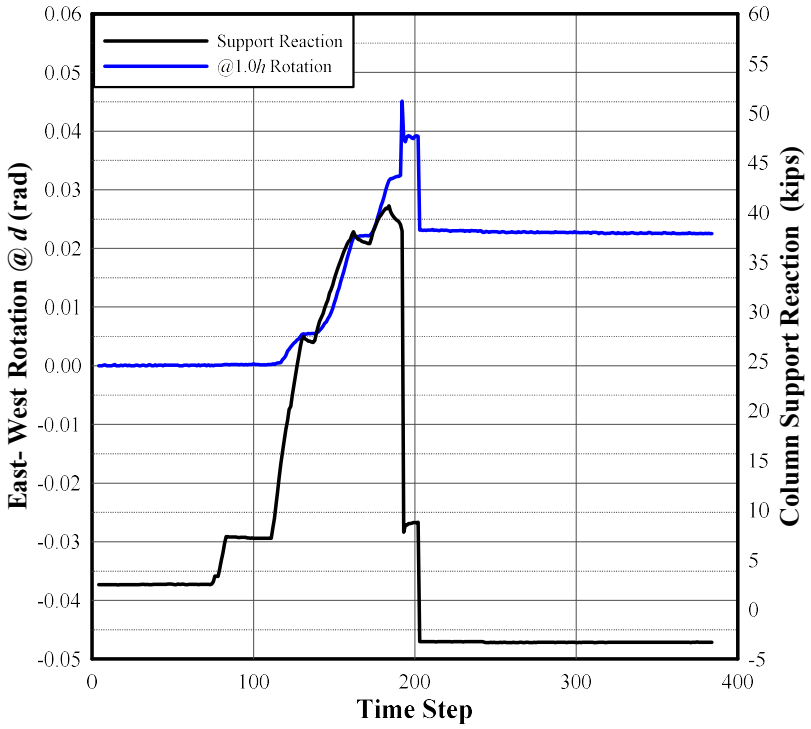

Fig. 4.86 – Slab Rotation and Support Reaction for Specimen G2

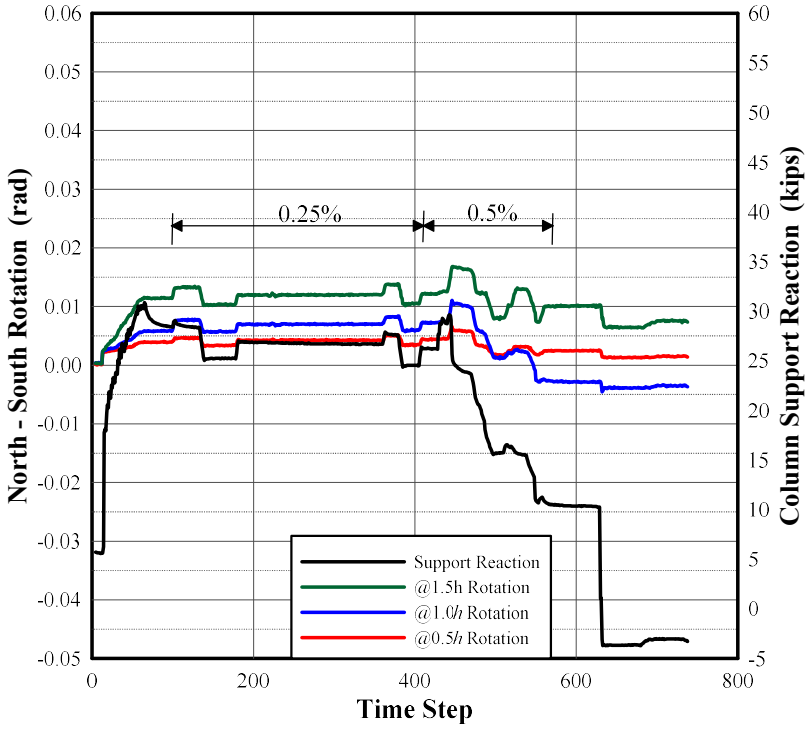

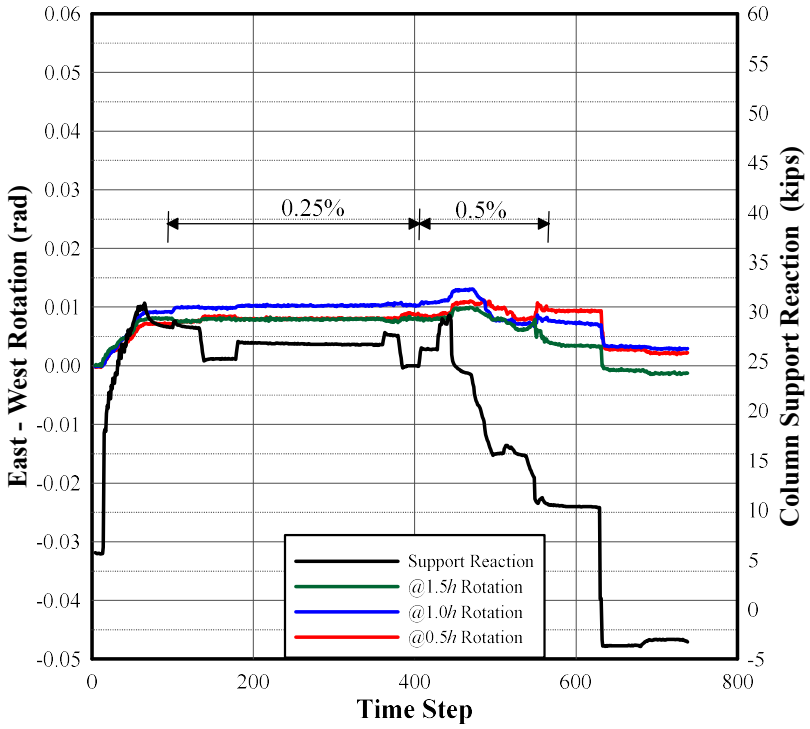

Fig. 4.87 – Slab Rotation and Support Reaction for Specimen G3

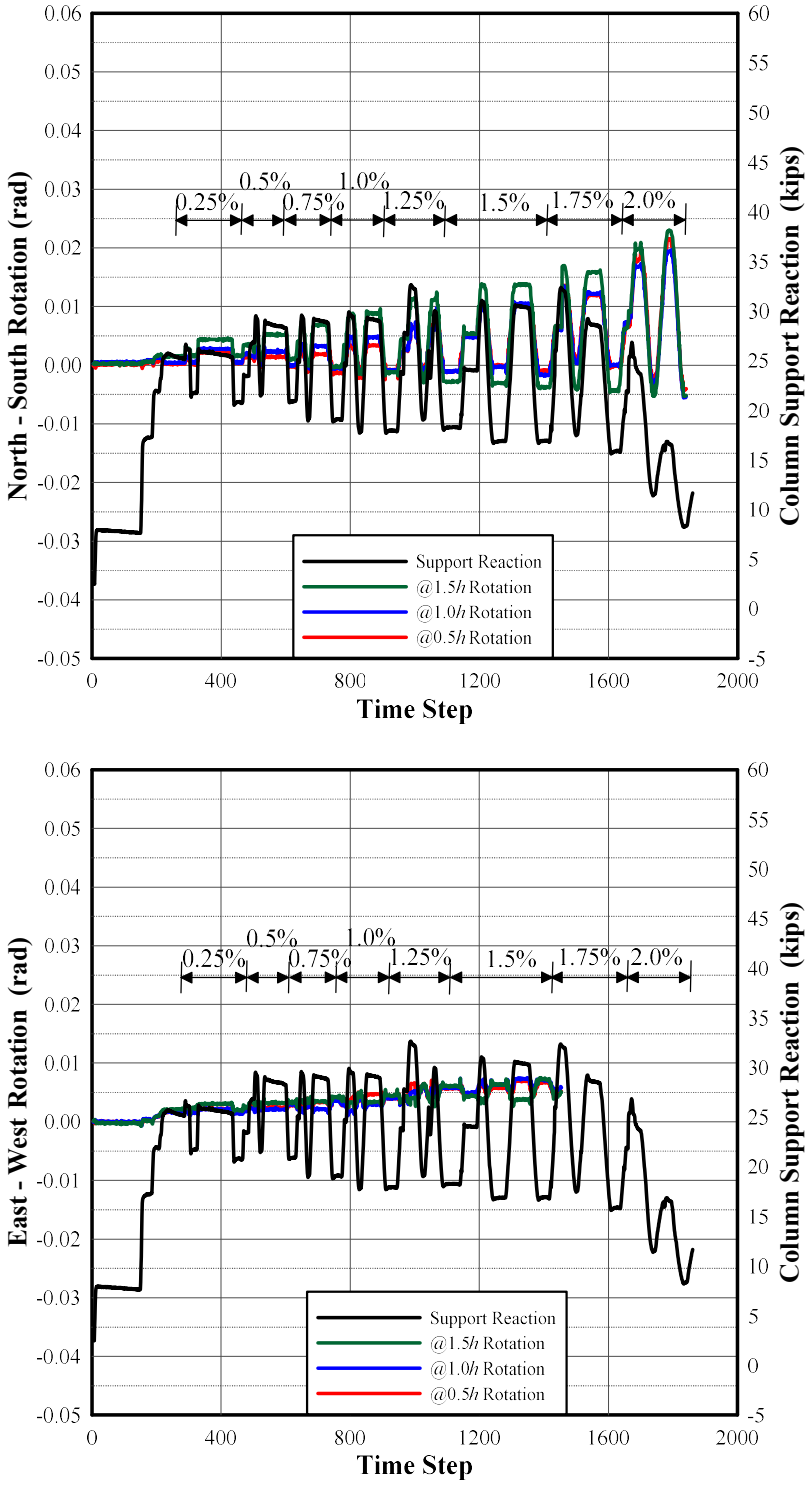

Fig. 4.88 – Slab Rotation and Support Reaction for Specimen R1

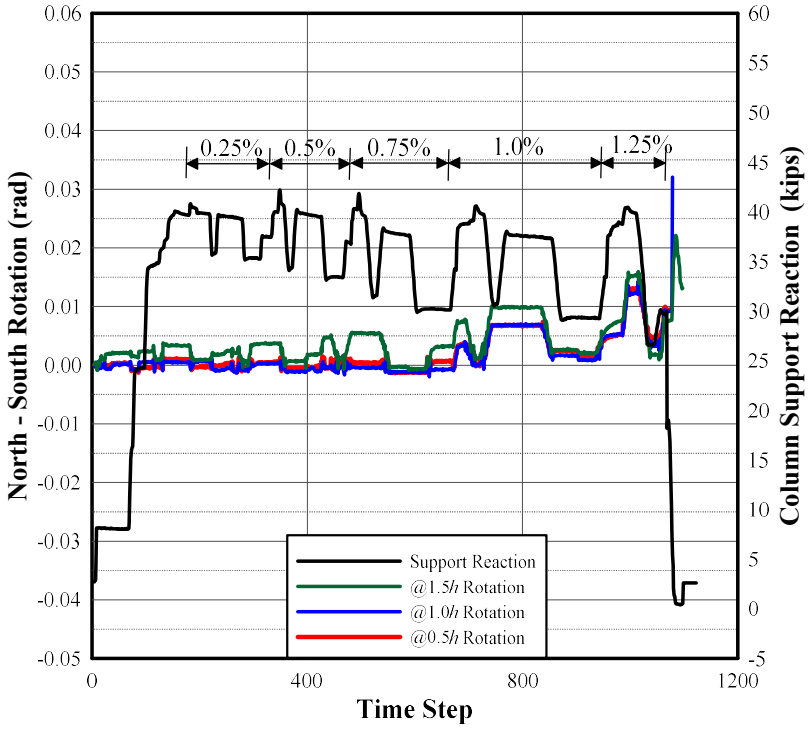

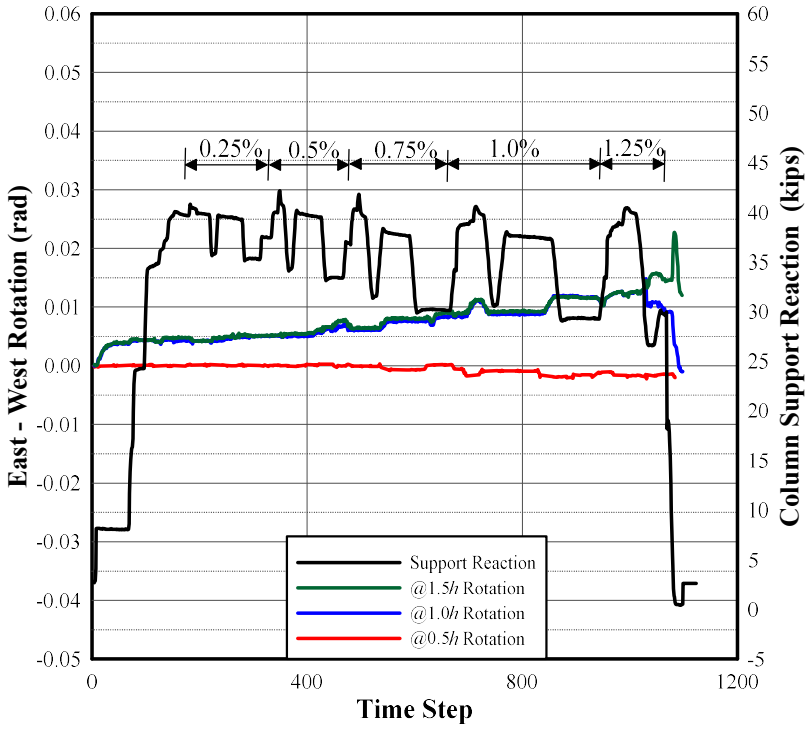

Fig. 4.89 – Slab Rotation and Support Reaction for Specimen R2

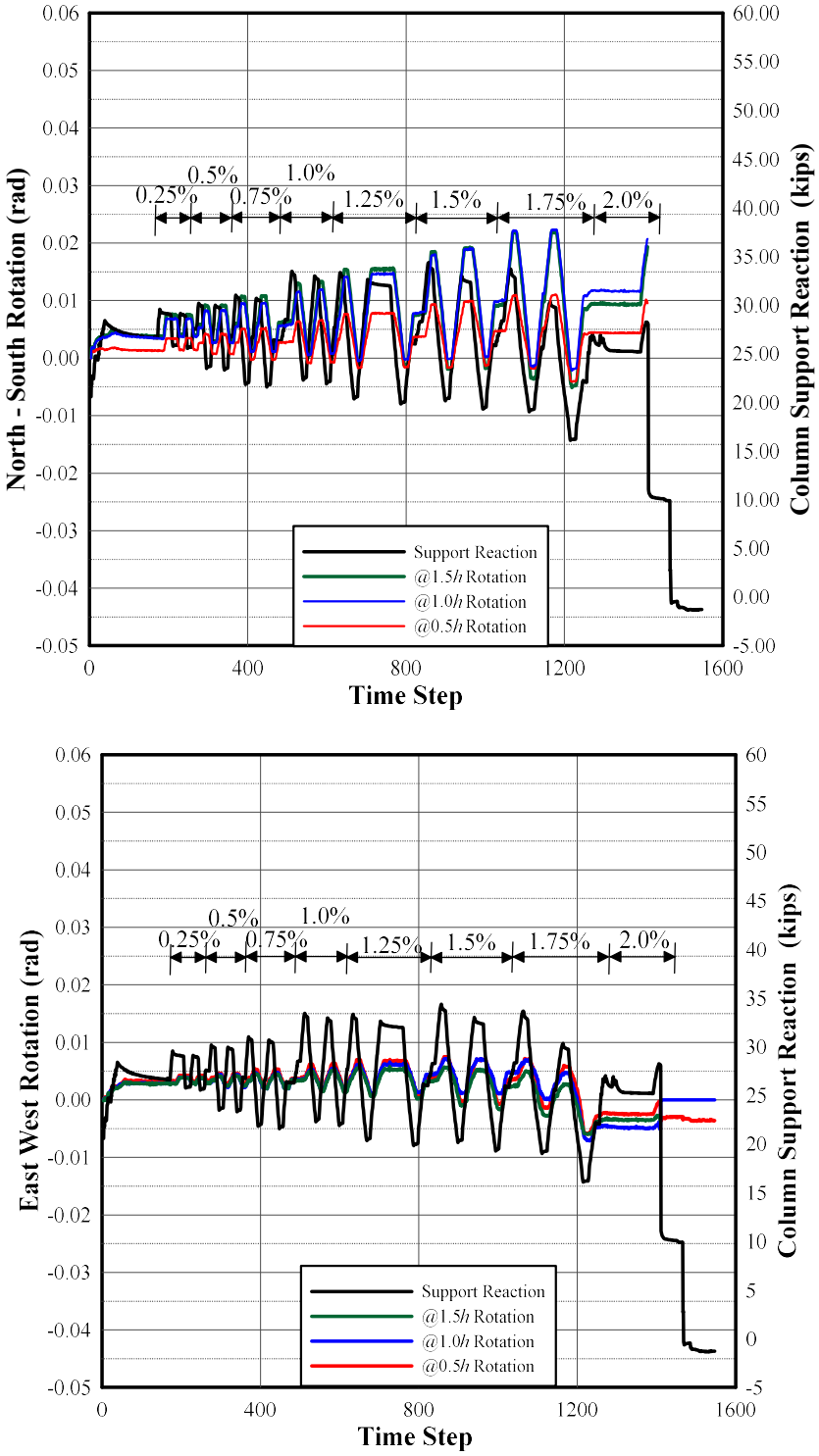

Fig. 4.90 – Slab Rotation and Support Reaction for Specimen R3

4.6 STRAIN GAUGE READINGS

Strain gauges were installed to monitor the strain of the slab flexural reinforcement. Strain gauges were also provided on some of the column longitudinal reinforcement of specimens G1, G2, R1 and R2 and readings of those strain gauge on the column sections were typically low (within elastic limit). With this, no strain gauge was attached on the column longitudinal reinforcement for specimens G3 and R3.

Based on strain gauge readings, the extent of yielding of all test specimens are presented in Fig. 4.91 to Fig. 4.96. In those figures, the solid rectangular symbols indicate strain gauges with readings exceeding yield strain while the hollow rectangular symbols are for strain gauges with readings within elastic limit. The drift level as well as the cycle number (in the parenthesis) when yielding strain was recorded are provided near the symbols. For all test specimens, it appears that strain gauges with readings exceeding yielding strain are primarily located within a 2*d* distance from the column faces.

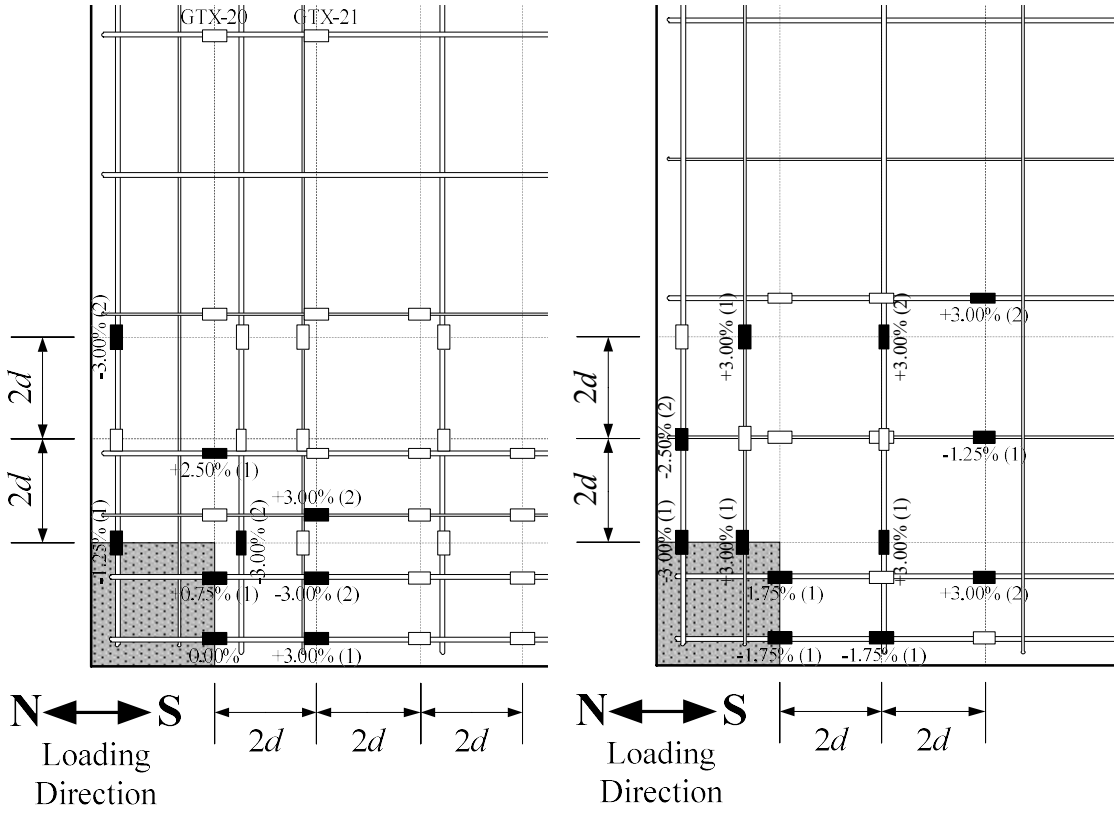

(a) Top Flexural Reinforcement (b) Bottom Flexural Reinforcement

Fig. 4.91 – Extent of Yielding of the Slab Flexural Reinforcement of Specimen G1

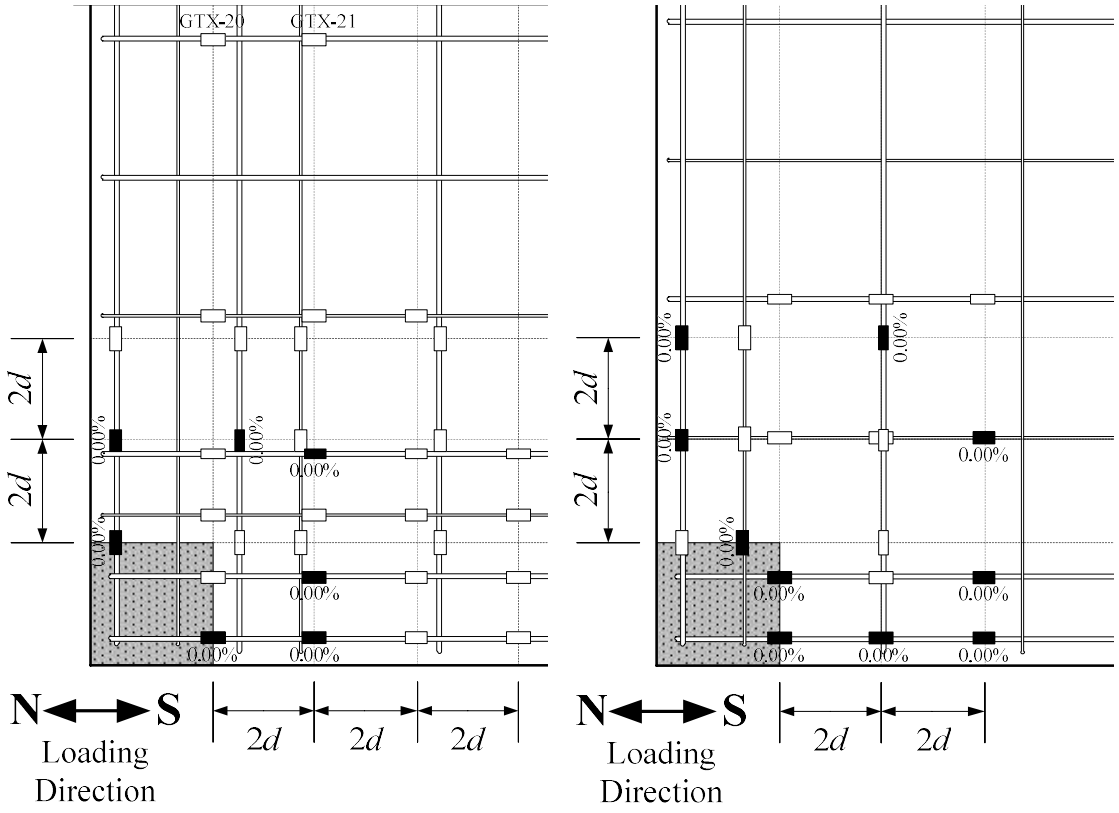

(a) Top Flexural Reinforcement (b) Bottom Flexural Reinforcement

Fig. 4.92 – Extent of Yielding of the Slab Flexural Reinforcement of Specimen G2

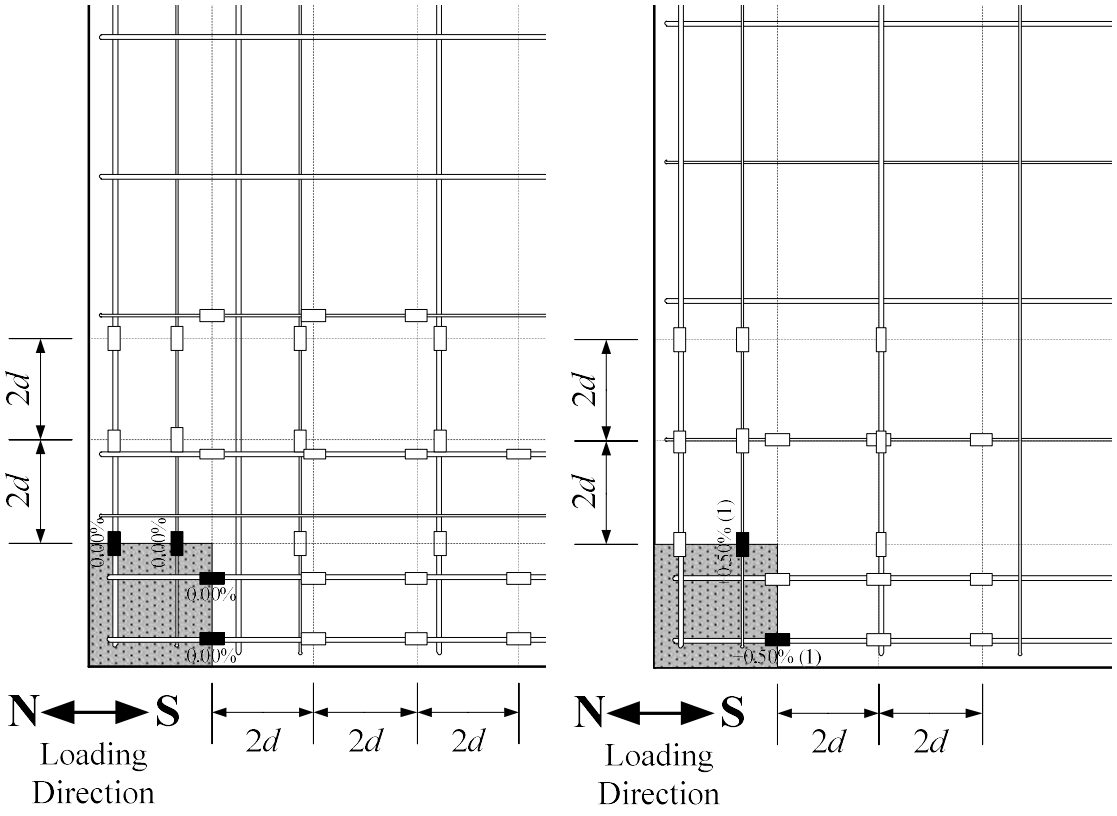

(a) Top Flexural Reinforcement (b) Bottom Flexural Reinforcement

Fig. 4.93 – Extent of Yielding of the Slab Flexural Reinforcement of Specimen G3

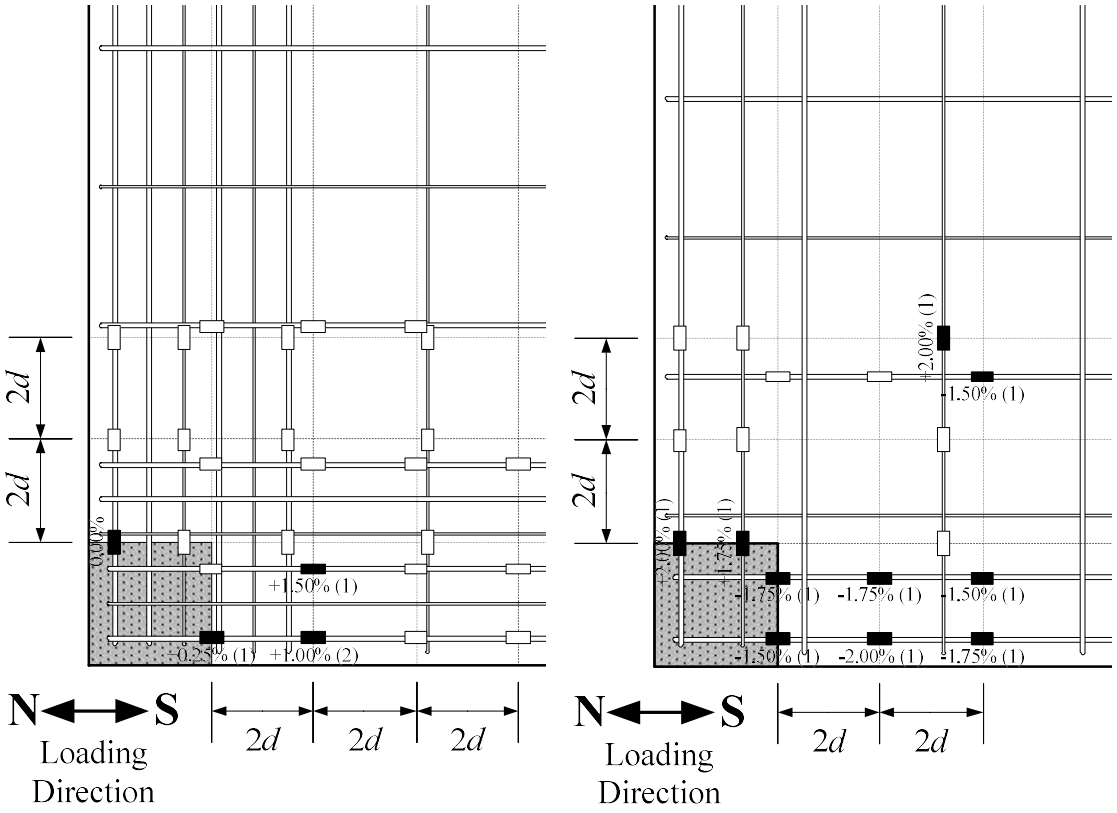

(a) Top Flexural Reinforcement (b) Bottom Flexural Reinforcement

Fig. 4.94 – Extent of Yielding of the Slab Flexural Reinforcement of Specimen R1

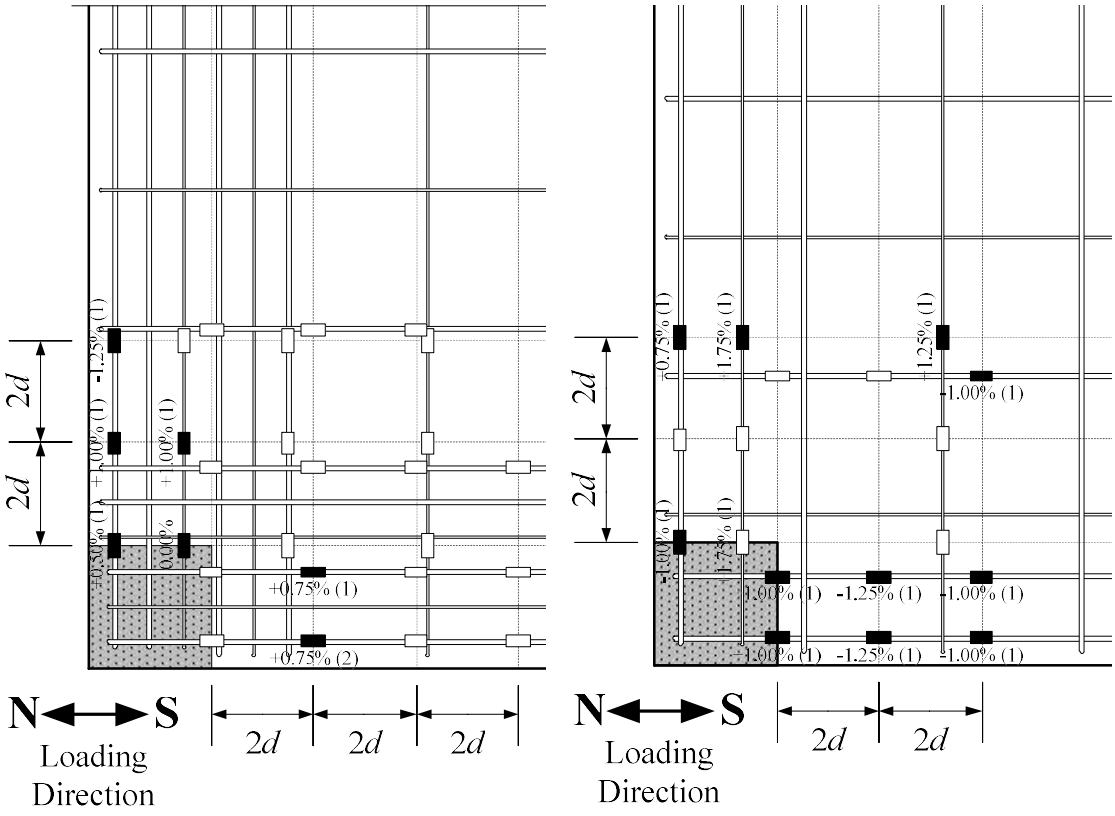

(a) Top Flexural Reinforcement (b) Bottom Flexural Reinforcement

Fig. 4.95 – Extent of Yielding of the Slab Flexural Reinforcement of Specimen R2

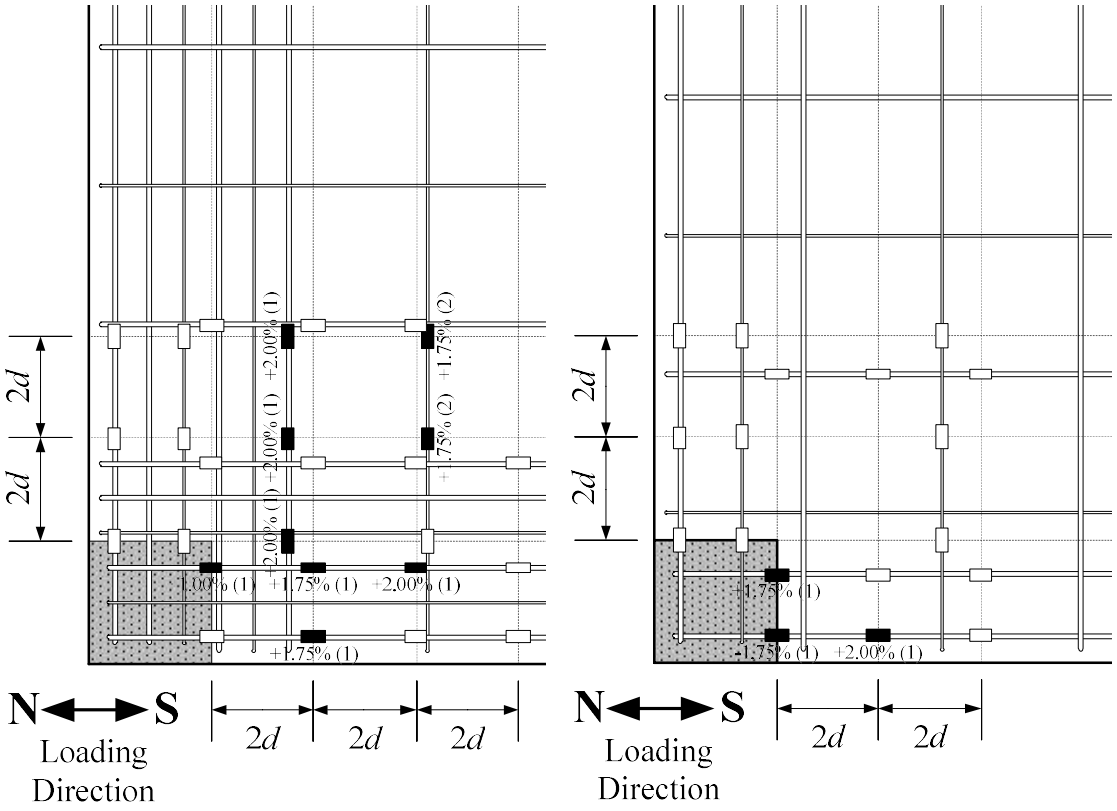

(a) Top Flexural Reinforcement (b) Bottom Flexural Reinforcement

Fig. 4.96 – Extent of Yielding of the Slab Flexural Reinforcement of Specimen R3

CHAPTER 5

ANALYSIS OF EXPERIMENTAL RESULTS

5.1 INTRODUCTION

This chapter discusses punching shear strengths and lateral deformation capacities of the corner slab-column connection. To be consistent with the design philosophy of the ACI 318-14, punching shear strength is evaluated using test results of specimens subjected to monotonically increased gravity-type load. A database consisting of a total of twenty specimens is developed for this purpose. In which, nineteen specimens were collected from previous researches and one specimen was collected from this study, i.e. specimen G2. Connection deformation capacity, on the other hand, is evaluated based on test results of the other five specimens tested in this study.

5.2 PUNCHING SHEAR STRENGTH

5.2.1 Database

A database that summarizes the key test results of the 20 corner slab-column connection specimens is provided in Table 5.1. The range of some design parameters for the collected specimens is summarized as follows: (1) specimens were subjected to monotonically increased gravity-type loading only, (2) slab thicknesses ranged between 3 in. and 8 in., (3) flexural reinforcement ratio within the effective width, b_{ew}, per ACI 318-14 ranged between 0.30% - 1.19% and 0.30% - 3.13% for top and bottom bars, respectively. The reinforcement ratio is evaluated using the total steel area within the b_{ew} divided by $b_{ew} \times d$, and (4) concrete cylinder strength was between 2.9 ksi and 7.1 ksi, and yield strength of slab flexural reinforcement was between 45.0 ksi and 104.0 ksi.

In Table 5.1, the gravity shear, V_g, is obtained from the reaction force at bottom of the column support. And, M_x and M_y is unbalanced moment transferred about the x- and y- axis at centroid of the column, respectively. Positive values for M_x and M_y refer to moments that create tension at top of the slab. The reinforcement ratio within the column width plus a 3d distance is determined using the total steel area within that width. The ρ_l and $\rho_{l,\,EC2}$ determined as $\sqrt{\rho_{tx}\rho_{ty}}$ and $\sqrt{\rho_{tx,\,EC2}\rho_{ty,\,EC2}}$, respectively, represents the reinforcement ratio within the width considered from the two principal directions.

Yield-line analysis was conducted for all test specimens. The yield-line pattern used for the test specimen is illustrated in Fig. 5.1. Details of the yield-line analysis can be found in Appendix B. Result of the yield-line analysis is converted to column reaction, and denoted as $V_{g,flex}$ in Table 5.1. As can be seen, all specimens have $V_g/V_{g,flex}$ less than 1.20 and using V_g as the shear capacity of the connection appears to be rational.

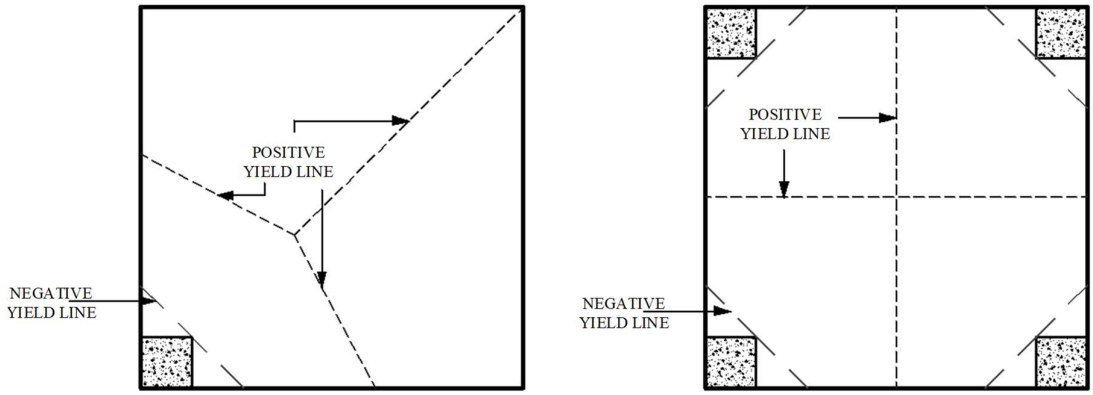

(a) Specimen G2 **(b) Specimens from Other Researchers**

Fig. 5.1 – Assumed Yield-Line Pattern

Table 5.1 – Database of Corner Slab-Column Connection Subjected to Gravity-Type Load

Specimen Data		Test Parameters												Load Data			Yield-Line Results
							Within b_{ew}			Within $c + 3d$							
Authors	Spec.	c_x, c_y	h	d	f_c'	f_y	ρ_{tx}	ρ_{ty}	ρ_l	$\rho_{tx,\ EC2}$	$\rho_{ty,\ EC2}$	$\rho_{l,\ EC2}$	V_g	M_x	M_y	$\frac{V_g}{V_{g,flex}}$
		in. (mm)	in. (mm)	in. (mm)	psi (MPa)	ksi (MPa)	%	%	%	%	%	%	kip (kN)	kip-ft (kN-m)	kip-ft (kN-m)	
Zaghlool et al. (1970)	I	5.50 (140)	5.50 (140)	4.50 (114)	3500 (24.1)	45.0 (310)	1.19	1.19	1.19	0.87	0.87	0.87	23.60 (105.0)	6.46 (8.80)	4.92 (6.70)	0.67
	III	6.50 (165)	5.5 (140)	4.5 (114)	3005 (20.7)	45.0 (310)	1.12	1.12	1.12	0.82	0.82	0.82	22.30 (99.0)	11.90 (16.1)	11.83 (16.0)	0.63
	IV	6.50 (165)	5.50 (140)	4.50 (114)	5185 (35.7)	45.0 (310)	1.12	1.12	1.12	0.82	0.82	0.82	26.50 (118.0)	11.60 (15.8)	16.20 (22.0)	0.69
Walker and Regan (1987)	SC1	11.8 (300)	4.90 (125)	3.90 (100)	6280 (43.3)	65.3 (450)	0.81	0.81	0.81	0.66	0.66	0.66	18.30 (81.4)	18.60 (25.2)	18.60 (25.2)	1.06
	SC2	11.8 (300)	4.90 (125)	3.90 (100)	6947 (47.9)	65.3 (450)	0.52	0.52	0.52	0.42	0.42	0.42	16.80 (74.7)	17.70 (24.0)	17.70 (24.0)	0.94
	SC3	11.8 (300)	4.90 (125)	3.90 (100)	5424 (37.4)	65.3 (450)	1.09	1.09	1.09	0.89	0.89	0.89	16.70 (74.3)	23.30 (31.6)	23.30 (31.6)	1.04
	SC4	8.70 (220)	4.90 (125)	3.90 (100)	5918 (40.8)	65.3 (450)	0.77	0.77	0.77	0.76	0.76	0.76	14.30 (63.6)	12.30 (16.7)	12.30 (16.7)	1.13
	SC5	8.70 (220)	4.90 (125)	3.90 (100)	6744 (46.5)	65.3 (450)	1.11	1.11	1.11	1.09	1.09	1.09	18.50 (82.3)	13.90 (18.8)	13.90 (18.8)	0.98
	SC7	8.70 (220)	4.90 (125)	3.90 (100)	6353 (43.8)	65.3 (450)	1.11	1.11	1.11	1.09	1.09	1.09	18.50 (82.3)	20.40 (27.6)	20.40 (27.6)	0.99
	SC8	6.30 (160)	3.20 (80)	2.50 (64)	5424 (37.4)	86.3 (595)	0.31	0.31	0.31	0.25	0.25	0.25	7.40 (32.9)	3.47 (4.70)	3.47 (4.70)	0.87
	SC9	6.30 (160)	3.20 (80)	2.50 (64)	4975 (34.3)	86.3 (595)	0.78	0.78	0.78	0.63	0.63	0.63	7.40 (32.9)	4.35 (5.90)	4.35 (5.90)	1.17
	SC11	6.30 (160)	3.20 (80)	2.40 (60)	3945 (27.2)	86.3 (595)	1.74	0.66	1.07	1.47	0.55	0.90	7.40 (32.9)	1.62 (2.20)	3.39 (4.60)	0.98
	SC12	11.8 (300)	3.20 (80)	2.40 (60)	5903 (40.7)	86.3 (595)	0.33	1.10	0.60	1.23	0.49	0.78	8.30 (36.9)	6.56 (8.90)	9.37 (12.7)	0.49
Desayi and Seshadri (1997)	S101	3.90 (100)	3.90 (100)	3.20 (80)	5221 (36.0)	104 (720)	0.57	0.57	0.57	0.52	0.52	0.52	7.34 (32.6)	6.50 (8.81)	6.50 (8.81)	0.72
	S201	3.90 (100)	3.90 (100)	3.20 (80)	5221 (36.0)	104 (720)	0.85	0.85	0.85	0.73	0.73	0.73	10.60 (47.0)	9.37 (12.70)	9.37 (12.70)	0.78
	S301	3.90 (100)	3.90 (100)	3.20 (80)	2901 (20.0)	104 (720)	1.13	1.13	1.13	0.94	0.94	0.94	12.40 (55.1)	11.0 (14.90)	11.0 (14.90)	0.82
	S102	3.90 (100)	3.90 (100)	3.20 (80)	3597 (24.8)	104 (720)	0.57	0.57	0.57	0.52	0.52	0.52	11.74 (52.2)	7.89 (10.70)	7.89 (10.70)	0.89
	S202	3.90 (100)	3.90 (100)	3.20 (80)	3945 (27.2)	104 (720)	0.85	0.85	0.85	0.73	0.73	0.73	9.16 (40.7)	6.16 (8.35)	6.16 (8.35)	0.50
	S302	3.90 (100)	3.90 (100)	3.20 (80)	3249 (22.4)	104 (720)	1.13	1.13	1.13	0.94	0.94	0.94	9.61 (42.7)	6.46 (8.76)	6.46 (8.76)	0.43
Current Study	G2	16.0 (406)	8.00 (203)	6.60 (168)	7090 (48.9)	61.6 (425)	0.67	0.67	0.67	0.52	0.52	0.52	40.40 (180.0)	40.20 (54.6)	40.20 (54.6)	0.37

5.3 EVALUATION

Each building code or design guide has its distinct approach in evaluating the punching shear in slab-column connections. Typically, the analytical model assumes non-uniform distribution of shear stress demand on the critical section and that results in maximum demand at a point or along one face of the critical section. As a result, points A, B, C have to be defined first as shown in Fig. 5.2 in order to better present the shear stress value and its corresponding location.

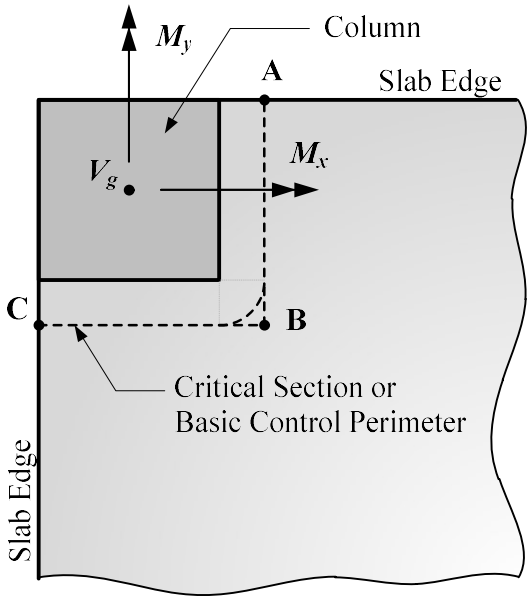

Fig. 5.2 – Points of Interests for a Corner Slab-Column Connection

5.3.1 ACI 318-14

Parameters needed for the shear strength model per ACI 318-14 are summarized in Table 5.2. Specimen shear demands considering uniaxial moment transfer, $v_{u,318u}$ per Eq. 2.10, and biaxial moment transfer, $v_{u,\,318b}$ per Eq. 2.9, are provided in Table 5.3. Connection shear capacity evaluated using Eq. 2.7 and Eq. 2.8 is also presented in Table 5.3. Results of the experimental-to-predicted shear strength ratios are summarized in the last two columns of Table 5.3. Values that are used to determine the experimental-to-predicted shear strength ratios are presented in

bold font style in Table 5.3. Please note, M_{ux} and M_{uy} listed in Table 5.3 refer to the unbalanced moments at the centroid of the critical section.

The influence of the slab flexural reinforcement ratio on punching shear capacity is then evaluated through the interaction between the specimen experimental-to-predicted shear strength ratio and equivalent slab top flexural reinforcement ratio, ρ_l, as shown in Fig. 5.3 and Fig. 5.4. The equivalent slab top flexural reinforcement ratio ρ_l is determined as $\sqrt{\rho_{tx}\rho_{ty}}$, much like the definition per EC2 and MC-10, to consider flexural reinforcement in both directions where ρ_{tx} and ρ_{ty} represents the slab top flexural reinforcement ratio within b_{ew} along the *x*- and *y*-direction, respectively.

As depicted in Figs. 5.3 and 5.4, the ACI 318-14 strength model does not provide a uniform result for specimens across the whole range of ρ_l. This scatteredness appears to increase as the ρ_l increases. More importantly, the predicted strength appears to be un-conservative for specimens with ρ_l around 0.75% or lower. When simultaneous biaxial moment transfer is considered, the shear demand prediction relatively increases due to the additional stress induced by the orthogonal moment transfer. For all specimens, the largest shear stress demand considering biaxial moment transfer is located at point B of the critical section (see Fig. 5.2). However, even biaxial moment transfer is considered, the strength model is still not conservative for specimens with ρ_l around 0.75% or lower.

Based on the analytical results in Table 5.3, the average of the ratios between the connection punching shear strength and demand of all collected specimens is 1.50 with a coefficient of variation (COV) of 0.55 when uniaxial moment transfer is considered, and is 2.08, with a COV of 0.62 when biaxial moment transfer is considered.

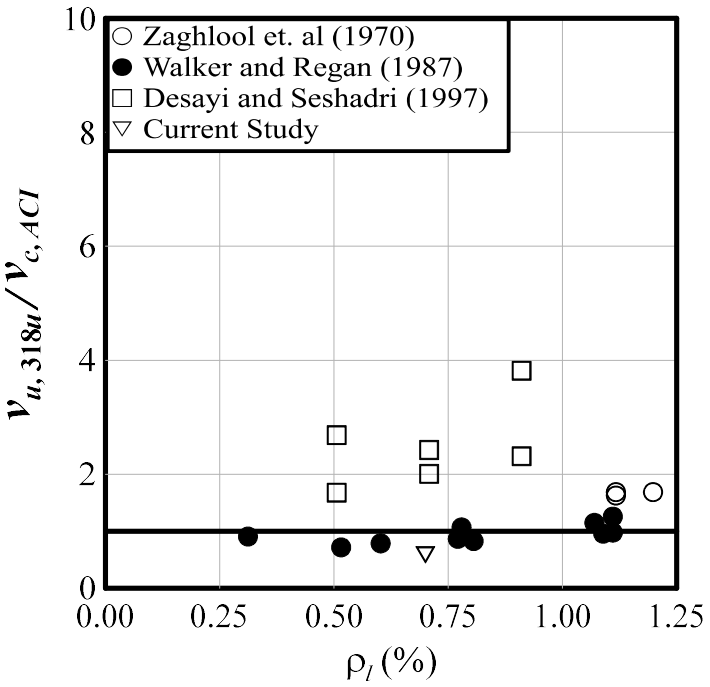

Fig. 5.3 – Punching Shear Strength Evaluation per ACI 318-14 Considering Uniaxial Moment Transfer

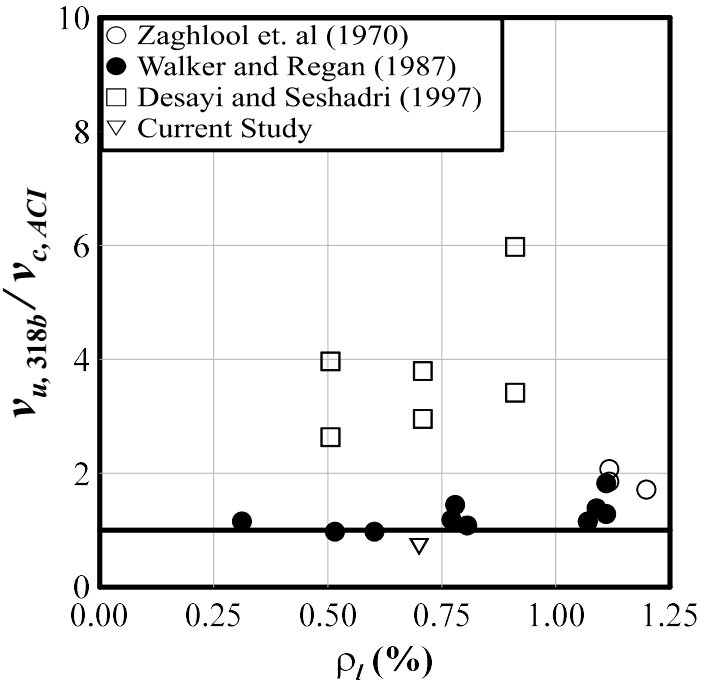

Fig. 5.4 – Punching Shear Strength Evaluation per ACI 318-14 Considering Biaxial Moment Transfer

Table 5.2 – Parameters for Punching Shear Strength Evaluation per ACI 318-14

Specimen Data			Critical Section Properties								Parameters	Load Data		
No.	Researcher	Specimen	b_1	b_2	b_o	d	C_{BC}	C_{AB}	J_x	J_y	$\gamma_{vx} = \gamma_{vy}$	V_g	M_x	M_y
			in. (mm)	in. (mm)	in. (mm)	in. (mm)	in. (mm)	in. (mm)	in.^{4} (10^6 mm^4)	in.^{4} (10^6 mm^4)		kip (kN)	kip-ft (kN-m)	kip-ft (kN-m)
1	Zaghlool et. al. (1970)	I	7.80 (197)	7.80 (197)	15.5 (394)	4.50 (114)	1.90 (49.2)	1.90 (49.2)	495 (206.0)	495 (206.0)	0.40	23.57 (104.8)	6.46 (8.8)	4.92 (6.7)
2		III	8.80 (222)	8.80 (222)	17.5 (445)	4.50 (114)	2.20 (55.6)	2.20 (55.6)	695 (289.0)	695 (289.0)	0.40	22.26 (99.0)	11.90 (16.1)	11.83 (16.0)
3		IV	8.80 (222)	8.80 (222)	17.5 (445)	4.50 (114)	2.20 (55.6)	2.20 (55.6)	695 (289.0)	695 (289.0)	0.40	26.50 (117.9)	11.64 (15.8)	16.20 (22.0)
4	Walker and Regan (1987)	SC1	13.80 (350)	13.8. (350)	27.6 (700)	3.90 (100)	3.40 (87.5)	3.40 (87.5)	2220 (922.0)	2220 (922.0)	0.40	18.30 (81.4)	18.60 (25.2)	18.60 (25.2)
5		SC2	13.80 (350)	13.8 (350)	27.6 (700)	3.90 (100)	3.40 (87.5)	3.40 (87.5)	2220 (922.0)	2220 (922.0)	0.40	16.80 (74.7)	17.70 (24.0)	17.70 (24.0)
6		SC3	13.80 (350)	13.8 (350)	27.6 (700)	3.90 (100)	3.40 (87.5)	3.40 (87.5)	2220 (922.0)	2220 (922.0)	0.40	16.70 (74.3)	23.30 (31.6)	23.30 (31.6)
7		SC4	10.60 (270)	10.6 (270)	21.3 (540)	3.90 (100)	2.70 (67.5)	2.70 (67.5)	1040.0 (433.0)	1040.0 (433.0)	0.40	14.30 (63.6)	12.32 (16.7)	12.32 (16.7)
8		SC5	10.6. (270)	10.6 (270)	21.3 (540)	3.90 (100)	2.70 (67.5)	2.70 (67.5)	1040.0 (433.0)	1040.0 (433.0)	0.40	18.50 (82.3)	13.90 (18.8)	13.90 (18.8)
9		SC7	10.60 (270)	10.6 (270)	21.3 (540)	3.90 (100)	2.70 (67.5)	2.70 (67.5)	1040.0 (433)	1040.0 (433)	0.40	18.50 (82.3)	20.40 (27.6)	20.40 (27.6)
10		SC8	7.60 (192)	7.60 (192)	15.1 (384)	2.50 (64)	1.90 (48.0)	1.90 (48.0)	237.0 (98.6)	237.0 (98.6)	0.40	7.40 (32.9)	3.47 (4.7)	3.47 (4.7)
11		SC9	7.60 (192)	7.60 (192)	15.1 (384)	2.50 (64)	1.90 (48.0)	1.90 (48.0)	237.0 (98.6)	237.0 (98.6)	0.40	7.40 (32.9)	4.35 (5.9)	4.35 (5.9)
12		SC11	7.50 (190)	7.50 (190)	15.1 (384)	2.40 (60)	1.90 (48.0)	1.90 (48.0)	214.0 (89.2)	214.0 (89.2)	0.40	7.40 (32.9)	1.62 (2.2)	3.39 (4.6)
13		SC12	13.0 (330)	13.0 (330)	26.0 (660)	2.40 (60)	3.20 (82.5)	3.20 (82.5)	1094 (455.0)	1090 (455.0)	0.40	8.30 (36.9)	6.56 (8.9)	9.37 (12.7)
14	Desayi and Seshadri (1997)	S101	5.5 (140)	5.50 (140)	11.0 (280)	3.20 (80)	1.40 (35.5)	1.4 (35.5)	124.0 (51.7)	124.0 (51.7)	0.40	7.34 (32.6)	6.50 (8.81)	6.50 (8.81)
15		S201	5.50 (140)	5.50 (140)	11.0 (280)	3.20 (80)	1.40 (35.5)	1.40 (35.5)	124.0 (51.7)	124.0 (51.7)	0.40	10.60 (47.0)	9.37 (12.70)	9.37 (12.70)
16		S301	5.50 (140)	5.50 (140)	11.0 (280)	3.20 (80)	1.40 (35.5)	1.40 (35.5)	124.0 (51.7)	124.0 (51.7)	0.40	12.40 (55.1)	11.0 (14.90)	11.0 (14.90)
17		S102	5.50 (140)	5.50 (140)	11.0 (280)	3.20 (80)	1.40 (35.5)	1.40 (35.5)	124.0 (51.7)	124.0 (51.7)	0.40	11.70 (52.2)	7.89 (10.70)	7.89 (10.70)
18		S202	5.50 (140)	5.50 (140)	11.0 (280)	3.20 (80)	1.40 (35.5)	1.40 (35.5)	124.0 (51.7)	124.0 (51.7)	0.40	9.16 (40.7)	6.16 (8.35)	6.16 (8.35)
19		S302	5.50 (140)	5.50 (140)	11.0 (280)	3.20 (80)	1.40 (35.5)	1.40 (35.5)	124.0 (51.7)	124.0 (51.7)	0.40	9.61 (42.7)	6.46 (8.76)	6.46 (8.76)
20	Current Study	G2	19.3 (490)	19.3 (490)	38.6 (980)	6.60 (168)	4.80 (122.6)	4.80 (122.6)	10400.0 (4310.0)	10400.0 (4310.0)	0.40	40.40 (179.7)	40.24 (54.6)	40.24 (54.6)

Table 5.3 – Punching Shear Strength Evaluation per ACI 318–14

Specimen Data			Load Data			Shear Demand			Shear Capacity			Demand / Capacity	
No.	Researcher	Specimen	V_g	M_{ux}	M_{uy}	$v_{u,318u}$ on face BC	$v_{u,318u}$ on face AB	$v_{u,318b}$	$v_c=4\sqrt{f'_c}$	$v_c=\left(2+\frac{\alpha_s d}{b_o}\right)\sqrt{f'_c}$	$v_c=\left(2+\frac{4}{\beta_o}\right)\sqrt{f'_c}$	$\frac{v_{u,318u}}{v_{c,ACI}}$	$\frac{v_{u,318b}}{v_{c,ACI}}$
			kip (kN)	kip-ft (kN-m)	kip-ft (kN-m)	ksi (MPa)	ksi (MPa)	ksi (MPa)	ksi (MPa)	ksi (MPa)	ksi (MPa)		
1	Zaghlool et. al. (1970)	I	23.57 (105.0)	0.44 (0.60)	-1.09 (-1.48)	0.346 (2.39)	**0.400 (2.75)**	**0.408 (2.81)**	**0.237 (1.63)**	0.462 (3.19)	0.356 (2.45)	1.69	1.72
2		III	22.26 (99.0)	5.76 (7.80)	5.69 (7.71)	**0.370 (2.55)**	0.369 (2.54)	**0.456 (3.14)**	**0.219 (1.51)**	0.392 (2.70)	0.329 (2.27)	1.69	2.08
3		IV	26.50 (118.0)	4.32 (5.86)	8.88 (12.00)	0.402 (2.77)	**0.471 (3.24)**	**0.536 (3.69)**	**0.288 (1.99)**	0.514 (3.55)	0.432 (2.98)	1.63	1.86
4	Walker and Regan (1987)	SC1	18.30 (81.4)	11.80 (16.10)	11.80 (16.10)	**0.257 (1.77)**	**0.257 (1.77)**	**0.345 (2.38)**	**0.317 (2.19)**	0.385 (2.65)	0.475 (3.28)	0.83	1.09
5		SC2	16.80 (74.7)	11.50 (15.60)	11.50 (15.60)	**0.241 (1.66)**	**0.241 (1.66)**	**0.326 (2.25)**	**0.333 (2.30)**	0.405 (2.79)	0.500 (3.45)	0.72	0.98
6		SC3	16.70 (74.3)	17.15 (23.30)	17.15 (23.30)	**0.282 (1.94)**	**0.282 (1.94)**	**0.410 (2.82)**	**0.295 (2.03)**	0.358 (2.47)	0.442 (3.05)	0.96	1.39
7		SC4	14.30 (63.6)	7.98 (10.80)	7.98 (10.80)	**0.269 (1.85)**	**0.269 (1.85)**	**0.367 (2.53)**	**0.308 (2.12)**	0.439 (3.03)	0.462 (3.18)	0.87	1.19
8		SC5	18.50 (82.3)	8.25 (11.20)	8.25 (11.20)	**0.322 (2.22)**	**0.322 (2.22)**	**0.424 (2.92)**	**0.329 (2.27)**	0.468 (3.23)	0.493 (3.40)	0.98	1.29
9		SC7	18.50 (82.3)	14.75 (20.00)	14.80 (20.00)	**0.402 (2.77)**	**0.402 (2.77)**	**0.583 (4.02)**	**0.319 (2.20)**	0.455 (3.14)	0.478 (3.30)	1.26	1.83
10		SC8	7.40 (32.9)	1.90 (2.58)	1.90 (2.58)	**0.268 (1.84)**	**0.268 (1.84)**	**0.341 (2.35)**	**0.295 (2.03)**	0.393 (2.71)	0.442 (3.05)	0.91	1.16
11		SC9	7.40 (32.9)	2.80 (3.80)	2.80 (3.80)	**0.301 (2.08)**	**0.301 (2.08)**	**0.408 (2.81)**	**0.309 (2.13)**	0.412 (2.84)	0.464 (3.20)	1.07	1.45
12		SC11	7.40 (32.9)	0.10 (0.14)	1.87 (2.54)	0.214 (1.47)	**0.288 (1.98)**	**0.292 (2.01)**	**0.251 (1.73)**	0.324 (2.23)	0.377 (2.60)	1.15	1.16
13		SC12	8.30 (36.9)	3.90 (5.29)	6.71 (9.10)	0.191 (1.31)	**0.231 (1.59)**	**0.287 (1.97)**	0.309 (2.12)	**0.293 (2.02)**	0.460 (3.18)	0.79	0.98
14	Desayi and Seshadri (1997)	S101	7.34 (32.6)	5.17 (7.01)	5.17 (7.01)	**0.487 (3.36)**	**0.487 (3.36)**	**0.763 (5.25)**	**0.289 (1.99)**	0.557 (3.84)	0.434 (2.99)	1.68	2.64
15		S201	10.60 (47.0)	7.46 (10.10)	7.46 (10.10)	**0.702 (4.84)**	**0.702 (4.84)**	**1.10 (7.57)**	**0.289 (1.99)**	0.557 (3.84)	434 (2.99)	2.43	3.80
16		S301	12.40 (55.1)	8.74 (11.90)	8.74 (11.90)	**0.822 (5.67)**	**0.822 (5.67)**	**1.29 (8.87)**	**0.215 (1.49)**	0.415 (2.87)	0.323 (2.23)	3.82	5.98
17		S102	11.70 (52.2)	5.77 (7.82)	5.77 (7.82)	**0.645 (4.45)**	**0.645 (4.45)**	**0.953 (6.56)**	**0.240 1.65)**	0.463 (3.19)	0.360 (2.48)	2.69	3.97
18		S202	9.16 (40.7)	4.50 (6.10)	4.50 (6.10)	**0.503 (3.47)**	**0.503 (3.47)**	**0.744 (5.12)**	**0.251 (1.73)**	0.485 (3.34)	0.377 (2.60)	2.01	2.96
19		S302	9.61 (42.7)	4.73 (6.41)	4.73 (6.41)	**0.528 (3.64)**	**0.528 (3.64)**	**0.780 (5.37)**	**0.228 (1.57)**	0.440 (3.03)	0.342 (2.36)	2.32	3.42
20	Current Study	G2	40.40 (180.0)	18.4 (25.0)	18.4 (25.0)	**0.200 (1.38)**	**0.200 (1.38)**	**0.241 (1.66)**	**0.337 (2.32)**	0.456 (3.15)	0.505 (3.48)	0.59	0.72
											Mean:	1.50	2.08
											COV:	0.55	0.64

5.3.2 ACI 421

The ACI 421 also uses Eq. 2.7 and Eq. 2.8 to evaluate punching shear capacity of the slab-column connection. However, shear demand per ACI 421 is interpreted differently despite using identical concepts of the eccentric shear stress model analogous to Eq. 2.11. Details to determine orientation of the "principal axes" and evaluation of J_{cx} and J_{cy} with respect to the principal axes can be found in Section 2.3 in this report or elsewhere (Joint ACI-ASCE Committee 421, 2008; Joint ACI-ASCE Committee 421, 2010). Parameters used to evaluate strength model per ACI 421 are summarized in Table 5.4. Analytical results are presented in Table 5.5 and the experimental-to-predict shear strength ratios for all specimens are presented in Fig. 5.5.

Despite the mean demand-to-capacity ratio is the largest among all shear strength models evaluated, the ACI 421 provisions are still not able to provide conservative prediction for all test specimens. As can be seen in Fig. 5.5, the largest $v_{u,421}/v_{c,ACI}$ ratio per ACI 421 (2008, 2010) is 9.83, while the smallest one is 0.90. Both the mean (3.08) and the COV (0.75) of the $v_{u,421}/v_{c,ACI}$ ratio are the largest values among all strength models.

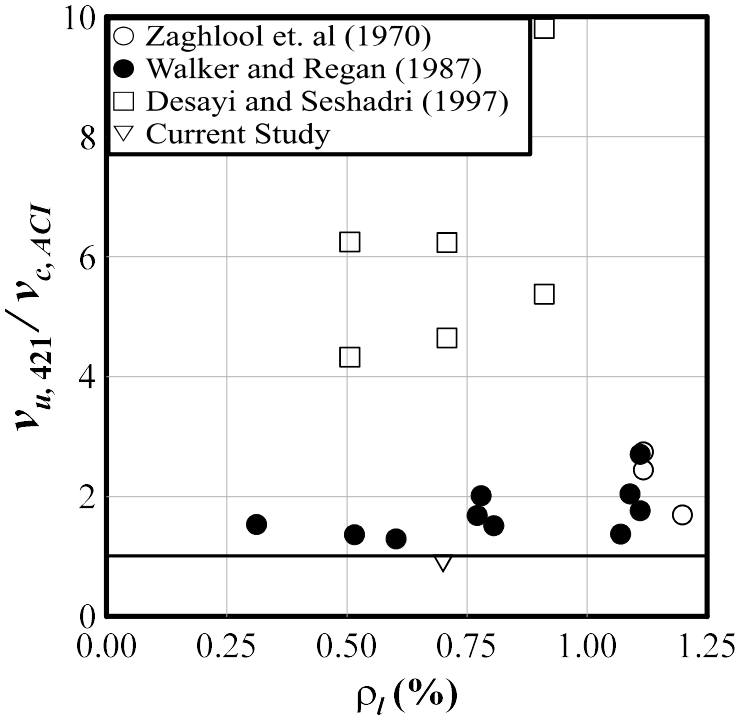

Fig. 5.5 – Punching Shear Strength Evaluation per ACI 421

Table 5.4 – Parameters for Punching Shear Strength Evaluation per ACI 421 (2008, 2010)

Specimen Data			Critical Section Properties							Parameters		Load Data		
No.	Researcher	Specimen	l_1	l_2	b_o	d	θ	I_1	I_2	γ_{v1}	γ_{v2}	V_g	M_1	M_2
			in. (mm)	in. (mm)	in. (mm)	in. (mm)	degree	10^2 in.^{4} (10^6mm^4)	10^2 in.^{4} (10^6mm^4)			kip (kN)	kip-ft (kN-m)	kip-ft (kN-m)
1	Zaghlool et al. (1970)	I	5.50 (139)	11.0 (278)	15.5 (394)	4.50 (114)	-45.0	698 (14.50)	175 (3.62)	0.40	0.27	23.60 (105.0)	1.09 (1.48)	8.05 (10.90)
2		III	6.20 (157)	12.4 (314)	17.5 (445)	4.50 (114)	-45.0	1010 (20.80)	251 (5.21)	0.40	0.27	22.30 (99.0)	0.05 (0.07)	16.80 (22.80)
3		IV	6.20 (157)	12.4 (314)	17.5 (445)	4.50 (114)	-45.0	1010 (20.80)	251 (5.21)	0.40	0.27	26.50 (118.0)	-3.23 (-4.38)	19.70 (26.70)
4	Walker and Regan (1987)	SC1	9.70 (247)	19.5 (494)	27.6 (700)	3.90 (100)	-45.0	3430 (70.10)	858 (17.80)	0.40	0.27	18.30 (81.4)	0.00 (0.00)	26.30 (35.64)
5		SC2	9.70 (247)	19.5 (494)	27.6 (700)	3.90 (100)	-45.0	3430 (71.10)	858 (17.80)	0.40	0.27	16.80 (74.7)	0.00 (0.00)	25.03 (33.90)
6		SC3	9.70 (247)	19.5 (494)	27.6 (700)	3.90 (100)	-45.0	3430 (71.10)	858 (17.80)	0.40	0.27	16.70 (74.3)	0.00 (0.00)	33.0 (44.70)
7		SC4	7.50 (191)	15.1 (383)	21.3 (540)	3.90 (100)	-45.0	1580 (32.60)	394 (8.15)	0.40	0.27	14.30 (63.6)	0.00 (0.00)	17.40 (23.60)
8		SC5	7.50 (191)	15.1 (383)	21.3 (540)	3.90 (100)	-45.0	1580 (32.60)	394 (8.15)	0.40	0.27	18.50 (82.3)	0.00 (0.00)	19.60 (26.60)
9		SC7	7.50 (191)	15.1 (383)	21.3 (540)	3.90 (100)	-45.0	1580 (32.60)	394 (8.15)	0.40	0.27	18.50 (82.3)	0.00 (0.00)	28.80 (39.10)
10		SC8	5.30 (136)	10.7 (271)	15.1 (384)	2.50 (64)	-45.0	363 (7.51)	91.0 (1.88)	0.40	0.27	7.40 (32.9)	0.00 (0.00)	4.90 (6.65)
11		SC9	5.30 (136)	10.7 (271)	15.1 (384)	2.50 (64)	-45.0	363 (7.51)	91.0 (1.88)	0.40	0.27	7.40 (32.9)	0.00 (0.00)	6.15 (8.34)
12		SC11	5.30 (136)	10.6 (269)	15.1 (384)	2.40 (60)	-45.0	330 (6.83)	82.0 (1.70)	0.40	0.27	7.40 (32.9)	-1.25 (-1.69)	3.54 (4.80)
13		SC12	9.20 (233)	18.4 (467)	26.0 (660)	2.40 (60)	-45.0	1730 (35.70)	432 (8.94)	0.40	0.27	8.30 (36.9)	-1.99 (-2.90)	11.26 (15.30)
14	Desayi and Seshadri (1997)	S101	3.90 (99)	7.80 (198)	11.0 (280)	3.20 (80)	-45.0	176 (3.65)	44.0 (0.91)	0.40	0.27	7.34 (32.6)	0.00 (0.00)	9.19 (12.50)
15		S201	3.90 (99)	7.80 (198)	11.0 (280)	3.20 (80)	-45.0	176 (3.65)	44.0 (0.91)	0.40	0.27	10.60 (47.0)	0.00 (0.00)	13.30 (18.0)
16		S301	3.90 (99)	7.80 (198)	11.0 (280)	3.20 (80)	-45.0	176 (3.65)	44.0 (0.91)	0.40	0.27	12.40 (55.1)	0.00 (0.00)	15.50 (21.01)
17		S102	3.90 (99)	7.80 (198)	11.0 (280)	3.20 (80)	-45.0	176 (3.65)	44.0 (0.91)	0.40	0.27	11.70 (52.2)	0.00 (0.00)	11.20 (15.20)
18		S202	3.90 (99)	7.80 (198)	11.0 (280)	3.20 (80)	-45.0	176 (3.65)	44.0 (0.91)	0.40	0.27	9.16 (40.7)	0.00 (0.00)	8.71 (11.80)
19		S302	3.90 (99)	7.80 (198)	11.0 (280)	3.20 (80)	-45.0	176 (3.65)	44.0 (0.91)	0.40	0.27	9.61 (42.7)	0.00 (0.00)	9.14 12.40)
20	Current Study	G2	13.7 (347)	27.3 (694)	38.6 (980)	6.60 (168)	-45.0	15900 (329.30)	3980 (82.40)	0.40	0.27	40.40 (180.0)	0.00 (0.00)	56.90 (77.20)

Table 5.5 – Punching Shear Strength Evaluation per ACI 421 (2008, 2010)

Specimen Data			V_g	M_{u1}	M_{u2}	Shear Demand			Shear Capacity			Demand / Capacity
No.	Researcher	Specimen				$v_{u,\,421}$ at A	$v_{u,\,421}$ at B	$v_{u,\,421}$ at C	$v_c=4\sqrt{f'_c}$	$v_c=\left(2+\frac{\alpha_s d}{b_o}\right)\sqrt{f'_c}$	$v_c=\left(2+\frac{4}{\beta_o}\right)\sqrt{f'_c}$	$\frac{v_{u\,421}}{v_{c,ACI}}$
			kip (kN)	kip-ft (kN-m)	kip-ft (kN-m)	ksi (MPa)	ksi (MPa)	ksi (MPa)	ksi (MPa)	ksi (MPa)	ksi (MPa)	
1	Zaghlool et al. (1970)	I	23.57 (104.8)	1.09 (1.48)	-0.460 (-0.624)	**0.402 (2.77)**	0.315 (2.17)	0.320 (2.21)	**0.237 (1.63)**	0.462 (3.19)	0.356 (2.45)	1.70
2		III	22.26 (99.0)	0.05 (0.06)	8.09 (11.0)	-0.036 (-0.25)	**0.602 (4.15)**	-0.039 (-0.27)	**0.219 (1.51)**	0.392 (2.70)	0.329 (2.27)	2.75
3		IV	26.50 (117.9)	-3.23 (-4.38)	9.34 (12.70)	-0.128 (-0.88)	**0.706 (4.86)**	-0.063 (-0.43)	**0.288 (1.99)**	0.514 (3.55)	0.432 (2.98)	2.45
4	Walker and Regan (1987)	SC1	18.30 (81.4)	0.00 (0.00)	16.70 (22.60)	-0.136 (-0.94)	**0.474 (3.27)**	-0.136 (-0.94)	**0.317 (2.19)**	0.385 (2.65)	0.475 (3.28)	1.49
5		SC2	16.80 (74.7)	0.00 (0.00)	16.30 (22.10)	-0.141 (-0.97)	**0.451 (3.11)**	-0.141 (-0.97)	**0.333 (2.30)**	0.405 (2.79)	0.500 (3.45)	1.35
6		SC3	16.70 (74.3)	0.00 (0.00)	24.30 (32.90)	-0.288 (-1.98)	**0.596 (4.11)**	-0.288 (-1.98)	**0.295 (2.03)**	0.358 (2.47)	0.442 (3.05)	2.02
7		SC4	14.30 (63.6)	0.00 (0.00)	11.30 (15.30)	-0.175 (-1.21)	**0.516 (3.56)**	-0.175 (-1.21)	**0.308 (2.12)**	0.439 (3.03)	0.462 (3.18)	1.68
8		SC5	18.50 (82.3)	0.00 (0.00)	11.70 (15.90)	-0.136 (-0.94)	**0.578 (3.98)**	-0.136 (-0.94)	**0.329 (2.27)**	0.468 (3.23)	0.493 (3.40)	1.76
9		SC7	18.50 (82.3)	0.00 (0.00)	20.90 (28.30)	-0.417 (-2.87)	**0.860 (5.93)**	-0.417 (-2.87)	**0.319 (2.20)**	0.455 (3.14)	0.478 (3.30)	2.70
10		SC8	7.40 (32.9)	0.00 (0.00)	2.71 (3.67)	-0.062 (-0.43)	**0.451 (3.11)**	-0.062 (-0.43)	**0.295 (2.03)**	0.393 (2.71)	0.442 (3.05)	1.53
11		SC9	7.40 (32.9)	0.00 (0.00)	3.95 (5.36)	-0.180 (-1.24)	**0.568 (3.91)**	-0.180 (-1.24)	**0.309 (2.13)**	0.412 (2.84)	0.464 (3.20)	1.84
12		SC11	7.40 (32.9)	-1.25 (-1.70)	1.40 (2.00)	-0.031 (-0.21)	**0.353 (2.43)**	0.162 (1.12)	**0.251 (1.73)**	0.324 (2.23)	0.377 (2.60)	1.41
13		SC12	8.30 (36.9)	-1.98 (-2.69)	7.51 (10.18)	-0.172 (-1.19)	**0.392 (2.70)**	-0.071 (-0.49)	0.309 (2.12)	**0.293 (2.02)**	0.460 (3.18)	1.34
14	Desayi and Seshadri (1997)	S101	7.34 (32.6)	0.00 (0.00)	7.32 (9.92)	-0.830 (-5.72)	**1.25 (8.61)**	-0.830 (-5.72)	**0.289 (1.99)**	0.557 (3.84)	0.434 (2.99)	4.34
15		S201	10.60 (47.0)	0.00 (0.00)	10.55 (14.30)	-1.20 (-8.27)	**1.810 (12.5)**	-1.200 (-8.27)	**0.289 (1.99)**	0.557 (3.84)	0.434 (2.99)	6.25
16		S301	12.40 (55.1)	0.00 (0.00)	12.40 (16.80)	-1.40 (0.00)	**2.12 (14.6)**	-1.400 (-9.65)	**0.215 (1.49)**	0.415 (2.87)	0.323 (2.23)	9.83
17		S102	11.70 (52.2)	0.00 (0.00)	8.16 (11.10)	-0.824 (0.00)	**1.50 (10.3)**	-0.824 (-5.68)	**0.240 1.65)**	0.463 (3.19)	0.360 (2.48)	6.25
18		S202	9.16 (40.7)	0.00 (0.00)	6.37 (8.64)	-0.643 (0.00)	**1.170 (8.06)**	-0.643 (-4.43)	**0.251 (1.73)**	0.485 (3.34)	0.377 (2.60)	4.66
19		S302	9.61 (42.7)	0.00 (0.00)	6.69 (9.07)	-0.674 (0.00)	**1.230 (8.47)**	-0.674 (-4.64)	**0.228 (1.57)**	0.440 (3.03)	0.342 (2.36)	5.39
20	Current Study	G2	40.40 (179.7)	0.00 (0.00)	26.03 (35.30)	0.014 (0.00)	**0.303 (2.09)**	0.014 (0.096)	**0.337 (2.32)**	0.456 (3.15)	0.505 (3.48)	0.90
											Mean:	3.08
											COV:	0.75

5.3.3 Eurocode 2 (2004)

Shear demands are required to be designed at the column perimeter and at the basic control section (critical section). The current study focuses on shear at the critical section only for comparison purposes. At the critical section, punching shear demand and capacity per EC2 is evaluated using Eq. 2.18 and Eq. 2.22, respectively. The critical section is defined in Fig. 2.13. In Eq. 2.18, V_{Ed} is the applied shear force on the critical section and d is the slab effective depth. Coefficient β is $b_{o,EC2}/b_{red,EC2}$ if load eccentricity is toward interior of the slab with respect to the center of the critical section, and $b_{red,EC2}$ is the reduced perimeter defined in Fig. 2.14. For connections with load eccentricity toward the exterior, β is $1+\sqrt{\left(k_x \frac{M_{ED,x}}{v_{ED}d}\frac{1}{W_{1,x}}\right)^2+\left(k_y \frac{M_{ED,y}}{v_{ED}d}\frac{1}{W_{1,y}}\right)^2}$ to consider bi-axial bending effects as suggested by German Annex (EN 1992-1-1/NA, 2013). In which, $k_x = k_y = 0.6$ applies to all collected specimens with a square column, $M_{ED,x}$ and $M_{ED,y}$ refers to moment at center of the critical section with axis along x- and y- direction, respectively, and $W_{1,x}$ and $W_{1,y}$ is the first moment area of the critical section with respect to x- and y- axis, respectively. Please see Appendix A for more details about $W_{1,x}$ and $W_{1,y}$.

In Eq. 2.22, the partial safety factor for concrete, γ_c, is taken as unity in the evaluation. For slabs with effective depth of 8 in. or less, size effect coefficient k_s is 2.0, which applies to all collected specimens. The parameter $\rho_{l,EC2}$ is $\sqrt{\rho_{tx,EC2}\rho_{ty,EC2}}$ and should not be larger than 0.02, where $\rho_{tx,EC2}$ and $\rho_{ty,EC2}$ represents the slab top reinforcement ratio within a width defined as the column width plus a 3d distance in the x- and y-direction, respectively. Please note, the characteristic concrete strength f_{ck}, originally used in EC2, is replaced by f'_c in Eq. 2.22.

Parameters used for the strength model per EC2 as well as the analytical results are summarized in Table 5.6. The experimental-to-predicted shear strength ratios of all specimens are presented in Fig. 5.6. Compared to other design provisions, EC2 appears to provide better and more uniform predicted strengths for the collected specimens. The mean of the $v_{u,EC2}/v_{c,\,EC2}$ ratios of the specimens is 1.41 and the COV is 0.31.

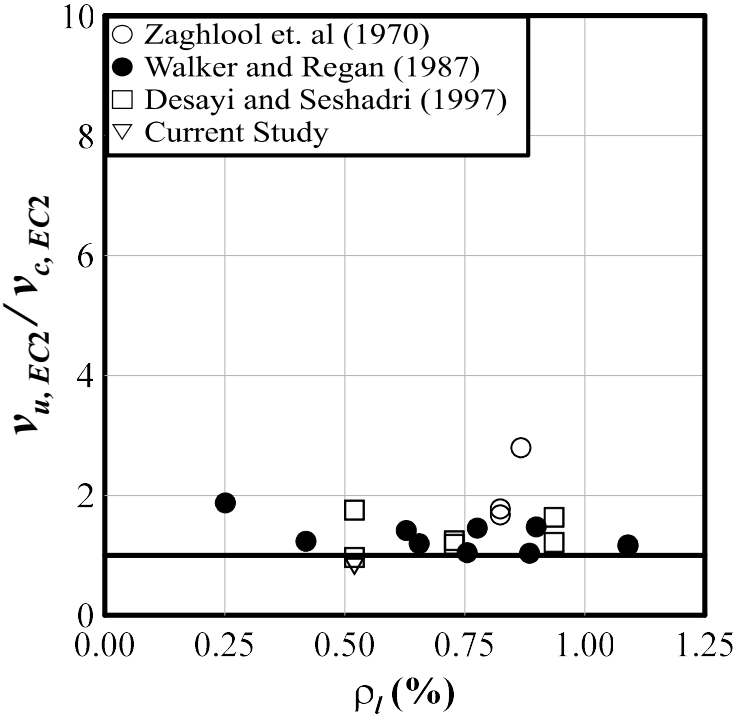

Fig. 5.6 - Punching Shear Strength Evaluation per Eurocode 2.

Table 5.6 – Punching Shear Strength Evaluation per EC2 (2004)

Specimen Data			Critical Section Properties							Load Data	Shear Demand	Shear Capacity	Demand / Capacity
No.	Researcher	Specimen	d	$b_{o,EC2}$	$b_{o,red,EC2}$	β	γ_c	k_s	$\rho_{l,EC2}$	V_g	$v_{u,EC2}$	$v_{c,EC2}$	$\frac{v_{u,EC2}}{v_{c,EC2}}$
			in. (mm)	in. (mm)	in. (mm)	in. (mm)	in. (mm)	in. (mm)	%	kip (kN)	ksi (MPa)	ksi (MPa)	
1	Zaghlool et al. (1970)	I	4.50 (114)	25.10 (639.0)	19.60 (499.0)	1.93	1.0	2.0	0.87	23.60 (105.00)	0.402 (2.77)	0.144 (0.992)	2.80
2		III	4.50 (114)	27.10 (689.0)	20.60 (524.0)	1.24	1.0	2.0	0.82	22.30 (99.00)	0.226 (1.55)	0.134 (0.927)	1.68
3		IV	4.50 (114)	25.10 (689.0)	20.60 (524.0)	1.32	1.0	2.0	0.82	26.50 (118.00)	0.288 (1.98)	0.161 (1.11)	1.78
4	Walker and Regan (1987)	SC1	3.90 (100)	36.00 (914.0)	24.20 (614.0)	1.49	1.0	2.0	0.65	18.30 (81.40)	0.192 (1.33)	0.159 (1.10)	1.20
5		SC2	3.9 (100)	36.00 (914.0)	24.20 (614.0)	1.49	1.0	2.0	0.42	16.80 (74.70)	0.177 (1.22)	0.142 (0.978)	1.24
6		SC3	3.90 (100)	36.00 (914.0)	24.20 (614.0)	1.49	1.0	2.0	0.88	16.70 (74.30)	0.176 (1.21)	0.168 (1.16)	1.04
7		SC4	3.90 (100)	26.70 (754.0)	21.00 (534.0)	1.41	1.0	2.0	0.76	14.30 (63.60)	0.173 (1.19)	0.164 (1.13)	1.05
8		SC5	3.90 (100)	26.70 (754.0)	21.00 (534.0)	1.41	1.0	2.0	1.09	18.50 (82.30)	0.224 (1.54)	0.193 (1.33)	1.16
9		SC7	3.90 (100)	26.70 (754.0)	21.00 (534.0)	1.41	1.0	2.0	1.09	18.50 (82.30)	0.224 (1.54)	0.189 (1.30)	1.18
10		SC8	2.50 (64.0)	20.50 (521.0)	14.20 (361.0)	1.44	1.0	2.0	0.25	7.40 (32.90)	0.207 (1.42)	0.110 (0.759)	1.88
11		SC9	2.50 (64.0)	20.50 (521.0)	14.20 (361.0)	1.44	1.0	2.0	0.63	7.40 (32.90)	0.207 (1.42)	0.145 (1.00)	1.42
12		SC11	2.40 (60.0)	20.00 (509.0)	13.70 (349.0)	1.43	1.0	2.0	0.90	7.40 (32.90)	0.224 (1.55)	0.152 (1.04)	1.48
13		SC12	2.40 (60.0)	31.00 (789.0)	14.50 (369.0)	2.14	1.0	2.0	0.78	8.30 (36.90)	0.242 (1.67)	0.165 (1.14)	1.46
14	Desayi and Seshadri (1997)	S101	3.20 (80.0)	17.80 (451.0)	13.80 (351.0)	1.28	1.0	2.0	0.52	7.34 (32.60)	0.135 (0.928)	0.139 (0.956)	0.97
15		S201	3.20 (80)	17.80 (451.0)	13.80 (351.0)	1.28	1.0	2.0	0.73	10.60 (47.00)	0.194 (1.34)	0.155 (1.07)	1.25
16		S301	3.20 (80)	17.80 (451.0)	13.80 (351.0)	1.28	1.0	2.0	0.93	12.40 (55.10)	0.228 (1.57)	0.139 (0.956)	1.64
17		S102	3.20 (80.0)	17.80 (451.0)	13.80 (351.0)	1.28	1.0	2.0	0.52	11.70 (52.20)	0.216 (1.49)	0.122 (0.844)	1.76
18		S202	3.20 (80.0)	17.80 (451.0)	13.80 (351.0)	1.28	1.0	2.0	0.73	9.16 (40.70)	0.168 (1.16)	0.141 (0.974)	1.19
19		S302	3.20 (80.0)	17.80 (451.3)	13.80 (351.3)	1.28	1.0	2.0	0.93	9.61 (42.7)	0.176 (1.22)	0.144 (0.992)	1.22
20	Current Study	G2	6.60 (168)	52.70 (1340.0)	36.80 (934.0)	1.08	1.0	2.0	0.52	40.40 (180.0)	0.126 (0.865)	0.154 (1.06)	0.82
												Mean:	1.41
												COV:	0.31

5.3.4 fib Model Code 2010

Per MC-10, punching shear demand, $v_{u,MC}$, is the applied shear stress on the basic control section with a perimeter $b_{o,MC}$ $b_{o,MC10}$ defined in Fig. 2.15. Shear capacity, $v_{c,MC}$, is determined using Eq. 2.24, where $f_c^{'}$ is the concrete strength (f_{ck} originally); $b_{red,MC10}$ defined in Fig. 2.16 is the reduced basic control perimeter intended to consider moment transfers from two directions; and d is the effective slab depth. Again, the partial safety factor for concrete, γ_c, is taken as unity. Coefficient k_ψ is provided to consider the effect of aggregate size, slab effective depth, and slab rotation (the larger value from the two directions). The partial safety factor γ_c for concrete material properties and the coefficient k_{dg} for aggregate size effect are taken to be unity for all specimens. Please note, the maximum aggregate size of 0.63 in. or greater is assumed for the test specimens by Desayi and Seshadri (1997) due to the lack of information.

Parameters used for the strength model per MC10 are summarized in Table 5.7. Analytical results are summarized in Table 5.8. The experimental-to-predicted shear strength ratios of all specimens per MC-10 are presented in Fig. 5.7. The ratios of the connection shear capacity and demand of all specimens have a mean value of 2.65 and a COV of 0.43.

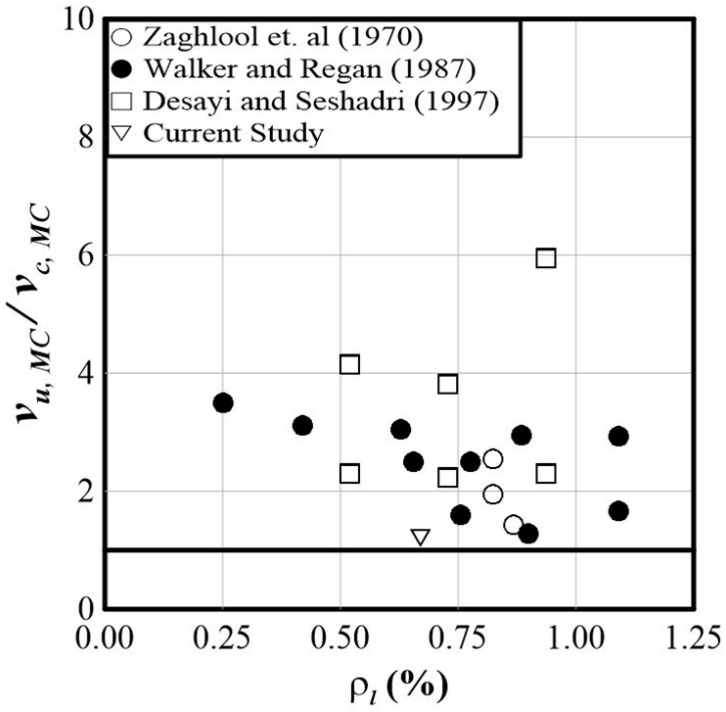

Fig. 5.7 – Punching Shear Strength Evaluation per fib Model Code 2010.

Table 5.7 – Parameters for Punching Shear Strength Evaluation per fib Model Code (2010))

Specimen Data			Load Data				Control Perimeter					Rotation Perimeter							
No.	Researcher	Specimen	V_g	M_x	M_y	M_d	d	e_u	b_u	k_e	$b_{o,MC}$	r_{sx}	r_{sy}	$b_{s,}$	b_r	m_{ux}	m_{uy}	m_{nx}	m_{ny}
			kip (kN)	kip-ft (kN-m)	kip-ft (kN-m)	kip-ft (kN-m)	in. (mm)	in. (mm)	in. (mm)	in. (mm)	in. (mm)	in. (mm)	in. (mm)	in. (mm)	in. (mm)	kip-ft/ft (kN-m/m)	kip-ft/ft (kN-m/m)	kip-ft/ft (kN-m/m)	kip-ft/ft (kN-m/m)
1	Zaghlool et al. (1970)	I	23.60 (105.0)	6.46 (8.80)	4.92 (6.70)	8.20 (11.10)	4.5 (114)	0.18 (4.47)	8.66 (220)	0.98	14.30 (362)	26.40 (671)	26.40 (671)	39.80 (1010)	11.00 (279)	11.80 (52.4)	11.80 (52.4)	14.50 (64.30)	14.50 (64.30)
2		III	22.30 (99.0)	11.90 (16.10)	11.80 (16.0)	16.70 (22.70)	4.5 (114)	4.33 (110)	9.80 (249)	0.69	11.50 (291)	26.40 (671)	26.40 (671)	39.80 (1010)	13.00 (330)	11.10 (49.5)	11.10 (49.5)	12.25 (54.50)	12.30 (54.50)
3		IV	26.50 (118.0)	11.60 (15.80)	16.20 (22.0)	20.0 (27.10)	4.5 (114)	4.33 (110)	9.80 (249)	0.69	11.50 (291)	26.40 (671)	26.40 (671)	39.80 (1010)	13.00 (330)	13.25 (59.00)	13.25 (59.00)	9.63 (42.80)	9.63 (42.80)
4	Walker and Regan (1987)	SC1	18.30 (81.30)	18.60 (25.20)	18.60 (25.2)	26.30 (35.70)	3.9 (100)	11.00 (279)	15.50 (394)	0.59	8.74 (222)	23.80 (605)	23.80 (605)	35.80 (908)	23.60 (600)	9.14 (40.70)	9.14 (40.70)	6.63 (29.50)	6.63 (29.50)
5		SC2	16.80 (74.70)	17.70 (24.00)	17.70 (24.00)	25.0 (33.90)	3.90 (100)	11.60 (295)	15.50 (394)	0.57	8.50 (216)	23.80 (605)	23.80 (605)	35.80 (908)	23.60 (600)	8.40 (37.40)	8.40 (37.40)	4.47 (19.90)	4.47 (19.90)
6		SC3	16.70 (74.30)	23.30 (31.60)	23.30 (31.60)	33.0 (44.70)	3.90 (100)	17.40 (442)	15.50 (394)	0.47	7.01 (178)	23.80 (605)	23.80 (605)	35.80 (908)	23.60 (600)	8.35 (37.10)	10.80 (48.00)	8.10 (36.00)	8.10 (36.00)
7		SC4	14.30 (63.60)	12.30 (16.70)	12.30 (16.70)	17.4 (23.60)	3.90 (100)	9.45 (240)	12.00 (304)	0.56	8.31 (211)	24.50 (623)	24.50 (623)	36.80 (934)	17.30 (440)	7.15 (31.80)	7.31 (32.50)	7.31 (32.50)	7.31 (32.50)
8		SC5	18.50 (82.30)	13.90 (18.80)	13.90 (18.80)	19.6 (26.60)	3.90 (100)	7.56 (192)	12.00 (304)	0.61	9.13 (232)	24.50 (623)	24.50 (623)	36.80 (934)	17.30 (440)	9.25 (41.10)	9.25 (41.10)	9.92 (44.10)	9.92 (44.10)
9		SC7	18.50 (82.30)	20.40 (27.60)	20.40 (27.60)	28.8 (39.00)	3.90 (100)	13.50 (344)	12.00 (304)	0.47	7.01 (178)	24.50 (623)	24.50 (623)	36.80 (934)	17.30 (440)	9.25 (41.10)	12.52 (55.70)	9.92 (44.10)	9.92 (44.10)
10		SC8	7.40 (32.90)	3.47 (4.70)	3.47 (4.70)	4.90 (6.60)	2.50 (64)	4.37 (111)	8.50 (216)	0.66	6.30 (160)	15.90 (405)	15.90 (405)	23.90 (607)	12.60 (320)	3.70 (16.50)	3.70 (16.50)	1.72 (7.66)	1.72 (7.66)
11		SC9	7.40 (32.90)	4.35 (5.90)	4.35 (5.90)	6.10 (8.34)	2.50 (64)	6.42 (163)	8.50 (216)	0.57	5.43 (138)	15.90 (405)	15.90 (405)	23.90 (607)	12.60 (320)	3.70 (16.50)	3.70 (16.50)	2.32 (10.30)	2.32 (10.30)
12		SC11	7.40 (32.90)	1.62 (2.20)	3.39 (4.60)	3.80 (5.10)	2.40 (60)	2.60 (66.0)	8.43 (214)	0.76	6.97 (177)	15.90 (405)	15.90 (405)	23.90 (607)	12.60 (320)	3.70 (16.50)	3.70 (16.50)	6.60 (29.30)	6.60 (29.30)
13		SC12	8.30 (36.90)	6.56 (8.90)	9.37 (12.70)	11.4 (15.50)	2.40 (60)	11.10 (282)	14.70 (373)	0.57	5.20 (132)	14.70 (374)	9.53 (242)	17.80 (451)	23.60 (600)	5.56 (24.80)	4.15 (18.50)	4.68 (20.80)	4.68 (20.80)
14	Desayi and Seshadri (1997)	S101	7.33 (32.60)	6.50 (8.81)	6.50 (8.81)	9.20 (12.50)	3.20 (80)	12.00 (304)	6.18 (157)	0.34	3.52 (89.3)	8.31 (211)	8.31 (211)	12.50 (317)	7.87 (200)	5.89 (26.20)	8.80 (39.20)	6.76 (30.10)	6.76 (30.10)
15		S201	10.60 (47.0)	9.37 (12.70)	9.37 (12.70)	13.20 (17.90)	3.20 (80)	12.00 (304)	6.18 (157)	0.34	3.52 (89.3)	8.31 (211)	8.31 (211)	12.50 (317)	7.87 (200)	8.50 (37.80)	12.69 (56.40)	8.19 (36.50)	8.19 (36.50)
16		S301	12.40 (55.10)	11.00 (14.90)	11.00 (14.90)	15.6 (21.10)	3.20 (80)	12.00 (304)	6.18 (157)	0.34	3.52 (89.3)	8.31 (211)	8.31 (211)	12.50 (317)	7.87 (200)	9.96 (44.30)	14.87 (66.20)	9.73 (43.3)	9.73 (43.3)
17		S102	11.70 (52.20)	7.89 (10.70)	7.89 (10.70)	11.1 (15.10)	3.20 (80)	8.35 (212)	6.18 (157)	0.42	4.41 (112)	8.31 (211)	8.31 (211)	12.50 (317)	7.87 (200)	7.02 (31.20)	10.30 (46.00)	6.51 (29.00)	6.51 (29.00)
18		S202	9.16 (40.70)	6.16 (8.35)	6.16 (8.35)	8.70 (11.80)	3.20 (80)	8.35 (212)	6.18 (157)	0.42	4.41 (112)	8.31 (211)	8.31 (211)	12.50 (317)	7.87 (200)	5.48 (24.40)	8.01 (35.60)	7.90 (35.20)	7.90 (35.20)
19		S302	9.61 (42.80)	6.46 (8.76)	6.46 (8.76)	9.10 (12.40)	3.20 (80)	8.35 (212)	6.18 (157)	0.42	4.41 (112)	8.31 (211)	8.31 (211)	12.50 (317)	7.87 (200)	5.75 (25.60)	8.41 (37.40)	10.20 (45.60)	10.20 (45.60)
20	Current Study	G2	40.40 (180.0)	40.20 (54.60)	40.20 (54.60)	56.9 (77.20)	6.60 (168)	7.76 (197)	21.70 (551)	0.74	18.40 (468)	22.80 (578)	22.80 (578)	34.20 (868)	32.00 (812)	20.20 (89.90)	20.20 (89.90)	16.60 (73.60)	16.60 (73.60)

Table 5.8 – Punching Shear Strength Evaluation per fib Model Code (2010)

Specimen Data			Punching Shear Strength Parameters							Shear Demand	Shear Capacity	Demand / Capacity
No.	Researcher	Specimen	$f_c^{'}$ psi (MPa)	d in. (mm)	$b_{o,MC}$ in. (mm)	ψ in x-direction	ψ in y-direction	k_ψ	γ_c	$v_{u,MC}$ ksi (MPa)	$v_{c,MC}$ ksi (MPa)	$\frac{v_{u,MC}}{v_{c,MC}}$
1	Zaghlool et al. (1970)	I	3500 (24.1)	4.50 (114)	14.30 (362)	0.012	0.012	0.362	1.0	0.368 (2.53)	0.258 (1.78)	1.43
2		III	3005 (20.7)	4.50 (114)	11.50 (291)	0.015	0.015	0.335	1.0	0.432 (2.98)	0.221 (1.52)	1.95
3		IV	5185 (35.7)	4.50 (114)	11.50 (291)	0.027	0.027	0.234	1.0	0.515 (3.55)	0.203 (1.40)	2.54
4	Walker and Regan (1987)	SC1	6280 (43.3)	3.90 (100)	8.74 (222)	0.033	0.033	0.224	1.0	0.533 (3.67)	0.213 (1.47)	2.50
5		SC2	6947 (47.9)	3.90 (100)	8.50 (216)	0.053	0.053	0.160	1.0	0.501 (3.45)	0.161 (1.11)	3.11
6		SC3	5424 (37.4)	3.90 (100)	7.01 (178)	0.021	0.031	0.231	1.0	0.605 (4.17)	0.205 (1.41)	2.95
7		SC4	5918 (40.8)	3.90 (100)	8.31 (211)	0.020	0.021	0.295	1.0	0.437 (3.01)	0.273 (1.88)	1.60
8		SC5	6744 (46.5)	3.90 (100)	9.13 (232)	0.019	0.019	0.312	1.0	0.515 (3.55)	0.309 (2.13)	1.67
9		SC7	6353 (43.8)	3.90 (100)	7.01 (178)	0.019	0.030	0.239	1.0	0.673 (4.63)	0.229 (1.58)	2.93
10		SC8	5424 (37.4)	2.50 (64.0)	6.30 (160)	0.089	0.089	0.151	1.0	0.467 (3.22)	0.134 (0.922)	3.49
11		SC9	4975 (34.3)	2.50 (64.0)	5.43 (138)	0.057	0.057	0.209	1.0	0.541 (3.72)	0.178 (1.22)	3.04
12		SC11	3945 (27.2)	2.40 (60)	6.97 (177)	0.013	0.013	0.458	1.0	0.444 (3.06)	0.346 (2.39)	1.28
13		SC12	5903 (40.7)	2.40 (60)	5.20 (132)	0.036	0.015	0.290	1.0	0.668 (4.60)	0.269 (1.85)	2.49
14	Desayi and Seshadri (1997)	S101	5221 (36.0)	3.20 (80)	3.52 (89.3)	0.012	0.021	0.330	1.0	0.663 (4.57)	0.287 (1.98)	2.30
15		S201	5221 (36.0)	3.20 (80)	3.52 (89.3)	0.015	0.028	0.287	1.0	0.955 (6.58)	0.250 (1.72)	3.82
16		S301	2901 (20.0)	3.20 (80)	3.52 (89.3)	0.015	0.027	0.291	1.0	1.12 (7.71)	0.189 (1.30)	5.94
17		S102	3597 (24.8)	3.20 (80)	4.41 (112)	0.016	0.028	0.283	1.0	0.848 (5.85)	0.204 (1.41)	4.15
18		S202	3945 (27.2)	3.2 (80)	4.41 (112)	0.008	0.015	0.392	1.0	0.662 (4.56)	0.297 (2.05)	2.23
19		S302	3249 (22.4)	3.2 (80)	4.41 (112)	0.006	0.011	0.442	1.0	0.695 (4.79)	0.303 (2.09)	2.29
20	Current Study	G2	7090 (48.9)	6.6 (168)	18.40 (468)	0.015	0.015	0.267	1.0	0.331 (2.28)	0.271 (1.87)	1.22
											Mean:	2.65
											COV:	0.43

5.4 PROPOSED PUNCHING SHEAR STRENGTH MODEL FOR CORNER SLAB - COLUMN CONNECTION UNDER GRAVITY-TYPE LOADING

Based on the findings mentioned above, there is still room for improvement on the shear strength model for corner slab-column connections. First of all, the interaction between the gravity shear and unbalanced moment of the specimens was examined. Test results of the five specimen pairs, each pair had identical dimensions and reinforcement ratios, are summarized in Table 5.9. The interactions between the unbalanced moments and gravity shear of those specimens are presented in Fig. 5.8. Each specimen pair is presented with the same symbol in Fig. 5.8. Because unbalanced moments are practically similar on both orthogonal directions, only the data along the x-direction are presented.

In Fig. 5.8, the straight solid line represents the shear capacity per ACI 318-14. As can be seen, instead of following this linear capacity line, test results show an opposite trend. The trend indicates that the assumed interaction between the unbalanced moment and gravity shear in the connection shear strength model per ACI 318-14 may not be appropriate. Further analysis is conducted without considering the unbalanced moment. If moment transfer is not considered, experimental data shows that connection shear capacity appears to be greatly influenced by b_o/d and ρ_l as shown in Fig. 5.9.

Based on data shown in Fig. 5.9, a shear capacity model for corner slab-column connection subjected to gravity-type loading only is proposed as shown in Eq. 5.1. The coefficient α is 10 when ρ_l =0.005 and 20 when ρ_l =0.015. Linear interpolation can be used for intermediate values of ρ_l. In addition, a shear strength of $2.00\sqrt{f_c'\,(\text{psi})}\,b_o d$ for the proposed model, consistent with one-way shear strength stipulated in the ACI 318-14, appears to an acceptable lower bound as shown in Fig. 5.9.

Based on the proposed model, punching shear strengths of the specimens in the database are evaluated and summarized in Table 5.10. The relationship between connection shear demand-to-capacity ratio based on the proposed model and the equivalent reinforcement ratio is presented in Fig. 5.10 The proposed model provides satisfactory results with an average experimental-to-predicted strength ratio of 1.12 with a COV of 0.21.

$$v_{c,prop} = \frac{\alpha d}{b_o}\sqrt{f_c'(\text{psi})} \geq 2.00\sqrt{f_c'(\text{psi})} \qquad \text{Eq. 5.1}$$

Table 5.9 – Influence of Moment on the Connection Shear

Specimen Pairs	d	b_o	V_g	M_x	Remarks
	in. (mm)	in. (mm)	kip-ft (kN-m)	kip-ft (kN-m)	
III	4.5	17.5	22.30 (99.0)	11.90 (16.1)	Different f_c'
IV	(114)	(445)	26.50 (118.0)	11.60 (15.8)	
SC5	3.90	21.3	18.50 (82.3)	13.90 (18.8)	Different connection integrity detailing
SC7	(100)	(541)	15.50 (82.5)	20.40 (27.6)	
S101	3.20	11.0	7.34 (32.6)	6.50 (8.81)	Different loading point distances
S102	(80)	(280)	11.70 (52.2)	7.89 (10.70)	
S201	3.20	11.0	10.60 (47.0)	9.37 (12.70)	Different loading point distances
S202	(80)	(280)	9.16 (40.7)	6.16 (8.35)	
S301	3.20	11.0	12.40 (55.1)	11.00 (14.90)	Different loading point distances
S302	(80)	(280)	9.61 (42.7)	6.46 (8.76)	

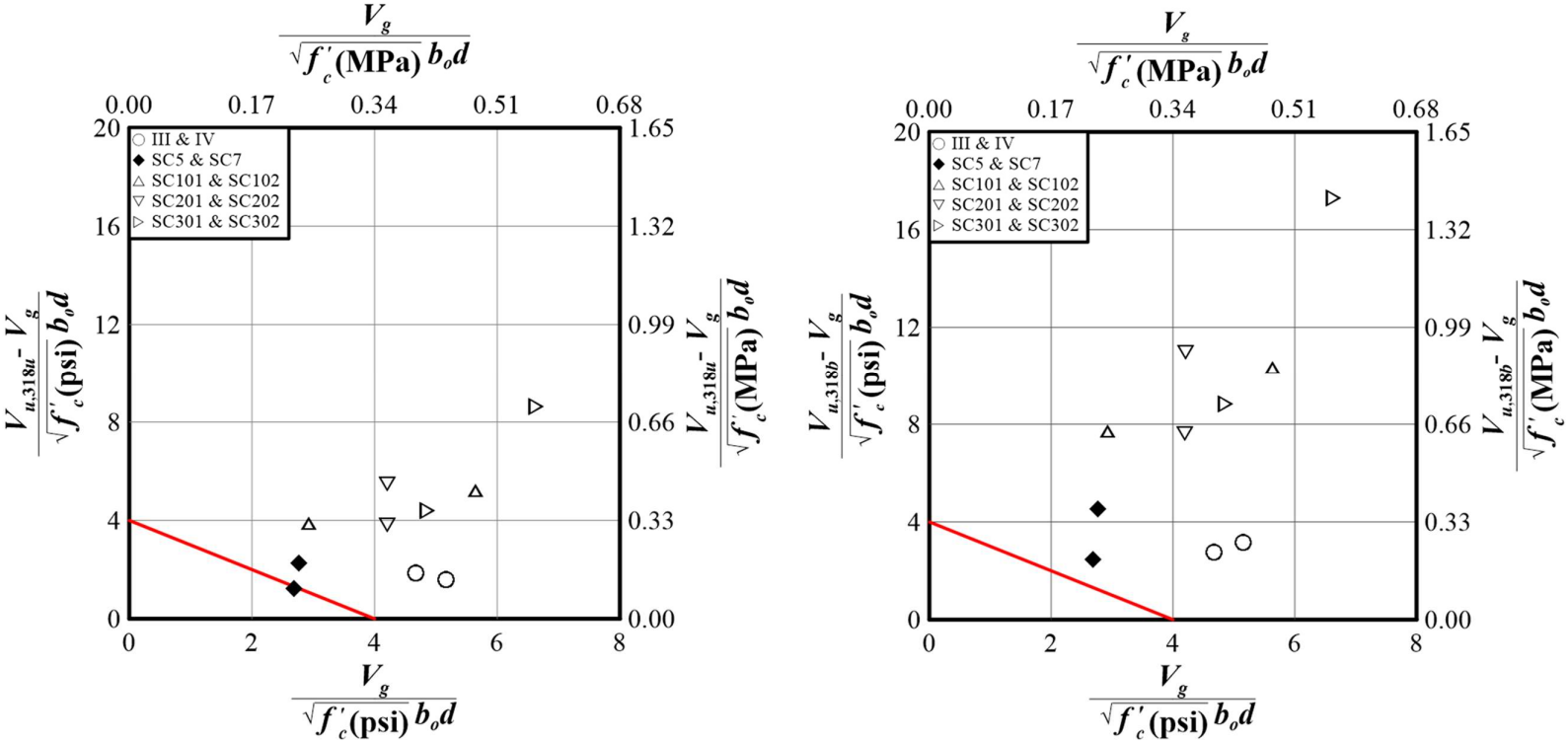

(a) Uniaxial Moment Transfer **(b) Biaxial Moment Transfer**

Fig. 5.8 – Evaluation of Connection Shear – Unbalanced Moment Interaction

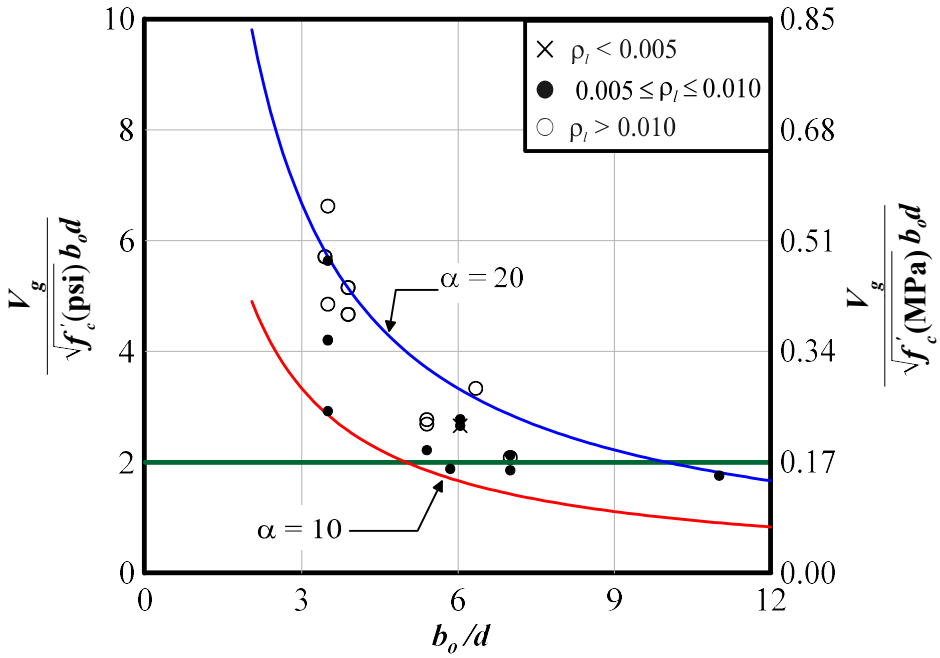

Fig. 5.9 – Effect of b_o/d Ratio on Connection Shear Strength

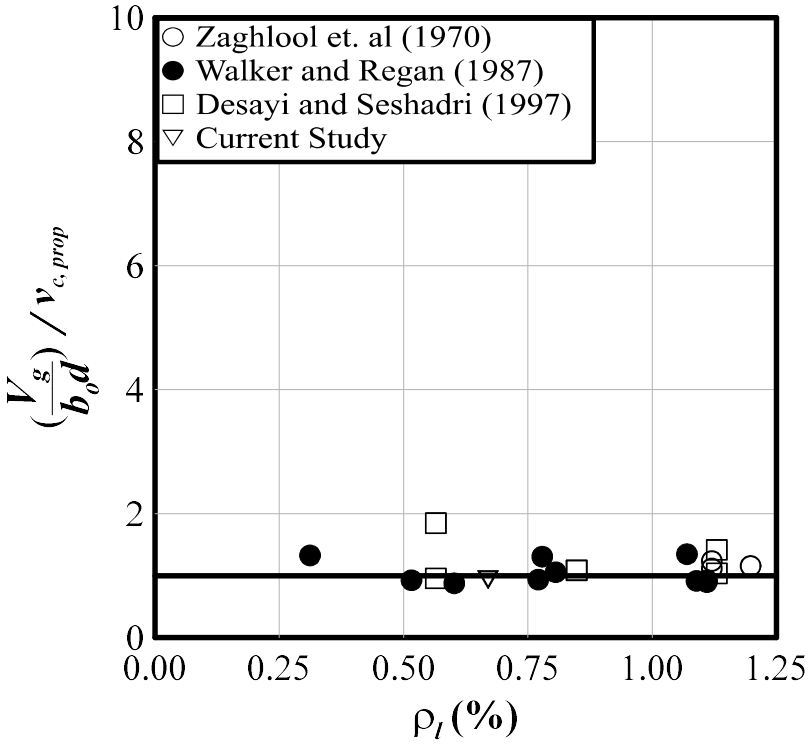

Fig. 5.10 – Proposed Punching Shear Evaluation.

Table 5.10 – Punching Shear Strength Evaluation using the Proposed Punching Shear Strength Model

Specimen Data			Punching Shear Strength Parameters							Shear Demand	Shear Capacity	Demand / Capacity
No.	Researcher	Specimen	f_c'	d	b_o	b_o/d	ρ_{tx}	ρ_{ty}	ρ_l	$\frac{V_g}{b_o d}$	$v_{c,prop}$	$\left(\frac{V_g}{b_o d}\right)/v_{c,prop}$
			psi. (MPa)	in. (mm)	in. (mm)		%	%	%	ksi. (MPa)	ksi. (MPa)	
1	Zaghlool et al. (1970)	I	3500 (24.1)	4.50 (114)	15.5 (394)	3.44	1.19	1.19	1.19	0.338 (2.33)	0.292 (2.01)	1.16
2		III	3005 (20.7)	4.50 (114)	17.5 (445)	3.89	1.12	1.12	1.12	0.283 (1.95)	0.228 (1.57)	1.24
3		IV	5185 (35.70)	4.50 (114)	17.5 (445)	3.89	1.12	1.12	1.12	0.337 (2.32)	0.299 (2.06)	1.12
4	Walker and Regan (1987)	SC1	6280 (43.3)	3.90 (100)	27.60 (700)	7.00	0.81	0.81	0.81	0.169 (1.16)	0.158 (1.09)	1.06
5		SC2	6947 (47.9)	3.90 (100)	27.60 (700)	7.00	0.52	0.52	0.52	0.155 (1.07)	0.167 (1.15)	0.93
6		SC3	5424 (37.40)	3.90 (100)	27.60 (700)	7.00	1.09	1.09	1.09	0.154 (1.06)	0.167 (1.15)	0.92
7		SC4	5918 (40.80)	3.90 (100)	21.30 (540)	5.40	0.77	0.77	0.77	0.171 (1.18)	0.181 (1.25)	0.94
8		SC5	6744 (46.50)	3.90 (100)	21.30 (540)	5.40	1.11	1.11	1.11	0.221 (1.52)	0.245 (1.69)	0.90
9		SC7	6353 (43.80)	3.90 (100)	21.60 (540)	5.40	1.11	1.11	1.11	0.221 (1.52)	0.238 (1.64)	0.93
10		SC8	5424 (37.40)	2.50 (64.0)	15.10 (384)	6.04	0.31	0.31	0.31	0.196 (1.35)	0.147 (1.02)	1.33
11		SC9	4975 (34.30)	2.50 (64.0)	15.10 (384)	6.04	0.78	0.78	0.78	0.196 (1.35)	0.149 (1.03)	1.31
12		SC11	3945 (27.20)	2.40 (60.0)	15.00 (380)	6.34	1.74	0.66	1.07	0.210 (1.44)	0.156 (1.07)	1.35
13		SC12	5903 (40.70)	2.40 (60.0)	26.00 (660)	11.00	0.33	1.10	0.60	0.135 (0.932)	0.154 (1.06)	0.88
14	Desayi and Seshadri (1997)	S101	5221 (36.0)	3.20 (80.0)	11.02 (280)	3.50	0.57	0.57	0.57	0.211 (1.46)	0.220 (1.52)	0.96
15		S201	5221 (36.0)	3.20 (80.0)	11.02 (280)	3.50	0.85	0.85	0.85	0.304 (2.10)	0.278 (1.92)	1.09
16		S301	2901 (20.0)	3.20 (80.0)	11.02 (280)	3.50	1.13	1.13	1.13	0.357 (2.46)	0.251 (1.73)	1.42
17		S102	3597 (24.8)	3.20 (80.0)	11.02 (280)	3.50	0.57	0.57	0.57	0.338 (2.33)	0.183 (1.26)	1.85
18		S202	3945 (27.2)	3.20 (80.0)	11.02 (280)	3.50	0.85	0.85	0.85	0.264 (1.82)	0.242 (1.67)	1.09
19		S302	3249 (22.4)	3.20 (80.0)	11.02 (280)	3.50	1.13	1.13	1.13	0.277 (1.91)	0.266 (1.83)	1.04
20	Current Study	G2	7090 (48.9)	6.60 (168)	38.6 (980)	5.85	0.67	0.67	0.67	0.159 (1.09)	0.169 (1.16)	0.94
											Mean:	1.12
											COV:	0.21

5.5 LATERAL DISPLACEMENT CAPACITY OF CORNER SLAB-COLUMN CONNECTIONS

The interaction between DR_u and gravity shear ratio, defined as the ratio between $V_g / b_o d$ and $v_{c,\,ACI}$ for all the collected specimens is presented in Fig. 5.11(a). As the gravity shear ratio increases, the DR_u in G-Series specimens with ρ_l = 0.67% degrade more quickly compared to R-Series specimens with ρ_l = 1.00%. The shear decay model per ACI 318-14, presented by solid line in Fig. 5.11(a), is not conservative for specimens with ρ_l = 0.67%. Results appear to be improved if the proposed punching shear strength model (Eq. 5.1) is used, as summarized in Table 5.11 and presented in Fig. 5.11(b).

Table 5.11– Drift Capacity of Corner Slab - Column Connections

Series	Specimen	$v_{c,ACI}$	$v_{c,prop}$	$\left(\frac{V_g}{b_o d}\right)$	$\frac{\left(\frac{V_g}{b_o d}\right)}{v_{c,\,ACI}}$	$\frac{\left(\frac{V_g}{b_o d}\right)}{v_{c,\,prop}}$	Drift (%)
		ksi (MPa)	ksi (MPa)	ksi (MPa)			
G-Series	G1	0.323 (2.22)	0.162 (1.11)	0.097 (0.667)	0.30	0.60	3.00
	G2	0.337 (2.32)	0.168 (1.16)	0.159 (1.09)	0.47	0.94	0.00
	G3	0.306 (2.11)	0.153 (1.05)	0.113 (0.780)	0.37	0.74	0.50
R-Series	R1	0.306 (2.11)	0.197 (1.36)	0.098 (0.675)	0.32	0.50	1.90
	R2	0.302 (2.08)	0.194 (1.34)	0.151 (1.04)	0.50	0.78	1.25
	R3	0.281 (2.22)	0.181 (1.25)	0.110 (0.756)	0.39	0.61	1.75

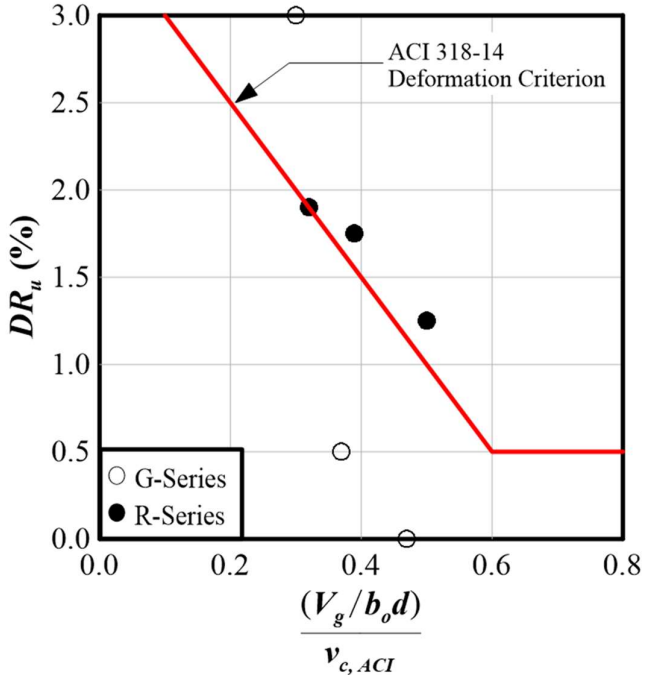

(a) ACI 318 -14

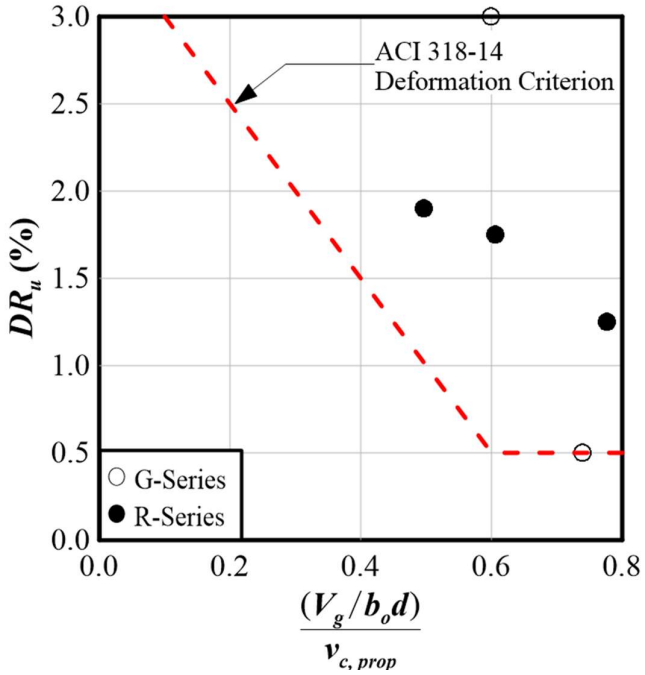

(b) Proposed Shear Strength Model

Fig. 5.11 - Specimen Drift Capacity

CHAPTER 6
CONCLUSION

In this study, a test program consisting of six specimens is conducted to investigate punching shear strength and deformation capacity of the corner slab-column connections. All test specimens were designed to be tested under combined gravity-type loading and lateral displacement reversals. Primary test parameters include (1) slab flexural reinforcement ratio, and (2) gravity shear ratio. Based on test results of the six specimens and additional nineteen specimens from previous researches, the following conclusions are drawn:

1. Although all test specimens were designed to be tested under combined gravity-type loading and lateral displacement reversals, specimen G2 failed by punching shear at a gravity shear level of $1.89\sqrt{f_c'(\text{psi})}\,b_o d$ before application of the lateral displacement reversals. Test results from the other five specimens indicate that lateral deformation capacity decreases as the connection gravity shear ratio increases.

2. Results from specimens (20 specimens) subjected to gravity-type loading indicate that punching shear strength model per current ACI 318-14 is not conservative, particularly for specimens with slab flexural reinforcement ratio (within the effective width, b_{ew}), ρ_l, of 0.75% or less. Among all strength models evaluated in this study, strength model per Eurocode 2 provides relatively better punching shear strength predictions.

3. Results from specimens G1, G3, R1, R2, and R3 also indicate that the shear decay model (gravity shear versus lateral deformation capacity curve) per current ACI 318-14 is not conservative when applied to the corner slab-column connections.

4. To be consistent with the design philosophy of the current ACI 318-14, a punching shear strength model considering effects of the aspect ratio b_o / d of the critical section and slab flexural reinforcement ratio within the effective width, ρ_l, is proposed for connections subjected to gravity-type loading only. This proposed model provides satisfactory prediction results to the collected specimens with a mean ratio between test results and the predicted

strength of 1.12 and a c.o.v. of 0.21.

5. Using the proposed shear capacity model to evaluate gravity shear ratio allows the shear decay model per ACI 318-14 to be applicable to specimens with ρ_l of either 0.67% or 1.0%.

REFERENCES

1. ACI Committee E-1, 1927, "Reinforced Concrete Building design and Specifications," Proceedings, Journal of American Institute, V.23, No.2, February, pp. 643-677.

2. ACI Committee 318, 1941, "Building Regulations for Reinforced Concrete (ACI 318-41)," American Concrete Institute, Detroit, MI, 63 pp.

3. ACI Committee 318, 1947, "Building Code Requirements for Reinforced Concrete (ACI 318-47)," American Concrete Institute, Detroit, MI, 64 pp.

4. ACI Committee 318, 1951, "Building Code Requirements for Reinforced Concrete (ACI 318-51)," Proceedings, Journal of American Concrete Institute, V. 47, No. 4, April, pp 589-652.

5. ACI Committee 318, 1956, "Building Code Requirements for Reinforced Concrete (ACI 318-56)," Proceedings, Journal of American Concrete Institute, V. 52, No. 5, May, pp 913-986.

6. ACI Committee 318, 1963a, "Building Code Requirements for Reinforced Concrete (ACI 318-63)," American Concrete Institute, Detroit, MI, 144 pp.

7. ACI Committee 318, 1963b, "Commentary on Building Code Requirements for Reinforced Concrete (ACI 318-63)," Publication SP-10 Special Publications, Detroit, MI, 91 pp.

8. ACI Committee 318, 1971a, “Building Code Requirements for Reinforced Concrete (ACI 318-71),” American Concrete Institute, Detroit, MI, 78 pp.

9. ACI Committee 318, 1971b, “Commentary on Building Code Requirements for Reinforced Concrete (ACI 318-71),” American Concrete Institute, Detroit, MI, 96 pp.

10. ACI Committee 318, 1974, “1974 Supplement to: Building Code Requirements for Reinforced Concrete (ACI 318-71) and Commentary on Building Code Requirements for Reinforced Concrete (ACI 318-71)” American Concrete Institute, Detroit, MI, 103 pp.

11. ACI Committee 318, 1977, “Building Code Requirements for Reinforced Concrete (ACI 318-77),” American Concrete Institute, Detroit, MI, 103 pp.

12. ACI Committee 318, 1983, “Building Code Requirements for Reinforced Concrete (ACI 318-83),” American Concrete Institute, Detroit, MI, 111 pp.

13. ACI Committee 318, 1989, “Building Code Requirements for Reinforced Concrete (ACI 318-89) and Commentary (ACI 318R-89)” American Concrete Institute, Detroit, MI, 353 pp.

14. ACI Committee 318, 1995, “Building Code Requirements for Structural Concrete (ACI 318-95) and Commentary (ACI 318R-95)” American Concrete Institute, Detroit, MI, 369 pp.

15. ACI Committee 318, 1999, “Building Code Requirements for Structural Concrete (ACI 318-99) and Commentary (ACI 318R-99)” American Concrete Institute, Farmington Hills, MI, 391 pp.

16. ACI Committee 318, 2002, “Building Code Requirements for Structural Concrete (ACI 318-02) and Commentary (ACI 318R-02)” American Concrete Institute, Farmington Hills, MI, 443 pp.

17. ACI Committee 318, 2005, “Building Code Requirements for Structural Concrete (ACI 318-05) and Commentary (ACI 318R-05)” American Concrete Institute, Farmington Hills, MI, 430 pp.

18. ACI Committee 318, 2008, “Building Code Requirements for Structural Concrete (ACI 318-08) and Commentary (ACI 318R-08)” American Concrete Institute, Farmington Hills, MI, 473 pp.

19. ACI Committee 318, 2014, “Building Code Requirements for Structural Concrete (ACI 318-14) and Commentary (ACI 318R-14)” American Concrete Institute, Farmington Hills, MI, 519 pp.

20. ACI Committee 501, 1936, “Building Regulations for Reinforced Concrete,” Proceedings, Journal of American Institute, V.32, No.3, March, pp. 407- 444.

21. Alexander, S. D. B., and Simmonds, S. H., 1992, “Bond Model for Concentric Punching Shear,” ACI Structural Journal, V. 89, No. 3 May-June, pp. 325-334.

22. ASCE/SEI 7, 2010, “Minimum Design Loads for Building and Other structures,” American Society of Civil Engineers, Reston, VA, 608 pp.

23. ASTM A370, 2012, “Standard Testing Methods and Definitions for Mechanical Testing Steel products,” ASTM International, West Conshohocken, PA, 48 pp.

24. ASTM A706/A706M, 2009, “Standard Specification for Low- Alloy Steel Deformed and Plain Bars for Concrete Reinforcement,” ASTM International, West Conshohocken, PA, 6 pp.

25. ASTM C143/C143M, 2015, “Standard Testing Methods for Slump of Hydraulic-Cement Concrete,” ASTM International, West Conshohocken, PA, 4 pp.

26. ASTM C617/C617M, 2015, “Standard Practice for Capping Cylindrical Concrete Specimens,” ASTM International, West Conshohocken, PA, 4 pp.

27. Broms, C. E., 2007, “Flat Plates in Seismic Areas: Comparison of Shear Reinforcement System,” ACI Structural Journal, V.104, No. 6, November- December, pp 712-721.

28. Cheng, M.-Y., and Giduquio, M. B., 2014a, “Seismic Design Issue of Corner Slab-Column Connection,” Journal of Earthquake Engineering, V. 18, No. 1, pp. 24-40, DOI: 10.1080/13632469.2013.816644.

29. Cheng, M.-Y., and Giduquio, M. B., 2014b, "Experimental Study of Corner Slab-Column Connection," ACI Structural Journal, V. 111, No. 5, September- October, pp. 1123- 1134.

30. Cheng, M-Y., and Parra-Montesinos, G. J., 2010a, "Evaluation of Steel Fiber Reinforcement for Punching Shear Resistance in Slab-Column Connections – Part I: Monotonically Increased Load," ACI Structural, V. 107, No. 1 January- February, pp. 101-109.

31. Cheng, M-Y., and Parra-Montesinos, G. J., 2010b, "Evaluaion of Steel Fiber Reinforcement for Punching Shear Resistance in Slab-Column Connections – Part II: Lateral Displacement Reversals," ACI Structural Journal, V. 107, No.1, January- February, pp. 110- 118.

32. Cheng, M-Y., and Parra-Montesinos, G. P.; and Shield, C. K.; 2010, "Shear Strength and Drift Capacity of Fiber- Reinforced Concrete Slab-column Connections Subjected to Biaxial Displacements," Journal of Structural Engineering, ASCE, V. 136, No. 9, September, pp. 1078-1088.

33. Cheng, M-Y., 2009, "Punching Shear Strength and deformation Capacity of fiber Reinforced Concrete Slab-Column Connection under Earthquake-Type Loading," PhD thesis, Civil and Environment Engineering Department, The University of Michigan, Ann Arbor, MI, 332pp.

34. Committee on Standard Building Regulations for the Use of Reinforced Concrete, 1920, "Standard Building Regulations for the Use of Reinforced Concrete," Standard

Specification No. 23, Proceedings, Journal of American Concrete Institute, V. 16, No. 2, pp. 283-302.

35. Committee on Reinforced Concrete and Building Laws, 1916, “Report of the Committee on Reinforced Concrete and Building Laws,” Proceedings, Journal of American Concrete Institute, V.12, No. 2, February, pp. 171-180.

36. Dam, Wight and Parra-Montesinos., “Behavior of Monotonically Loaded slab-column connections Reinforced with Shear studs: ACI structural journal, 2017.

37. DECON EXPERT Studrails 4.2.0.23, 2017, Computer program for Design of Shear reinforcement for Slabs, Decon, Brampton, Ontario.

38. Desayi, P., and Seshadri, H. K., 1997, “Punching Shear Strength of Flat Slab Corner Column Connections. Part 1. Reinforced Concrete Connections,” Proceedings of the Institute of Civil Engineers, Structures and Buildings, V.122, No. 1, February, pp. 10-20.

39. Di Stasio, J., and van Buren, M. P., 1960, “Transfer of Bending Moment between Flat Plate Floor and Column,” Journal of the American Concrete.

40. DIN EN 1992-1-1/NA: 2013-04. National Annex - National Pertermined Parameters - Eurocode 2: Design of concrete structures - Part 1-1: general rules and rules for buildings.

41. Dilger, W., Birkle, G., and Mitchell, D., 2005, "Effect of Flexural Reinforcement on Punching Shear Resistance," Special Publication 232 - Punching Shear in Reinforced Concrete Slabs, American Concrete Institute, 2005, pp. 57-74.

42. Einpaul, J.; Ruiz-Fernandez, M.; and Muttoni, A., 2015, "Influence of moment Redistribution and Compressive Member Action on Punching Strength of Flat Slabs," Engineering Structures, V. 86, March pp 43-57.

43. Elgabry, A. A., 1991, "Shear and Moment Transfer of Concrete Flat Plates," PhD thesis, Department of Civil Engineering, The University of Calgary, Calgary, Alberta, Canada, 266 pp.

44. Elgabry, A. A., and Ghali, A., 1996, "Transfer of Moments between columns and Slabs: Proposed Code Revision," ACI Structural Journal, V. 93, No. 1, January- February, pp. 56-61.

45. European Committee for Standardization, 2004, "Eurocode 2: Design of Concrete Structures – Part 1-1: General rules and Rules for Buildings," European Standard, Brussels, 225 pp.

46. Garner, N. J., and Shao, X.Y., 1996, "Punching Shear of Continuous Flat Reinforced Concrete Slabs," ACI Structural Journal, V. 93, No. 2 march-April, pp. 218-228.

47. Gasparini, D. A.; 2002, “Contributions of C.A.P. Turner to Development of Reinforced Concrete Flat Slabs 1905-1909,” Journal of Structural Engineering, ASCE, V. 128, No. 10, October, pp. 1243-1252.

48. Ghali, A., 1989, Discussions of “Proposed Revisions to Building Code Requirements for Reinforced Concrete (ACI 318-83),” ACI Structural Journal, V. 86, No. 3, May-June, pp. 328-330.

49. Ghali, A.; Gayed. R. B.; and Dilger, W., 2015, “Design of Concrete Slab for Punching Shear: Controversial Concepts,” ACI Structural Journal, V.112, No. 4, July-August, pp. 505-514.

50. Ghali, A., and Magally, S., 1999, “Design for Punching Shear Strength with ACI 318-95,” ACI Structural Journal, V. 96, No. 4, July-August, pp. 539-548.

51. Grossman, J. S., 1989, “Code Procedures, History, and Shortcomings: Column-Slab Connections,” Concrete International, V.11, No. 9, September, pp. 73-77.

52. Hammil, N., and Ghali, A., 1994, “Punching Shear Resistance of Corner Slab-Column Connections,” ACI Structural Journal, V. 91, No. 6, November- December, pp. 697-705.

53. Hanson, N. W., and Hanson, J. M., 1968, “Shear and Moment Transfer between Concrete Slabs and Columns,” Journal, PCA Research and Development Laboratories, V. 10, No. 1, January, pp. 2-16.

54. Henley, H. C., 1908, “Report of Committee on Laws and Ordinances,” National Association of Cement Users (NACU), Proceedings of the Fourth Annual Convention, V. 4 January, pp. 233-239.

55. Hueste, M. D. B.; Browning, J; Lepage, A.; and Wallace, J. W., 2007, “Seismic Design Criteria for Slab-Column Connections,” ACI Structural Journal, V. 104, No. 4, July-August, pp. 448-458.

56. Hueste, M. D. B.; Kang, H.-K.; and Robertson, I. N., 2009, “Lateral Drift Limits for Structural Concrete Slab-Column Connections, Including Shear Reinforcement Effects,” Proceedings, Structures 2009: Don’t Mess with Structural Engineers, ASCE, May, Austin, TX.pp 1515-1524.

57. Hueste, M. B. D., and Wight, J. k., 1999, “Nonlinear Punching Shear Failure Model for Interior Slab-Column Connections,” Journal of Structural Engineering, ASCE, V. 125, No. 9, September, pp. 997-1008.

58. Hwang, S.-J., and Moehle, J.P., 1990, “An Experimental Study of Flat-Plate Structures under Vertical and lateral Loads,” Report No. UCB/SEMM-90/11, Department of Civil Engineering, University of Carlifornia at Berkeley, CA, July, 271 pp.

59. International Federation for Structural Concrete, 2010, “fib Model Code for Concrete Structures,” International Federation for Structural Concrete, Lausanne, Switzerland, 402 pp.

60. Joint ACI-ASCE Committee 326, 1962, “Shear and Diagonal Tension,” American Concrete Institute, Detroit, MI, 124 pp.

61. Joint ACI-ASCE Committee 426, 1974, “The Shear Strength of Reinforced Concrete Members – Slabs,” Proceedings, ASCE, V. 100, No. ST8, August, pp. 1543-1591.

62. Joint ACI- ASCE Committee 352, 1988, “Recommendations for Design of Slab-Column Connections in Monolithic Reinforced Concrete Structures,” (ACI 352.1R-89), ACI Structural Journal, V. 85, No. 6, November – December, 1988, pp. 675-696.

63. Joint Committee of Concrete and Reinforced Concrete, 1913, “Report on Concrete and reinforced Concrete,” Proceedings, ASTM, V. 13, pp. 224-281.

64. Joint Committee of Concrete and Reinforced Concrete, 1917, “Final Report on Joint Committee on Concrete and reinforced Concrete,” Proceedings, ASTM, V. 17, pp. 202-262.

65. Joint Committee on Standard Specifications for Concrete and Reinforced Concrete, 1921, “Tentative Specifications for Concrete and Reinforced Concrete,” Committee Progress report, June, 73 pp.

66. Joint Committee on Standard Specifications for Concrete and Reinforced Concrete, 1924, “Standard Specifications for Concrete and Reinforced Concrete,” American Concrete Institute, Detroit, MI, August, 152 pp.

67. King, S., and Delatte, N. J., 2004, “Collapse of 2000 Commonwealth Avenue: Punching Shear Case Study,” Journal of Performance of Conctructed Facilities, ASCE, V. 18, No. 1, pp. 54-61.

68. Luo, Y., and Durrani, A. J., 1995, “Evaluation, Modeling, and Seismic Retrofit of Flat-Slab Buildings,” Structural Research at Rice, Report N. 44, Department of Civil Engineering, Rice University, Houston, Texas, 141 pp.

69. Matzke, E. M.; Lequesne, R. D.; Parra- Montesinos, G.J.; and Shield, C. K., 2015, Behavior of Biaxially Loaded Slab- Column Connections With Shear Studs,” ACI Structural Journal, V. 112, No. 3, May-June, pp.335-346.

70. McHarg, P. J.; Cook, W. D.; Mitchell, D.; and Yoon, Y.-S., 2000, “Benefits of Concentrated Slab Reinforcement and Steel Fibers on Perfomance of Slab-Column Connections,” ACI Structural Journal, V.97, No. 2, March- April, pp. 225-235.

71. Moe, J., 1961, “Shearing Strength of Reinforced Concrete Slabs and Footings under Concentrated Loads,” Development Department Bulletin D47, Research and Development Laboratories, Portland Cement Association, April Skokie, IL, 130 pp.

72. Moehle, J. P., 1988, “Strength of Slab-Column Edge Connections,” ACI Structural Journal, V.85, No.1, January- February, pp. 89-98.

73. NACU, 1910, “Standard Building Regulations for the Use of Reinforced Concrete,” Standard No. 4, Proceedings of the sixth Annual Convention, National Association of Cement Users, V. 6, February, pp. 349-361.

74. Pan, A. D., and Moehle, J. P., 1989, “Lateral Displacement Ductility of Reinforced Concrete Flat Plates,” ACI Structural Journal, V. 86, No. 3, May-June, pp. 250-258.

75. Pan, A. D., and Moehle, J. P., 1992, “An Experimental Study of Slab-Column Connections,” ACI Structural Journal, V. 89, No. 6, November- December, pp 626-638.

76. Park, T.-W., 2012, “Inspection of Collapse Cause of Sampoong Department Store,” Forensic Science International, Elsevier, V.217, No. 1-3, April, pp.119-126.

77. “Peikko Designer Ex. 1.0.2.75, 2017” Punching Reinforcement Software, Peikko, Lahti, Finland.

78. Rha, C.; Kang, T. H.-K.; Shin, M.; and Yoon, J. B., 2014, “Gravity and Laod- Carrying Capacity of Reinforced Concrete Flat Plate Systems,” ACI Structural Journal, V. 111, No. 4, July- August, pp. 753-764.

79. Robertson, I. N.; Kawai, T.; Lee, J.; and Enomoto, B., “Cyclic Testing of Slab-Column Connection with Shear Reinforcement,” ACI Structural Journal, V. 99, N. 5, September-October, pp. 605-613.

80. Shaaban, A. M., and Gesund, H., 1994, “Punching Shear Strength of Steel Fiber Reinforced Concrete Flat Plates,” ACI Structural Journal, V.91, No.3, July-August, pp. 406-414.

81. Sozen, M. A., and Siess, C. P., 1963, “Investigation of Multi-Panel Reinforced Concrete Floor Slabs: Design Methods- Their Evolution and Comparison,” Journal of the American Concrete Institute, Proceedings, V. 60, 8, August, pp. 999- 1028.

82. Sudarsana, I. K., 2001, “Punching Shear Behavior of Reinforced Slab-Column Connections of Flat Plate Structures,” PhD thesis, Department of Civil Engineering, University of Ottawa, Ottawa, ON, Canada, 225 pp.

83. Swamy, R. N., and Ali, S. A.R., 1982, “Punching Shear Behavior of Reinforced Slab-Column Connections Made with Steel Fiber Concrete,” Proceedings, ACI Journal, V. 79, No.5, September –October, pp. 392-406.

84. Walker, P. R., and Regan, P. E., 1987, “Corner Column-slab Connections in Concrete Flat Plate Floors,” Journal of Structural Engineering, ASCE, V. 113, No. 4, April, pp. 704-720.

85. Widianto, Oguzhan Bayrak, James O. Jirsa., “Two-way shear strength of slab-column connection”: Reexamination of ACI 318 provision. Mar. 2009.

86. Widjaja, S., 2008, “Behavior of Corner Column- Slab Connections in Irregular Flat Plate Floors under Gravity and Bidirectional Lateral Loading,” PhD thesis, School of Civil and Environmental Engineering, Nanyang Technological University, Singapore, 482 pp.

87. Wight, J. K., 2016, “Reinforced Concrete: Mechanics and Design,” Seventh Edition, Pearson Education Inc., Hoboken, NJ, 1144 pp.

88. Wight, J. K., and Falconer, D., 2005, "Concrete Q & A: Checking Punching Shear Strength by the ACI Code,' Concrete International, V. 27, No. 11, pp. 76.

89. Wood, J. G. M., 2004, "Pipers row Car Park, Wolverhampton: Quantitative Study of the Cause of the partial Collapse on 20th March 1997," Press Release, health and Safety Executive, UK, January, 197 pp.

90. Zaghlool, E. R. F., 1971, "Strength and Behavior of Corner and Edge Column-Slab Connections in Reinforced Concrete Flat Plates," PhD thesis, Department of Civil Engineering, University of Calgary, AB, Canada, 366 pp.

91. Zaghlool, E. R. F., and de Paiva, H. A. R., 1973, "Test of Flat- Plate Corner Column-Slab Connections," Proceedings, Journal of the Structural Division, ASCE, V. 99., No. ST3, March, pp. 551-572.

92. Zaghlool, E. R. F.; de Paiva, H. A. R.; and Glockner, P. G., 1970, "Test of Reinforced Concrete Flat Plate Floors," Proceedings, Journal of the Structural Division, ASCE, V. 96., No. ST3, March, pp. 487-507.

APPENDIX

Appendix A:

W_1 FORMULA DERIVATION

Square corner column derivation of W_1, the shear distribution along the basic control perimeter.

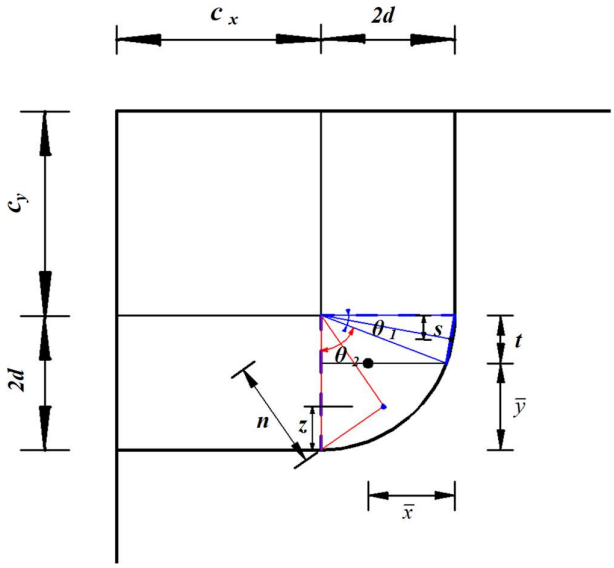

Figure 1: W_1 formula derivation for a typical critical section

In the above sketch of a corner column connection:

$$t = 2d - \bar{y} \quad , \quad \theta_1 = \sin^{-1}\left[\frac{t}{2d}\right] \quad , \quad \theta_2 = \frac{\pi}{2} - \theta_1$$

$$n = \frac{2d \sin\frac{\theta_2}{2}}{\frac{\theta_2}{2}}$$

$$z = 2d - \frac{2d \sin\frac{\theta_2}{2}}{\frac{\theta_2}{2}} \cos\frac{\theta_2}{2}$$

$$s = \frac{2d \sin\frac{\theta_1}{2}}{\frac{\theta_1}{2}} \sin\frac{\theta_1}{2}$$

$$\bar{x} = \frac{c_x\left(2d + \frac{c_x}{2}\right) + \left(\frac{(4\pi d)}{4}\right)\left(2d - \frac{4d}{\pi}\right)}{2c_x + \frac{4\pi d}{4}}$$

$$\bar{y} = \frac{c_y\left(2d + \frac{c_y}{2}\right) + \left(\frac{(4\pi d)}{4}\right)\left(2d - \frac{4d}{\pi}\right)}{2c_y + \frac{4\pi d}{4}}$$

Therefore W_1 was derived using the formula below:

$$W_1 = c_x\left(\frac{c_x}{2} + 2d - \bar{y}\right) + c_x\bar{y} + 2d\theta_1(t - s) + 2d\theta_2(\bar{y} - z)$$

Appendix B

YIELD LINE ANNALYSIS

Current Study:

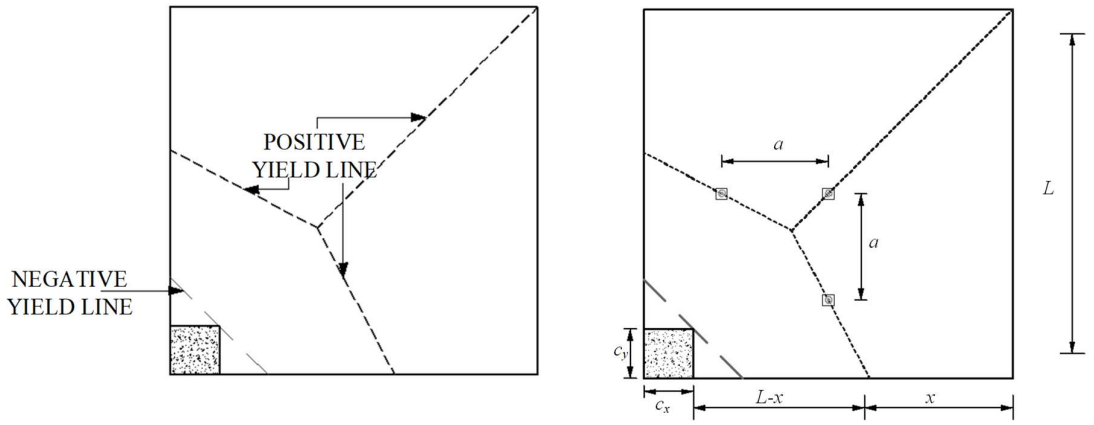

(a) Yield Line pattern (b) Load distribution pattern

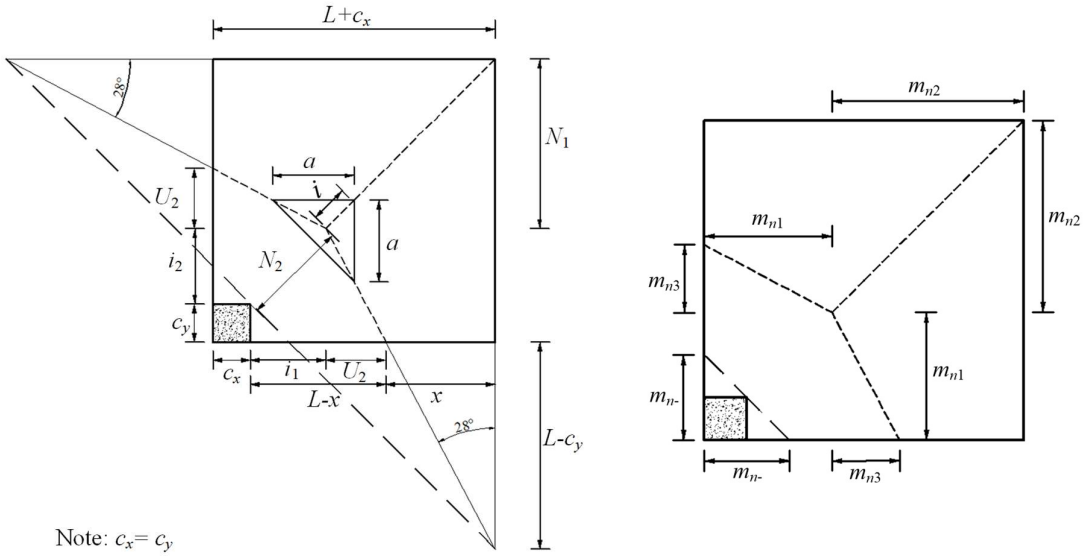

(c) Formula derivation

Figure 2: Yield Line Pattern and $V_{flex.}$ *formula derivation*

Specimen *G2*:

Positive Yield Line V_{flex} Calculations:

Positive External Work:

$$EW^{+} = 3P.\,\delta$$

Positive Internal Work:

Internal Work 1:

$$IW_1 = m_{n_1}\frac{\delta}{\left(\frac{L}{2}-\frac{1}{\sqrt{2}}i\right)}\left(\frac{L}{2}-\frac{1}{\sqrt{2}}i\right)+\ m_{n_2}\frac{\delta}{\left(\frac{L}{2}+\frac{1}{\sqrt{2}}i\right)}\left(\frac{L}{2}+\frac{1}{\sqrt{2}}i\right)$$

Internal work 2:

$$IW_2 = \left[\ m_{n_1}\left(\frac{L}{2}-\frac{1}{\sqrt{2}}i\right)\frac{\delta}{i_2}+\ m_{n_3}.U_2.\frac{\delta}{i_2}\right]$$

Where i = 16.9in., i_1= 31.8 in, i_2= 31.8 in, U_2= 22.67in., N_1= 70.69in. and N_2= $\sqrt{i_1^2+ i_2^2}$ = 44.97in.

Positive $V_{flex.}$ Calculations:

Total external work = total internal work

$EW^{+} = IW^{+}$

Therefore:

$$3p = 2\left(0.6907\ m_{n_1}+ m_{n_2}\right)+\left(1.536\ m_{n_1}\right)+\left(0.713\ m_{n_3}\right)$$
$$= \mathbf{2.9174}\ m_{n_1}\mathbf{+2}\ m_{n_2}+0.713\ m_{n_3}$$

Negative Yield Line $V_{flex.}$ Calculations:

Negative Internal Work:

$$(IW^{-}) = m_n^{-}\left(2\sqrt{2}c_y\right)\frac{\delta}{\left(i_1^2+ i_2^2\right)}+ m_{n_1}^{-}\frac{\delta}{\left(\frac{L}{2}-\frac{1}{\sqrt{2}}i\right)}\left(\frac{L}{2}-\frac{1}{\sqrt{2}}i\right)+ m_{n_2}^{-}\frac{\delta}{\left(\frac{L}{2}+\frac{1}{\sqrt{2}}i\right)}\left(\frac{L}{2}+\frac{1}{\sqrt{2}}i\right)$$

External work for the negative yield line will be the same as the one for the positive yield line.

$$EW^{+} = 3P.\,\delta$$

Negative V_{flex} Calculations:

Total external work = total internal work

$$3p^- = 2\left(0.6907\, m_{n_1}^- + m_{n_2}^-\right) + (1.006 m_n^-)$$
$$= \mathbf{1.3814}\, m_{n_1}^- + \mathbf{2}\, m_{n_2}^- + \mathbf{1.006} m_n^-$$

Moment strength, positive m_n and negative m_n were calculated using the Sp-column software, using the bottom and the top reinforcement areas from the provided reinforcement layout. Since the yield line pattern is not straight line, it's an incline line, therefore the moment was calculated considering both x- and y- directions.

The table below shows all the values of positive m_n and negative m_n calculated using the software and the calculated $V_{flex.}$:

Spec.	Negative m_n (k-in/in.)			Positive m_n (k-in/in.)			P^- (kip)	P^+ (kip)	$V_{flex.}$ (kip)
	m_{n1}^-	m_{n2}^-	m_n^-	m_{n1}^+	m_{n2}^+	m_{n3}^+			
G1	11.8	8.22	16.4	13.9	8.22	6.48	49.3	61.6	**110.8**
G2	14.04	8.26	16.5	12.0	8.26	6.49	52.5	56.2	**108.7**
G3	12.3	8.72	17.1	14.5	8.72	6.88	51.5	64.5	**116.1**
R1	19.9	10.9	25.2	12.9	9.41	7.22	74.9	61.6	**136.5**
R2	20.1	10.9	25.2	12.8	9.39	7.21	75.1	61.4	**136.4**
R3	18.8	8.86	23.7	8.32	10.4	6.83	67.5	49.9	**117.4**

Desayi and Seshadri 1997

Specimen *S*101, *S*201 and *S*301:

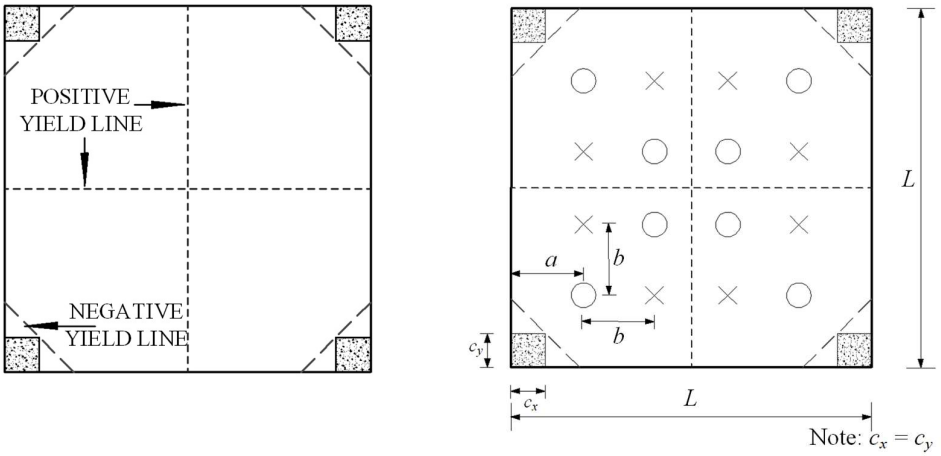

(a) Yield Line pattern (b) Load distribution pattern

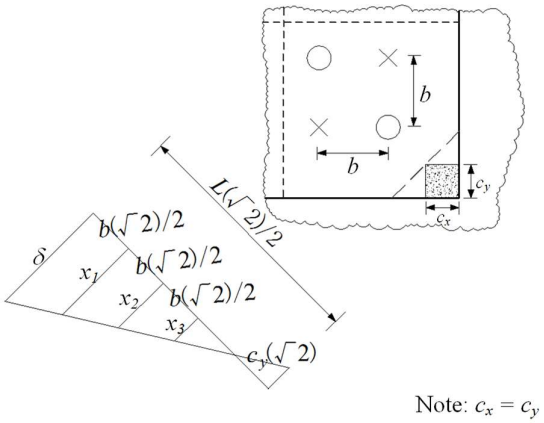

(c) Formula derivation

Figure 3*: Yield Line Pattern and* $V_{flex.}$ *formula derivation*

Positive Yield Line V_{flex} Calculations:

As per the above sketch:

$$\frac{\delta}{\frac{\sqrt{2}}{2}(L\text{-}2c_y)} = \frac{x_1}{\frac{\sqrt{2}}{2}(L\text{-}2c_y\text{-}b)} = \frac{x_2}{\frac{\sqrt{2}}{2}(L\text{-}2c_y\text{-}2b)} = \frac{x_3}{\frac{\sqrt{2}}{2}(L\text{-}2c_y\text{-}3b)}$$

Positive External Work:

$$EW^{+} = (0.05Px_1 + 0.075P.2x_2 + 0.05Px_3).4$$

$$= \left[0.05P\frac{\left(k - \frac{\sqrt{2}}{2}b\right)+\left(k - \frac{3\sqrt{2}}{2}b\right)}{k} + 0.075\frac{2(k - \sqrt{2}b)}{k}\right]4\delta$$

$$= \frac{k - \sqrt{2}b}{k}P\delta \qquad \text{where:} \quad k = \frac{\sqrt{2}}{2}(L - 2c_y)$$

Positive Internal Work:

$$IW^{+} = m_n\left(4L\frac{\sqrt{2}}{2}\right)\frac{\delta}{k}$$

Positive V_{flex} Calculations:

$$EW^{+} = IW^{+}$$

$$\frac{k - \sqrt{2}b}{k}P\delta = m_n\left(4L\frac{\sqrt{2}}{2}\right)\frac{\delta}{k}$$

Therefore:

$P^{+} = \frac{2\sqrt{2}\,L}{k - \sqrt{2}\,b}\,m_n$ For: $L = 41.7$in., $c_y = 3.94$in., $b = 8.27$in. *and* $k = 23.9$in.

$\boldsymbol{P^{+} = 9.636\ m_n^{+}}$

Negative Yield Line V_{flex} Calculations:

Negative External Work:

$$EW^{-} = \frac{k - \sqrt{2}b}{k}P\delta$$

Negative Internal Work:

$$IW^{-} = m_n\left(8\sqrt{2}\,c_y\right)\frac{\delta}{k}$$

Negative V_{flex} Calculations:

$$EW^{-} = IW^{-}$$

$$\frac{k - \sqrt{2}b}{k}P\delta = m_n\left(8\sqrt{2}\,c_y\right)\frac{\delta}{k}$$

Therefore, the value of P will be as follows:

$$P^{-} = \frac{8\sqrt{2}\,c_y}{k - \sqrt{2}\,b}m_n$$

Where k = 23.9in., c_y= 3.94in. and b = 8.27in.

$\boldsymbol{P^- = 3.636\ m_n^-}$

Specimen *S*201, *S*202 and *S*302:

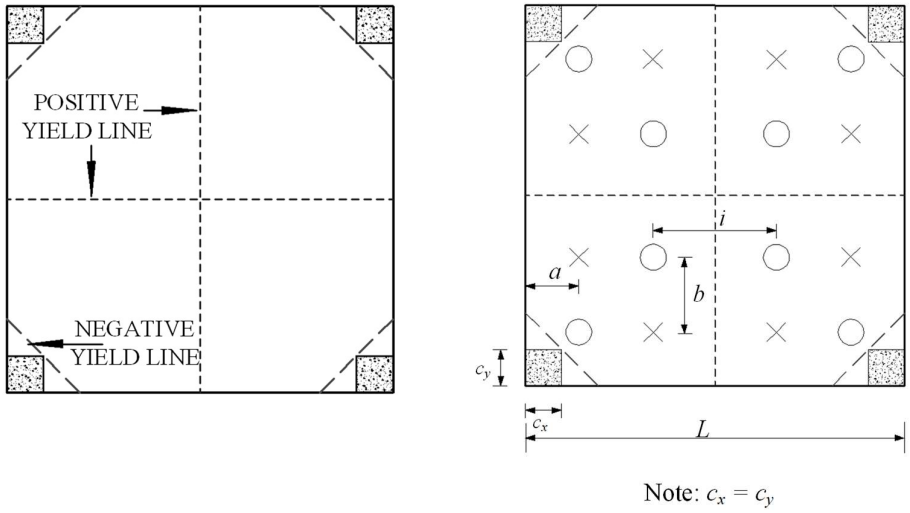

(a) Yield Line pattern (b) Load distribution pattern

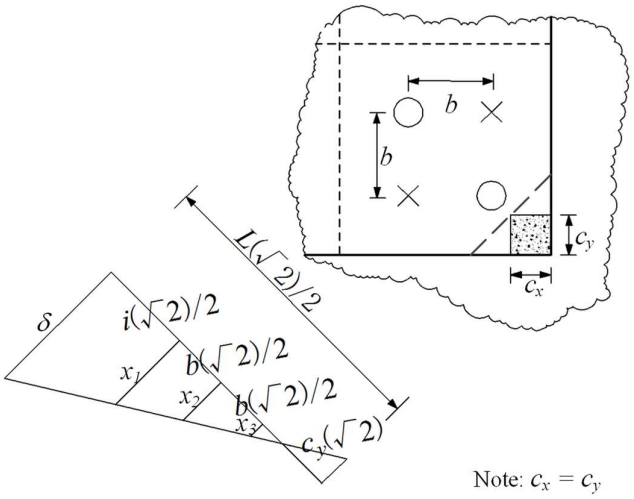

(c) Formula derivation

Figure 4*: Yield Line Pattern and* $\boldsymbol{V_{flex.}}$ *formula derivation*

For these specimens, the $V_{flex.}$ formula is also derived from the figure above, (figure: 4c)

$$\frac{\delta}{\frac{\sqrt{2}}{2}(L\text{-}2c_y)} = \frac{x_1}{\frac{\sqrt{2}}{2}(L\text{-}2c_y) - \frac{\sqrt{2}}{2}i} = \frac{x_2}{\frac{\sqrt{2}}{2}(L\text{-}2c_y) - \frac{\sqrt{2}}{2}i - \frac{\sqrt{2}}{2}b} = \frac{x_3}{\frac{\sqrt{2}}{2}(L\text{-}2c_y) - \frac{\sqrt{2}}{2}i - \sqrt{2}b}$$

Positive External Work (*EW*):

$$EW^{+} = (0.05Px_1 + 0.075P.2x_2 + 0.05Px_3).4$$

$$= \left[0.05P\frac{\left(k - \frac{\sqrt{2}}{2}b\right) + \left(k - \frac{\sqrt{2}}{2}b - \sqrt{2}b\right)}{k} + 0.075\frac{2\left(k - \frac{\sqrt{2}}{2}b - \frac{\sqrt{2}}{2}b\right)}{k}\right]4\delta$$

$$= \frac{2k - \sqrt{2}i - \sqrt{2}b}{k}0.5P\delta \qquad \text{where:} \qquad k = \frac{\sqrt{2}}{2}\left(L\text{-}2c_y\text{-}b\right)$$

Positive Internal Work:

$$IW^{+} = \left(4L\frac{\sqrt{2}}{2}\right)\frac{\delta}{k}m_n$$

Positive V_{flex} Calculations:

$EW^{+} = IW^{+}$

Therefore, this leads to the value of P as follows:

$$P^{+} = \frac{4\sqrt{2}L}{2k - \sqrt{2}i - \sqrt{2}b}m_n$$

For L= 41.7in., c_y = 3.94in., b = 8.3in., i = 13.4in. and k = 23.9in.

$$\boldsymbol{P^{+} = 13.67m_n^{+}}$$

Negative Yield Line $V_{flex.}$ Calculations:

Negative External Work:

$$EW^{-} = \frac{2k - \sqrt{2}b - \sqrt{2}i}{k}\ 0.5P\delta$$

Negative Internal Work:

$$IW^{-} = m_n\left(8\sqrt{2}\,c_y\right)\frac{\delta}{k}$$

Negative $V_{flex.}$ Calculations:

$EW^{-} = IW^{-}$

Therefore:

$$P^{-} = \frac{16\sqrt{2}\, c_y}{2k - \sqrt{2}\, i - \sqrt{2}\, b} m_n$$

Where k = 23.9in., c_y = 3.94in., i = 13.4in. and b = 8.3in.

$\boldsymbol{P^{-} = 5.159\ m_n^{-}}$

Moment strength, positive m_n and negative m_n were calculated using the Sp-column software, using the bottom and top steel rebar reinforcement areas from the provided reinforcement layout. Since the reinforcement layout is different along the column strip and the middle strip of the slab span, therefore the moment strength was calculated separately and the average moment used for $V_{flex.}$ calculations.

The table below shows all the values of positive m_n and negative m_n calculated using the software:

Spec.	Negative m_n	Positive m_n			P^{-} (kip)	P^{+} (kip)	$V_{flex.}$ (kip)
	m_n^{-} (kip-in./in.)	m_{n1}^{+} (kip-in./in.)	m_{n2}^{+} (kip-in./in.)	$m_{n\,aver.}^{+}$ (kip-in./in.)			
S101	5.00	2.49	2.19	2.34	18.2	22.6	**10.20**
S201	7.13	3.75	2.19	2.97	25.9	28.6	**13.60**
S301	8.11	4.46	1.98	3.22	29.5	31.0	**15.10**
S102	4.65	2.37	1.86	2.09	24.0	28.6	**13.20**
S202	6.77	3.55	1.99	2.77	34.9	37.9	**18.20**
S302	8.27	4.56	2.15	3.36	42.7	45.9	**22.20**

Walker and Regan 1987

Specimen *Sc*1, *Sc*2 and *Sc*3:

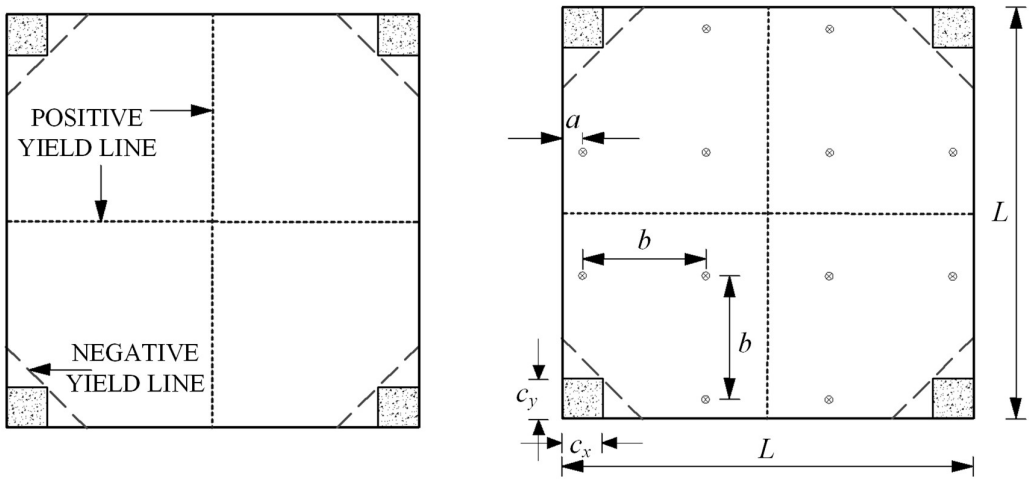

(a) Yield Line pattern (b) Load distribution pattern

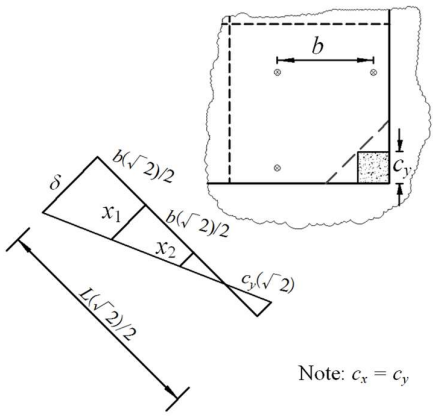

(c) Formula derivation

Figure 5: Yield Line Pattern and $V_{flex.}$ formula derivation

Positive Yield Line V_{flex} Calculations:

As per the above sketch (figure:5c)

$$\frac{\delta}{\frac{\sqrt{2}}{2}(L\text{-}2c_y)} = \frac{x_1}{\frac{\sqrt{2}}{2}(L\text{-}2c_y\text{-}b)} = \frac{x_2}{\frac{\sqrt{2}}{2}(L\text{-}2c_y\text{-}2b)}$$

Positive External Work:

$$EW^{+} = 4(Px_1 + 2Px_2)$$

$$= 4P\frac{(L-2c_y-b)+2(L-2c_y-2b)}{L-2c_y}$$

$$= \frac{3L - 6c_y - 5b}{L - 2c_y}\ 4P$$

Positive and Negative Internal Work:

$$IW^{+} = m_n^{+}\ (2L\sqrt{2})\theta + m_n^{-}(8\sqrt{2}\ c_y)\ \theta$$

Where $\theta = \frac{\delta}{\frac{\sqrt{2}}{2}(L-2c_y)}$

Positive and Negative $V_{flex.}$ Calculations:

$$EW^{+} = IW^{+}$$

Therefore, it will lead to the value of P as follows:

$$P = \left(\frac{(L-2c_y)}{4(3L-6c_y-5b)}\right)\left(\frac{2\sqrt{2}}{\frac{\sqrt{2}}{2}(L-2c_y)}\right)\left[m_n^{+}L+4c_y m_n^{-}\right]$$

$$= \frac{\boldsymbol{m_n^{+}\,L+4c_y m_n^{-}}}{\boldsymbol{(3L-6c_y-5b)}}$$

where: L = 120in., c_y = 11.8in. and b = 36in. *(for Sc1 to Sc3)*

where: L = 120in., c_y = 8.66in. and b = 36in. *(for Sc4 to Sc7)*

Therefore, for specimen *Sc*1-*Sc*3 and specimen *Sc*4-*Sc*7, the yield line pattern and the formula derivation will be the same, only the column size changes from 11.8x11.8in. for *Sc*1-*Sc*4 to 8.66x8.66in. for *Sc*4-*Sc*7.

The results of the V_{flex} were calculated as listed below;

Specimen	Positive V_{flex}	Negative V_{flex}
*Sc*1- *Sc*3	$\boldsymbol{P = 1.099 m_n^{+}}$	$\boldsymbol{P = 0.432 m_n^{-}}$
*Sc*4- *Sc*7	$\boldsymbol{P = 0.937 m_n^{+}}$	$\boldsymbol{P = 0.27 m_n^{-}}$

Specimen *Sc*8 and *Sc*9:

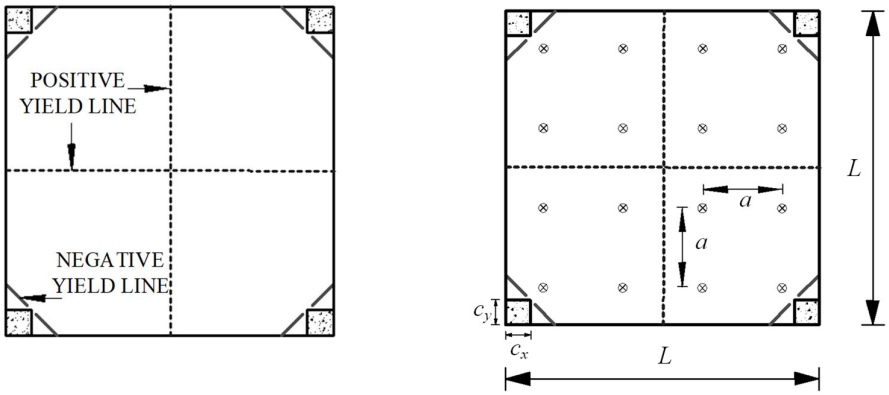

(a) Yield Line pattern (b) Load distribution pattern

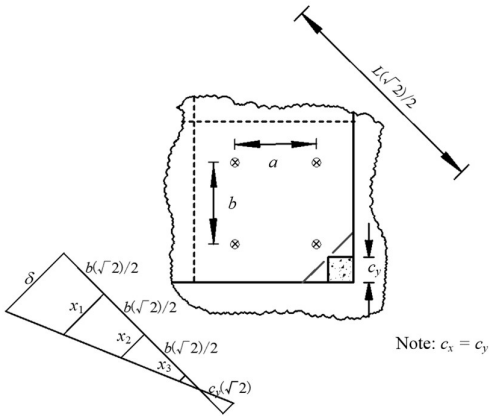

(c) Formula derivation

Figure 6: *Yield Line Pattern and* $V_{flex.}$ *formula derivation*

Positive Yield Line V_{flex} Calculations:

As per the above sketch (figure 6c):

$$\frac{\delta}{\frac{\sqrt{2}}{2}(L\text{-}2c_y)} = \frac{x_1}{\frac{\sqrt{2}}{2}(L\text{-}2c_y)\text{-}\frac{\sqrt{2}}{2}a} = \frac{x_2}{\frac{\sqrt{2}}{2}(L\text{-}2c_y)\text{-}\sqrt{2}a} = \frac{x_3}{\frac{\sqrt{2}}{2}(L\text{-}2c_y)\text{-}\frac{3\sqrt{2}}{2}a}$$

Positive External Work:

$EW^{+} = 4(Px_1 + 2Px_2 + Px_3)$, Let $L\text{-}2c_y = k$

$$= 4P\frac{(k-a)+2(k-2a)+(k-3a)}{k} = \frac{4k-8a}{k}\,4P\delta$$

Positive Internal Work:

$$IW^{+} = m_n^{+}\left(\frac{\sqrt{2}}{2}4L\right)\frac{\delta}{\frac{\sqrt{2}}{2}k}$$

$$= m_n^{+}(4L)\frac{\delta}{k}$$

Positive V_{flex} Calculations:

$EW^{+} = IW^{+}$

Therefore, this leads to the value of P as follows:

$$EW^{+} = IW^{+}$$

$$\frac{4k-8a}{k}\,4P\delta = m_n^{+}(4L)\frac{\delta}{k}$$

$$\boldsymbol{P = \frac{L}{4k-8a}m_n^{+}}$$

$\boldsymbol{P = 0.735m_n^{+}}$ where: L = 78.7in., c_y = 6.30in., a = 19.7in. and k = 66.1in.

Negative Yield Line V_{flex} Calculations:

Negative External Work:

$$EW^{-} = \frac{4k-8a}{k}\,4P\delta$$

Negative Internal Work:

$$IW^{-} = 4m_n\left(2\sqrt{2}\,c_y\right).\frac{\delta}{\left(\frac{\sqrt{2}}{2}k\right)}$$

$$= 4c_y\frac{\delta}{k}m_n$$

Negative V_{flex} Calculations:

$EW^{-} = IW^{-}$

Therefore:

$$P^{-} = \frac{4c_y}{4k-8a}\,m_n^{-}$$

$\boldsymbol{P^{-} = 0.235\,m_n^{-}}$, where: L = 78.7in., a = 19.7in., k = 66.1in. and c_y = 6.3in.

Specimen	Positive V_{flex}	Negative V_{flex}
*Sc*8- *Sc*9	$\boldsymbol{P = 0.735\ m_n^+}$	$\boldsymbol{P = 0.235 m_n^-}$

Specimen *Sc*11 and *Sc*12:

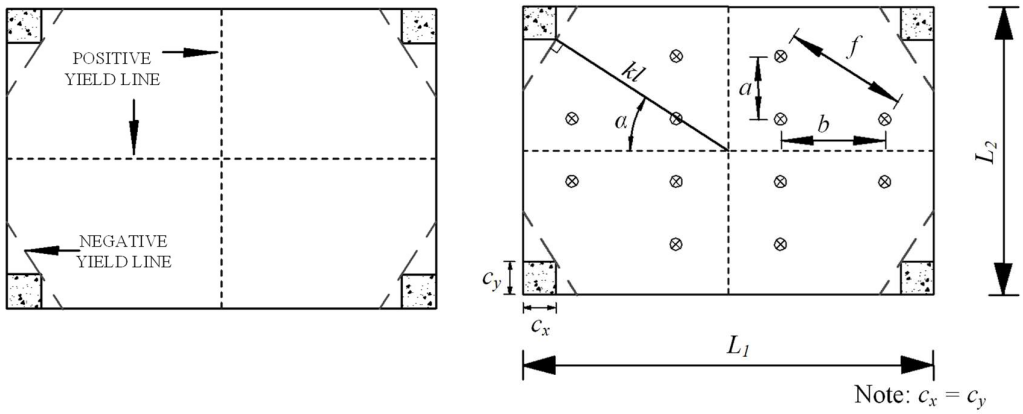

(a) Yield Line pattern (b) Load distribution pattern

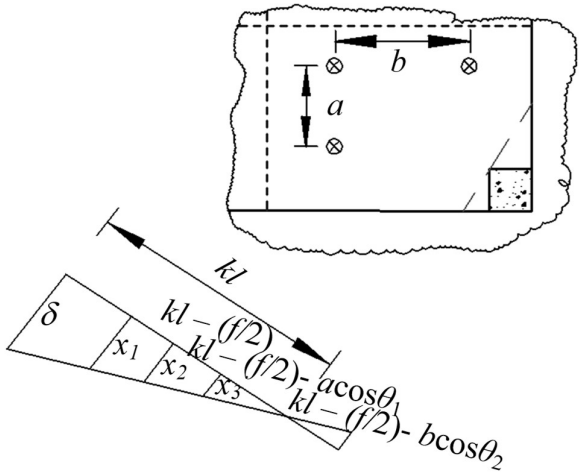

(c) Formula derivation

Figure 7: *Yield Line Pattern and* $V_{flex.}$ *formula derivation*

Positive Yield Line $V_{flex.}$ Calculations:

As per the above sketch (figure 7c):

$$\frac{\delta}{kl} = \frac{x_1}{kl - \frac{f}{2}} = \frac{x_2}{kl - \frac{f}{2} - a\cos\theta_1} = \frac{x_3}{kl - \frac{f}{2} - b\cos\theta_2}$$

Positive External Work:

$$EW^{+} = P\,(x_1 + x_2 + x_3) \;=\; \delta P \frac{3kl - \frac{3}{2}f - (2a\cos\theta_1 + b\cos\theta_2)}{kl}$$

Positive Internal Work:

$$IW^{+} = m_n^{+}\left(L + \frac{7}{10}L\right)\frac{\delta}{4kl}$$

Positive V_{flex} Calculations:

$EW^{+} = IW^{+}$

Therefore, the value of P is derived as follows:

$$EW^{+} = IW^{+}$$

$$\delta P \frac{3kl - \frac{3}{2}f - (2a\cos\theta_1 + b\cos\theta_2)}{kl} = m_n^{+}\left(L + \frac{7}{10}L\right)\frac{\delta}{4kl}$$

$$P^{+} \;=\; \frac{(L + \frac{7}{10}L)\frac{1}{4}}{3k\,l - \frac{3}{2}f - (2a\cos\theta_1 + b\cos\theta_2)}\; m_n^{+}$$

$\boldsymbol{P^{+} = 0.557\, m_n^{+}}$ *where* c_y = 6.3in., a =11.8in., b = 19.7in., kl = 39.1in. *and* f = 22.9in.

$\boldsymbol{P^{+} = 0.638\, m_n^{+}}$ *where* c_y = 11.8in., a = 11.8in., b = 19.7in., kl = 31.4in. *and* f = 22.9in.

Negative Yield Line V_{flex} Calculations:

Negative External Work:

$$EW^{-} = \delta P \frac{3kl - \frac{3}{2}f - (2a\cos\theta_1 + b\cos\theta_2)}{kl}$$

Negative Internal Work:

$$IW^{-} = m_n\left(2\sqrt{2}\,c_y\right)\frac{\delta}{k}$$

$$P^{-} \;=\; \frac{2\sqrt{2}\,c_y}{3kl - \frac{3}{2}f - (2a\cos\theta_1 + b\cos\theta_2)}\; m_n^{-}$$

$\boldsymbol{P^{-} = 0.297\, m_n^{-}}$ *where* c_y = 6.3in., a = 11.8in., kl = 39.1in, f = 22.9in., b = 19.7in. *and* $\Delta = \alpha$.

$\boldsymbol{P^{-} = 0.915\, m_n^{-}}$ *where* c_y = 11.8in., a = 11.8in., kl = 31.4in., f = 22.9in., b = 19.7in. *and* $\Delta = \alpha$.

Specimen	Positive V_{flex}	Negative V_{flex}
*Sc*11	$\boldsymbol{P = 0.557\ m_n^+}$	$\boldsymbol{P = 0.297 m_n^-}$
*Sc*12	$\boldsymbol{P = 0.638\ m_n^+}$	$\boldsymbol{P = 0.915 m_n^-}$

Moment strength, positive m_n and negative m_n were calculated using the Sp-column software, using the bottom and the top reinforcement areas from the provided reinforcement layout. Though the reinforcement layout is different along the column strip and the middle strip of the slab span, therefore the moment strength was calculated using the whole slab span length reinforcement area and divided by the total length to get the moment per unit length.

The table below shows all the values of positive m_n and negative m_n and the calculated $\boldsymbol{V_{flex.}}$:

Spec.	**Negative m_n** $\boldsymbol{m_n^-}$ (kip-in./in.)	**Positive m_n** $\boldsymbol{m_n^+}$ (kip-in./in.)	$\boldsymbol{P^-}$ (kip)	$\boldsymbol{P^+}$ (kip)	$\boldsymbol{V_{flex.}}$ (kip)
S_{c1}	6.75	2.59	2.92	2.84	**17.30**
S_{c2}	4.88	3.48	2.11	3.83	**17.80**
S_{c3}	8.21	1.64	3.55	1.80	**16.03**
S_{c4}	6.69	2.57	1.81	2.41	**12.60**
S_{c5}	9.38	3.99	2.53	3.74	**18.80**
S_{c7}	10.70	3.98	2.52	3.72	**18.70**
S_{c8}	1.12	2.55	0.26	1.88	**8.55**
S_{c9}	1.63	1.63	0.38	1.20	**6.34**
S_{c11}	3.07	2.89	0.91	1.61	**7.56**
S_{c12}	3.82	3.32	3.49	2.12	**16.8**

Zaghlool 1970

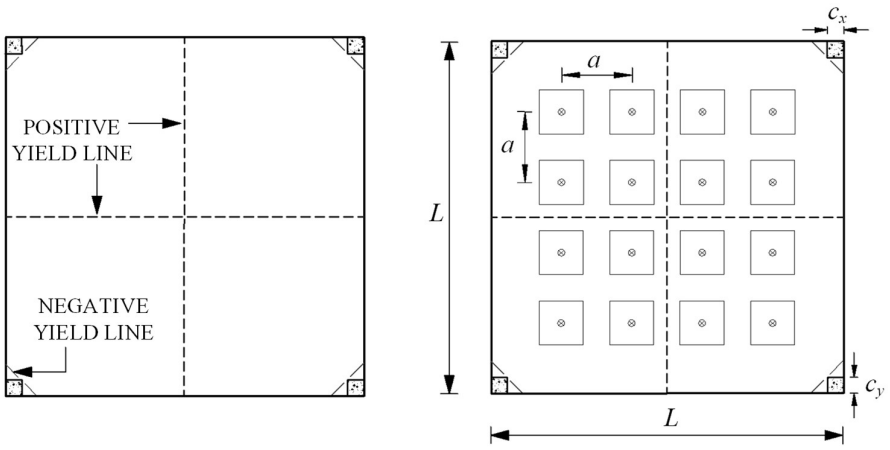

(a) Yield Line pattern (b) Yield Line pattern

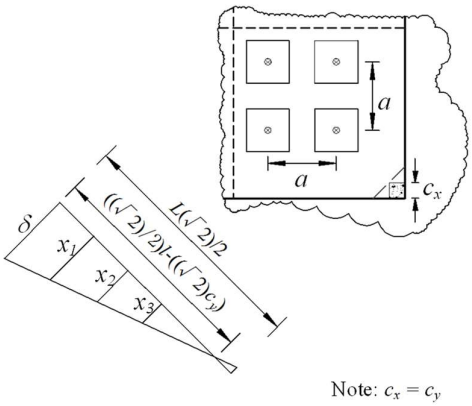

(c) Formula derivation

Figure 8: *Yield Line Pattern and* $V_{flex.}$ *formula derivation*

Positive Yield Line $V_{flex.}$ Calculations:

As per the above sketch:

$$\frac{\delta}{\frac{\sqrt{2}}{2}(l - c_y)} = \frac{x_1}{\frac{\sqrt{2}}{2}(l - c_y - a)} = \frac{x_2}{\frac{\sqrt{2}}{2}(l - c_y - 2a)} = \frac{x_3}{\frac{\sqrt{2}}{2}(l - c_y - 3a)}$$

Where: $l = L - c_y$

Positive External Work (*EW*):

$EW^{+} = 4P(x_1+2x_2+x_3)$

$$= 4P\delta\left(\frac{l - c_y - a}{l - c_y} + 2\frac{l - c_y - 2a}{l - c_y} + \frac{l - c_y - 3a}{l - c_y}\right)$$

$$= 4P\delta\left(\frac{4l - 4c_y - 8a}{l - c_y}\right)$$

Positive Internal Work (IW):

$IW^{+} = m_n^{+}\, L\, \theta$

$$= m_n^{+}\left(2\sqrt{2}\right)L\frac{\delta}{\frac{\sqrt{2}}{2}(l - c_y)}$$

Positive V_{flex} Calculations:

$EW^{+} = IW^{+}$

Therefore, the value of *P* will be as follows:

$$EW^{+} = IW^{+}$$

$$4P\delta\left(\frac{4l - 4c_y - 8a}{l - c_y}\right) = m_n^{+}\left(2\sqrt{2}\right)L\frac{\delta}{\frac{\sqrt{2}}{2}(l - c_y)}$$

$\boldsymbol{P = \frac{L}{4(l - c_y - 2a)}m_n^{+}}$ where: l = 120in., c_y= c_y = 5.5in (6.5in. for specimen III and IV), L = $c_y + l$ and a = 24in.

$\boldsymbol{P = 0.472m_n^{+}}$ ***(for specimen I)***

$\boldsymbol{P = 0.483m_n^{+}}$ ***(for specimen III and IV)***

Negative Yield Line V_{flex} Calculations:

Negative External Work:

$EW^{-} = \frac{4l - 4c_y - 8a}{l - c_y}\ 4P\delta$

Negative Internal Work:

$IW^{-} = m_n\left(2\sqrt{2}c_y\right).\frac{\delta}{\frac{\sqrt{2}}{2}(l - c_y)}$

Negative V_{flex} Calculations:

$$EW^{+} = IW^{+}$$

Therefore, the value of P will be as follows:

$$EW^{+} = IW^{+}$$

$$\frac{4l - 4c_y - 8a}{l - c_y} \; 4P\delta = m_n\left(2\sqrt{2}c_y\right).\frac{\delta}{\frac{\sqrt{2}}{2}(l - c_y)}$$

$\boldsymbol{P^{-} = \frac{c_y}{4(l - c_y - 2a)} m_n^{-}}$ where: l = 120in., c_y = 5.5in (6.5in. for specimen III and IV), $L = c_y + l$ and a = 24in.

$\boldsymbol{P^{-} = 0.0207 m_n^{-}}$ ***(for specimen I)***

$\boldsymbol{P^{-} = 0.0249 m_n^{-}}$ ***(for specimen III and IV)***

Moment strength, positive m_n and negative m_n were calculated per unit length using the Sp-column software, using the bottom and the top reinforcement areas from the provided reinforcement layout.

The table below shows all the values of positive m_n and negative m_n calculated using the software:

Spec.	Negative m_n			Positive m_n			P^{-} (kip)	P^{+} (kip)	$V_{flex.}$ (kip)
	m_{n1}^{-} (k-ft)	m_{n2}^{-} (k-ft)	$m_{n,\text{aver.}}^{-}$ (k-in/in)	m_{n1}^{+} (k-ft)	m_{n2}^{+} (k-ft)	$m_{n,\text{aver.}}^{+}$ (k-in/in)			
I	13.26	13.30	**14.50**	133.4	160.7	**14.70**	1.46	33.85	**35.32**
III	12.84	13.27	**12.05**	130.6	156.7	**14.37**	1.46	33.97	**35.43**
IV	14.14	14.15	**13.06**	139.8	169.5	**15.46**	1.59	36.56	**38.15**